DigiWest: a high throughput Western-Blot and its application for comprehensive signaling analysis of microdissected liver tissue

Dissertation

der Mathematisch-Naturwissenschaftlichen Fakultät

der Eberhard Karls Universität Tübingen

zur Erlangung des Grades eines

Doktors der Naturwissenschaften

(Dr. rer. nat.)

vorgelegt von

Fridolin Treindl

aus Binsdorf

Tübingen

2015

Gedruckt mit Genehmigung der Mathematisch-Naturwissenschaftlichen Fakultät der Eberhard Karls Universität Tübingen.

Tag der mündlichen Qualifikation:	14.10.2015
Dekan:	Prof. Dr. Wolfgang Rosenstiel
1. Berichterstatter:	Prof. Dr. Michael Schwarz
2. Berichterstatter:	Prof. Dr. Stefan Stevanović

The presented doctoral thesis was carried out at the Natural and Medical Sciences Institute at the University of Tuebingen (NMI) in Reutlingen, in the group of Markus Templin, Protein Profiling and Assay Development, from 2010 to 2013 under the supervision of Prof. Dr. Michael Schwarz, Department of Toxicology, Institute of Experimental and Clinical Pharmacology and Toxicology, University of Tuebingen and Prof. Dr. Stefan Stevanović, Department of Immunology, Interfaculty Institute for Cell Biology, University of Tuebingen.

Table of contents

1 Abstracts

1.1 Summary

Proteins play a pivotal role in cellular processes. As proteins represent the major ‘workforce’ of biomolecules, changes in protein abundances and in posttranslational modifications indicate changes in the behavior of cells on the molecular level. Analysis of proteins improves our understanding of physiological and pathophysiological mechanisms. Today, there are numerous technologies and methods available for protein analysis. For semi-quantitative detection, Western-Blotting still represents the gold standard and is probably the most widespread method for protein analysis.

The DigiWest approach which is described in this thesis is based on the Western-Blot. Transfer onto a bead-based microarray platform creates hundreds of replicas of an initial blot. Proteins are separated by SDS-PAGE and blotted onto a membrane as performed for a classical Western-Blot. The membrane containing the size-separated proteins is then cut into molecular weight fractions. Proteins are eluted from the molecular weight fractions and each fraction is loaded onto a distinct color-coded Luminex bead set. The color code of the bead sets retains the molecular weight information and allows pooling of all bead sets loaded with proteins into a bead-mix which represents the initial Western-Blot with a resolution of 0.5 mm. As only a small aliquot of a bead-mix is required for an antibody-incubation, a bead-mix loaded with protein from a single Western-Blot is sufficient for hundreds of antibody incubations which are performed in microtiter plates. After fluorescence-based readout on the Luminex instrument, the color code of the beads allows digital reconstruction of the initial Western-Blot lanes using the antibody specific signal obtained on the different bead-sets representing molecular weight fractions of the initial blot. Therefore, the method was named ‘DigiWest’. The digital data allow fast quantification of the antibody specific signal without image processing and the data can also be used to create gray-scale images mimicking classical Western-Blot images. Although hundreds of replicas are generated, allowing hundreds of antibody incubations in fast and automatable assays, DigiWest uses the same sample amount that is usually used for a single Western-Blot while it keeps sensitivity and signal linearity comparable to high-end Western-Blot readout platforms. The results are robust and highly comparable to classical Western-Blots. Application of the DigiWest method allowed a comprehensive analysis of laser capture microdissected samples which are barely sufficient for a single Western-Blot.

Mouse models play an important role in toxicology and the liver, the most important organ for drug metabolism, gains special attention. Besides its homogenous appearance the liver is built from lobules as repeated units and zonation results in different metabolic competences for the hepatocytes dependent

on their position within a lobule. Proximal periportal and pericentral zones from liver lobules were isolated by LCM from formalin fixed mouse liver sections derived from a time-course treatment study with the non-genotoxic carcinogen TCPOBOP. About 200 Western-Blot equivalents were performed with the resulting samples. The analysis of the isolated zones provided new insights into cellular signaling in liver zonation and changes occurring during the treatment time course. An important role for serine and threonine phosphorylations and phosphatases was found for regulation of zone specific metabolism. Inhibition of the phosphatase PP2A in the periportal zone was found to direct insulin dependent signaling. The TCPOBOP treatment time-course analysis showed that mainly the pericentral zone is exposed to oxidative stress resulting in activation of a stress-survival response while other TCPOBOP induced effects were found to affect both zones. TCPOBOP was found to induce a pronounced disturbance in cellular signaling within the first 24 hours after treatment.

1.2 Zusammenfassung

Proteine spielen eine zentrale Rolle in zellulären Prozessen. Da Proteine unter den Biomolekülen die wichtigsten „Arbeitskräfte“ darstellen, deuten Änderungen in der Menge an Proteinen und an posttranslationalen Modifikationen auf Änderungen im Verhalten von Zellen auf molekularer Ebene. Die Analyse von Proteinen verbessert unser Verständnis von physiologischen und pathophysiologischen Vorgängen. Heutzutage steht uns eine große Anzahl an Technologien und Methoden zur Proteinanalyse zur Verfügung. Für den semiquantitativen Nachweis stellt der Western-Blot immer noch den Gold-Standard dar und ist wahrscheinlich die am weitesten verbreitete Methode für die Proteinanalyse.

Die DigiWest Methode die in dieser Doktorarbeit beschrieben wird basiert auf dem Western-Blot. Durch Überführung auf eine Bead-basierte Mikroarray Plattform werden aus einem initialen Blot hunderte Repliken erzeugt. Proteine werden mittels SDS-PAGE aufgetrennt und auf eine Membran geblottet wie es für einen klassischen Western-Blot durchgeführt wird. Die Membran, die die nach Größe aufgetrennten Proteine enthält, wird dann in Molekulargewichtsfraktionen geschnitten. Die Proteine werden aus den Molekulargewichtsfraktionen eluiert und jede Fraktion wird auf eine unterscheidbare, farbkodierte Luminex Bead-Population geladen. Die Farbkodierung der Beads bewahrt die Molekulargewichtsinformation und erlaubt es, alle mit Proteinen beladenen Bead-Populationen in einem Bead-Mix zu vereinigen welcher den ursprünglichen Western-Blot mit einer Auflösung von 0.5 mm darstellt. Da nur ein kleines Aliquot eines Bead-Mixes für eine Antikörperinkubation benötigt wird, ist ein Bead-Mix der mit Protein aus einem einzelnen Western-Blot beladen ist ausreichend für hunderte Antikörperinkubationen welche in Mikrotiter-Platten durchgeführt werden. Nach dem

fluoreszenzbasierten Auslesen auf einem Luminex-Gerät erlaubt die Farbkodierung die digitale Rekonstruktion der ursprünglichen Western-Blot Spuren unter Verwendung des Antikörper-spezifischen Signals welches auf den unterschiedlichen Bead-Populationen erhalten wurde die die Molekular-gewichts-Fraktionen des ursprünglichen Blots darstellen. Daher wurde die Methode „DigiWest“ genannt. Die digitalen Daten erlauben eine schnelle Quantifizierung des Antikörperspezifischen Signals ohne Bildverarbeitung wobei die Daten auch dazu verwendet werden können Graustufenbilder zu erzeugen welche klassische Western-Blot Bilder nachahmen.

Obwohl hunderte Repliken erzeugt werden, welche hunderte Antikörperinkubationen in schnellen und automatisierbaren Assays erlauben, verwendet die DigiWest Methode die selbe Proben-Menge die üblicherweise für einen einzelnen Western-Blot verwendet wird während eine Sensitivität und Signal-Linearität beibehalten wird die mit High-End Western-Blot Auslese-Systemen vergleichbar ist. Die Ergebnisse sind robust und bestens mit klassischen Western-Blots vergleichbar. Die Anwendung der DigiWest Methode erlaubte eine umfangreiche Analyse von mittels Laser-Mikrodissektion isolierter Proben welche kaum für einen einzelnen Western-Blot ausreichen.

Maus-Modelle spielen eine wichtige Rolle in der Toxikologie und die Leber als wichtigstes Organ für Medikamenten-Metabolismus bekommt besondere Aufmerksamkeit. Abgesehen vom homogenen Erscheinungsbild der Leber ist diese aus Läppchen als sich wiederholende Einheiten aufgebaut deren Zonierung darin resultiert dass Hepatozyten unterschiedliche metabolische Kompetenzen besitzen, abhängig von ihrer Position innerhalb eines Läppchens. Stammnahe periportale und perizentrale Zonen der Leberläppchen wurden mittels LCM aus Formalin fixierten Mausleberschnitten isoliert welche aus einer Behandlungszeitreihen-Studie mit dem nicht-genotoxischen Karzinogen TCPOBOP stammten. Ungefähr 200 Western-Blot Äquivalente wurden mit den resultierenden Proben durchgeführt. Die Analyse der isolierten Zonen brachte neue Einblicke in die zelluläre Signalübertragung in der Leberzonierung und in Änderungen während der Behandlungs-Zeitreihe. Es wurde eine wichtige Rolle von Serin- und Threonin-Phosphorylierungen und Phosphatasen für die Regulation des Zonen-spezifischen Metabolismus gefunden. Es stellte sich heraus dass die Inhibierung der Phosphatase PP2A in der periportalen Zone die Insulin-vermittelte Signalübertragung lenkt. Die Analyse der TCPOBOP Behandlunszeitreihe zeigte dass hauptsächlich die perizentrale Zone oxidativem Stress ausgesetzt ist was eine Stress-Überlebens-Antwort hervorruft während andere TCPOBOP-induzierte Effekte beide Zonen betreffen. Es stellte sich heraus dass TCPOBOP eine ausgeprägte Störung der zellulären Signalüber-tragung innerhalb der ersten 24 Stunden nach der Behandlung verursacht.

2 Introduction

2.1 Of signaling and cancer

An adult human being is composed of about $3.7x10^{13}$ cells (Bianconi et al., 2013). Perfect interplay and communication between all these cells and tight regulation of their behavior is vital to maintain homeostasis and adapt to changes of the inner and outer environment (Scanlon, 2007). Yet being a human is more than just homeostasis. Although all cells possess the same almost invariable genes, they are highly differentiated to fulfil their purposes. Therefore, they express different proteins for metabolism and signaling. There are various molecular mechanisms for regulation of intercellular communication and intracellular signaling. Cell surfaces are strewn with receptors and other proteins which receive signals from outside the cells or transmit signals from inside the cells (Gomperts, Kramer, & Tatham, 2009; Karp, 2009).

While several fundamental principles are known on cellular signaling, yet we are still at the beginning of under-standing the complexity of signaling networks and of deciphering the nexuses. One important and frequently employed mechanism of cellular signaling starts with binding of a ligand, often a soluble extracellular protein, to a receptor at the surface of a cell. The receptor changes its conformation or forms a dimer and thereby transmits the signal to the inside of the cell. The activated receptor can provide a binding platform for intracellular proteins and enzymes. Many receptors themselves contain enzymatic subunits which are activated by ligand binding. A wide spread enzymatically transmitted signal is phosphorylation. Kinase activity leads to phosphorylation of proteins at specific hydroxyl-groups and thereby induces a conformational change. This conformational change leads to activation or inactivation of enzymatic activity, a change of specificity or it can lead to uncovering or hiding of interaction sites. Thereby, phosphorylation provides a powerful signaling mechanism. Activation of few receptor proteins or even a single receptor protein activates a kinase which may then phosphorylate and thereby activate many target proteins which can themselves be kinases that can activate many new target proteins. This phenomenon is known as a kinase cascade which has a strong amplifying effect. Important substrates for kinases are transcription factors resulting in transcriptional changes. Phosphatases can dephosphorylate proteins and thereby inverse the signal (Chang & Karin, 2001; Gomperts et al., 2009; Krauss, 2006).

Most signaling pathways depend on kinase activity and mechanisms to keep the amplifying effect of kinase cascades under control have evolved. The so called G-proteins can control initial steps of a cascade and have the function of a time switch getting inactivated after a short period of time to prevent signaling from getting out of control (Chang & Karin, 2001; Gomperts et al., 2009; Krauss, 2006).

Most kinases involved in signaling have a number of targets and the outcome of their activation depends on many factors. Formation of complexes with other proteins influences their microenvironment such as location, interaction partners and substrate availability. Therefore, cellular signaling has to be seen as a complex spatiotemporal process with different cell types responding differently upon signaling events (Kholodenko, 2006; Krauss, 2006; Volmat & Pouysségur, 2001).

Diseases which are not caused by pathogens directly are often based on defects in cellular signaling. Disturbances in signaling are a frequent cause of cancer development. Most tumors bear one or more mutations in genes which code for proteins that play central roles in cellular signaling. These mutations often lead to constitutively active signaling (Hanahan & Weinberg, 2000, 2011; Weber, 2007). For example, two thirds of all malignant melanoma bear an activating mutation in the B-RAF gene coding for a kinase involved in the MAP-kinase cascade leading to a constitutive active signaling status that promotes tumor growth (H. Davies et al., 2002). But cancer is not a defined disease and a single mutation in a gene coding for an important signaling protein is not sufficient for carcinogenesis. Current research postulates six hallmarks of cancer which are required for a cell to become malignant (Hanahan & Weinberg, 2000, 2011). Most tumor types are highly diverse in respect to mutations and this characteristic makes treatment difficult (Gabriel, 2007).

Errors in DNA replication are naturally occurring in our genome. Most of them get repaired by specific repair mechanisms, while cells with major defects undergo apoptosis or are eliminated by the immune system. Not all initial mutations are repaired and thereby, mutations accumulate during life time resulting in increased cancer risk with prolonged life (Hoeijmakers, 2009; Lombard et al., 2005).

Besides DNA replication, major causes for mutation are radiation and chemicals. Substances known to be mutagenic are classified as carcinogens (Weber, 2007). A special subgroup of carcinogens is known as non-genotoxic carcinogens (NGCs). These substances do not cause mutations directly but still induce tumor formation. Their mode of action has not yet been elucidated but they are thought to promote tumor formation from preneoplastic lesions i.e. genetically and phenotypically altered cells (Hernández, van Steeg, Luijten, & van Benthem, 2009).

In an attempt to get a closer understanding of NGCs, rodent tumor models can be employed. A common experimental system is based on tumor initiation and promotion. Rodents are injected with a single dose of a genotoxic agent like DEN (diethylnitrosamine) to induce mutations followed by long term treatment with a tumor promoting agent (Boorman, Maronpot, & Eustis, 1994; Schulte-Hermann, 1985). The mutagen DEN initiates mouse liver tumor formation and analysis of the tumor cells showed that they frequently harbor mutations in the MAP-kinase cascade, mutations in H-RAS in ~50% or B-RAF in ~20% of tumors were found (Jaworski, Buchmann, Bauer, Riess, & Schwarz, 2005). When this initiation is followed

by tumor promotion with a phenobarbital-like promoter, a NGC, the resulting tumors harbor almost exclusively mutations in Ctnnb1, the gene coding for β-catenin (Aydinlik, Nguyen, Moennikes, Buchmann, & Schwarz, 2001; Loeppen et al., 2002). These chemical substances seem to provide a growth advantage to preneoplastic lesions harboring activating β-catenin mutations in the liver. Phenobarbital-like inducers activate the nuclear receptor CAR which is a central regulator of xenobiotic metabolism. Activation of CAR results in induction of several drug metabolizing enzymes and hepatomegaly which is based on liver hypertrophy and hyperplasia. The strongest known phenobarbital-like tumor promoter is TCPOBOP (1,4-Bis[2-(3,5-Dichloropyridyloxy)] Benzene) (W. Huang et al., 2005; Kodama & Negishi, 2008).

Although different classes of NGCs seem to have different modes of action, they are often referred to epigenetic carcinogens as their tumor promoting effect coincides with epigenetic perturbations including DNA methylation. The effects of non-genotoxic carcinogens are dose and time dependent. Carcinogenic effects only occur beyond a certain threshold and usually only in long term treatment (Bolt, Foth, Hengstler, & Degen, 2004; Fukushima et al., 2005; Klein & Costa, 1997). The liver is the main organ for drug metabolism and several known NGCs promote tumors in the liver. Therefore, the liver gains special attraction for investigation of NGCs in rodents (Melnick, Kohn, & Portier, 1996; S. P. S. Monga & Cagle, 2010).

2.2 The liver

The liver is the largest visceral organ and the second most complex after the brain. The most important function is to maintain homeostasis of the blood. It regulates content of nutrients and other blood components and removes disused components. An important part of this function is metabolism and removal of xenobiotics – foreign chemical substances like drugs. There are at least a dozen different cell types present in the liver of which hepatocytes account for about 60% of the total cell number and 80% of the volume. Other prevalent cells are sinusoidal endothelial cells, Kupffer cells, hepatic stellate cells and biliary epithelial cells (Arias, 2009; Malarkey, Johnson, Ryan, Boorman, & Maronpot, 2005; S. P. S. Monga & Cagle, 2010).

Most nutrients enter our body through our intestine and are delivered to the liver by the portal vein. Oxygen rich blood is supplied to the liver by the hepatic artery. In combination with the biliary duct, these blood vessels form the so called portal triad. The three vessels of the portal triad form a unit and branch into smaller vessels interfusing the liver. Blood leaves the liver through the central vein which forms from fusion of smaller vessels which interfuse the liver. The functional unit of the liver is the liver

lobule. Lobules are defined by final branches of the central vein surrounded by final branches of the portal triad with a distance of about 10 hepatocytes from central vein to portal triad in a mouse liver. The hepatocytes are arranged in cell plates which are interfused by sinusoids and biliary ducts. Sinusoids are tiny, fenestrated blood vessels connecting the central veins and the portal triads. The lobules are arranged as repeated units throughout the liver. Blood flows along the porto-central axis from the portal triad to the central vein while bile, which is secreted from the liver into the biliary ducts, flows into the opposing direction and leaves the liver through the bile duct. The oxygen rich blood supplied by the hepatic artery leads to an oxygen gradient with a higher oxygen pressure close to the portal triad. Within each lobule the hepatocytes are equipped with different enzymes depending on their position along the porto-central axis. Therefore, three functional or metabolic zones can be defined which provide different metabolic competences. The periportal zone contains the hepatocytes surrounding the portal triad, the pericentral zone the ones surrounding the central vein whereas the midlobular zone is located in between (Arias, 2009; S. P. S. Monga & Cagle, 2010; Ruijter, Gieling, Markman, Hagoort, & Lamers, 2004).

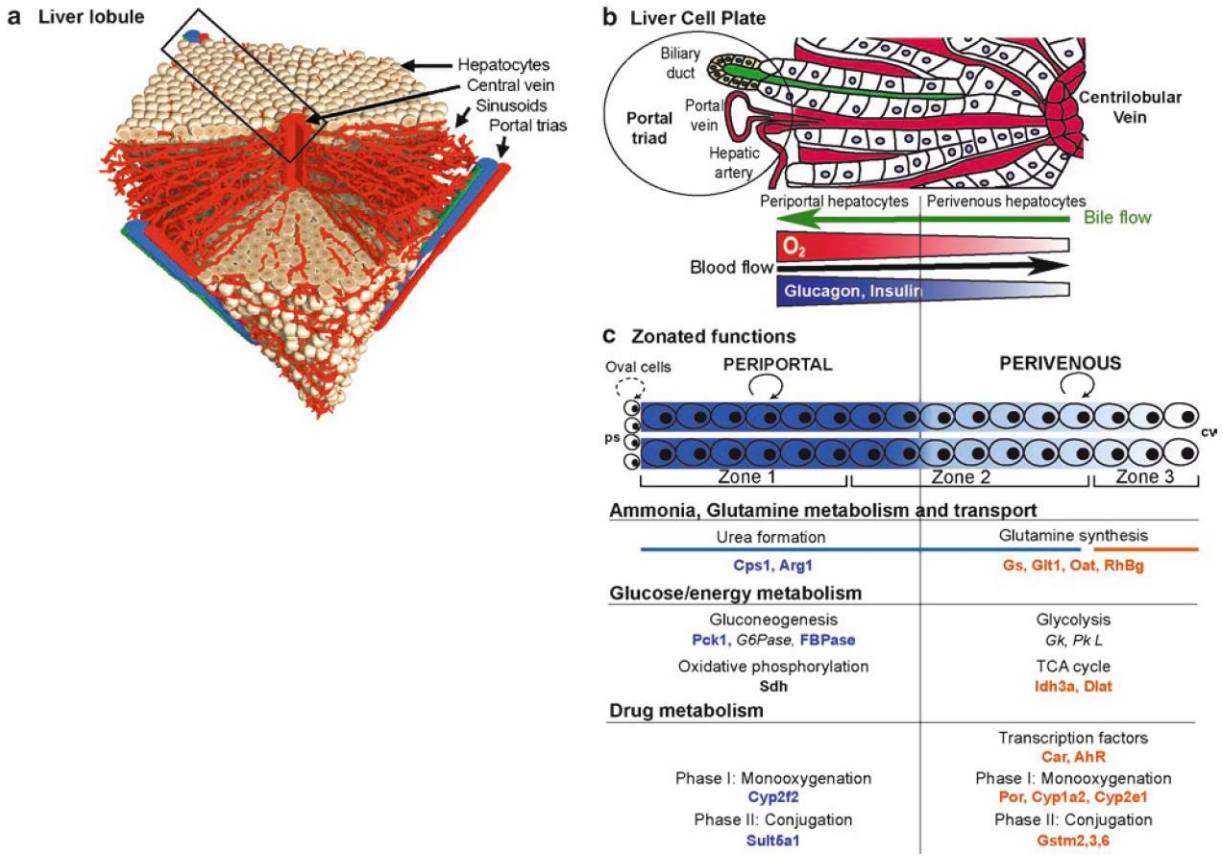

FIGURE 1 STRUCTURE AND FUNCTIONS OF THE ZONATED LIVER LOBULE.

a) *Overview of a liver lobule as three-dimensional draft. Lobules are defined by a branch of the central vein in the middle and branches of the portal triad at the edges connected by liver plates.* ***b)*** *Detail of a liver cell plate: A branch of the portal triad on the periportal side and a branch of the central vein on the pericentral side connected by sinusoidal blood vessels and biliary ducts interfusing the hepatocytes. Blood flow and bile flow are indicated, blood flows from the portal triad through the lobule to the central vein.* ***c)*** *Zonal functions: Hepatocytes provide different metabolic competences depending on their position along the porto-central axis. Three zones can be defined, the periportal zone (zone 1), the midlobular zone (zone 2) and the pericentral zone (zone 3). Zonation of some metabolic competences is indicated. Besides several zonated enzymes for energy and ammonia metabolism there are also several drug metabolizing enzymes underlying zonation. Taken from Sabine Colnot and Christine Perret,* (S. P. S. Monga & Cagle, 2010).

Removal of xenobiotics is one of the important functions of the liver and is performed by hepatocytes expressing drug metabolizing enzymes. There is a repertoire of nuclear receptors like CAR (constitutive androstane receptor) which serve as xenobiotic sensors and are activated by presence of certain xenobiotic substances. They induce transcription of defined sets of drug metabolizing enzymes. These enzymes are functionally grouped in phase I, II and III drug metabolizing enzymes. Phase I enzymes perform modifications by introducing reactive or polar groups into their substrates, many phase I enzymes are oxygenases including the prominent cytochrome P450 family of monooxygenases. Phase II enzymes perform conjugations. Thereby they increase the molecular weight of their substrates leading to decreased activity and increased solubility and they support transport and excretion of the xenobiotics. Phase III enzymes are transporters which excrete the conjugated xenobiotics (Arias, 2009; Dufour & Clavien, 2009; R Gebhardt, 1992; Malarkey et al., 2005; S. P. S. Monga & Cagle, 2010; Ruijter et al., 2004).

2.3 Antibody based protein detection

Cellular signaling is a complex spatiotemporal process influenced by many factors. This complexity demands for analysis of many proteins and protein modifications to uncover their interplay.

Cells or tissues commonly analyzed in life science research contain a complex mixture of biomolecules including a large number of different proteins. Some proteins are highly abundant others are rare and concentration differences are ranging over several orders of magnitude. Most proteins contain post-translational modifications which can be indicative of cellular signaling events. Antibodies proved to be versatile tools for detection of proteins in complex mixtures (N. L. Anderson, 2002; Hagen, 2011; Wild, 2013).

Utilizing the capabilities of the immune system provides life science research with the possibility to generate antibodies against a broad range of molecular structures. The highly specific binding of antibodies to their antigen makes them invaluable tools for research and diagnostics. Selective antibodies able to recognize protein variants that carry defined posttranslational modifications are available and are used for analyzing cellular signaling processes. A large number of companies have commercialized antibody production and today there are thousands of antibodies available (Baker, 2015; Taussig et al., 2007). An ambitious project is the human protein atlas aiming to generate antibodies against all human proteins – the human proteome (M. Uhlen et al., 2015; Mathias Uhlen et al., 2010). Versatile methods and technologies have been developed for life science research and diagnostics which use antibodies as detection reagents.

The Western-Blot is a protein detection method developed by Towbin et al. and was first published in 1979 (Towbin, Staehelin, & Gordon, 1979). Proteins are separated by gel electrophoresis and blotted onto a membrane. Specific antibodies are employed to detect proteins which are visualized by a labelled secondary antibody that specifically binds to the first one. In the resulting images, the specific signal shows a band at the molecular weight of the protein the antibody detected. Due to its simplicity and to the highly informative results this approach is still a gold standard and routinely used in most laboratories working on protein based life science research. In the last 35 years, Western-Blot readout has evolved resulting in highly sensitive readout platforms based on chemiluminescence or fluorescence. As the Western-Blot became a standard method, the majority of commercially available antibodies are suitable for Western-Blot.

Disadvantages of the Western-Blot are the fact that it is designed for detection of one protein and that there are limitations in the number of samples that can be analyzed. Different strategies have been developed to overcome these limitations. Some readout platforms allow analysis of two or three prote-

ins on the same blot, for analysis of more proteins it is necessary to process several blots which is time consuming and also multiplies the amount of sample needed.

Antibodies are often not completely selective for one protein but also bind other proteins containing similar epitopes (Baker, 2015; Michaud et al., 2003) or show background signal. The information of the molecular weight provided by the Western-Blot proved to be especially valuable as it allows discrimination of specific and unspecific signals.

The evolution of life science research demands methods that are capable of handling more samples and that provide the possibility to detect more analytes to cope with the complexity of cellular signaling. Therefore, protein microarray platforms have been developed which employ the principles of miniaturization and parallelization of the analysis. Miniaturization results in lower consumption of samples and detection reagents which is especially important for limiting amounts of samples and parallelization results in higher throughput for samples and analytes (Korf, 2011; Templin et al., 2002).

Directly addressing the limitations of the Western-Blot, reverse phase protein microarrays (RPPMs) were developed which are based on a dot blot. In this approach the proteins are not separated by gel electrophoresis but the samples are directly immobilized on a membrane or another hydrophobic carrier resulting in so called planar arrays. The molecular weight resolution is sacrificed for higher throughput. Employment of spotting robots allows highly reproducible immobilization of very small sample amounts. This gives the opportunity to print many samples, up to several hundred, onto an area of a few square centimeters. The sample spots are arranged in an array and it is possible to print hundreds of these arrays (Kambhampati, 2006). For example the contactless printers used for the ZeptoSens platform use only 0.5 nl sample per spot and the resulting spots have a diameter of about 100 µm allowing to print hundreds of arrays from microliters of samples (Voshol, Ehrat, Traenkle, Bertrand, & van Oostrum, 2009).

This approach substantially increases sample and analyte throughput compared to a Western-Blot. Yet it demands advanced and expensive equipment and requires a complex workflow which is a general disadvantage of microarray platforms that employ planar arrays. RPPMs mainly use Western-Blot antibodies and a disadvantage of RPPM data is that the signal obtained on a sample is represented by a spot without molecular weight resolution which does not allow discrimination of specific and unspecific signal.

Other protein microarray variants are based on binding molecules, usually antibodies, immobilized on a surface. These binders can capture proteins from a complex sample followed by washing and removal of the remainder of the sample. For detection, the proteins in the samples can be labelled in a direct labelling approach or a detection antibody targeting another epitope on the same protein than the

binder can be employed. This sandwich assembly employing two antibodies improves specificity for the target protein but for analysis of several proteins there is a limitation in the number of detection antibodies which can be employed per array. Therefore, these microarrays allow high throughput in respect to the number of samples but are limited in the number of analytes. This qualifies them for diagnostic approaches but often makes their use in research applications difficult (Kambhampati, 2006).

For microarrays, the binders can be immobilized on planar carriers as used for RPPM. Another possibility is to use microspheres, often called beads, for immobilization. There are several bead-based microarray platforms available. Luminex as a commercially important technology employs beads in micrometer scale which provide carboxyl groups for covalent immobilization. The microspheres contain up to three internal fluorescent dyes in different concentrations which are used as a color code for bead identification and classification. Thereby the instrument can distinguish up to 500 different bead sets. This platform can be used for different kinds of bio-assays. The distinguishable bead sets can be loaded with different binders, mixed and used for measuring several parameters in multiplex. Readout employs the principle of flow cytometry. The beads are soaked through a needle and pass the laser based detection system which performs the classification of the bead sets by detecting the internal dyes and quantification of the assay signal which is based on a reporter fluorescent dye. The resulting data represent the median fluorescence intensities (MFIs) for the reporter dye on each bead sets in each well (Korf, 2011; Wild, 2013).

2.4 Aim of this work

The complexity of cellular signaling demands for comprehensive analyses. Western-Blot has proved to be a valuable tool for detection of proteins and protein modifications involved in cellular signaling and is probably the most wide spread method for semi-quantitative protein detection. The vast number of commercially available antibodies for Western-Blot analysis underlines the importance of this method.

The major limitation of the Western-Blot is the fact that only one or very few proteins can be analyzed by this approach. Methods like reverse phase protein microarrays address this limitation and allow analysis of more samples and more analytes but they do sacrifice data quality. It is the separation of proteins by gel electrophoresis and the resulting molecular weight information that proved to be an important advantage of Western-Blot. Discrimination of specific and unspecific signal results in more reliable data.

Aim of this work was development of a method that bridges the gap between Western-Blot and reverse phase protein microarrays. The method should be based on a Western-Blot and allow generation of many copies or replicas of the blot. This would give the possibility to analyze many more proteins than from a single Western-Blot without losing the molecular weight separation.

For analysis of cellular signaling it is helpful to examine tissue samples as the complex signaling and communication between cells depends on their environment and the natural environment of a cell is the associated tissue. But tissues usually contain different types of cells and the behavior of a cell also depends on its position and environment within the tissue. For example hepatocytes in the liver express different enzymes and fulfill different metabolic functions depending on their position within a liver lobule. Laser capture microdissection is a method which allows isolation of small areas or even single cells from tissue sections but results in very limited amounts of samples. With an approach that allows analysis of proteins and posttranslational modifications in these cells, novel information on cellular signaling within the different functional zones of liver lobules might be obtained. Isolation of hepatocytes from different functional zones within liver lobules is elaborate but possible. It is worth the effort when a comprehensive analysis can be performed on the limited number of cells. These samples would hardly be sufficient for a single Western-Blot but having a method that creates many replicas from a Western-Blot could allow a comprehensive analysis.

Therefore, a method which creates many replicas of a Western-Blot might be a valuable tool for protein detection and bring the Western-Blot towards a proteomic tool allowing systems biology approaches.

3 Results

3.1 The DigiWest project

Is it possible to generate copies of Western-Blots? It started with an idea. Markus came up with the idea of transferring a Western-Blot onto the Luminex platform. That meant generating molecular weight size-fractions by cutting a Western-Blot membrane into defined pieces and coupling of the proteins contained in the resulting membrane-snippets onto Luminex beads. As the Luminex platform uses color-coded beads, the molecular weight information could be retained in the up to 500 distinct bead sets which could then be pooled into a bead-mix containing the whole Western-Blot.

The beads generated from one Western-Blot lane should be sufficient for dozens or even several hundred antibody incubations. The signal obtained from each antibody on the different molecular-weight fractions could be used to digitally reconstruct the initial Western-Blot lanes. Good antibodies should show stable and low background signal for most fractions and a peak composed of few fractions representing the Western-Blot band at the corresponding molecular weight. The digital nature of Luminex data could be used to easily quantify these peaks. We named this method 'DigiWest' because it represents digital reconstructions of Western-Blots.

Approaching this idea, the workflow should be composed of the following steps:

- **a)** Separation of proteins by molecular weight, that means a classical SDS-PAGE.
- **b)** Blotting the proteins onto a Western-Blot membrane.
- **c)** Cutting the membrane into defined pieces, each containing the separated proteins of a certain molecular weight range followed by elution of the proteins from the generated molecular weight fractions.
- **d)** Coupling of the proteins from each molecular weight fraction onto distinct, color coded Luminex bead sets.
- **e)** Pooling of the Luminex bead sets into a bead-mix retaining the size fraction information in the color code.
- **f)** Incubation of aliquots of the pooled bead-mixes using standard Western-Blot antibodies followed by fluorescent secondary antibodies for Luminex readout.
- **g)** Analysis of the Luminex signals obtained from the different bead sets representing the molecular weight fractions and graphical representation of the generated data.

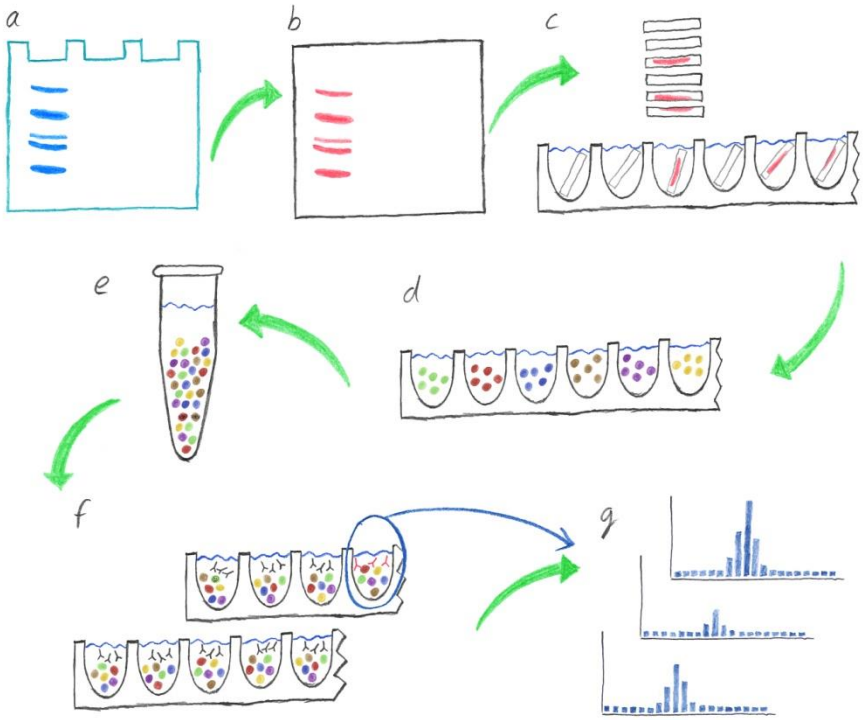

FIGURE 2 WORKFLOW OF THE DIGIWEST METHOD

*Proposed workflow of the DigiWest method, steps **a)** to **g)** as described on the previous page.*

Transfer of the Western-Blot to a Luminex bead-mix would allow easy handling as it could be handled like a liquid or in case of magnetic Luminex beads appropriate equipment could be employed. Antibody incubations could be performed in microtiter plates with quick and automatable washing steps followed by fast and automated readout on a Luminex machine.

3.2 Technical considerations

3.2.1 Sensitivity and comparison with existing Western-Blot readout platforms

Readout of a Western-Blot is usually based on chemiluminescence or fluorescence. For chemiluminescence as readout, horseradish peroxidase-labelled (HRP) secondary antibodies are commonly used. HRP catalyzes the oxidation of luminol to 3-aminophtalate using hydrogen peroxide as oxidizing reagent. This reaction causes emission of photons. The photons can be detected by high-end CCD cameras over long periods of time (up to several hours) as long as no substrate depletion occurs and unspecific background signal does not emerge. This makes chemiluminescent readout a very sensitive technology. Alternatively, fluorescence based labels are used which provide a wider linear range of the obtained signals. Sensitive confocal laser scanners are available for readout. The infrared fluorescence based Licor

Odyssey platform has a similar sensitivity than chemiluminescent readout. (Durrant, 1994; Mathews, Plaisance, & Kim, 2009; Thorpe, Kricka, Moseley, & Whitehead, 1985)

One big concern at the beginning of the project was whether Luminex readout is capable of competing with these highly sensitive readout systems. Chemiluminescence based readout can be exposed for prolonged times to increase signal and fluorescence based systems can use increased laser power to gain the same effect. As Luminex is a flow based readout system there is no comparable possibility to further increase the signals.

3.2.2 Protein transfer from membrane to beads

The use of the standard protein coupling method for Luminex-beads – activation of the carboxyl-groups on the surface of the beads to NHS-esters followed by reaction of these NHS-esters with primary amine-groups to form covalent amide-bonds – leads to a loading density that is directly dependent on protein concentration. Since a large number of fractions are generated, protein concentration was expected to be low and varying between the fractions, therefore this was seen as a principle problem. In addition, the quick hydrolysis of the activated ester was seen to be critical. This hydrolysis prevents the quantitative coupling of all protein-molecules contained in the solution onto the NHS-activated beads using prolonged reaction times. The half-life of NHS-esters in aqueous solutions is in a range from 10 minutes to 5 hours dependent on pH and temperature (Hermanson, 2008). Therefore another coupling strategy was chosen.

Streptavidin is a protein originally purified from the bacterium Streptomyces avidinii. It is a homo-tetramer containing a biotin binding site in each subunit. The interaction of biotin and streptavidin is one of the strongest non-covalent interactions known. It has a K_d of about 10^{-15} mol/L. The valeric acid substituent of biotin makes it ideal for attaching it covalently to e.g. proteins, a process called biotinylation. Due to these advantages the streptavidin biotin interaction is routinely used in molecular biology approaches (Hermanson, 2008).

There is a huge variety of commercially available biotinylation reagents. Due to the availability and good accessibility in proteins, amino-reactive biotinylation reagents were chosen. These kinds of reagents are usually composed of biotin followed by a spacer, which defines the distance of the biotin from the biotinylated protein, the solubility of the reagent and the flexibility, followed by an amine-reactive NHS-ester (Dundas, Demonte, & Park, 2013; Häfeli, Schütt, Teller, & Zborowski, 1997; Hermanson, 2008).

The coupling strategy chosen for method development was biotinylation of the proteins and loading onto streptavidin coated beads.

3.3 Method development

The proposed workflow of the method is suggested in section 3.1. All steps of the workflow contribute to the final results and none of them could be neglected. Method development started with best-guess conditions followed by optimization of each part of the workflow. Several rounds of re-optimization were necessary for each step till the finally optimized conditions were defined. An important aspect for decisions throughout the method development process was applicability in a routine workflow as the final workflow needed to be robust and reproducible.

The following section does not represent the whole method development which included more than hundred experiments but an overview containing some crucial examples of experiments for each step.

3.3.1 Western-Blotting

Western-Blotting is a standard method and each laboratory has its established procedure. In our group, the commercial NuPAGE system (Life Technologies) is used. Optimized conditions for gel electrophoresis and blotting onto membranes were already established. These conditions were used as basis for method development.

3.3.2 Protein biotinylation

The idea of the DigiWest method is to transfer proteins from a Western-Blot onto Luminex beads. The strategy chosen to achieve efficient loading of the proteins onto the beads was biotinylation of the proteins and loading onto streptavidin coated beads. Therefore, protein biotinylation was the first step of the workflow that had to be optimized. Typical samples used for Western-Blotting are cell or tissue lysates. Besides proteins they contain many ‘contaminants’ which might interfere with the biotinylation reaction including the routinely used Tris-based lysis buffers. Excess biotinylation reagent needs to be removed after biotinylation as it competes with the biotinylated proteins for binding sites on the strept-avidin coated beads.

Biotinylation of proteins immobilized on the membrane after blotting seemed to be straight forward as membranes can easily be handled and excess biotinylation reagent can be washed off. It also allows removal of all the buffer substances and other interfering substances from the sample preparations which could disturb the biotinylation reaction. This allows flexibility in respect to selection of samples and lysis buffers and also in respect to running and blotting buffers and prevents loss of proteins during the washing steps.

After blotting, membranes were washed excessively in PBST to remove the Tris-based transfer buffer and other molecules which could interfere with the biotinylation reaction. PVDF and nitrocellulose membranes bind proteins and other molecules mainly through hydrophobic interactions. When performing classical Western-Blots, membranes are blocked using an excess amount of protein, usually BSA or milk powder, to saturate membranes with protein after blotting. For biotinylation, this blocking step had to be omitted. Only the detergent Tween-20 present in PBST is used for partial blocking of the membranes. This blocking effect proved to be sufficient to prevent biotinylation reagent from binding to the membranes.

In the initial experiments NHS-LC-LC-Biotin was used as biotinylation reagent which provides an effective spacer length of 30.5 Å. Later and in the final workflow, NHS-PEG12-Biotin is used which provides a spacer length of 56 Å. The PEG-structure of the spacer is also contained in Tween-20 which might contribute to the observation that no excess biotinylation reagent was bound to the membrane after washing.

Different biotinylation conditions and concentrations were evaluated. The following experiment is taken from investigation of the effect of different concentrations of biotinylation reagent. A lysate of the mouse hepatoma cell line 55.1c was used as sample. 4 Lanes of a gel were loaded, each with 40 µg protein. After electrophoresis and blotting, a 12 mm high and 2 mm wide piece was cut from each lane covering the molecular weight range from about 48 kDa to 28 kDa. These pieces were biotinylated using NHS-LC-LC-Biotin. The excess of biotinylation reagent relative to the amount of protein was based on an estimation of the number of proteins bound on the membrane pieces which was assumed to be about 0.2 nmol. An excess of biotinylation reagent of factor 5, 50, 200 and 500 was used for biotinylation in a constant volume of 350 µl PBST. After biotinylation and washing, the membrane pieces were each cut into 24 molecular weight fractions with a height of 0.5 mm each. Proteins were eluted and loaded onto streptavidin coated Luminex bead-sets. After loading, the beads were pooled into bead-mixes and used for a Luminex assay applying a selection of Western-Blot antibodies. Primary antibodies were incubated overnight followed by PE-labelled secondary antibody incubation for 1 hour and read-out on a Luminex 100. The data are represented as diagrams (Fig. 3) showing the signal obtained on the 24 molecular weight size fractions.

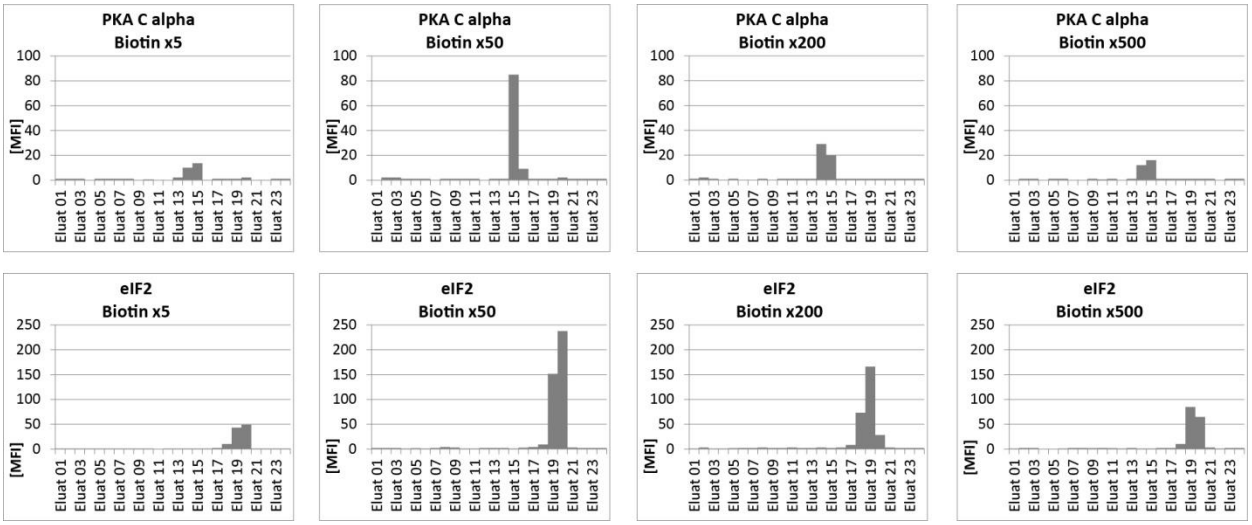

FIGURE 3 EFFECT OF THE EXCESS OF BIOTINYLATION REAGENT ON ASSAY SIGNAL

55.1c cell lysate was subjected to SDS-PAGE and protein fractions were generated. The eluates 01 to 24 represent 24 molecular weight fractions covering the range from about 48 to 28 kDa. Biotinylation reagent was used in a 5-, 50-, 200- and 500-fold excess relative to the estimated number of proteins. Shown are the results from PKA C alpha (42 kDa) and eIF2 (38 kDa) specific antibodies. Data are shown as diagrams representing the MFI values obtained on each of the 24 molecular weight size fractions for each concentration of biotinylation reagent. The 50-fold excess of biotinylation reagent resulted in the highest signals for the two antibodies shown here. The same effect was observed for the other antibodies used in this assay.

The results of this experiment show that there is an optimum in the amount of used biotinylation reagent. The signals obtained in the Luminex assay were the highest using a 50-fold excess of biotinylation reagent.

As mentioned before, there are different biotinylation reagents available. The NHS-PEG12-Biotin has an increased spacer length when compared to the NHS-LC-LC-Biotin or the even shorter NHS-LC-Biotin. The following experiment compares the long PEG12- to the short LC-spacer containing biotinylation reagent. A 55.1c cell lysate was used as sample and, after electrophoresis and blotting, 12 mm high membrane pieces were cut covering the molecular weight range from about 48 to 28 kDa. Both biotinylation reagents were used in a 50-fold excess relative to the estimated number of proteins. The membrane pieces were cut into 24 molecular weight fractions, eluted and loaded onto streptavidin coated Luminex beads. The resulting bead-mixes were used to perform an assay employing a selection of Western-Blot antibodies.

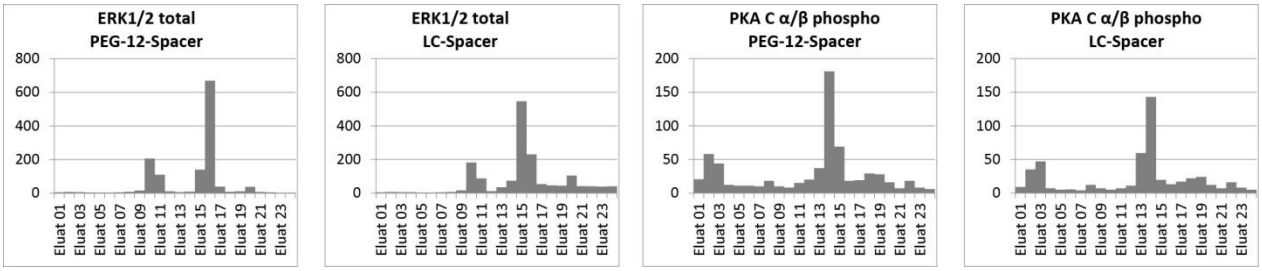

FIGURE 4 COMPARISON OF TWO BIOTINYLATION REAGENTS

55.1c cell lysate was subjected to SDS-PAGE and protein fractions were generated. The eluates 01 to 24 represent 24 molecular weight fractions covering the range from about 48 to 28 kDa. Biotinylation reagents were used in a 50-fold excess relative to the estimated number of proteins. Shown are the data obtained from ERK1/2 (42/44 kDa) and PKA C α/β phospho (42 kDa) specific antibodies. Data are represented as diagrams with the MFI values obtained on the 24 molecular weight fractions for each biotinylation reagent. The longer PEG-12 spacer results in slightly better signals compared to the shorter LC-spacer. The same effect was observed for the other antibodies used in this assay.

The NHS-PEG12-Biotin with the longer spacer results in slightly better signals compared to the biotinylation reagent with the shorter spacer. Although the spacer length seems to have only minor effects in the experiment shown here the NHS-PEG12-Biotin was chosen for the final workflow conditions. The NHS-PEG12-Biotin has an additional property which is often seen as disadvantage but for workflow optimization it was seen as advantage. This biotinylation reagent comes as a wax-like substance which needs to be dissolved in an organic solvent while the LC-spacer based reagents come as powders which are completely water soluble. As NHS-esters hydrolyze in aqueous solutions the reagents cannot be stored in a dissolved state. The PEG12-spacer based reagent was dissolved in DMSO and stored at -20°C in aliquots. Using these aliquots helped achieving reproducible biotinylation.

For the final workflow, the excess of biotinylation reagent was translated into a defined concentration and the blots are biotinylated as a whole.

3.3.3 Cutting membranes

During most time of method development, membranes were cut using ruler and scalpel. Single lanes were processed and cut into a smaller number of molecular weight fractions representing a selection of the Western-Blot lane. An important milestone during method development was size reduction of the molecular weight fractions. Smaller fractions not only improved the resolution of the data but also lead to an increase in sensitivity and to a reduced background. This observation might be due to the fact that

an increase in fraction numbers and the corresponding reduction of the fraction size result in relative enrichment for a given protein within a size fraction and also the unspecific background signal is lowered by distribution over several fractions. The binding surface of the Luminex beads is limited. An increased number of fractions might also contribute to more robust results by increase of the overall binding capacity.

The following experiment directly compares a resolution of 1 mm per molecular weight fraction to a resolution of 0.5 mm. The sample used for this experiment was the mouse hepatoma cell line 55.1c. The molecular weight range used was about 48 to 28 kDa. The membrane pieces were either cut into 12 molecular weight fractions with a height of 1 mm or 24 fractions with a height of 0.5 mm. In this experiment NeutrAvidin coated Luminex beads were used.

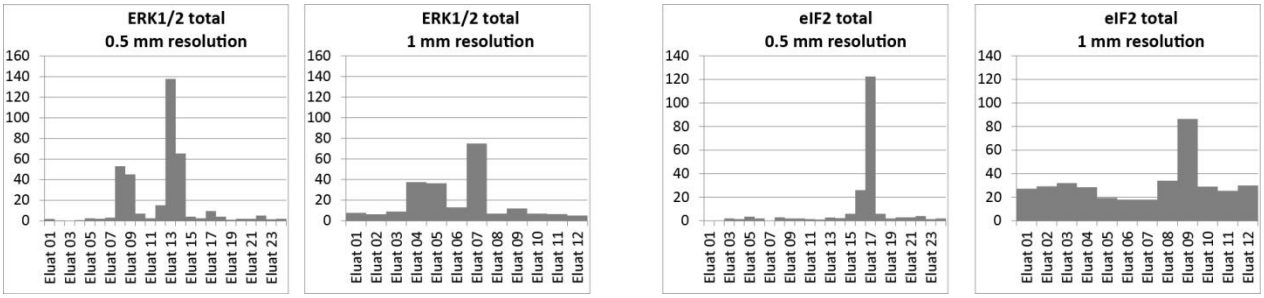

FIGURE 5 EFFECT OF RESOLUTION

55.1c cell lysate was subjected to SDS-PAGE and protein fractions were generated. The eluates 01 to 24 represent 24 molecular weight fractions covering the range from about 48 to 28 kDa. This experiment shows a direct comparison of a resolution of 1 mm and 0.5 mm. Shown are two analytes from the Luminex assay. The higher resolution results in higher data quality and more peak-like structures. The decrease in background which can be seen here might be due to distribution of the unspecific signal over more fractions.

The resolution has an obvious effect on data quality. The resulting data show more peak-like structures and the background signal is reduced for the higher resolution.

A whole lane representing the molecular weight range from more than 400 kDa to about 10 kDa from a Western-Blot based on the mini gel format results in 96 molecular weight fractions when a resolution of 0.5 mm is used. As 96 well plates or 384 well plates are standard formats for laboratory equipment, this resolution was chosen. A higher resolution would demand for more bead sets while the Luminex platform is limited to 500 bead sets.

In the final workflow, 384 bead sets are used allowing 4 samples with 96 fractions each to be pooled into one DigiWest bead-mix. As cutting these fractions manually is time consuming and error prone, a cutting plotter was employed. The plotter cuts the lanes to a comb like structure and the 0.5 mm molecular weight fractions are sorted into 96 well plates using a forceps.

3.3.4 Protein elution from membranes

There are several published protocols for efficient protein elution from Western-Blot membranes. Most of them were developed for mass spectrometry applications and many of them claim to be able to elute the membrane bound proteins quantitatively applying very different approaches. Some methods employ organic solvents. One interesting approach tested is to use nitrocellulose membranes and dissolve the membrane snippets containing the molecular weight fractions in acetone (e.g. (P. J. Anderson, 1985)). The dissolved nitrocellulose can be precipitated by adding an aqueous buffer. When a buffer containing carrier protein, e.g. 10 mg/ml BSA, was added, this method worked nicely. But the acetone is not ideal for polystyrene-based Luminex beads and could therefore not be used for workflow development. Other methods described in literature use detergents, usually in alkaline buffers or even in a moderate sodium hydroxide solution (e.g. (Jørgensen et al., 2004)). Several of these recipes were tested using Triton X-100, Tween-20, SDS or mixtures of detergents.

An experiment comparing different elution buffers is shown in detail. As the protein elution efficacy from nitrocellulose and PVDF membranes might differ, both membranes were used. The sample was a mouse whole liver lysate. 2D well gels were used which provide one lane for a molecular weight marker and one 6 cm wide lane which was used to separate 400 µg of mouse liver lysate. One gel was blotted onto a PVDF membrane and one onto a nitrocellulose membrane. Areas surrounding the position of glutamine synthetase (42 kDa) were cut from each membrane, each 4.5 mm high and 10 mm wide. After biotinylation, these areas were cut into 3 molecular weight fractions each 1.5 mm high and 10 mm wide. These stripes were cut into 5 snippets each 2 mm wide for elution under 5 different conditions. The buffer used for preparation of the elution buffers was 100 mM Tris-HCl with a pH of 9.5. The composition of the elution buffers used in this experiment was as follows:

‘Detergent-Mix’	0.4% PVP 10000, 0.4% PVP 40000, 0.7% Triton X100 and 0.5% Tween-20
‘Detergent-Mix Urea’	same as ‘Detergent-Mix’ with additional 4 M Urea
‘1% Triton 8 M Urea’	1% Triton X100 and 8 M Urea
‘1% Triton 4 M Urea’	1% Triton X100 and 4 M Urea
‘1% Triton’	1% Triton

For each elution buffer there are 3 molecular weight fractions for each membrane type resulting in 30 eluates. Elution was performed in a volume of 50 µl for 2 hours at 70°C with heavy shaking (1200 rpm). Eluates were diluted 1:5 in PBS and used for loading onto streptavidin coated Luminex beads. An assay was performed applying a selection of antibodies.

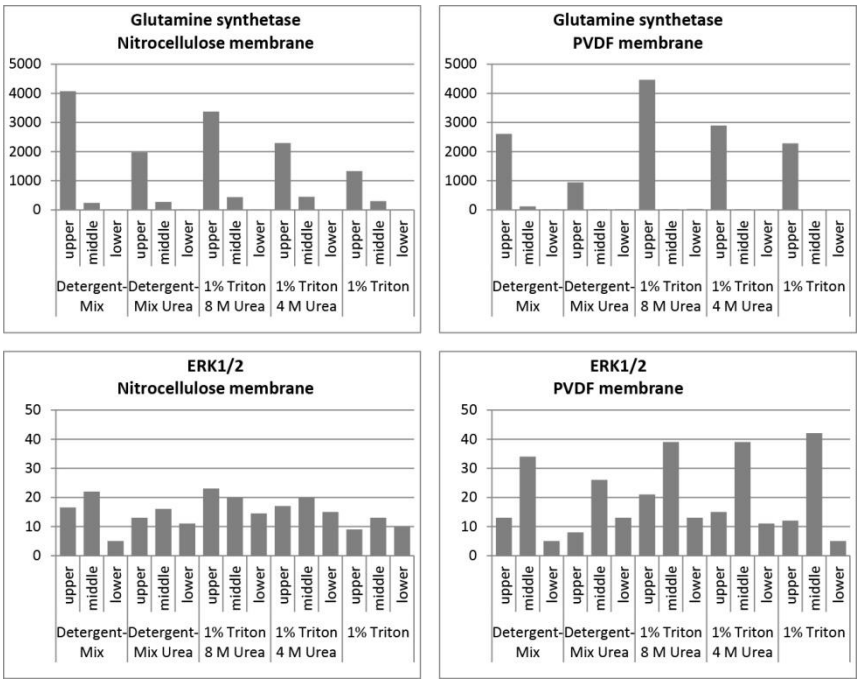

FIGURE 6 COMPARISON OF DIFFERENT ELUTION BUFFERS

Mouse liver proteins were separated by SDS-PAGE in 6 cm wide lanes. One gel was blotted onto a nitrocellulose membrane and one onto a PVDF membrane. Areas with a height of 4.5 mm and 10 mm wide were cut from the membranes at the molecular weight around 42 kDa. After biotinylation, the membrane pieces were cut into 1.5 mm high stripes (molecular weight fractions) and each stripe was cut into 5 pieces each 2 mm wide. The resulting 5 replicates of the 3 molecular weight fractions (upper, middle, lower fraction) for each membrane were used for elution with 5 different elution buffers.
The eluates were loaded onto streptavidin coated beads and used to perform an assay with a selection of antibodies.

The differences in the pattern seen for glutamine synthetase between the membranes might be based on slightly different cutting positions. From this selection of elution buffers in this experiment, the 'Detergent-Mix' seems to be the best buffer for elution from nitrocellulose membrane while for PVDF membrane the '1% Triton 8 M Urea' buffer performed best. For the ERK1/2 antibody the patterns on the 3 molecular weight fractions are more distinct on the PVDF membrane than on the nitrocellulose

membrane. This could also be based on the cutting positions of the fractions and the fact that 1.5 mm molecular weight fractions were used which do not provide a good resolution.

This is just one out of many experiments performed for optimization of protein elution conditions from membranes. As cutting of the membrane pieces into 1.5x2 mm snippets by hand is not so precise there might also be a bias from the cutting procedure in this experiment.

The best working method which made it into the final workflow is 1% Triton X-100 and 8 M urea in an alkaline buffer, Tris-HCl at pH 9.5 as also described by (Jørgensen et al., 2004). The combination of urea and Triton changes their behavior. Urea or Triton alone is way less effective. This effect is also described (Jørgensen et al., 2004). Besides the better performance on PVDF membranes, this elution buffer is so harsh that it partially degrades nitrocellulose membranes. Therefore it was decided to use PVDF membranes in the final workflow which are chemically more stable.

Elution in the urea-Triton based elution buffer and most of the other methods were tested under different conditions. Elution for 90 minutes with heavy shaking at room temperature resulted in reproducible protein recovery. A helpful property of the elution buffer is that the PVDF membrane snippets turn transparent and thereby almost invisible in this buffer. After dilution of the elution buffer, they turn white again.

3.3.5 Loading proteins onto Luminex beads

For immobilization of the biotinylated proteins, beads were coated with either streptavidin or NeutrAvidin. NeutrAvidin (pI 6.3) has a more neutral isoelectric point than streptavidin (pI 4.6). It is a deglycosylated avidin which has a similar affinity for biotin (K_d 10^{-15} M) compared to streptavidin and can be used interchangeably. In one phase of method development, NeutrAvidin and streptavidin coated beads were used in parallel and loaded with biotinylated proteins in multiplex. NeutrAvidin showed a better overall performance for this application which might be due to the more neutral isoelectric point. The difference between the two biotin binding proteins varied for different analytes. The isoelectric point of NeutrAvidin rendered it more universal and therefore NeutrAvidin was chosen for the final workflow.

As urea is a strong denaturing reagent and even the very stable NeutrAvidin and streptavidin cannot tolerate 8 M urea, the elution buffer had to be diluted after elution of the proteins. During method development, eluted proteins were usually transferred to new vials and diluted in PBS. In the final workflow, where elution is performed in 96 well plates, the membrane snippets remain in the plate while the proteins are being loaded onto the Luminex beads. The dilution buffer in the final workflow is PBST containing BSA which meant to block the membrane snippets and prevent rebinding of the

biotinylated proteins. Loading of the eluted biotinylated proteins onto streptavidin or NeutrAvidin coated beads was usually performed overnight at 4°C or later at room temperature with gentile shaking.

To avoid aggregation of the beads, they were blocked with an excess of biotin after being loaded with biotinylated proteins. Deactivated biotinylation reagent in a Tris-buffer or a biotinylated peptide was used to occupy the remaining biotin binding sites on the Luminex beads. The peptide moiety was used to measure remaining free biotin binding sites on the beads after protein loading by incubation with a peptide specific antibody. All bead sets were able to bind peptide showing that the beads were not completely saturated with biotinylated protein. The blocking step might not be required as the beads did not tend to aggregate during the overnight loading procedure. On the other hand most proteins contain more than one biotin after biotinylation and there are free biotins detectable on the surface of the beads. This can be exploited to perform an on-bead protein loading control by simply incubating the beads with PE-labelled streptavidin which will be discussed in detail later.

The following experiment compares the performance of streptavidin and NeutrAvidin coated Luminex beads directly. In this experiment a lysate from the mouse hepatoma cell line 55.1c was used and 400 µg lysate were separated on a 2D well gel in a 6 cm wide lane. An area with a height of 12 mm and 4 mm wide was cut from the membrane covering the molecular weight range from about 48 to 28 kDa. After biotinylation, the stripe was cut into 24 molecular weight fractions with a height of 0.5 mm each. The resulting 24 protein eluates were used to simultaneously load streptavidin and NeutrAvidin coated Luminex beads in multiplex. An assay was performed with the resulting bead-mixes applying a selection of antibodies.

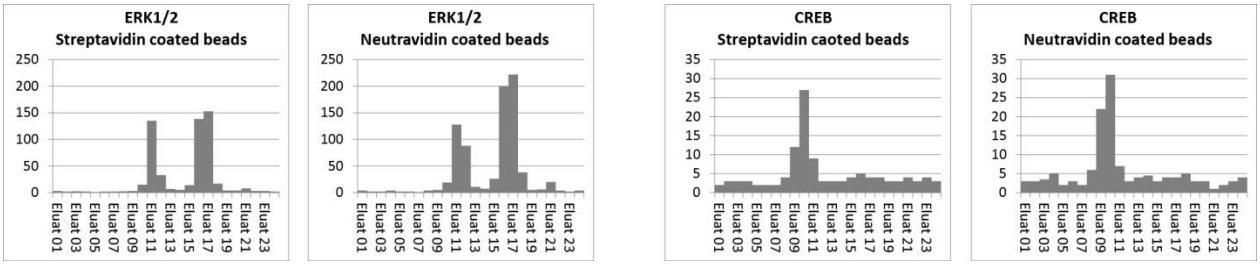

FIGURE 7 COMPARISON OF STREPTAVIDIN AND NEUTRAVIDIN COATED LUMINEX BEADS

Lysate from 55.1c cell line was separated by SDS-PAGE and blotted. An area covering the molecular weight from about 48 to 28 kDa was used for biotinylation and cut into 24 molecular weight fractions. Proteins were loaded onto streptavidin and NeutrAvidin coated Luminex beads in multiplex. The resulting bead-mixes were used to perform assays. The NeutrAvidin coated beads show a slightly better performance.

As NeutrAvidin coated Luminex beads showed a slightly better overall performance in all experiments where both kinds of beads were used, the NeutrAvidin coated beads were chosen for the final workflow.

3.3.6 Luminex bead preparation

In the experiments described so far, 12 bead-sets of MicroPlex Luminex beads were used and the 24 fractions shown in most experiments were distributed on 2 bead-mixes. The magnetic MagPlex Luminex beads provide additional options for bead handling. Therefore, it was decided to integrate these into the final workflow.

The Luminex beads for the final workflow were MagPlex beads coated with NeutrAvidin in a modified procedure employing a KingFisher magnetic particle processor which allows parallel coupling of 96 bead sets in 96 well plates. 400 bead sets were coated with NeutrAvidin and used to arrange 384 bead sets into 4 times 96 sets. The coupling procedure is the same than for manual bead coupling except for the fact that the beads are transferred sequentially to new plates containing the next reagent or washing buffer instead of removing the buffer or reagent from the vials. Due to the stickiness of the KingFisher consumables, all buffers were supplemented with Triton X-100. Beads were washed in activation buffer and the carboxyl groups were activated to sNHS-esters using EDC and sNHS. After washing in coupling buffer they were coated with NeutrAvidin in coupling buffer. Followed by blocking in a BSA containing buffer and washing they were transferred back to vials and adjusted to a defined volume of 1 ml. After bead count on a Luminex FlexMap 3D, they were adjusted to a defined concentration. The biotin binding capacity, as determined using a biotinylated peptide and an antibody directed against this peptide, showed a CV of less than 3% for the 384 bead sets used for the main experiments in this thesis. The same was true for repeated coupling rounds.

The Beads, for the final workflow 384 sets, were then arranged to 4 times 96 bead sets which were used to generate master plates and bead plates. The master plates contained a defined volume with a defined bead concentration. A pipetting robot equipped with a head for 96 pipetting tips was employed to generate bead plates containing a defined number of beads per well. These bead plates were vacuum sealed and stored at 4°C. For DigiWest experiments, the beads were transferred into the plates containing the biotinylated and eluted proteins using a 96-well magnet head from a KingFisher magnetic particle processor. The 4 different bead-plates were used to pool 4 samples, each represented by 96 molecular weight fractions, into one bead-mix.

3.3.7 DigiWest assays: merging two worlds

Although most immunoassays run on Luminex instruments employ ELISA-suitable antibodies and buffers based on ELISA buffers, DigiWest uses Western-Blot antibodies. As Western-Blot is a standard method in molecular biology, a vast number of Western-Blot qualified antibodies are available. Most of them are not suitable for ELISA. The DigiWest method successfully employs Western-Blot antibodies on the Luminex platform giving access to this huge repertoire. As we are also working with reverse-phase protein microarrays (RPPM) which do employ Western-Blot antibodies, a large repertoire of antibodies was available in the lab.

In case of DigiWest, the Luminex beads are NeutrAvidin coated and loaded with biotinylated proteins. Each bead set represents a molecular weight fraction from the initial Western-Blot. These beads are incubated with the primary antibodies followed by species specific, PE-labelled secondary antibodies.

Several buffers were tested during method development. The buffer with the best overall performance, in the following sections called 'assays buffer' is 'Blocking Reagent for ELISA' (Roche) supplemented with 0.2% milk powder, so a hybrid of an ELISA buffer and a Western-Blot buffer. This is not too surprising as the method is a hybrid of a Western-Blot and a bead-based Luminex assay.

The buffer has a major impact on the DigiWest results. As for every buffer used for immunoassays, it needs to stabilize the interaction of the antibody and the antigen but it also needs to prevent unspecific binding and reduce background. The following experiment compares a classical Western-Blot buffer – 1% BSA in TBST – with an ELISA buffer –Blocking Reagent for ELISA (Roche). A cell lysate of the human hepatocyte cell line HepG2 was used as sample. 24 molecular weight fractions were cut representing the molecular weight range from about 65 to 25 kDa. An assay was performed employing a selection of antibodies in each of the buffers.

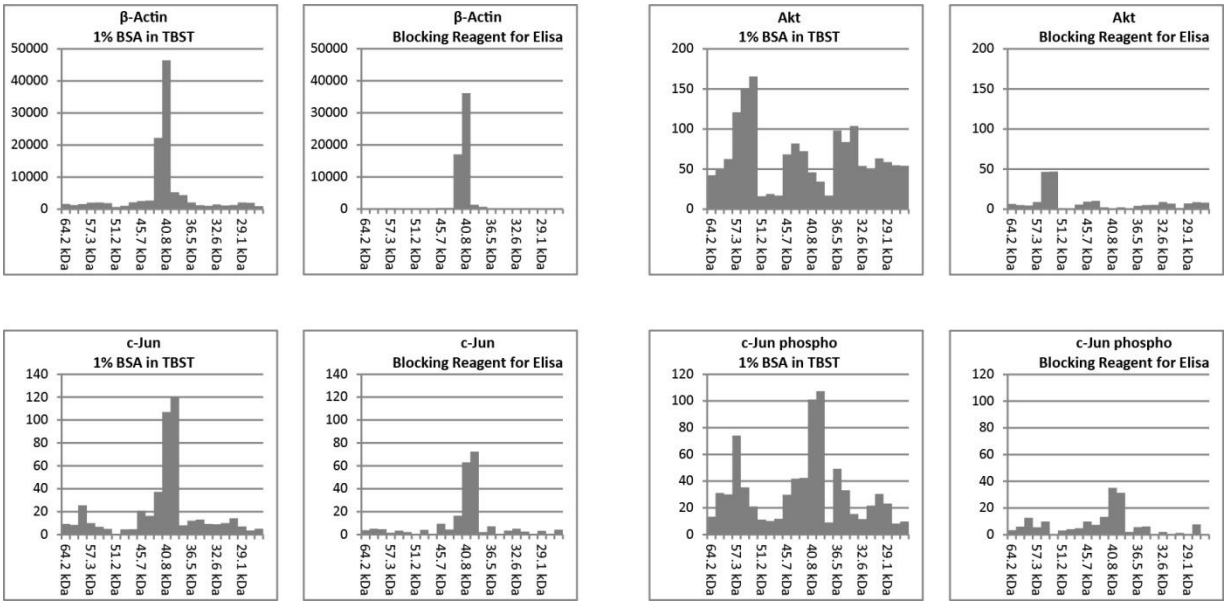

FIGURE 8 COMPARISON OF A WESTERN-BLOT AND AN ELISA BUFFER FOR DIGIWEST

In this assay the same bead-mixes loaded with proteins from a HepG2 cell lysate were incubated with antibodies either in 1% BSA in TBST or in Blocking Reagent for ELISA. Results from four antibodies are shown. In all four cases the ELISA buffer results in massively reduced background combined with reduced specific signal.

Although the ELISA buffer results in reduced signals compared to the Western-Blot buffer, the decreased background still results in a better signal-noise ratio for the ELISA buffer. The other classical Western-Blot buffer – 1% milk powder in TBST – resulted in almost complete loss of the background but also of the specific signal.

Both, the specific signal and unspecific signal depend on the antibody which is applied. Although the ELISA buffer performed well for many antibodies, there were still some antibodies which showed a high unspecific signal. As mentioned, the milk powder based Western-Blot buffer had a massive blocking effect. When the Blocking Reagent for ELISA was supplemented with 0.2% milk powder, the blocking effect of the milk powder still resulted in decreased specific signal but also in a decrease of the unspecific signal and therefore it resulted in a better signal-noise ratio for antibodies which tended to high unspecific signals.

The following experiment shows the effect of milk powder for an antibody which showed a massive background. In this experiment a lysate from a human cell line was used and the whole molecular weight range from about 420 to 14 kDa was used to generate a DigiWest bead-mix with 96 molecular weight

fractions. In this experiment the Blocking Reagent for ELISA was used with and without 0.25% milk powder supplemented.

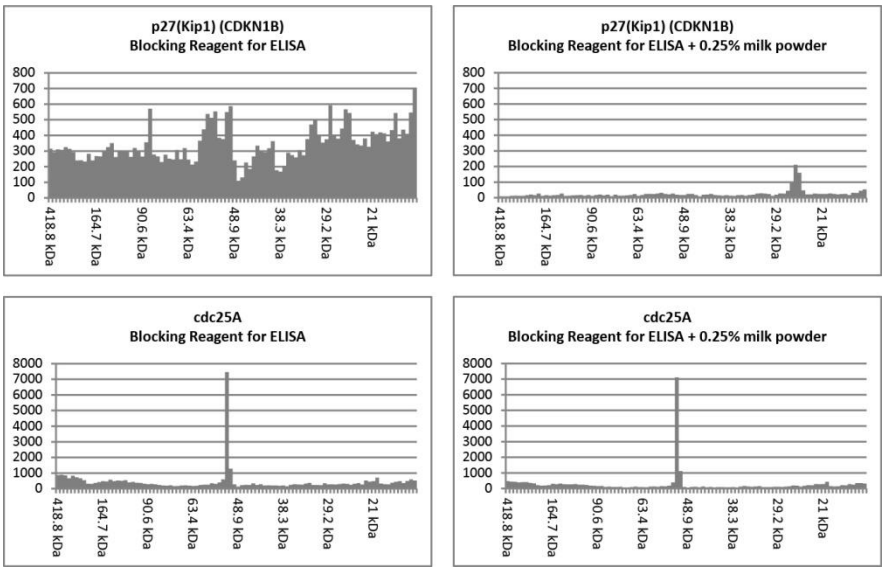

FIGURE 9 COMPARISON OF AN ELISA BUFFER WITH AND WITHOUT MILK POWDER

The two antibodies selected for this figure are not representative. Shown is an antibody detecting p27 which showed massive background in the DigiWest assay using the ELISA buffer. It is compared to incubation in the same ELISA buffer supplemented with 0.25% milk powder. Only few antibodies showed that strong effects when milk powder was supplemented. The second antibody shown is more representative. The milk powder results in a slightly reduced specific signal but also reduces the unspecific signal resulting in a better signal-noise ratio.

For the final workflow, the Blocking Reagent for ELISA supplemented with 0.2% milk powder is used referred to as 'assay buffer' in the following sections.

3.3.8 DigiWest assays in general

DigiWest assays contain the following steps: Dilution of the antibodies in assay buffer. Usually a dilution of factor 5 less than recommended for Western-Blots and not more than 1 µg/ml is used. For example an antibody which is recommended to be diluted 1:1000 for Western-Blots is diluted 1:200. One big advantage of the DigiWest method is that it requires only 30 µl antibody dilution per well.

An assay plate is filled with 50 µl per well assay buffer. An aliquot of the DigiWest bead-mix or if more than 4 samples are used the bead-mixes is added to the assay buffer. For readout on the Luminex

machine, 200 beads per set and well are sufficient for a good assay performance. So, if for example 40000 beads are loaded from each molecular weight fraction, the resulting DigiWest bead-mixes are sufficient for 200 antibody incubations. After pre-incubation of the bead-mixes in assay buffer, the assay plates are placed on a 96-well magnet plate, the buffer is discarded and 30 µl per well of the antibody-dilutions in assay buffer are added. They are incubated overnight on a cooled shaker.

The next day the beads are washed twice with PBST on a magnet plate and PE-labelled secondary antibodies are added. They are usually diluted 1:200 in assay buffer. 30 µl are added per well and incubated for 1 hour at room temperature. The beads are washed twice with PBST and PBST is added for readout. The 96-well plate format gives the opportunity to incubate up to 96 different antibodies and therefore test 96 different analytes in 1 plate. Readout takes about 45 minutes to one hour per plate and has to be performed on the Luminex FlexMAP 3D as this is the biggest Luminex instrument and capable of handling 384 or more different bead sets, the other instruments have limitations in multiplexing. The Luminex instrument provides relative fluorescence intensities for each bead set and each well of the assay plate. The fluorescence intensities represent the median intensities (MFI) of all measured beads for each bead set in each well.

3.3.9 Improvements during method development

The following figure shows a comparison of an experiment which was performed in the middle of the method development process and a comparable experiment performed under final workflow conditions. For both experiments a lysate of the mouse hepatoma cell line 55.1c was used as sample. For the final workflow condition 20 µg protein was used, the earlier experiment used approximately 27 µg protein. The early experiment was presented before (see Fig. 7) for comparison of streptavidin and NeutrAvidin coated Luminex beads. The data were taken from the NeutrAvidin coated beads. In this experiment 24 molecular weight fractions were used covering the molecular weight range from about 48 to 28 kDa with a fraction size of 0.5 mm. In the experiment performed under final workflow conditions, the whole molecular weight range was used covering the range from about 600 to 12 kDa represented by 96 molecular weight fractions with a resolution of also 0.5 mm.

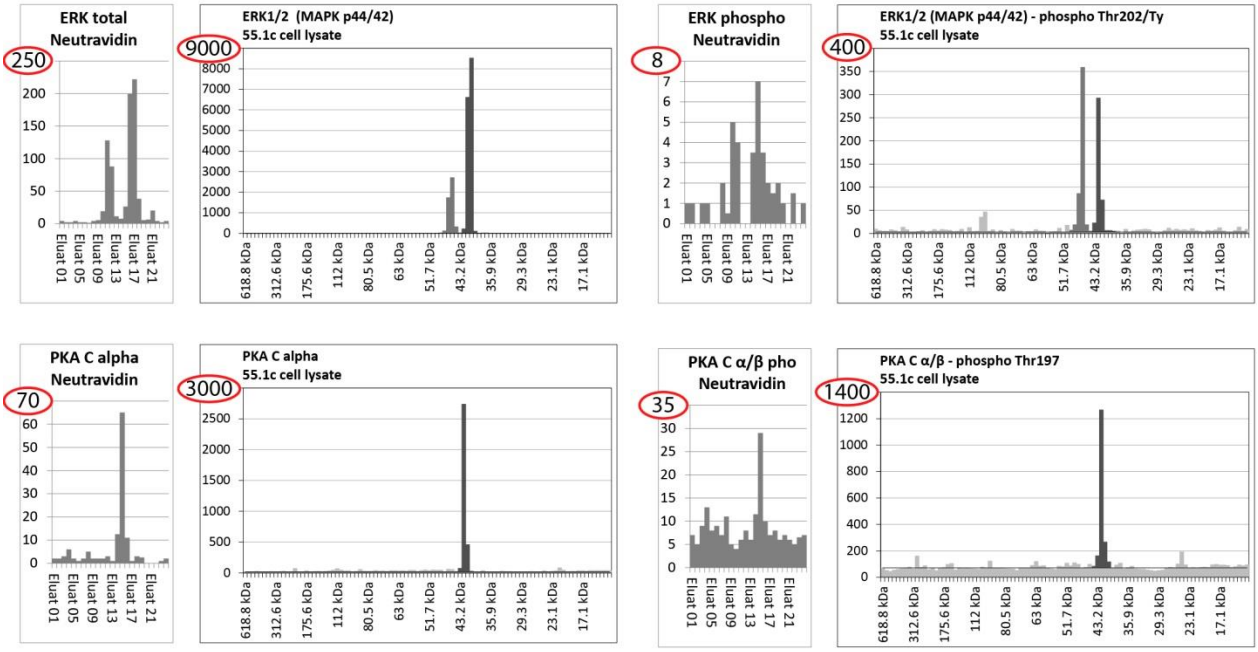

FIGURE 10 COMPARISON OF FINAL WORKFLOW CONDITIONS TO AN EARLIER EXPERIMENT

Direct comparison of four antibody incubations from an experiment performed in the middle of the method development process and an experiment performed under final workflow conditions. The same sample was used for both experiments and the same antibodies were used for the assays. The smaller diagrams show data from the earlier experiment, the bigger diagrams show data from the final workflow condition. Data quality and signal intensities are massively improved when the final conditions are used.

This figure demonstrates the improvements made during method development. The overall improvements are the payoff from all the optimization and re-optimization steps. As mentioned in the beginning, all steps of the workflow needed to be optimized as each step is essential for making the DigiWest method work. One technical difference between the final workflow conditions and earlier experiments is that the photo-multiplier of the Luminex instrument was set to the high PMT mode to increase signals. This increases all signals, specific and unspecific, by about 10-fold. The data obtained under final workflow conditions give analyzable signals for most antibodies.

3.3.10 Enhancing signal intensities

As readout platforms for Western-Blots have the possibility to increase signals by longer exposure times or higher laser intensities, one question was whether a similar effect can be applied to the DigiWest method besides the setting for the photo multiplier.

A possibility to increase signals in the DigiWest method is to use polymer-based buffers. The so called 'polymer effect' can be described as an increase in the local concentration of antibody and antigen as they are excluded from the volume of the solvated polymer which implies a dependency on the polymer concentration (Milone, 2012). Addition of high molecular weight polymers like PVA or PVP in concentrations of 2-4% to the assay buffer increases the signals in DigiWest assays by several folds. But this also demands addition of more blocking reagent like milk powder to restrain the background signal. As for increased exposure times or higher laser intensities, it does not improve the signal-noise ratio but increases all signal, specific and unspecific.

The following experiment shows the effect of a polymer based buffer. It is the same experiment as presented in the previous section under final workflow conditions with 55.1c cell lysate as sample. The same DigiWest bead-mix was used for an assay with different buffers. One buffer was the DigiWest assay buffer (Blocking Reagent for ELISA supplemented with 0.2% milk powder) the other buffer was a polymer buffer which was also based on the ELISA buffer supplemented with 4% PVP (average MW 360.000) and 1% milk powder.

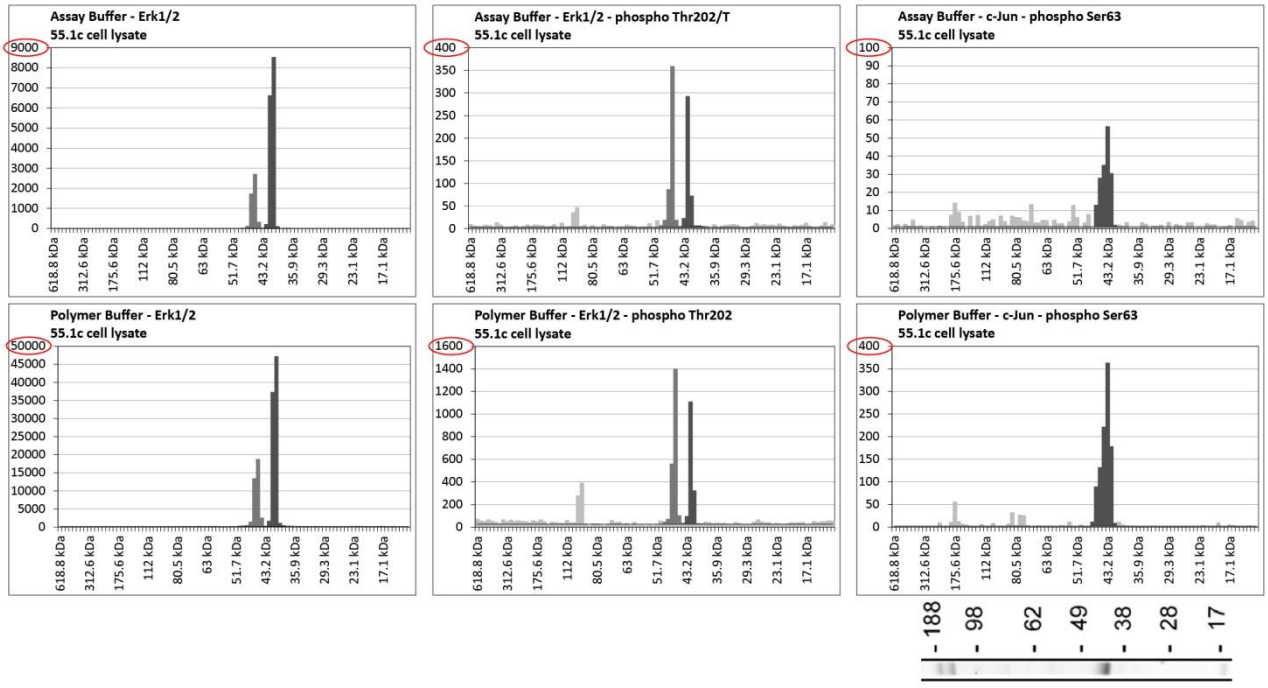

FIGURE 11 SIGNAL IMPROVEMENT USING POLYMER BUFFER

Comparison of two assays using the DigiWest assay buffer and a polymer based variation. The upper diagrams show the DigiWest data for a selection of antibodies using the DigiWest assay buffer, the lower diagrams show the same antibodies using a polymer based variation. Signals are improved by about 4-

fold in this experiment when the polymer buffer is used. The unspecific signals are also increased. The Western-Blot image at the bottom right (turned 90°) represents the same antibody on the same sample as the DigiWest data above (c-Jun pSer63). The image was taken using chemiluminescence readout on a Kodak imager with an exposure time of 30 minutes.

The c-Jun phospho antibody shown at the right in the previous figure showing weak signal in the assay buffer is giving a more stable signal in the polymer-based buffer. The Western-Blot image shown under these diagrams (turned 90° to the left) shows the same antibody on the same sample (55.1c lysate). The image was taken using chemiluminescence readout on a Kodak Image Station 440 CF with an exposure time of 30 minutes (1800 seconds).

All antibodies used in our group are routinely validated for application in RPPMs using Western-Blots. Therefore, a Western-Blot image collection for several hundred antibodies is available. The 30 minutes exposure time which was used for the c-Jun phospho antibody shown in the previous figure is the longest exposure time which can be found in this collection. This antibody still gives analyzable signals for DigiWest. So the DigiWest under final workflow conditions has a sensitivity which might be able to compete with Western-Blotting.

Polymers can increase the signals of DigiWest assays but the increased viscosity makes polymer based buffers difficult to handle. The effect of pushing the signals correlates with the concentration of polymer in the buffer but concentrations higher than 4% cannot be handled anymore. They cannot be pipetted properly due to high viscosity and the washing steps become difficult. Several experiments were performed testing different polymers and buffer compositions. The one shown here based on ELISA buffer and supplemented with PVP and milk powder proved to be one of the best combinations which were tested.

Nevertheless, this buffer is not routinely used for DigiWest assays due to the described handling issue. But it can be used if pushing signals seems to be necessary.

3.3.11 Summary of the final workflow conditions

This section represents a summary of the workflow. More details are described in the materials and methods section. The commercial NuPAGE system is used for protein separation and blotting. The gels are precast 4-12% BisTris gradient gels with a size of 8x8 cm. The MES buffer system as described in the manual is usually used as running buffer. The blotting modules are based on the wet blotting procedure and proteins are blotted onto PVDF membranes. The membranes are washed in PBST and a Ponceau S

stain is performed to visualize the transferred proteins. The positions of the lanes are labelled using a pencil before the blots are destained in PBST.

After washing in PBST, biotinylation of the whole membrane is performed in 20 ml PBST containing 50 µM NHS-PEG12-Biotin for one hour at room temperature. After washing, the membrane is dried. Membrane cutting is performed on a Silhouette SD cutting plotter. Each lane is cut into 96 molecular weight fractions with a resolution of 0.5 mm resulting in a comb-like structure. The fractions are picked with a forceps and sorted into 96 well plates.

For protein elution, 10 µl of the elution buffer are added to each well. It is necessary to ensure that the membrane snippets are completely covered with buffer. A helpful property of the elution buffer is that the membrane snippets turn transparent and thereby almost invisible in this buffer, after dilution of the elution buffer, they turn white again. The plates are sealed and placed on a shaker for 90 minutes with 1200 rpm at room temperature.

The eluted proteins are diluted by adding 90 µl BSA containing buffer per well. As described, ready to use bead plates are used. There are 4 different bead plates each equipped with 96 different NeutrAvidin coated Luminex bead sets. The bead plates contain a defined number of beads per well. A 96-well magnet comb is used to transfer the beads from the bead plate to the diluted protein eluates. The plates are sealed and incubated overnight at room temperature with gentile shaking.

The next day, an excess of Tris-inactivated biotinylation reagent is added and incubated for one hour to block remaining biotin binding sites. Then the beads from up to 4 plates are pooled together using the 96-well magnet comb and an 8-channel magnet comb. The beads are transferred to a vial and after washing in CBS they are adjusted to a defined concentration. The resulting bead-mix contains up to 384 bead sets representing 4 samples with 96 molecular weight fractions each. The number of samples can be scaled by generating several DigiWest bead-mixes. A typical DigiWest bead-mix contains 40000 beads from each bead-set and is sufficient for 200 antibody incubations. This number is also scalable.

DigiWest assays are performed in 96 well plates. Plates are pre-incubated with assay buffer and an aliquot of the DigiWest bead-mix(es) is added. The buffer is discarded and 30 µl per well of the anti-bodies diluted in assay buffer are added. Primary antibodies are incubated overnight. The assay plates are placed on magnet plates and the buffer is discarded, PBST is added and discarded again. Plates are washed twice. PE-labelled secondary antibodies are diluted in assay buffer and 30 µl are added per well. After incubation for 1 hour at room temperature and two washing steps, the plates are filled with PBST for readout which is performed on a Luminex FlexMAP 3D. A full plate with 4 samples on 384 bead sets and 96 wells results in almost 37000 data points representing 384 Western-Blot lane equivalents. The Luminex data are used for data analysis.

3.4 Data analysis

The DigiWest method creates hundreds of Western-Blot equivalents. For analysis of this amount of data it is necessary to identify, integrate and quantify the specific signals. The initial Western-Blot lanes need to be reconstructed and the antibody specific signals need to be identified. An advantage of the digital nature of Luminex based DigiWest data is that the antibody signals can be quantified without any image processing as usually performed for Western-Blot quantification. Therefore, I created an Excel based analysis tool which is able to handle the data.

The Luminex output file contains several blocks of data. One of the data blocks contains the median of the reporter dye (PE) fluorescence for each bead set in each well. Luminex uses a relative fluorescence unit called MFI (median fluorescence intensities). The Luminex data for DigiWest contain data for up to 96 wells per plate and up to 384 bead sets resulting in almost 37000 data points per plate. Each of the antibody incubations on each sample is represented by 96 values which are represented as diagrams for visualization during data analysis. These diagrams represent equivalents of Western-Blot lanes and the antibody specific signals appear as peaks which are equivalent to bands in Western-Blot images.

The analysis tool contains three visible sheets. The first sheet is meant for input of the Luminex data, the second is for data analysis and the third contains the quantified signals from the selected peaks. The analysis tool can handle all the data derived from one 96 well plate. The whole data block from the Luminex output file can be pasted in one. Information on which antibodies were incubated in which well and which bead-mix containing which samples was used can be added.

There are some options built in for background subtraction including species specific background subtraction which needs additional information on the species the antibodies are derived from. Background subtraction is mandatory as the Luminex beads themselves show some background fluorescence and the species specific secondary antibodies can also show background signal.

The tool can handle antibodies derived from 5 different species at a time and a sixth option for streptavidin-PE which is used for on-bead protein determination as shown in section 3.6.

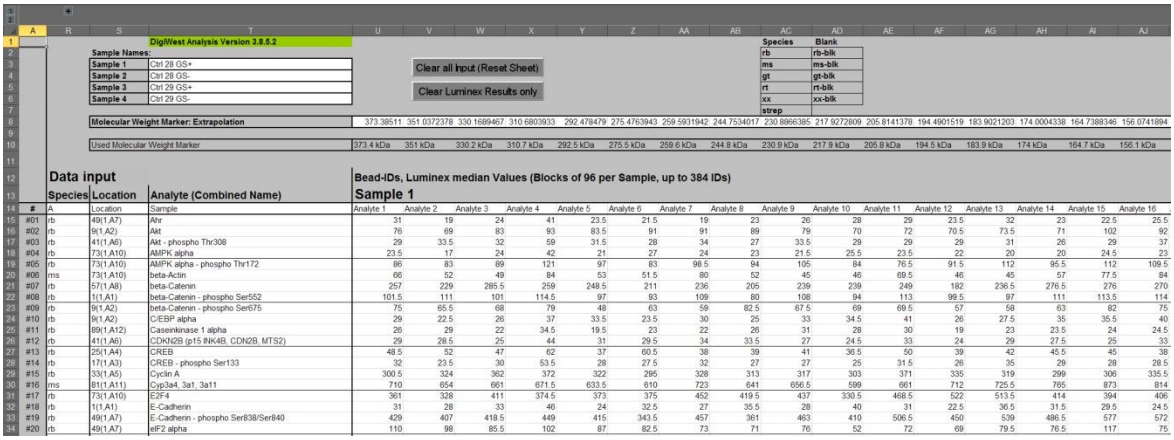

DigiWest Analysis Version 3.8.5.2

Sample Names:

Sample 1	Ctrl 28 GS+
Sample 2	Ctrl 28 GS-
Sample 3	Ctrl 29 GS+
Sample 4	Ctrl 29 GS-

Clear all Input (Reset Sheet)

Clear Luminex Results only

Species	Blank
rb	rb-blk
ms	ms-blk
gt	gt-blk
rt	rt-blk
xx	xx-blk
strep	

Molecular Weight Marker: Extrapolation: 373.38511 351.0372378 330.1689467 310.6803933 292.478479 275.4763943 259.5931942 244.7534017 230.8866385 217.9272809 205.8141378 194.4901519 183.9021203 174.0004338 164.7388346 156.0741894

Used Molecular Weight Marker: 373.4 kDa | 351 kDa | 330.2 kDa | 310.7 kDa | 292.5 kDa | 275.5 kDa | 259.6 kDa | 244.8 kDa | 230.9 kDa | 217.9 kDa | 205.8 kDa | 194.5 kDa | 183.9 kDa | 174 kDa | 164.7 kDa | 156.1 kDa

Data input

Bead-IDs, Luminex median Values (Blocks of 96 per Sample, up to 384 IDs)

Species	Location	Analyte (Combined Name)	Sample 1															
#	A	Location	Sample	Analyte 1	Analyte 2	Analyte 3	Analyte 4	Analyte 5	Analyte 6	Analyte 7	Analyte 8	Analyte 9	Analyte 10	Analyte 11	Analyte 12	Analyte 13	Analyte 14	Analyte 15	Analyte 16
#01	rb	49(1,A7)	Ahr	31	19	24	41	23.5	21.5	19	23	26	28	29	23.5	32	23	22.5	25.5
#02	rb	9(1,A2)	Akt	76	69	83	93	83.5	91	91	89	79	70	72	70.5	73.5	71	102	92
#03	rb	41(1,A6)	Akt - phospho Thr308	29	33.5	32	59	31.5	28	34	27	33.5	29	29	29	31	26	29	37
#04	rb	73(1,A10)	AMPK alpha	23.5	17	24	42	21	27	24	23	21.5	25.5	23.5	22	20	20	24.5	23
#05	rb	73(1,A10)	AMPK alpha - phospho Thr172	86	83	89	121	97	83	98.5	94	105	84	76.5	91.5	112	95.5	112	109.5
#06	ms	73(1,A10)	beta-Actin	66	52	49	84	53	51.5	80	52	45	46	69.5	46	45	57	77.5	84
#07	rb	57(1,A8)	beta-Catenin	257	229	285.5	259	248.5	211	236	205	239	239	249	182	236.5	276.5	276	270
#08	rb	1(1,A1)	beta-Catenin - phospho Ser552	101.5	111	101	114.5	97	93	109	80	108	94	113	99.5	97	111	113.5	114
#09	rb	9(1,A2)	beta-Catenin - phospho Ser675	75	65.5	68	79	48	63	59	82.5	67.5	69	69.5	57	58	63	82	75
#10	rb	9(1,A2)	C/EBP alpha	29	22.5	26	37	33.5	23.5	30	25	33	34.5	41	26	27.5	35	35.5	40
#11	rb	89(1,A12)	Caseinkinase 1 alpha	26	29	22	34.5	19.5	23	22	26	31	28	30	19	23	23.5	24	24.5
#12	rb	41(1,A6)	CDKN2B (p15 INK4B, CDN2B, MTS2)	29	28.5	25	44	31	29.5	34	33.5	27	24.5	33	24	29	27.5	25	33
#13	rb	25(1,A4)	CREB	48.5	52	47	62	37	60.5	38	39	41	36.5	50	39	42	45.5	45	38
#14	rb	17(1,A3)	CREB - phospho Ser133	32	23.5	30	53.5	28	27.5	32	27	27	25	31.5	26	35	29	28	28.5
#15	rb	33(1,A5)	Cyclin A	300.5	324	362	372	322	295	328	313	317	303	371	335	319	299	306	335.5
#16	ms	81(1,A11)	Cyp3a4, 3a1, 3a11	710	654	661	671.5	633.5	610	723	641	656.5	599	661	712	725.5	765	873	814
#17	rb	73(1,A10)	E2F4	361	328	411	374.5	373	375	452	419.5	437	330.5	468.5	522	513.5	414	394	406
#18	rb	1(1,A1)	E-Cadherin	31	28	33	46	24	32.5	27	35.5	28	40	31	22.5	36.5	31.5	29.5	24.5
#19	rb	49(1,A7)	E-Cadherin - phospho Ser838/Ser840	429	407	418.5	449	415	343.5	457	361	463	410	506.5	450	539	486.5	577	572
#20	rb	49(1,A7)	eIF2 alpha	110	98	85.5	102	87	82.5	73	71	76	52	72	69	79.5	76.5	117	75

FIGURE 12 LUMINEX DATA-INPUT FOR ANALYSIS

Shown is a detail from the data-input sheet of the DigiWest analysis tool. The data block containing the measured MFI values is copied from the Luminex output file. The information on which well the data are derived from is adopted from the Luminex output file for quality control. Antibody or analyte labels and species information are added for each well. The molecular weight assigned to each bead set is shown. There is an additional block where more antibody and assay related data can be added which can be used for additional information and quality control. This block is hidden in this screenshot.

An extrapolated molecular weight marker which assigns a molecular weight to each Luminex bead set is the key for the following data analysis. The basis for this marker can be the molecular weight marker which is run together with the samples and contained on the blot. The positions of the marker bands can be measured and used for marker calculation. For a more precise marker the peak-positions of a selection of analytes in the assay can be used. The Excel plug-in XLfit is used for fitting the molecular weight marker followed by extrapolation of the marker for all 96 bead-sets representing the molecular weight fractions. This extrapolated marker can be used for all 4 samples or it can be calculated for each sample individually.

The data-analysis sheet is the core component of the analysis tool. In the upper-left is a control panel with buttons which are linked to Visual Basic based macros. Right to the control panel there are 4 diagrams representing the DigiWest data. The diagrams represent the data of the selected analyte which can be changed by clicking onto the analyte names. The diagrams can be scaled individually or they can be aligned to the same scale for all 4 samples. There is also an option for manual scaling of all four diagrams which can be used to zoom into the data. The lower part contains information on the selected peaks for up to 4 samples and up to 96 analytes. The tool can select and integrate two peaks from each diagram.

A major part of this analysis sheet is a control system which validates all input data including the raw Luminex data and all calculation steps resulting in error messages in case something went wrong or invalid data or values were used. An error report can be shown using the control panel. This control system also detects which analytes and which samples are being used for calculation and dismisses the unused ones.

The main function of this sheet is to integrate the peaks in the diagrams representing specific signal of the applied antibodies on the indicated samples. Therefore the data need to be background subtracted. The correct peaks need to be selected and integrated which needs calculation of a baseline. There are several options built into this tool which allow integration of (almost) every peak-like structure.

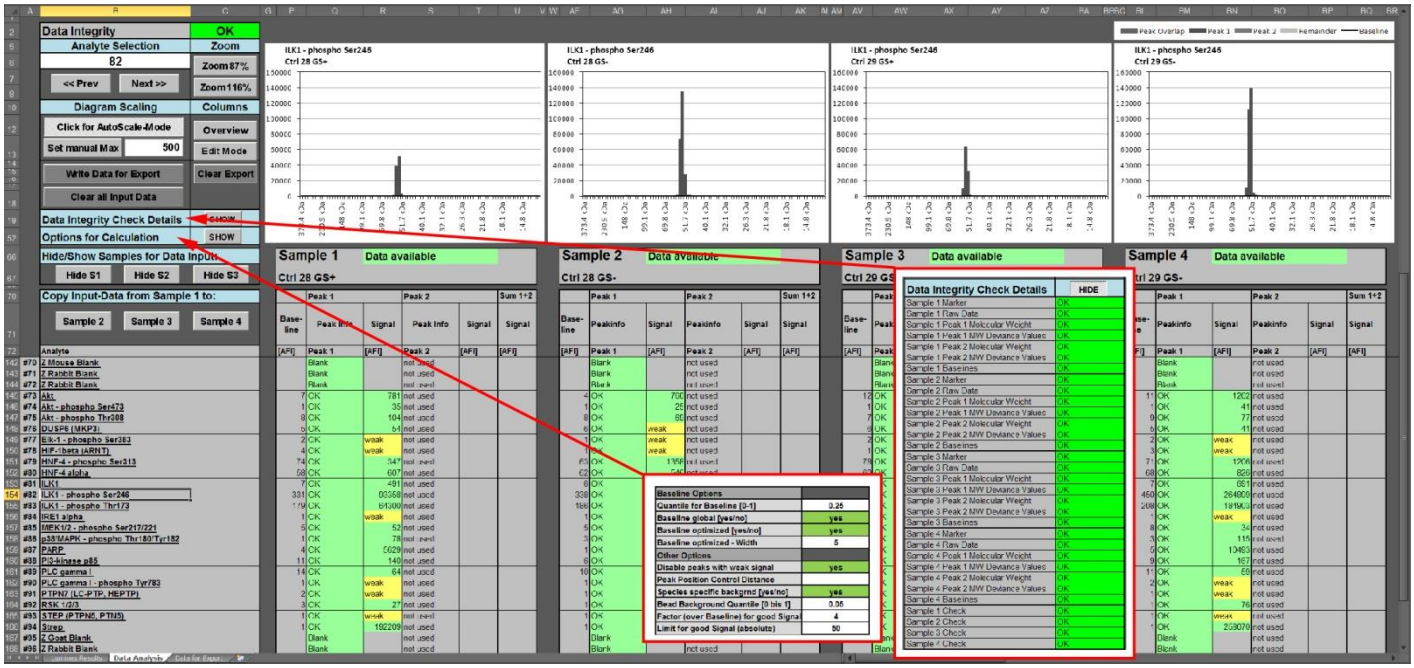

FIGURE 13 DIGIWEST DATA ANALYSIS SHEET: SCREEN SHOT OF THE DIGIWEST ANALYSIS SHEET

The analysis shown is taken from the mouse liver LCM experiment which is presented later in this thesis. The control panel is in the upper-left and the 4 diagrams representing the selected analyte on the 4 samples used in this DigiWest bead-mix are right of the panel. The sheet is in the overview mode showing the results only. The detailed error report from the control system and the panel with additional options for calculation (explained in detail in the text and next figure) are superimposed. They can be shown using the corresponding buttons from the control panel. The tool can select and quantify 2 peaks from each diagram. In the overview mode there are 6 columns for each sample which contain the baseline position, information on peak 1, integrated signal of peak 1, and if the second peak is used also information and signal of peak 2 and the integrated signal for both peaks. Details for calculation will be discussed.

The main function of this sheet is quantification of signals by integration of the specific peaks for each antibody on each sample. The first calculation is subtraction of background signal. As mentioned, the beads show some background which is bead set specific. The secondary antibodies for rabbit and mouse which are used for DigiWest often do not show any specific background. Therefore it is sufficient to subtract the general, bead-derived background. But in many situations, also for this example where some mouse-derived antibodies are used on mouse tissue samples, it is mandatory to subtract the signal derived from the secondary antibody as well. Therefore, there are some options integrated in the options panel. One option is to use species-specific background subtraction so that for each antibody derived from the same species the corresponding blank is subtracted. The blank is the secondary antibody control which is therefore mandatory for each assay. Alternatively, a background independent of the secondary antibody and only dependent on the bead-set can be subtracted. This option subtracts a given quantile over all measured wells for each bead-set. Setting this quantile to 0 results in subtraction of the minimum but as the Luminex data underlie some variation of a few fluorescence units (about +/- 5 MFI for stable measurements, about +/- 10 MFI for less stable ones) the preset value is 0.05 so the 5% quantile which means that 95% of the values are higher and 5% are lower resulting in more stable data. Negative values are eliminated and set to 0.

After background subtraction, peaks are selected. The peak selection process is based on the molecular weight marker. The analysis tool allows one or two peaks to be selected. When the molecular weight of the analyte is entered, the tool searches for the peak (local maximum) in a definable area around this molecular weight. The preset for the first peak is +/- 20% of the given molecular weight and for the second peak, because related proteins often have similar molecular weights, the preset is +/- 10%. For good data with clear peaks and no or minor additional peaks it is sufficient to give the molecular weight for selection and integration of the peaks. As it can happen that a peak is only partially contained in the defined area, an algorithm validates that the selected maximum is a real maximum and in case it is positioned in a slope of a peak a warning is given.

The peaks are defined by the local maximum with declining values left and right. The neighboring values need to be same or smaller. Sometimes peaks are not shaped that perfectly but are bogus and show for example a ‘shoulder’. To select these peaks, a factor was introduced with the inglorious name ‘Bad Peak Factor’ which is set to 1 by default. If it is increased for example to 1.1 the neighboring values can be up to this factor, in this case 10% higher, which helps selecting a bogus peak. The factor can also be set smaller than 1 resulting in a decline which needs to be reached by neighboring values to be included in the peak. The borders of the peaks are defined by the positions where the given criteria are not met anymore. Another option is the selection of two peaks and integration of both peaks into one. So double

peaks can be selected as two separate peaks or integrated into one peak. This function can also be used for selection of bogus peaks. The combination of the 'Bad Peak Factor' and the possibility to integrate two peaks into one allows selection of almost all peak-like structures.

For integration of the peak areas it is necessary to define baselines. There are several options for calculation of these baselines. The default setting is that the local background around the peaks is used for baseline calculation. The number of data points left and right of the peak which are used can be specified, the default setting is 5 data points from each side. A quantile is used again for calculation of the baseline from these by default 10 values. The default setting is 25% so the baseline is set at the position that 25% of the values are below and 75% are above the baseline. The quantile is set globally for all calculations in the sheet. This global setting can also be switched off which unlocks the possibility to change the setting for each sample and analyte individually.

The preset values are empirically determined and give good results for the vast majority of analyses. An alternative option is to calculate the baseline by the given quantile over all 96 values in the diagram independent of the peak position.

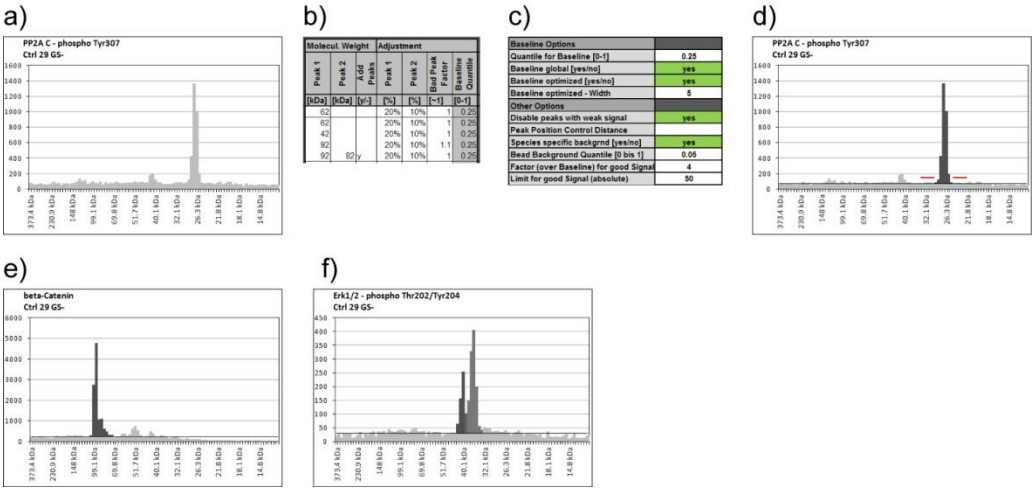

FIGURE 14 DIGIWEST DATA ANALYSIS: PEAK SELECTION

Shown are some examples for graphical illustration of the peak quantification procedure.

a) *Diagram showing the 96 values from the background subtracted Luminex data for one analyte on one sample. The molecular weight marker is shown on the x-axis and the values of the 96 Luminex data points on the y-axis are shown as light gray bars.*

b) *Detail of the input screen. When the analysis tool is switched to the 'Edit Mode' these columns are shown for each sample allowing selection of the peaks for all analytes. The molecular weight of the analyte needs to be given for one or two peaks in the first 2 columns. For most analyses this is sufficient*

for integration of the peaks and quantification of the analyte specific signal. The next column allows integration of both peaks to one peak by placing a 'y'. The next 2 columns define the allowed deviance from the given molecular weight for the peak-search algorithm which can be adjusted. The next column contains the described 'Bad Peak Factor' and the last column is locked. It can be unlocked to set individual quantiles for baseline calculation. By default a global quantile is used for all analytes and samples in the sheet.

***c)** Shows the options for calculation. Options which are switched on are highlighted in green. The global quantile for baseline calculation can be set followed by the option for global or individual quantile usage. The option 'Baseline optimized' switches between the algorithm for local background around the peak or the quantile over all 96 data points. The next option disables highlighting of peaks when the corresponding signal is dismissed as 'weak'. The Peak-Position control is inactive by default. If a number is given, for example 2, then the positions of the peaks for each analyte are compared between the 4 samples for their relative position which in this example has to be smaller or equal 2 data points. This validates that peaks with the same molecular weight are selected for all samples. The next options are for background subtraction mentioned earlier. The last two options represent cut-off filters for low signals. This is necessary as the algorithms always find a local maximum even in background noise. The first filter uses the signal-noise ratio and the second filter the integrated peak signal. Both filters need to be passed to give an analyzable signal. The default setting is factor 4 over baseline and an integrated signal of more than 50.*

***d)** Shown are the same data as in a) with the peak selected. The peak-area which is being integrated is represented in dark gray, the remainder in light gray. The baseline is shown. The data-points under the red bars were used for baseline calculation (local background, 5 data points from each side).*

***e)** An example of a peak with a 'shoulder' where the 'Bad Peak Factor' was used for peak selection.*

***f)** An example where two peaks were selected. The first peak is highlighted in dark gray, the second peak in medium gray. The overlap is highlighted in striped dark/medium gray. The area of the overlap is attributed half to each peak.*

The integrated signals for each peak are shown in the analysis sheet. Peaks which failed passing the cut-off filters are dismissed as 'weak'. There is an option build-in to switch off highlighting of the peaks when the signals are dismissed. The integrated signals still have a relative unit now called AFI for 'assembled fluorescence units'. An export macro writes all AFI values into the last sheet of the analysis tool from where the data can be copied and used for further analysis and statistics.

3.5 Benchmarking DigiWest performance

As the Western-Blot represents the ancestor of the DigiWest method it was mandatory to perform a direct comparison between these methods. In the 35 years since Western-Blot was invented there were permanent efforts for optimizing the method. These efforts lead to development of several highly sensitive readout systems. A widely used readout is the enhanced chemiluminescence (ECL) combined with high end cameras, other systems use fluorescence based readout employing confocal laser scanners. The methods which were used for comparison of the DigiWest method were chemiluminescence readout employing the commercial substrate 'Super Signal West Pico' and readout on the Fuji LAS 4000 imaging system and the infrared fluorescence based Licor Odyssey scanner. The DigiWest method was compared to Western-Blots under qualitative and quantitative aspects.

3.5.1 Qualitative comparison to Western-Blot

A sample frequently used during method development was HepG2 cell lysate. This material has also been used for the antibody validation approach for reverse phase protein microarrays in our group. Therefore, a collection of Western-Blot images is available for several hundred antibodies. The image collection was used for a qualitative comparison to the DigiWest data.

20 µg HepG2 lysate were used to generate a DigiWest bead-mix containing 40000 beads per set, so sufficient for 200 antibody incubations. The bead-mix represented 96 molecular weight fractions at a resolution of 0.5 mm. Assays with more than 100 antibodies were performed using this bead-mix to generate DigiWest data which were compared to the corresponding Western-Blot images.

The digital data obtained from the Luminex instrument can be used to reconstruct Western-Blot-like images (see Fig. 15) by translating the 96 values into a grayscale image. The MEV software package was used to create such grayscale maps from the background subtracted data. These maps represent the initial Western-Blot lanes as 96 rectangles with no signal represented in white and the maximum values in black. The values in between are represented in different gray-values. The resulting maps look edgy due to the 96 rectangles but after application of a Gaussian diffusor the resulting images show high similarity to real western-Blot images. Images generated by this method were named 'Western-Blot mimics'. Using this approach, Western-Blot images from our image collection and DigiWest data from more than 100 antibodies could be compared. Some examples are shown here, a comprehensive collection of 104 antibodies is shown in Appendix 1.

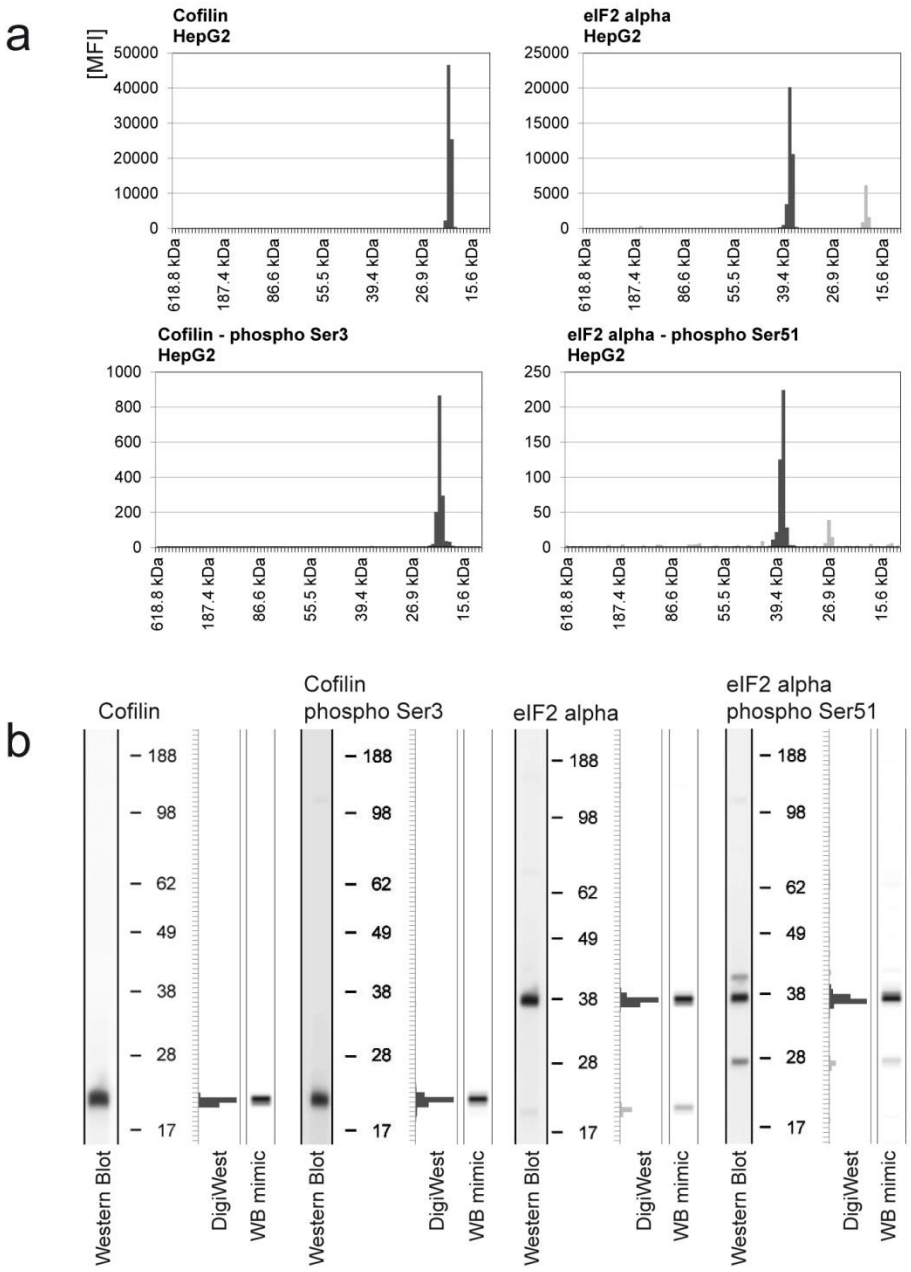

FIGURE 15 QUALITATIVE COMPARISON OF WESTERN-BLOT AND DIGIWEST

Direct comparison of Western-Blots and DigiWest data. HepG2 lysate was used as sample, antibodies as indicated. Data from 4 antibodies are shown. ***a)*** *Full diagrams of the DigiWest data used for generation of the Western-Blot mimics. The diagrams represent the signal obtained on the 96 molecular weight fractions. Specific signal is shown in black, unspecific signal in gray.* ***b)*** *Comparison to Western-Blots. The left columns show Western-Blot images, the diagrams in the middle show the Luminex data (same data as in a)) in reduced diagram form with the specific band highlighted in black, the right columns show the Western-Blot mimics generated from the DigiWest data.*

Using the Western-Blot mimics for representation, the similarity of DigiWest and Western-Blot becomes obvious. Unlike the diagram representation of the DigiWest data, this Western-Blot-like representation is familiar. The additional bands which can be seen in the Western-Blots for the eIF2 alpha antibodies can also be seen in the DigiWest data which underlines the similarity. The following figure shows a collection of 96 different antibodies incubated on the HepG2 lysate loaded DigiWest bead-mix.

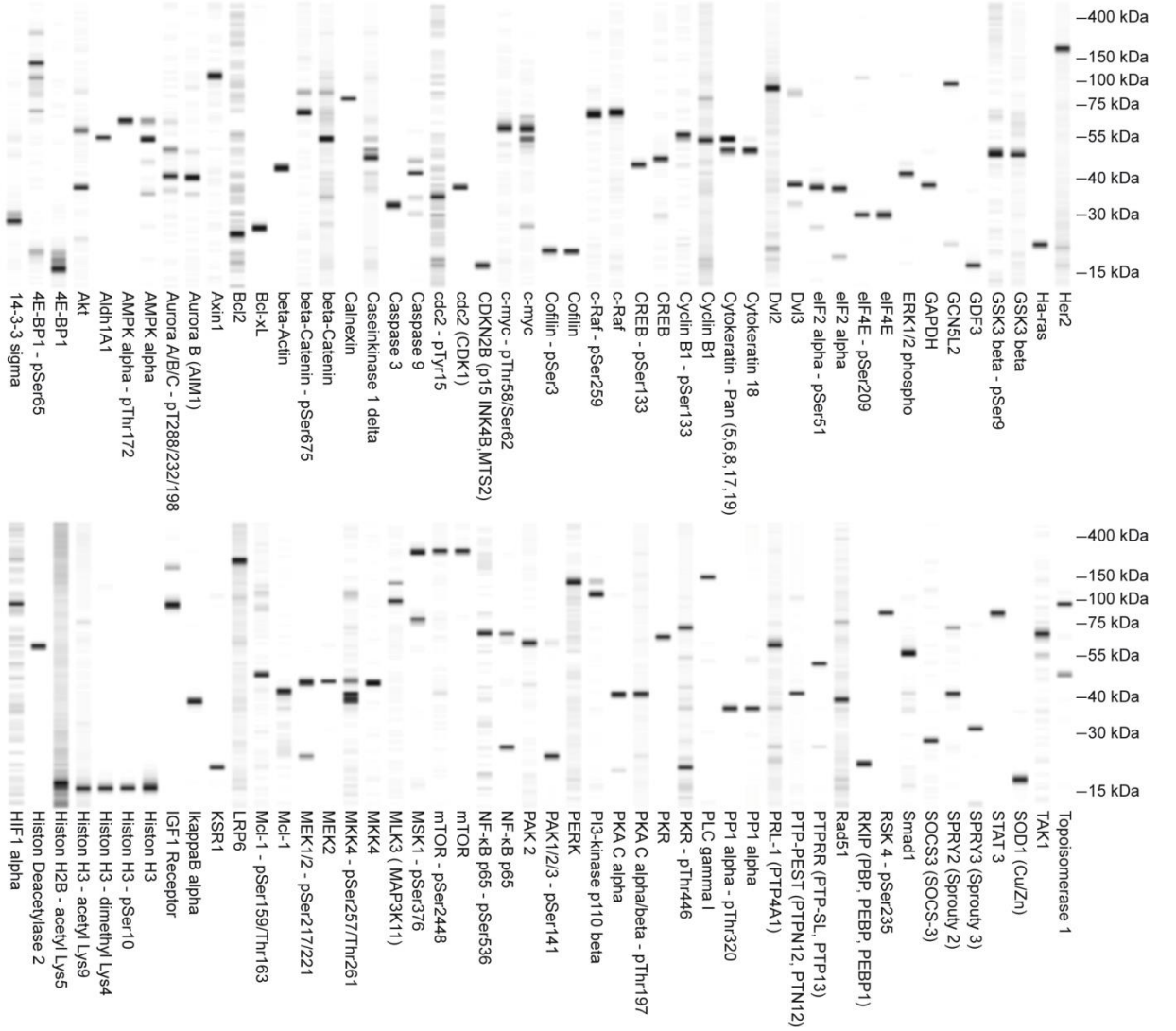

FIGURE 16 DIGIWEST DATA FROM A COLLECTION OF ANTIBODIES

DigiWest data from a collection of 96 antibodies on HepG2 lysate represented as Western-Blot mimics. Antibodies recognizing large, small or medium-size proteins were selected, also antibodies showing a single band at the correct molecular weight and antibodies showing additional bands. A comparison to Western-Blot images for all of these and some more antibodies is shown in Appendix 1.

Data generated by the DigiWest method correlate well with Western-Blots. Almost all antibodies tested which gave a specific signal on Western-Blot on this sample also gave a specific signal on DigiWest. For many antibodies which showed additional bands on the Western-Blot the same additional bands were visible on DigiWest data. In some cases the additional bands showed different intensities when compared to Western-Blot and in some cases additional bands appeared or disappeared. But these differences are not more distinctive than the differences between Western-Blots which are blocked with BSA or blocked with milk powder. For Western-Blots, a BSA based buffer was used while for DigiWest an ELISA buffer supplemented with milk-powder was used. Even antibodies which were imaged with long exposure times on Western-Blots gave acceptable signals for the DigiWest method.

3.5.2 Long term stability

An important aspect is the long-term stability of the DigiWest bead-mixes. The NeutrAvidin biotin interaction, which is used to immobilize the proteins, might show low off-kinetics resulting in exchange of biotinylated proteins in between the bead sets which are stored in a mix containing all 384 bead sets representing 4x96 molecular weight size fractions from the initial blots. This might lead to a loss of specific signal and disintegration in the DigiWest bead-mixes over time. The use of bead-mixes after 6 months or even two years storage showed good performance and sharp peaks and no measurable effect on the quality of the DigiWest assays was detected. A planned and scheduled long term storage experiment is still missing.

3.5.3 Linearity, sensitivity and quantification in comparison to Western-Blot

Important aspects for validation of the new method are the analyte-signal relationship i.e. linearity and linear range, reproducibility and direct comparison to a high-end Western-Blot readout system in regard to sensitivity. To determine these aspects, an experiment was designed in which DigiWest was compared to the infrared fluorescence based Licor Odyssey.

In the experiment, a dilution series of a GST fusion protein was spiked into a constant amount of cell lysate. The spiked lysates were used to perform blots for a DigiWest experiment and classical Western-Blots. HepG2 lysate was spiked with GST-ERK2. The GST-tag has a molecular weight of 26 kDa and shifts the 42 kDa ERK2 to 68 kDa which allows discrimination of the spiked protein and the intrinsic ERK2 in the cell lysate. The dilution series covered a dilution factor of 1024 in 6 different dilutions and ranged from 20 ng GST-ERK2 per 10 µg HepG2 lysate to about 20 fg GST-ERK2 per 10 µg HepG2 lysate. These samples were used to prepare 4 Western-Blots and blots for DigiWest.

For DigiWest, each sample was applied in triplicates resulting in 18 lanes each containing 10 µg HepG2 lysate. For the Western-Blots the higher spike-amounts were applied in duplicates and the lower ones in triplicates resulting in 15 lanes. As the PVDF membranes which are used for DigiWest are not suitable for fluorescence readout, 2 of the Western-Blots were performed using Nitrocellulose membranes and 2 using PVDF membranes.

The 18 lanes from the DigiWest blots were used to prepare DigiWest bead-mixes sufficient for 100 antibody incubations. To reduce the number of bead-mixes, only a limited molecular weight range from about 115 to about 40 kDa represented by 32 molecular weight fractions was used. A DigiWest assay was performed employing a monoclonal ERK1/2 specific antibody which detects the intrinsic ERK1/2 and the spiked GST-ERK2. As there were enough beads for 100 antibody incubations for DigiWest assays, the assay was performed with 4 repeated measurements.

The Western-Blots were either blocked with BSA or blocked with milk-powder and used for chemiluminescent readout on the Fuji LAS-4000 and for fluorescent readout on the Licor Odyssey. For the blots blocked with BSA, the obtained GST-ERK2 specific signal from chemiluminescent readout on PVDF membrane massively levelled out and showed more a curve than a linear relationship. The signal from fluorescent readout using the 800 nm channel of the Odyssey scanner on nitrocellulose membrane also levelled out and showed only linearity for the lower 4 spike amounts. Therefore, the blot on nitrocellulose blocked with milk-powder was used for fluorescent readout. The GST-ERK2 specific signal showed good linearity for all spike-amounts.

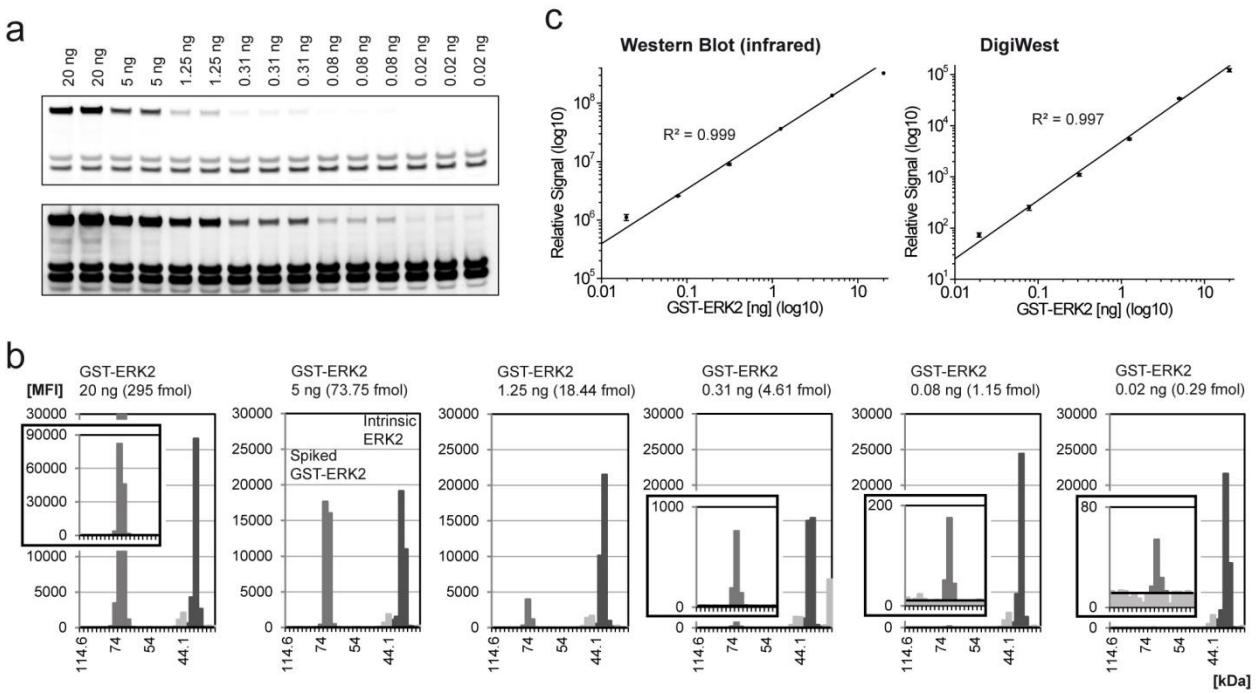

FIGURE 17 SENSITIVITY AND SIGNAL LINEARITY OF DIGIWEST COMPARED TO LICOR ODYSSEY

a) *The Western-Blot on nitrocellulose membrane blocked with milk powder on the Licor Odyssey using Licor secondary antibody on the 800 nm channel. The lower image is the same than the upper one with changed gray-scale settings to visualize the weaker bands. The laser power used for readout was the highest possible without saturated pixels within the area of interest.*

b) *Representative examples from the DigiWest measurement for each spike amount shown as diagrams. The peaks corresponding to the spiked GST-ERK2 are shown in medium gray and the peaks corresponding to the intrinsic ERK2 from the HepG2 lysate are shown in black. The peak in light gray corresponds to intrinsic ERK1 which is also detected by the antibody. The different peak shapes* which are very obvious for the intrinsic (black) ERK2 *correspond to differences in the exact cutting position.*

c) *Signal linearity: both methods show a slight s-curve which is typical for fluorescence based immuno-assays. The diagrams are in log10 scale on both axes. The coefficients of determination are good for both methods. Error bars are shown representing standard deviations, for the Western-Blot only for the 3 lower spike-amounts because there are only 2 values available for the higher spike amounts. The DigiWest data contain error bars for all spike-amounts including the repeated measurements.*

The whole dataset for the DigiWest measurement including the 4 repeated measurements is shown in Appendix 2. The DigiWest assay was performed under final workflow conditions using the DigiWest assay buffer. Utilization of a polymer based buffer might further increase the detection limit. Licor based

Western-Blot and DigiWest were both able to detect the 20 pg GST-ERK2 but both methods seem to be close to their detection limit. The Western-Blots with chemiluminescent readout on the LAS 4000 and with BSA-based buffer on the Licor Odyssey were both also able to detect the 20 pg spiked GST-ERK2 but they were both very close to their detection limits as the intensities of the bands were close to the background signal.

The peaks in the DigiWest data obtained from the intrinsic ERK2 show that the shape of the peaks varies dependent of the exact cutting position of the molecular weight fractions. But independent of the shape of the peaks, the integrated signals are robust.

The signal obtained from the intrinsic ERK2 in the Western-Blot (15 lanes, 1 blot) shows a CV of 6.44%, the signal obtained from DigiWest (18 lanes, 3 blots) shows a CV of 9.57%. This shows that reproducibility of the DigiWest method is good even for 18 lanes which are distributed over 3 blots. Distribution over 3 blots was necessary because empty lanes are needed in between for cutting the membranes for DigiWest. The increased variation of the DigiWest data compared to the Western-Blot can mainly be imputed to the three blots. In smaller spike-in experiments, where only one blot was used for generation of the DigiWest bead-mixes, the variation was lower.

The signals obtained from the spiked GST-ERK2 can be used as standard curve for absolute quantification. The intrinsic ERK2 in 10 µg HepG2 lysate can be calculated to 62.25 fmol (6.2 fmol/µg) using the Western-Blot and 70.99 fmol (7.1 fmol/µg) from the DigiWest data. For these calculations the standard curves from the GST-ERK2 spikes were fitted using XL-Fit and the different molecular weights of ERK2 and GST-ERK2 were taken into account. The discrepancy in between the two methods of about 14% is in an acceptable range for two different methods for protein quantification (Wild, 2013).

This experiment shows that DigiWest performs well in respect to signal linearity, reproducibility and sensitivity. It can compete with the highly sensitive Licor Odyssey platform. One aspect which should be mentioned here again is that for the DigiWest experiment the same sample and spike amount was used but the resulting DigiWest bead-mixes were sufficient for 100 antibody incubations, so only 1/100 of the sample amount was used per measurement compared to the Western-Blot.

3.6 On bead protein determination

Protein biotinylation usually results in the covalent attachment of more than one biotin per protein. Since the immobilization of biotinylated proteins on the Luminex beads only requires one biotin, there are still biotins available that are detectable on the bead-bound proteins. These biotins can be used for on-bead protein estimation. In this example, HepG2 lysate was used again as sample. To address the

limited sample amount in the following laser capture microdissection experiment, a linear dilution series from 6 to 1.5 µg HepG2 lysate was loaded. The DigiWest bead-mix was incubated with streptavidin-PE in assay buffer in 3 different dilutions (1:50, 1:200, 1:800) in duplicates. As milk powder contains biotin, a milk powder free buffer (CBS: 1% BSA, 0.05% Tween-20, 0.05% sodium azide in PBS) was also tested. Streptavidin-PE was incubated under secondary antibody conditions, 1 hour at 23°C.

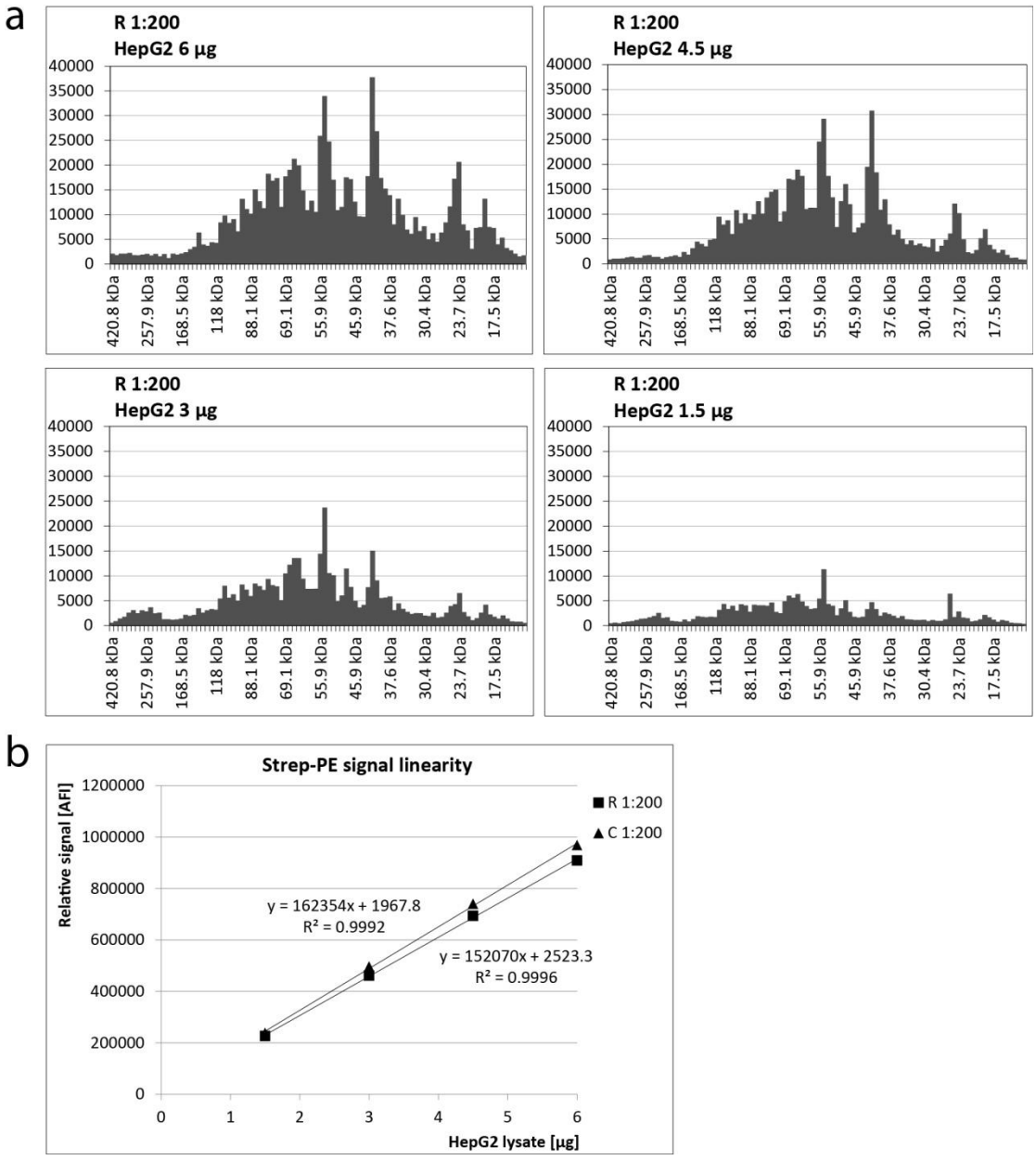

FIGURE 18 *ON-BEAD PROTEIN DETERMINATION*

a) *DigiWest diagrams taken from the DigiWest analysis table, the whole molecular weight ranges were used for signal integration. HepG2 lysate dilution series: 6 µg, 4.5 µg, 3 µg and 1.5 µg protein. Incubated*

with streptavidin-PE, diluted 1:200 in assay buffer. A clear correlation of signal and sample amount can be seen. ***b)*** *Quantified signal from the dilution series in assay buffer (R) and in CBS (C) both as means of duplicated measurements. The signal obtained from streptavidin-PE shows good linearity.*

The signal of streptavidin-PE in this assay represents free biotins on the Luminex beads. There is a clear linear correlation of the streptavidin-PE signal and the sample amount loaded onto the Luminex beads.

The signals in assay buffer are marginally lower than in CBS but signal linearity is still good. Other dilutions of Streptavidin-PE have been tested, all showed good signal linearity. The 1:200 dilutions resulted in the lowest Y-axis-intercept of the linear fit. The milk powder contained in the assay buffer which might contain biotin does not affect the measurement except for slightly lower signals.

This experiment proves that simple incubation of DigiWest bead-mixes with streptavidin-PE can be used for relative on-bead protein determination which results in good signal linearity. Another method involving a reactive dye has also been tested but there was no need for this as streptavidin-PE is simple and robust.

On-bead protein determination is useful for data normalization on total protein in the samples. The on-bead protein determination can be used as loading control and for normalization of the data as an alternative to β-Actin or GAPDH.

3.7 Lapatinib resistance in a cell line model

Lapatinib (GlaxoSmithKline) is a kinase inhibitor specifically inhibiting the receptor tyrosine kinases Her2 and EGFR (Her1). It is used in cancer therapy especially in cases where tumors overexpress one of these receptors. An important issue in cancer treatment is that tumors frequently develop resistance to anti-cancer drugs and relapse (C. R. Chong & Jänne, 2013).

In this experiment, the mucoepidermoid pulmonary carcinoma cell line H292 was employed to study this phenomenon. The motivation was to identify differences that occur during development of resistance to Lapatinib. The experiment was performed in collaboration with Benjamin Ruprecht in the group of Bernhard Küster (Chair of Proteomics and Bioanalytics, TUM) at the Technical University of Munich.

First, a Lapatinib resistant cell line was established in the laboratory of Bernhard Küster. By cultivating the cells in very low doses of Lapatinib which the cells managed to survive, the dose was slowly increased over several months so that the cells adapted to the drug and developed resistance. The resulting resistant cell line was able to grow in presence of high concentrations of Lapatinib. The IC_{50} of the resistant cell line was about 800 nM compared to about 10 nM of the parental cell line. The resistant cell line had to be cultured in presence of Lapatinib to conserve the generated resistance; the term 'resistant' is used here although the term 'tolerating' might be more appropriate.

3.7.1 Kinase enrichment using Kinobeads

Kinases play a pivotal role in cellular signaling and are therefore often targets in drug development. Most kinases use ATP as substrate for phosphorylation of hydroxyl groups on their target proteins or molecules. The main target of kinase inhibitors is the ATP binding site which allows efficient inhibition of the enzymatic activity but often results in inhibition of more than one kinase due to high similarity of ATP binding sites. This observation led to the development of Kinobeads as a tool for kinase enrichment. They are based on a collection of broad-selectivity kinase inhibitors immobilized on sepharose. This allows them to bind the majority of the kinome – the entity of all kinases. Thereby Kinobeads can be used to enrich kinases from complex samples usually followed by mass-spectrometry readout. For testing selectivity or binding affinity of a kinase inhibitor to a kinase, the Kinobeads can be used in a competitive experimental setup where the free target drug is used to compete with kinase binding to the Kinobeads (Bantscheff et al., 2007).

3.7.2 Experimental setup and correlation of mass spectrometry and DigiWest

In an experiment performed by Benjamin at TUM, Kinobeads were used to enrich the kinome of both the Lapatinib resistant and the parental H292 cell line. Besides the kinases, the Kinobead pulldows also contained some kinase-interacting proteins.

Benjamin analyzed the Kinobead pulldowns in mass spectrometry. For mass spectrometry analysis, Kinobead bound kinases and non-kinases were analyzed but only the kinases were taken into account. The mass spectrometry data analysis identified a set of 24 kinases which showed statistically significant changes for resistant versus parental H292 cell line.

For further analysis, DigiWest bead-mixes sufficient for 200 antibody incubations were generated from whole cell lysates and Kinobead pulldowns from Lapatinib resistant and parental H292 cell lines.

In the first part of the experiment, the set of 24 kinases from the mass spectrometry analysis was re-analyzed using DigiWest. The semi-quantitative results obtained from mass spectrometry and DigiWest were compared in respect to their correlation.

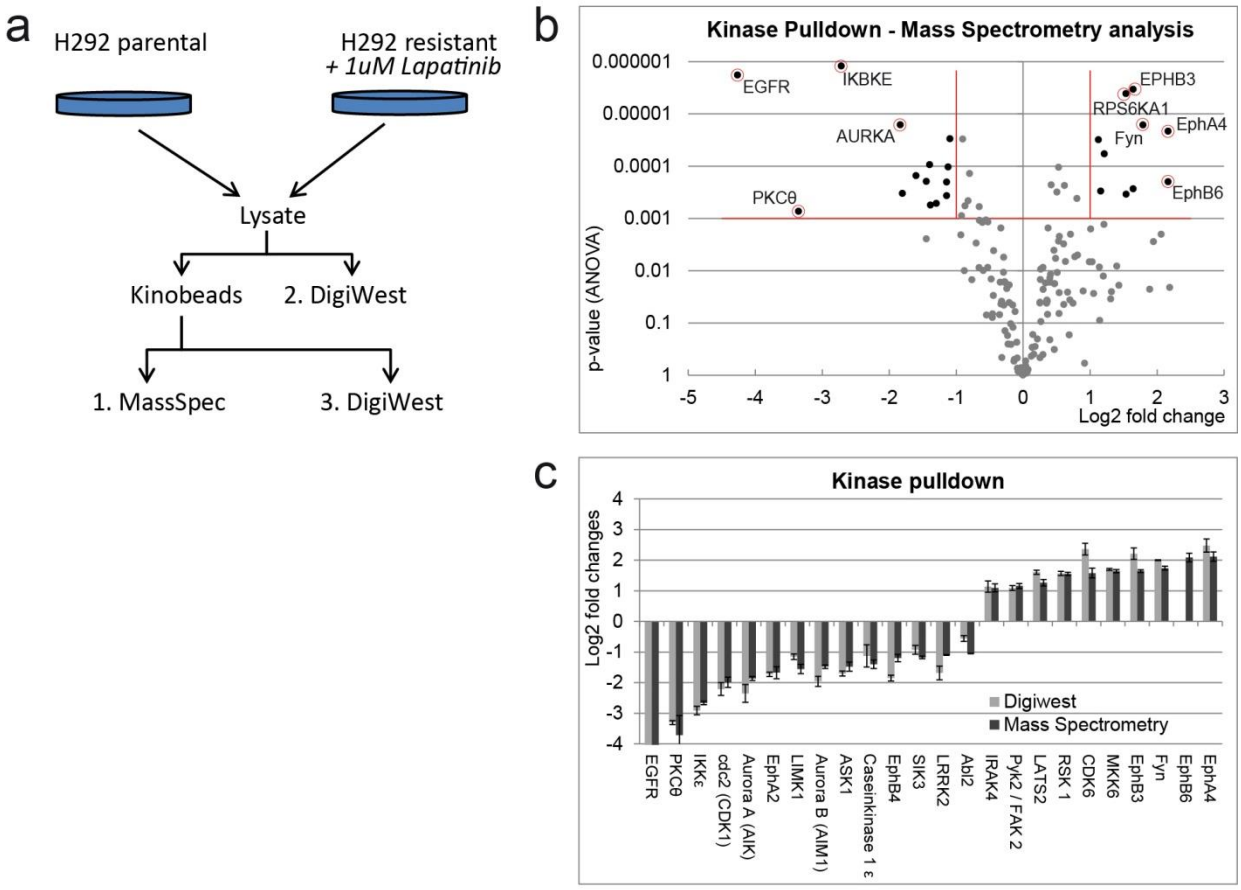

FIGURE 19 EXPERIMENTAL SETUP AND MASS SPECTROMETRY ANALYSIS

a) *Overview of the experimental setup. Parental and resistant cell lines were lysed. One part was used for DigiWest analysis, the other for Kinobead pulldown. Pulldowns were analyzed using mass spectrometry and DigiWest. All analyses were performed in triplicates.* ***b)*** *Volcano plot of the MS analysis. Significantly changed kinases were determined by the following criteria: p-value (ANOVA) < 0.001, fold change > 2 (Log2 >1), number of peptides ≥ 2.* ***c)*** *The set of 24 significantly changed kinases was analyzed using DigiWest and compared to the MS analysis. There was no working antibody available for EphB6. The correlation coefficient for mass spectrometry and DigiWest analysis was 0.98.*

One protein (EphB6) could not be detected in DigiWest because none of the tested antibodies worked. Her2 and EGFR, which are inhibited by Lapatinib and are therefore inhibited from binding to Kinobeads, were underrepresented. Her2 was not detectable and EGFR was massively reduced in the Kinobead pull-downs of the resistant cell line. EGFR was almost undetectable in the DigiWest analysis leading to an even bigger Log2 fold change than in the MS analysis. The correlation coefficient for the two methods (excluding EGFR) was calculated to be 0.98.

Although mass spectrometry and DigiWest are completely different methods for protein quantification this experiment shows that they correlate well. One important aspect for this correlation is the quality of the antibodies. All antibodies used here seem to be highly specific for their targets.

3.7.3 Analysis of cell lysates and Kinobead pulldowns using DigiWest

In a second experimental part, the crude cell lysates were analyzed by DigiWest. This type of sample is difficult to be analyzed by mass spectrometry due to the complex sample composition. The immuno-assay based DigiWest method can – like Western-Blot – handle such complex samples. The Kinobead pulldowns were also further investigated. This gave the opportunity to investigate non-kinase analytes and phosphorylation of proteins within the Kinobead pulldowns and the initial cell lysates.

Analytes were selected based on the set of significantly changed kinases including several phosphory-lations of these kinases. Other analytes were associated proteins and analytes based on literature on receptor tyrosine kinase inhibitor mechanisms.

The DigiWest bead-mixes can be stored and used to perform several assays. Some beads were kept for follow up analyses. Benjamin performed an Ingenuity pathway analysis of the interim results.

For this analysis, all DigiWest data available at this time (all except for 5 analytes including p53) were analyzed by use of the Ingenuity (Qiagen) software package. If data were available for whole cell lysates and Kinobead pulldowns, the data from the whole cell lysates were used. As Ingenuity cannot handle

phosphorylation of proteins, the data on total protein abundance and phosphorylation were separately used to perform two analyses. Both analyses pointed towards down-regulation of p53 as the top upstream regulator.

As p53 is not a kinase, this down-regulation was not visible in the Kinobead pulldown analyses. Therefore some of the remaining DigiWest beads were used to analyze p53 in the whole cell lysates. The down-regulation of p53 was confirmed.

A study on resistance mechanisms for EGFR inhibitors using the inhibitor Cetuximab and clonal selection for resistant H292 cells already showed that loss of p53 is the key player in this setup (S. Huang et al., 2011). Our results show that p53 is the key player for Lapatinib resistance as well and that resistance is based on down-regulation of p53 for reversible Lapatinib resistance in H292 without clonal selection.

As the DigiWest results showed low variance within the replicates, no normalization was performed. For statistical analysis, the DigiWest data were normalized on the mean of the parental cell line (control) and log2 transformed. The resulting data represent the log2 fold change of the Lapatinib resistant H292 cell line relative to the parental cell line. T-tests with Welch approximation were performed using MEV. All analytes with a fold change greater than 2 (log2 >1) and a p-value below 0.02 were defined as statistically significant.

Cell lysates

Log 2 fold change of Lapatinib resistant relative to parental cell line

Analyte	log2 fold	p-Value
DUSP6 (MKP3)	-4.046	8.08E-05
IRAK4 Phospho Thr345/Ser346	2.537	0.00299
IKK ε	-2.525	0.00023
DUSP9 (MKP4)	2.387	0.00025
Aurora A - phospho Thr288	2.382	0.00219
p27(Kip1) - phospho - (CDKN1B) Ser10	2.312	0.00097
PKC θ	-2.290	0.00538
CDK6	2.236	0.00020
EGFR - phospho Tyr1068	-2.212	0.00033
Cyclin B1	-2.211	0.00053
LATS2	2.140	0.00871
PKC θ Phospho Thr538	-2.113	0.00046
Cytokeratin 8	-2.011	0.00056
Caveolin-1	-1.902	0.00017
Aurora A (AIK)	-1.864	0.00334
Caspase 9	1.774	0.00323
p53	-1.753	0.00168
p27(Kip1) (CDKN1B)	1.703	0.00329
EGFR	1.685	0.00407
EphA2	-1.652	0.00193
Aurora B (AIM1)	-1.633	0.01806
EGFR - phospho Tyr845	-1.476	0.00019
RSK 1/2/3	1.468	0.00198
Src - phospho Tyr416	-1.453	0.00026
Pyk2 / FAK 2	1.448	0.00651
Erk1/2 (MAPK p44/42) - phospho Thr202/Tyr204	-1.436	0.00118
YAP - phospho Ser127	1.383	0.00405
Her2 - phospho Tyr1248	-1.378	0.00773
RSK 1	1.351	7.24E-05
Her2	1.232	0.00254
p21/Waf1/Cip1	-1.224	0.00063
cdc2 (CDK1)	-1.205	0.00144
Caspase 8	-1.175	0.00394
MKK6	1.158	0.00787
ABL2 (phosphorylated)	-1.148	0.00778
p53 - phospho Ser392	-1.112	0.00488
GSK3 beta - phospho Ser9	-1.100	0.00018
AMPK alpha - phospho Thr172	-1.063	0.00234
Caspase 7	1.061	0.00016
MEK1	-1.034	0.00231
HIF-1beta (ARNT)	-1.017	0.00250

Kinobead pulldowns

Log 2 fold change of Lapatinib resistant relative to parental cell line

Analyte	log2 fold	p-Value
EGFR	-9.778	9.07E-05
Cyclin B1	-4.027	0.00058
EphA2 Phospho Ser897	-3.915	0.00026
PKC θ Phospho Thr538	-3.407	0.00344
PKC θ	-3.363	0.00469
IKK ε	-2.954	0.00025
JNK/SAPK - phospho Thr183/Tyr185	-2.744	0.00015
LRRK2 Phospho Ser935	-2.465	0.00517
IRAK4 Phospho Thr345/Ser346	2.374	0.00590
EphA4	2.360	0.00126
cdc2 (CDK1)	-2.355	0.00090
Aurora A (AIK)	-2.244	0.00326
EphB3	2.117	0.00073
Fyn	2.063	0.00126
EphB4	-1.904	0.00097
Aurora B (AIM1)	-1.879	0.00114
LRRK2	-1.824	0.00332
ASK1 Phospho Thr845	-1.762	6.43E-05
ATM	-1.746	0.00507
Cytokeratin 8	-1.720	0.00394
EphA2	-1.712	0.00073
MKK6	1.702	0.00446
Caveolin-1	-1.677	0.00218
ASK1	-1.648	0.00022
LATS2	1.639	0.00015
MKK3/6 - phospho Ser189/207	1.603	0.00142
RSK 1	1.597	0.01071
EphB6	-1.511	0.00712
RSK 1 (p90RSK) - phospho Ser380	-1.422	0.00168
RSK 4 - phospho Ser235	1.378	0.01601
Caspase 7	1.325	0.00365
IRAK4	1.296	0.00532
MKK3/MKK6 Phospho S218/T222 S207/T211	1.295	0.00347
Erk1/2 (MAPK p44/42) - phospho Thr202/Tyr204	-1.271	0.00658
RSK 1/2/3	1.234	0.00611
CDK6 (phospho-Tyr24)	-1.216	0.00620
Aurora A/B/C - phospho Thr288/Thr232/Thr198	-1.170	0.01950
Mnk1 - phospho Thr197/202	-1.167	0.00082
GSK3 beta - phospho Ser9	-1.165	0.01106
LIMK1	-1.101	0.01594
Pyk2 / FAK 2	1.048	0.00051

TABLE 1 DIGIWEST ANALYSIS OF LAPATINIB RESISTANT H292 CELL LYSATES AND KINOBEAD PULLDOWNS

DigiWest results of Lapatinib resistant and parental H292 cell lysates and Kinobead pulldowns. The table shows the significantly changed analytes in the Lapatinib resistant cell line relative to the parental cell line as log2 fold changes. Analytes are sorted by absolute log2 fold changes. P-values are derived from t-tests with Welch approximation. Significantly changed analytes were defined as log2 fold change >1 and p-value <0.02. Within the cell lysates and the Kinobead pulldowns 41 analytes were significantly changed. All analytes from all assays including the follow-up containing p53 are included.

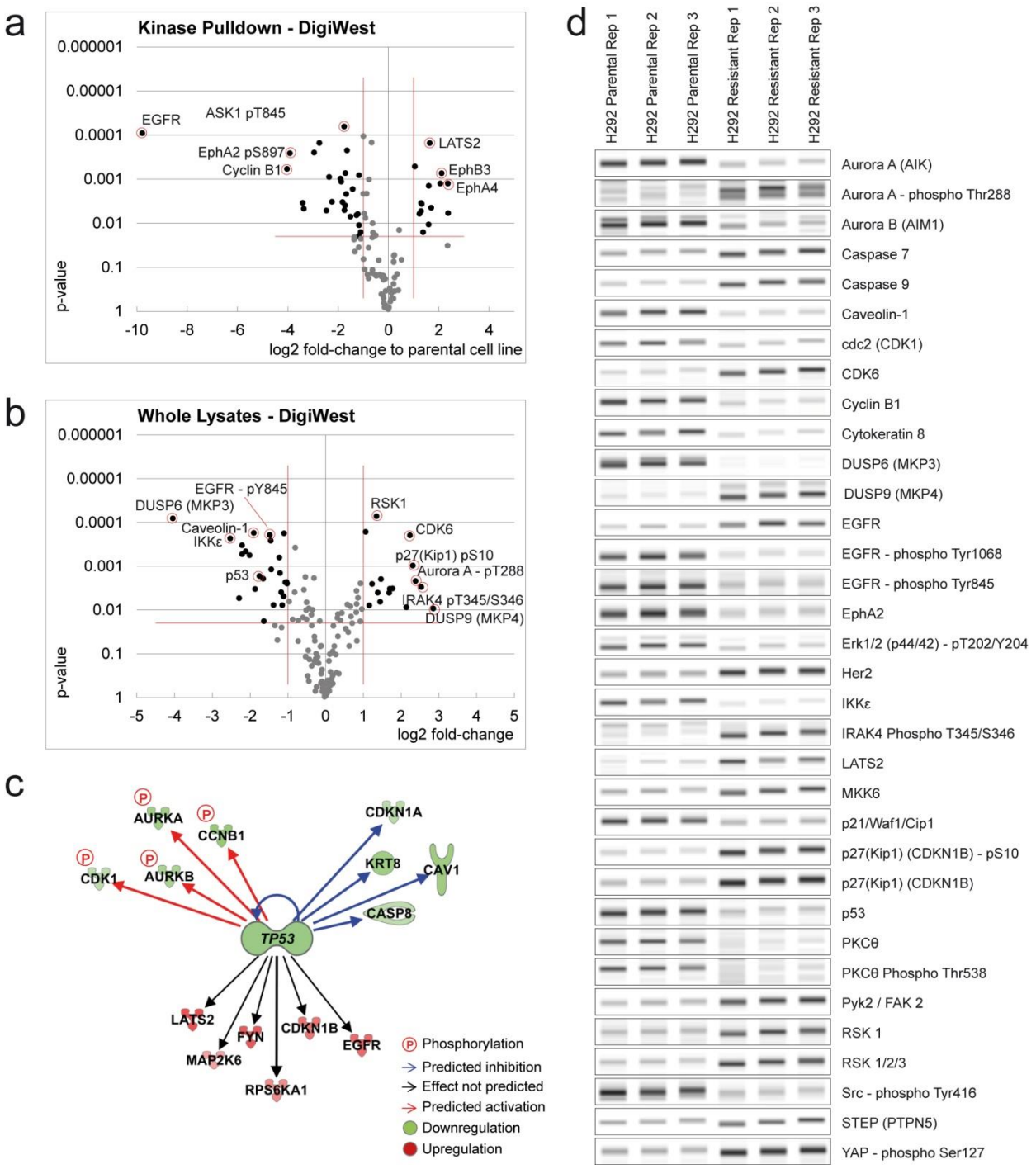

FIGURE 20 DIGIWEST DATA ANALYSIS

a) *Volcano plot representing the DigiWest results of the Kinobead pulldowns. These data include all data from all assays performed. Shown are the log2-fold changes of the Lapatinib resistant relative to the parental H292 cell line on the x-axis and the p-values of the t-test on the y-axis. The data contained in the volcano plots are derived from almost 1000 Western-Blot lane equivalents.* ***b)*** *Volcano plot of the results from whole cell lysate analysis.* ***c)*** *Detail of the Ingenuity pathway analysis of the first large part of*

DigiWest data indicating that p53 should be down-regulated as a key player. This is only a detail of the analyses summarizing the identified targets of p53 (4 phosphorylations and 10 total protein abundances). ***d)*** *Western-Blot mimics representing the 34 most significantly changed analytes in the cell lysates sorted alphabetically. p53 from the last assay is included.*

The combination of unbiased mass spectrometry combined with DigiWest as high-output Western-Blot-like approach and combined with Ingenuity pathway analysis proved to be a powerful team although the slim experiment without follow-up represents more a feasibility study than a serious investigation of the resistance mechanism. Nevertheless this approach resulted in identification of p53 as the top upstream regulator for induced Lapatinib resistance in H292 lung cancer cells and the experiment showed that mass spectrometry and DigiWest, which use completely different principles for protein detection, show a good correlation.

3.8 Mouse liver zonation and zonal response to TCPOBOP treatment

Animal models play an important role in pharmaceutical and toxicological research as the effects of drug treatment are different in cell culture when compared to the effects of drug in an organ or the whole organism. The liver, the most important organ for drug metabolism, is a target of known non-genotoxic carcinogens and thereby serves as a model to detect these substances. Non-genotoxic carcinogens promote tumor growth and the NGC TCPOBOP induces hepatomegaly and liver hypertrophy followed by liver tumors in mice (Donthamsetty et al., 2011; S. P. S. Monga & Cagle, 2010).

Most studies on mouse liver and drug treatment use whole liver lysates and do not take the architecture of the liver into account. The liver is organized in lobules which are defined by centrilobular veins and portal triads which are connected by sinusoids and hepatocytes with a distance of about 10 hepatocytes from portal triad to central vein in mice. Depending on their position within a lobule, the hepatocytes have different metabolic competences and are equipped with different enzymes. Some of the enzymes involved in drug metabolism are also known to underlie zonation (S. P. S. Monga & Cagle, 2010; Ruijter et al., 2004).

Separation of the different functional zones in the liver is technically possible by laser capture micro-dissection (LCM) which results in very limited sample amounts and demands for appropriate methods for analysis. The DigiWest method allows detection and relative quantification of several hundred proteins and protein modifications from limited material. This gave the opportunity to investigate laser capture microdissected material from the different liver zones. The aim of the following experiment was to investigate the pericentral and periportal zones separately upon TCPOBOP treatment to get new and more detailed insights into the processes and changes with a focus on cellular signaling. This is the first time that a drug treatment time course was investigated with zonal resolution on protein level.

3.8.1 Protein analysis of a TCPOBOP treatment time course with zonal resolution

The experiment was performed in cooperation with Albert Braeuning at the Department of Toxicology at University of Tuebingen in the group of Michael Schwarz. At the Department of Toxicology, four groups of C3H/He mice were treated with intraperitoneal injections of corn oil as control or TCPOBOP dissolved in corn oil (3 mg/kg) for 24, 48 and 72 hours. Details of the experimental setup of the time course study can be found in Braeuning et al. (Braeuning et al., 2011). As it is known that there is a gender difference and that female mice show a stronger response to TCPOBOP treatment (Braeuning et al., 2011) only female mice were chosen for this experiment.

Fresh frozen mouse liver sections were used as source material. The 10 µm thick sections were placed on LCM slides (MembraneSlide 1.0 PEN), formalin fixed and stained with a mouse derived glutamine synthetase (GS) antibody to visualize liver zonation. This was performed by Elke Zabinsky in the Department of Toxicology. These stained sections were kept frozen till used for LCM. The formalin fixation step was found to be necessary to prevent loss of phosphorylations. Formalin fixation is not ideal for lysis of tissue sections and impairs protein quality and yield but without fixation there was a massive loss of phosphorylations observed in initially performed experiments.

LCM was performed on a PALM MicroBeam (Zeiss). The MembraneSlide is based on a microscopy slide and a membrane which holds the section. Slide and usable area of the membrane are separated by a thin air bed. This allows cutting of the tissue section together with the membrane using an UV laser. The cut areas are then catapulted onto a cap which is placed above the section (AdhesiveCap 200 opaque, Zeiss) by a defocused laser shot. Areas surrounding the portal triad (GS negative vessels) and areas surrounding the central veins (GS positive vessels) were cut using the UV laser and collected.

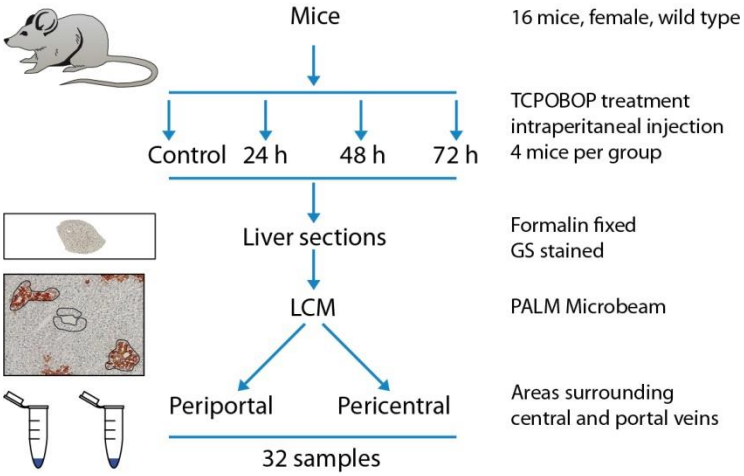

FIGURE 21 STUDY DESIGN: MOUSE LIVER AND DRUG TREATMENT

This study consisted of 16 female C3H/He mice in 4 groups. A control group and groups treated with TCPOBOP for 24, 48 and 72 hours. Liver sections were formalin fixed and GS stained. Periportal and pericentral areas from the liver sections were isolated by LCM for DigiWest analysis.

As indicated in figure 21 only the proximal 1-2 cell layers surrounding the blood vessels were collected representing the proximal pericentral and proximal periportal zones. An area of about 3.7 mm² was collected for each zone which represents most areas of interest surrounding vessels which can be found in one section. The liver sections from the 16 mice resulted in 32 samples. These were analyzed in a

DigiWest experiment. 8 bead-mixes were generated, each containing 4 samples and sufficient for 200 antibody incubations.

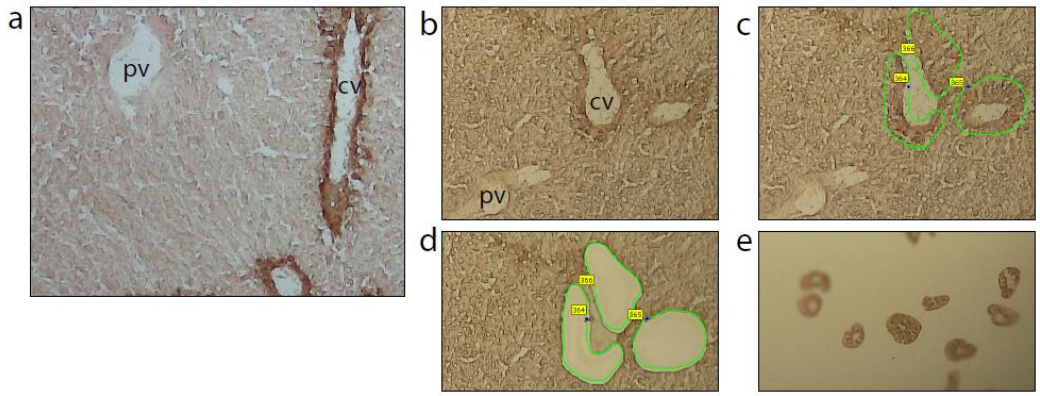

FIGURE 22 LASER CAPTURE MICRODISSECTION

a) *GS stained mouse liver section. Central vein (cv) and portal vein (pv) are clearly visible.* ***b)*** *GS stained mouse liver section as seen under the PALM MicroBeam. Staining was still visible but contrast was pretty bad, this might be based on settings of the microscope. The contrast was better for lower magnifications.* ***c)*** *Areas selected for cutting.* ***d)*** *Section after cutting.* ***e)*** *Cut areas collected on the LCM cap.*

As the number of cells isolated by LCM is low, antibodies were tested on less precious material. This were smaller sets of LCM samples (one set contained periportal and pericentral LCM material from a control mouse, another set additionally contained LCM material from a mouse treated with TCPOBOP for 48 hours) or on 3 µg of a mouse whole liver lysate. A bulk of about 660 antibodies was tested, several antibodies using up to 6 different assay conditions resulting in far more than 1000 test assays.

The proteins of interest were selected based on literature on liver zonation and on literature on TCPOBOP treatment but as the main interest was cellular signaling and changes thereof in respect to zonation and drug treatment, a large set of antibodies covering signaling pathways was included.

204 antibodies were finally selected for the DigiWest analysis on the 32 mouse liver LCM samples and the intense pretesting ensured that most of them gave analyzable signals. Some of the assays were performed using the polymer buffer.

As the resulting samples were very limited, no protein determination of the samples was performed. Based on protein determination for pre-experiments the protein amount was expected to be about 2.5 µg. The data were normalized on the signal obtained with Streptavidin-PE which can be used for relative on-bead protein determination as demonstrated.

As GS staining was used for visualization of zonation (see Fig. 22) and areas surrounding blood vessels showing GS staining were collected as pericentral areas and unstained areas surrounding blood vessels were collected as periportal areas, purity of the collected cells was tested using an anti-GS antibody in a DigiWest assay. The average ratio of the GS signal obtained for GS positive (pericentral) relative to GS negative (periportal) areas was 470 (mean) or 480 (median) over all 32 samples (16 mice). The periportal marker E-cadherin did only give analyzable signal on the periportal samples and no analyzable signal on the pericentral samples. So the periportal and pericentral areas were properly separated. Different cytochrome P450 antibodies were also included as an additional quality control. For cytochrome P450s which have been described to be induced by TCPOBOP treatment, antibodies recognizing members of the Cyp3A, Cyp2B and Cyp2C families were used. All three cytochrome P450 antibodies showed the expected induction.

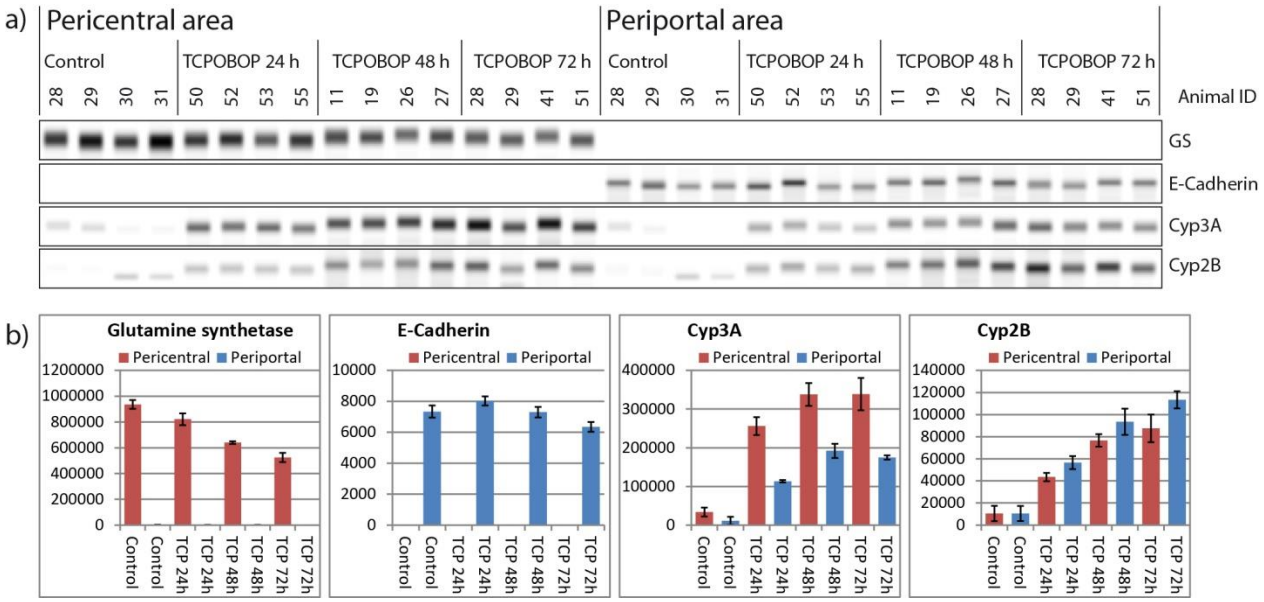

FIGURE 23 QUALITY CONTROL OF THE LCM EXPERIMENT

As quality control, the zonal markers glutamine synthetase (pericentral) and E-cadherin (periportal) and cycochrome P450 antibodies (Cyp3A and Cyp2B) were used. ***a)*** *Western-Blot mimics generated from background subtracted raw data. The slight differences in the positions of the bands are based on the initial Western-Blots and the cutting positions for the molecular weight fractions.* ***b)*** *Diagrams representing the integrated signals of the peaks (AFI). The median of the 4 mice in each group is shown with standard error. Data are normalized on total protein using Streptavidin-PE as mentioned. The zonal markers confirm a good separation of the zones and the cytochrome P450s respond to TCPOBOP treatment as expected.*

3.8.2 Issue with unspecific recognition

An additional band was observed for some analytes at about 40 kDa which showed complete pericentral zonation and a signal decay over the time course. Therefore, this band showed similar behavior than GS (glutamine synthetase) and exactly overlaid the bands for GS. This band was observed for Cyclin A, IDH2, IRAK4, HDAC1, PKA C alpha and PTCH2 but was not observed in experiments using fresh frozen liver lysates. The molecular weight resolution of the DigiWest method allowed identification of those additional bands and kept analyzability of the bands at the proper molecular weight. Interestingly, when some of these antibodies were used for validation of the results in immunohistochemical staining (IHC) by Elke Zabinsky, the antibodies showed a staining pattern resembling the GS stain but only when formalin fixed (FFPE) sections were used. The GS-like stain was not visible on fresh-frozen sections. So probably the formalin treatment created cross-reactivity for GS that was recognized by several antibodies. The same phenomenon was observed for some more antibodies showing an additional band at about 50 kDa which showed pericentral zonation and an induction in the time course. The additional band was observed for the antibodies recognizing Cox1, Cox2, DKK1, E2F4 and Elk1.

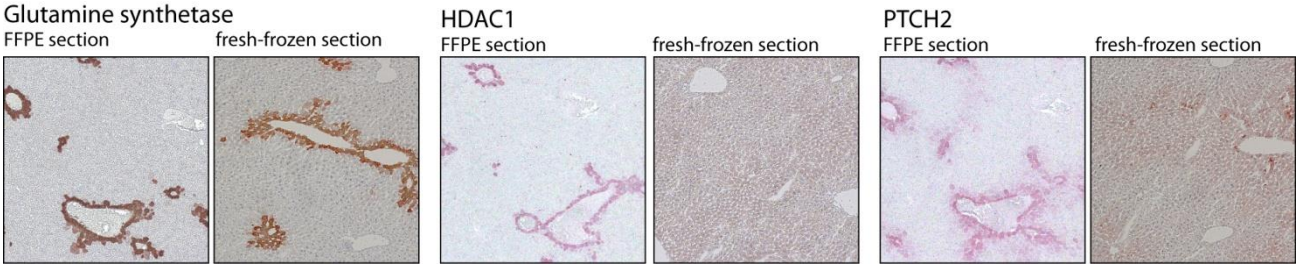

FIGURE 24 ADDITIONAL BANDS OBSERVED FOR SOME ANTIBODIES

Shown is the staining of glutamine synthetase on FFPE and fresh-frozen liver sections. Some analytes showed additional bands at 40 kDa which were completely zonated and showed similar behavior than GS. HDAC1 is one of these. The GS-like staining pattern only appeared on FFPE sections, the same was observed for cyclin A. PTCH2 showed the 40 kDa additional band but also a completely zonated band at the correct molecular weight (120 kDa). The FFPE-stain should represent an overlap of these two bands while on the fresh-frozen section the signal should be PTCH2-specific.

The molecular weight resolution of the DigiWest method allowed differentiation of the bands and kept analyzability for those analytes. Besides these additional bands there some more analytes which showed additional bands at 'wrong' molecular weights. In some cases these additional bands could be allocated to specific isoforms or variants of the proteins but in some cases they could not be allocated and were

discarded. The antibody recognizing RXRα showed an additional band which might represent RXRβ or might be an additional band and the antibody recognizing RAD23B showed an additional band which might represent RAD23B isoform 2 or RAD23A. The 40 kDa and 50 kDa bands observed for some analytes mentioned above were discarded.

3.8.3 Liver zonation

The first part of data analysis focused on proteins that showed a zonated distribution in the untreated animals. For this analysis all signals were normalized on the median of the pericentral zone of the control group and log2 transformed. Therefore, the following data represent the differences in the periportal zone (median) relative to the pericentral zone (median). The median was chosen because it is more stable to outliers and there is some variation in between the individual animals.

T-tests were performed for statistical analysis using the MEV software package for all analytes that gave analyzable signals on both zones. The following analytes are not shown because they were only detectable in one zone: E-cadherin (periportal only), PTCH2 (pericentral only) and Cyclin A (periportal only). To represent the complete data set in one graph, the volcano plot representation was chosen.

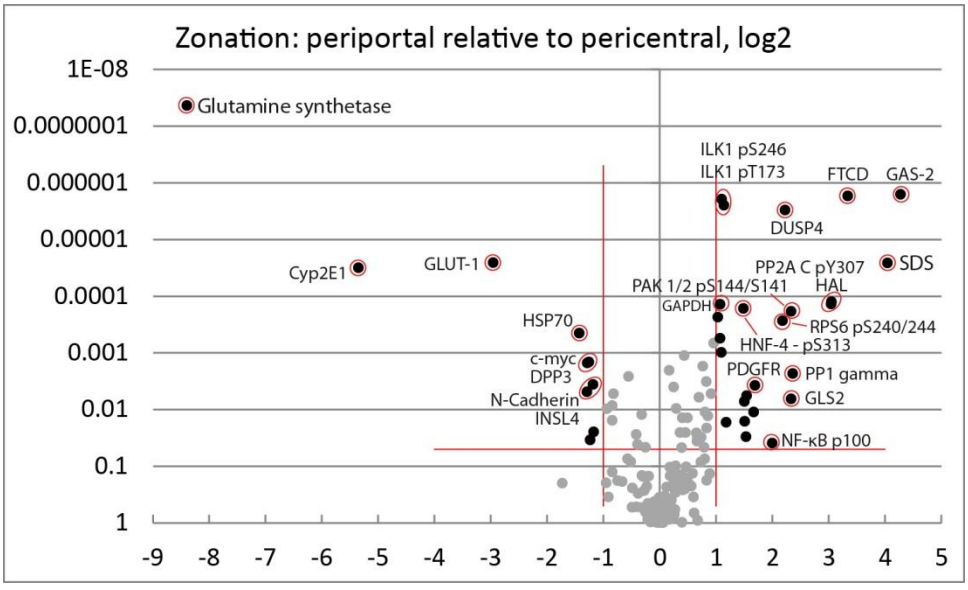

FIGURE 25 ZONATED ANALYTES

Volcano plot: Shown are all analytes which gave analyzable signal on pericentral and periportal samples from the control group. The data contained in this plot are derived from more than 1500 Western-Blot lane equivalents. The log2 fold difference of the periportal zone relative to the pericentral zone is shown on the x-axis and the statistical significance represented by the p-value of the t-test on the y-axis.

Significant analytes (Log2 fold difference >1, p<0.05) are shown in black, non-significant ones in gray. Several of the analytes which show significant zonation are highlighted.

The following table contains all significantly zonated analytes from this analysis.

Analyte	Ratio GS-/GS+	Log2 Fold	p-Value
Cyclin A	Periportal	NA	NA
E-Cadherin	Periportal	NA	NA
GAS-2	19.42	4.28	1.62E-06
SDS (serine dehydratase)	16.53	4.05	2.63E-05
FTCD	10.16	3.34	1.72E-06
HAL (histidine ammonia lyase)	8.31	3.05	0.00013
PP2A C - pY307	8.29	3.05	0.00014
PP1 gamma	5.15	2.37	0.0023
PAK 1/2 - p S144/S141	5.06	2.34	0.00019
GLS2 (Glutaminase 2)	5.06	2.34	0.0065
DUSP4	4.69	2.23	3.04E-06
RPS6 - pS240/244	4.54	2.18	0.00027
NF-κB p100/p52 - p100	4.01	2.00	0.039
PDGF Receptor beta	3.24	1.70	0.0038
ASL (argininosuccinate lyase)	3.19	1.67	0.011
RAD23B (hHR23b) - Isoform 1	2.92	1.55	0.0057
PGC1 alpha - pS571	2.90	1.54	0.030
p53	2.85	1.51	0.016
c-Jun	2.84	1.51	0.0072
HNF-4 - pS313	2.81	1.49	0.00017
AMPK alpha	2.28	1.19	0.017
ILK1 - pThr173	2.21	1.14	2.50E-06
ILK1 - pS246	2.15	1.11	1.95E-06
PTPN7 (LC-PTP, HEPTP) - 52 kDa Isoform 3	2.15	1.10	0.00099
PKC alpha/beta II - pT638/641	2.11	1.08	0.00055
GAPDH	2.11	1.08	0.00014
PTPN7 (LC-PTP, HEPTP) - 40 kDa Isoform 1	2.05	1.04	0.00023
MEK1/2 - p Ser217/221	0.446	-1.17	0.025
N-Cadherin	0.441	-1.18	0.0036
RAD23B (hHR23b) - Isoform 2 (or RAD23A)	0.427	-1.23	0.034
c-myc	0.419	-1.25	0.0015
DPP3 (Dipeptidyl-peptidase 3)	0.412	-1.28	0.0015
INSL4	0.410	-1.29	0.0049
HSP70	0.373	-1.42	0.00045
GLUT-1	0.129	-2.95	2.58E-05
Cyp2E (Cyp2E1)	0.0246	-5.35	3.18E-05
Glutaminsynthetase	0.0030	-8.39	4.39E-08
PTCH2	Pericentral	NA	NA

TABLE 2 ANALYTES WHICH SHOWED STATISTICALLY SIGNIFICANT ZONATION IN THE CONTROL GROUP

This table shows all significantly zonated analytes with a ratio periportal to pericentral > 2 (log2 >1) and a p-value < 0.05. 38 analytes hit these criteria. Shown is the median of the periportal (GS-) relative to

pericentral (GS+) samples with Log2 fold difference and p-value (t-test) sorted by fold difference. The analytes which were only detectable in one zone are included.

Several of the statistically significant analytes are enzymes known to be zonated. But the set also contains some kinases, phosphatases and transcription factors involved in cellular signaling. Some analytes showed a high variance between the animals within one group resulting in larger p-values and less significance; some seem to be very stably expressed.

These results confirm some published knowledge on zonation of enzymes. SDS (serine dehydratase) is known to be periportllay zonated (Ogawa & Kawamata, 1995), Cyp2E1 is known to be pericentrally zonated (Kai O. Lindros, 1997) as is GLUT-1 (Bilir et al., 1993). FTCD (glutamate formiminotransferase) and HAL (histidine ammonia lyase) are zonated periportally and others have been described based on mRNA data (Braeuning et al., 2006).

For a more familiar visualization of the DigiWest data, a collection of significantly zonated analytes was used to generate Western-Blot mimics.

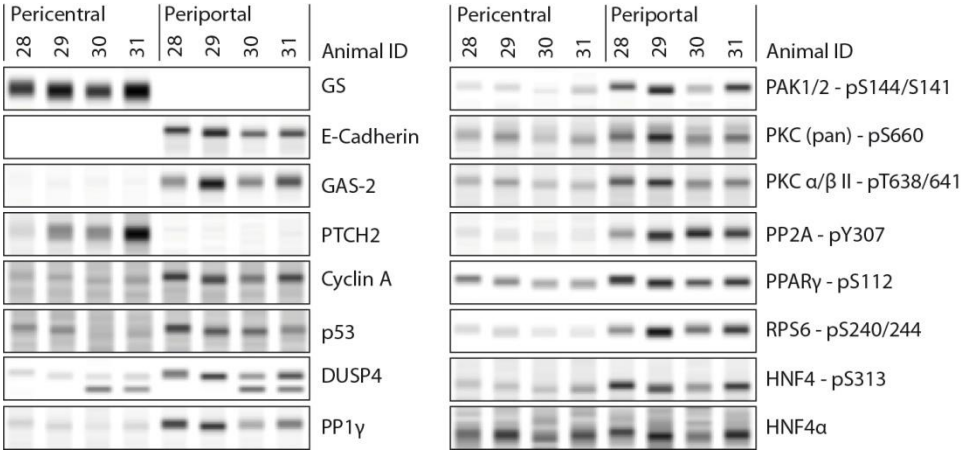

FIGURE 26 COLLECTION OF ZONATED ANALYTES AS WESTERN-BLOT MIMICS

A collection of statistically significantly zonated analytes represented as Western-Blot mimics. The images are based on the background subtracted DigiWest data without normalization. Normalization on protein amount was performed after quantification of the bands/peaks. The analytes with complete zonation which were not contained in the statistical analysis (E-Cadherin, PTCH2 and Cyclin A) are also included.

GS and E-Cadherin are known zonation markers and show perfect localization in the periportal and pericentral hepatocytes. PTCH2 is a Hedgehog receptor which has not yet been described as being

zonated. HNF4α protein which is also included in the Western-Blot mimics did not show significant zonation but the phosphorylation of HNF4α at Ser313 showed a periportal zonation.

GAS-2 has been shown to be zonated on mRNA level (Braeuning et al., 2006) which fits the observation on protein level. GAS-2 is an inhibitor for the protease calpain and was shown to stabilize p53 (Benetti et al., 2001) which is in agreement with the localization of the p53 protein in this dataset.

Several phosphatases, kinases and phosphorylations are found to show a zonal distribution. A prominent phenomenon is that several serine and threonine phosphorylations show periportal zonation which is part of the discussion.

3.8.4 Zonation and drug response: a short overview

The data set contains the TCPOBOP treatment time course and the zonation. Depending on the analysis, data were either normalized on the median of the zone specific control group or on the median of all controls (periportal and pericentral). The following figure represents the whole data set (median values of the groups) for a first overview. Data for each zone were normalized on the median of the corresponding control group and log2-transformed.

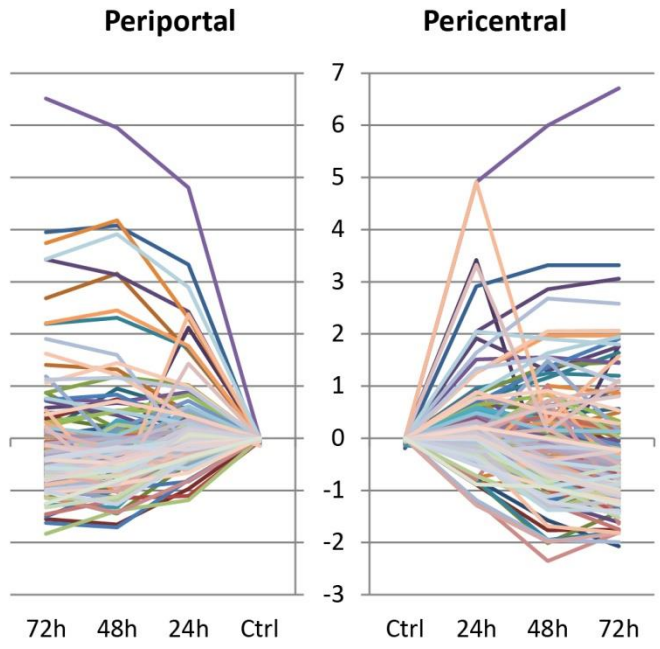

FIGURE 27 OVERVIEW OF THE COMPLETE TIME COURSE DATA-SET

Shown are the log2-fold changes (median values) relative to the control (normalized on the median of the corresponding control group) for all analytes in the time course representing the whole data set.

Besides some analytes showing strong effects, the data show a global tendency of a slight decrease over the time course. This phenomenon might be based on hypertrophy during TCPOBOP treatment and will be part of the discussion.

Two microarray analysis techniques capable of time course analysis for groups of samples were employed for detecting drug effects over time. For analysis of the whole data set, the data were normalized on the median of all controls (pericentral and periportal) and log2 transformed. In a first analysis, LIMMA (Linear Model for Microarray Analysis) was employed which uses two conditions, in this case the periportal and the pericentral location. The 4 time points (control, 24, 48 and 72 hours TCPOBOP treatment) were used for time course analysis. P-values for each condition and each time point could be calculated and the cut-off was set to $p < 0.05$. The results are lists giving significant analytes for each time point and condition. The data shown in the following figure are the significant analytes detected for all time points and both conditions (overall significant).

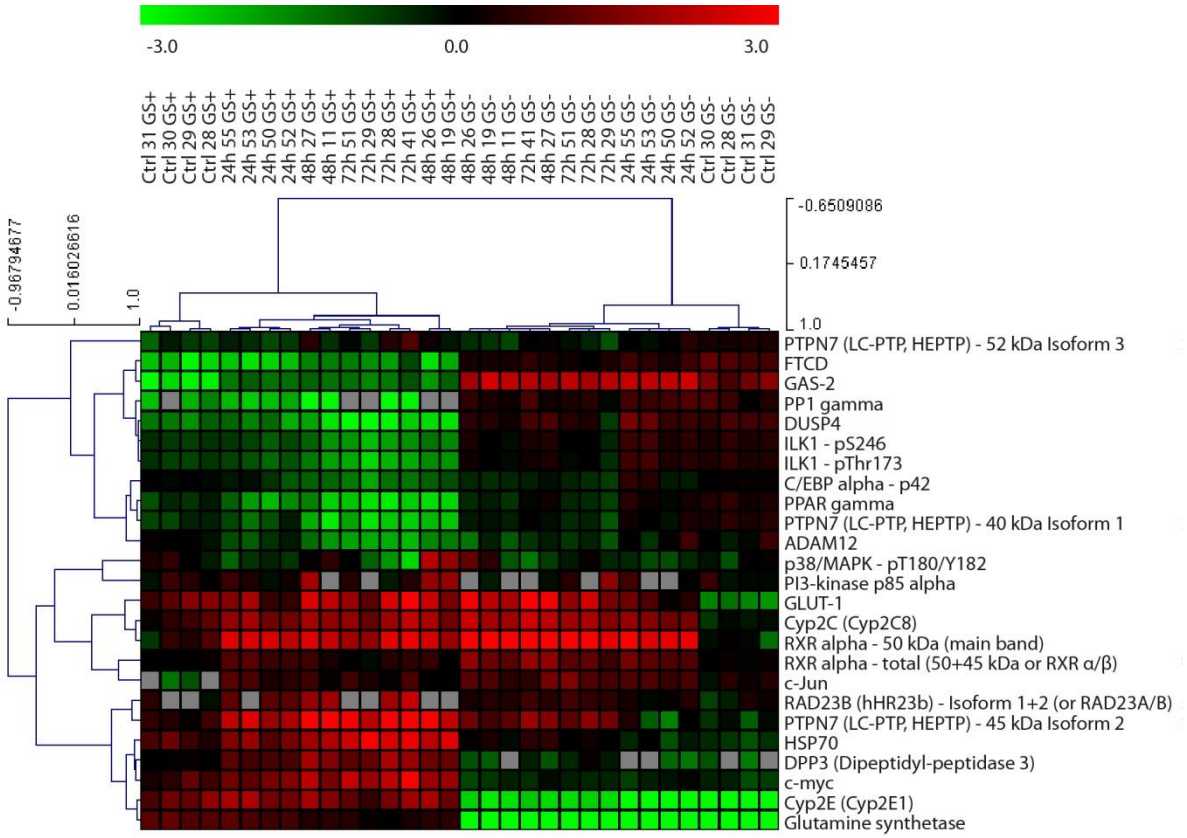

FIGURE 28 LIMMA ANALYSIS OF THE WHOLE DATA SET

Shown are the overall significant analytes (all time points, both conditions (zones)) from LIMMA analysis with p<0.05 in a heat map. The data are clustered by Pearson correlation. Some analytes were skipped

because there were no or not enough data for one or more time points for one of the conditions and the test needs data for both conditions and all time points.

For statistical significance the overall significant analytes from the LIMMA analysis have to show significant changes over the time course and between the zones. Several analytes show similar changes in the periportal and the pericentral zones and are therefore not contained in this analysis. This test is not perfectly suited for this data set as the two zones do not exactly represent two conditions to be compared like treatment and control. Time course effects are not represented well on the heat map representation, still the subset of significant analytes clustered in the correct groups and only the 48 hours and 72 hours treatment time points are not clustered correctly in the time course. Although the heat map shows only the group of overall significant analytes between all time-points and both conditions, there are still 25 analytes which show significant time course and zonation effects.

As DigiWest represents a new method, there are no established standards for data representation. Depending on the aspect of the data which should be highlighted, there are different representations favorable.

A collection of some analytes is represented as Western-Blot mimics in the next figure. This representation is useful as it is very similar to Western-Blots and familiar to scientists who are used to Western-Blot images. It focuses on molecular weight and also highlights variations between the samples or animals. The data represent paired samples as from each animal a periportal and a pericentral zone was isolated. As mentioned, background subtracted raw data are used for these representations without normalization on total protein.

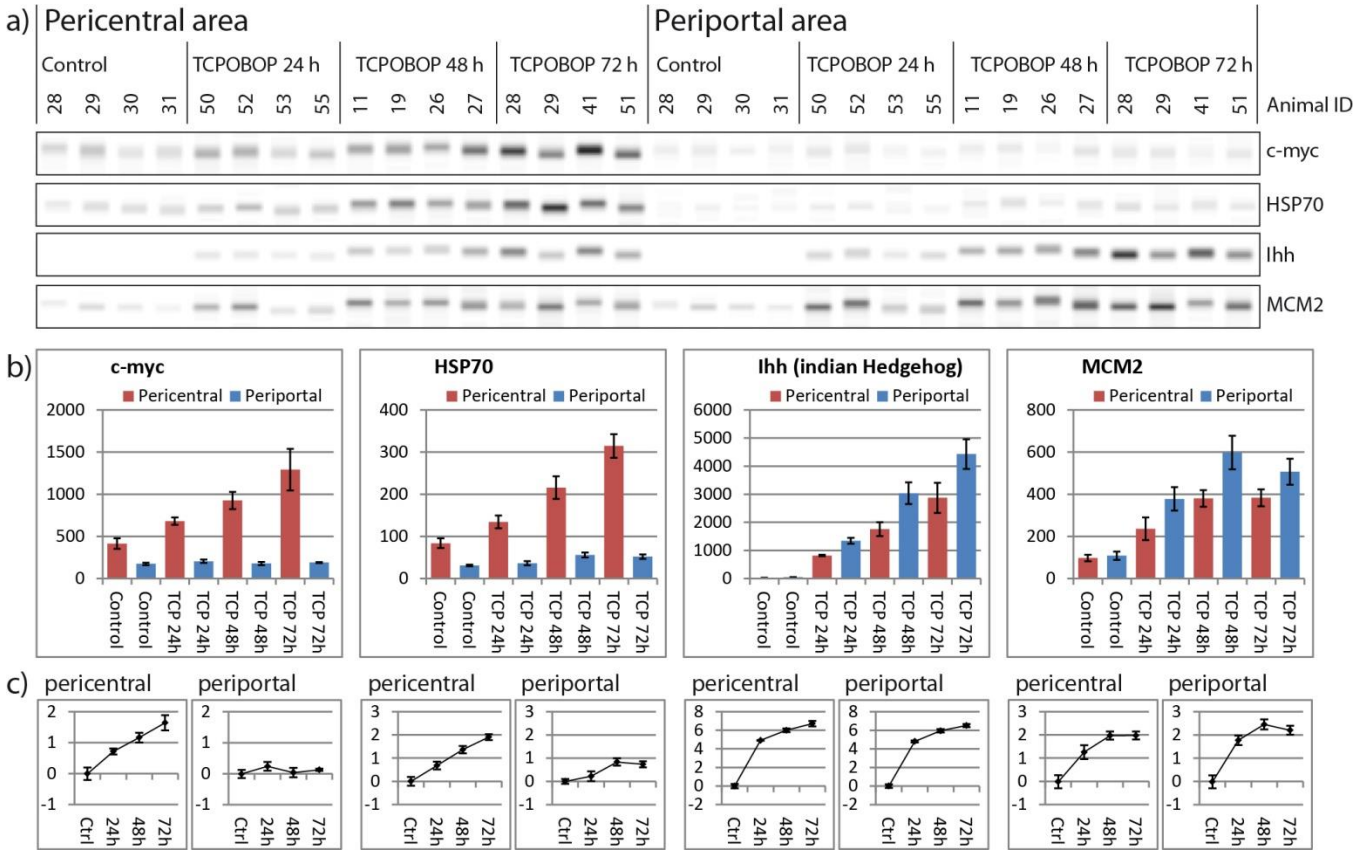

FIGURE 29 SELECTION OF WESTERN-BLOT MIMICS REPRESENTING THE WHOLE SAMPLE SET

Shown is a selection of some analytes on all 32 samples in different representations. Shown are c-Myc, HSP70, Ihh and MCM2. ***a)*** *Western-Blot mimics generated from background subtracted raw data.* ***b)*** *Same data shown as diagrams representing the integrated signal intensities (AFI) normalized on total protein, median with standard error.* ***c)*** *Same data again, shown as log2 fold change relative to control for each zone with standard error.*

It is known that c-Myc is induced upon TCPOBOP treatment in the mouse liver (Blanco-Bose et al., 2008; Donthamsetty et al., 2011). But it was not known yet that this effect is completely restricted to the peri-central zone, there is no change detectable in the periportal zone. HSP70 has not yet been described in context with TCPOBOP but as it is a stress related protein this is not surprising. HSP70 induction is also restricted to the pericentral zone but there is a lower induction in the periportal zone.

Ihh (indian Hedgehog) is a ligand from hedgehog signaling and is induced in periportal and pericentral zones. Hedgehog signaling plays an important role in liver development and regeneration and induction of Ihh has been reported after partial hepatectomy and under conditions which might induce apoptosis (Ochoa et al., 2010; Omenetti, Choi, Michelotti, & Diehl, 2011).

MCM2 (Minichromosome maintenance protein 2) has been observed on mRNA level to be induced by TCPOBOP (Leoni et al., 2011). It is induced in both zones to a similar extend.

The molecular weight resolution allows identification of additional bands which could be isoforms but can also be additional bands. All analytes which are described as isoforms here could be isoforms as there are known isoforms with the appropriate molecular weight but they could also be additional bands from other proteins which cross react with the antibody.

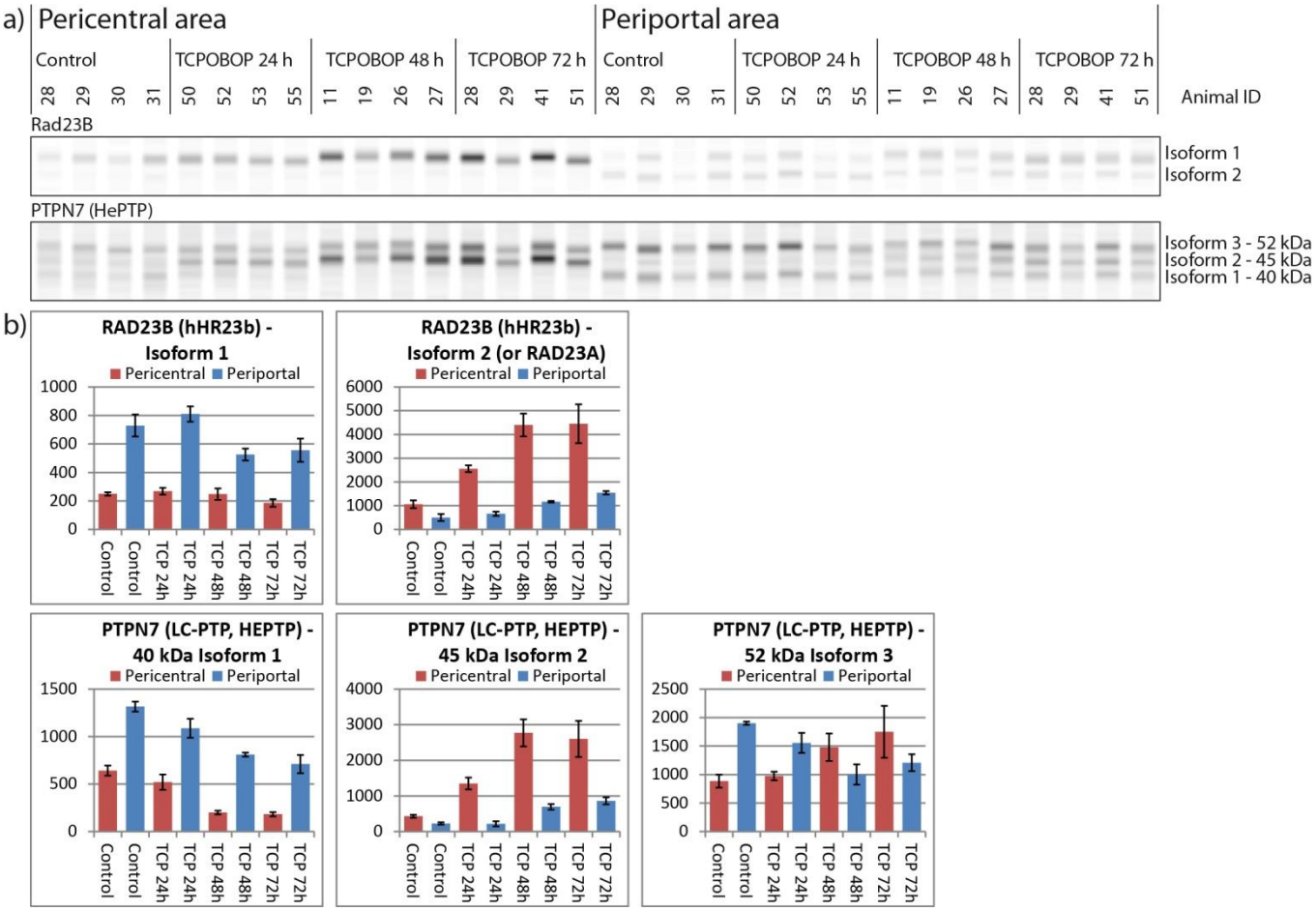

FIGURE 30 SELECTION OF ANALYTES SHOWING POTENTIAL ISOFORMS

Shown are RAD23B and PTPN7 as examples of observable isoforms. UV excision repair protein RAD23 homolog B has 2 known isoforms (in humans) but it is also possible that the observed additional band might represent RAD23A. The phosphatase PTPN7 has 3 known isoforms (in humans). ***a)*** *Western-Blot mimics of RAD23B and PTPN7.* ***b)*** *Integrated signals for the individual isoforms in [AFI] with standard error. RAD23B isoform 1 is zonated periportally and does not respond to TCPOBOP treatment while isoform 2 (or RAD23A) is pericentrally zonated and induced by TCPOBOP. The 3 isoforms of PTPN7 also*

show different behavior. Isoform 1 is periportally zonated and down regulated by TCPOBOP while isoform 2 is pericentrally zonated and induced. Isoform 3 shows high variation within the groups with a tendency to induction in the pericentral zone and down regulation in the periportal zone.

As mentioned before these isoforms could also represent additional bands. There is no knowledge about the meaning or regulatory differences for these potential isoforms at this time. The UV excision repair protein RAD23 homolog B is involved in DNA repair. It might be possible that the 2 bands correspond to RAD23B and RAD23A. The hematopoietic tyrosine phosphatase PTPN7 is a mitogen-activated protein kinase phosphatase which can inactivate Erk and p38 (Nika et al., 2006). There is nothing known yet about the potential functions of the different isoforms.

3.8.5 Zonation and drug response: pericentral effects

In this analysis only the pericentral areas were analyzed to further investigate the TCPOBOP treatment time course. Data were normalized on the median of the control group of the pericentral samples. BETR (Bayesian Estimation of Temporal Regulation) was used as microarray analysis technique which is also implemented in MEV. BETR takes sample and time point information into account to detect differential expression in time-series data (Aryee, Gutiérrez-Pabello, Kramnik, Maiti, & Quackenbush, 2009). Significance was calculated based on a p-value <0.05 resulting in 66 significant analytes.

To identify analytes with similar response to TCPOBOP treatment, the significant analytes were clustered by Pearson correlation.

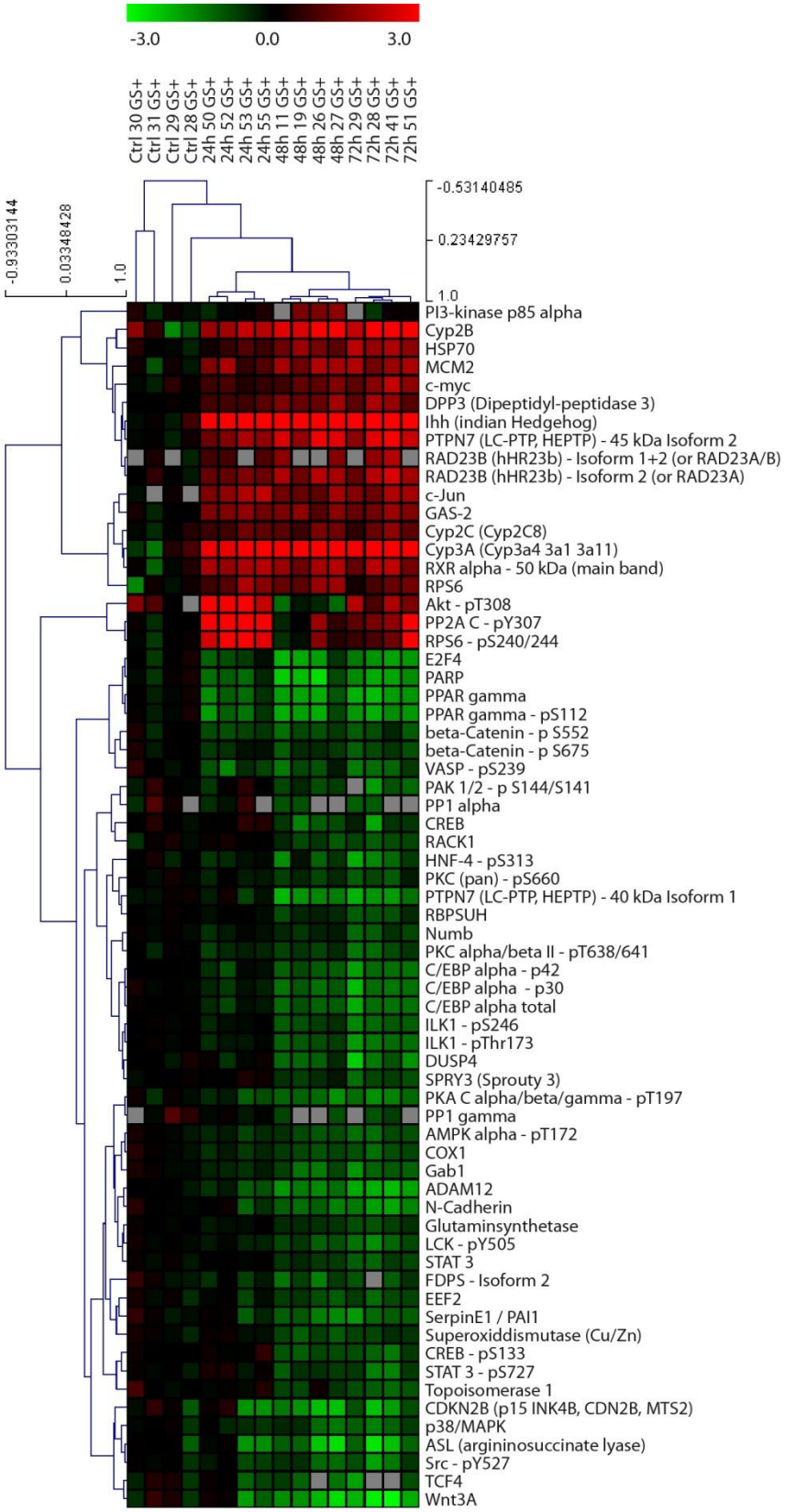

FIGURE 31 BETR TIME COURSE ANALYSIS OF THE PERICENTRAL AREAS

The heat map shows all 66 analytes which were significant ($p < 0.05$) in the BETR analysis clustered by Pearson correlation. The analyte tree on the left represents the similarity of the analyte behaviors. All samples are clustered in the correct order.

There are many interesting changes on protein level in the pericentral areas and all samples cluster in the correct order. The time course effects are not well visualized in the heat map. Therefore, small diagrams were generated showing the log2-fold change relative to control and standard error within the groups. The same 66 analytes were used and grouped based on Pearson correlation corresponding to the analyte tree of the heat map in figure 31.

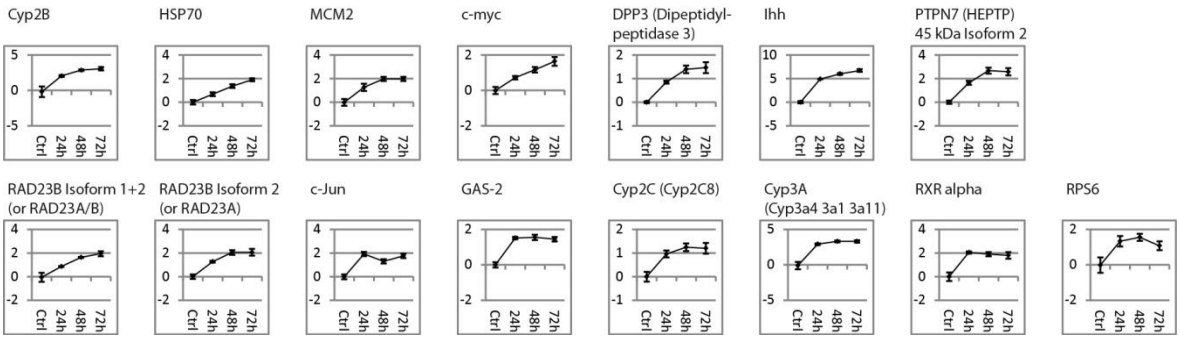

FIGURE 32 UP-REGULATED ANALYTES IN PERICENTRAL AREAS

Up-regulated analytes in pericentral areas based on BETR analysis. Data are medians of the groups shown in log2 fold change relative to the control group with standard error. Analytes are grouped by Pearson correlation corresponding to the analyte correlation tree of the previous heat map.

Besides the analytes shown as examples in the short overview section there are several more analytes which are induced upon TCPOBOP treatment.

As TCPOBOP induces hepatocyte hyperplasia with a proliferation peak at 24 to 48 hours (Donthamsetty et al., 2011) it is expected that some analytes show peaks at these time points.

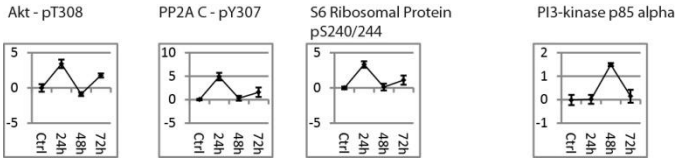

FIGURE 33 ANALYTES WITH MAXIMA AT 24 OR 48 HOURS TREATMENT IN PERICENTRAL AREAS

Data represented in log2 fold change with standard error. RPS6 (S6 ribosomal protein) phosphorylation, PP2A C (protein phosphatase 2 catalytic sub unit) phosphorylation and Akt Thr308 phosphorylation show a peak at 24 hours TCPOBOP treatment. PI3-kinase p85 shows a peak at 48 hours treatment.

S6 ribosomal protein phosphorylation is associated with increased proliferation and protein synthesis (Stewart & Thomas, 1994). Akt (PKB) is phosphorylated at Thr308 by PDK1 and has been shown to be involved in liver regeneration (Haga et al., 2009). Akt and S6 kinase, the kinase phosphorylating S6 ribosomal protein, are both phosphorylated by PDK1 and are both dephosphorylated by the phosphatase PP2A (Bononi et al., 2011; Shiojima & Walsh, 2006). The phosphorylation of PP2A catalytic subunit at Tyr307 inhibits phosphatase activity (J. Chen, Martin, & Brautigan, 1992) which fits to the observation of the phosphorylation peaks. PI3-kinase shows a peak at 48 hours.

There are more analytes which show peaks at either 24 or 48 hours, but their changes were not found to be statistically significant. As can be observed in figure 27 representing the whole time course data-set, there are several analytes which show a slight and not significant peak at the 24 hour time point.

A large number of analytes showed down-regulation in the pericentral zone during the TCPOBOP time course.

FIGURE 34 DOWN-REGULATED ANALYTES IN PERICENTRAL AREAS

Down-regulated analytes on pericentral side based on BETR analysis. Data are shown in log2 fold change relative to the control group with standard error. Analytes are grouped by Pearson correlation corresponding to the analyte tree of the heat map in figure 31.

Most of the phosphorylations with significant changes are down-regulated during the time course and also a large number of proteins. There are also some phosphorylations which are pericentrally zonated and some which do not decrease but they are not statistically significant. There are several possibilities which might explain this. It could be due to hypertrophy and increase in cell size and the induction of drug metabolizing enzymes during the time course which might lead to a decrease of phosphorylated proteins relative to the total protein in the samples. Phosphatases could also play a role. This observation is part of the following discussion.

The following figure shows some of the significantly changed analytes from the previous figures as Western-Blot mimics.

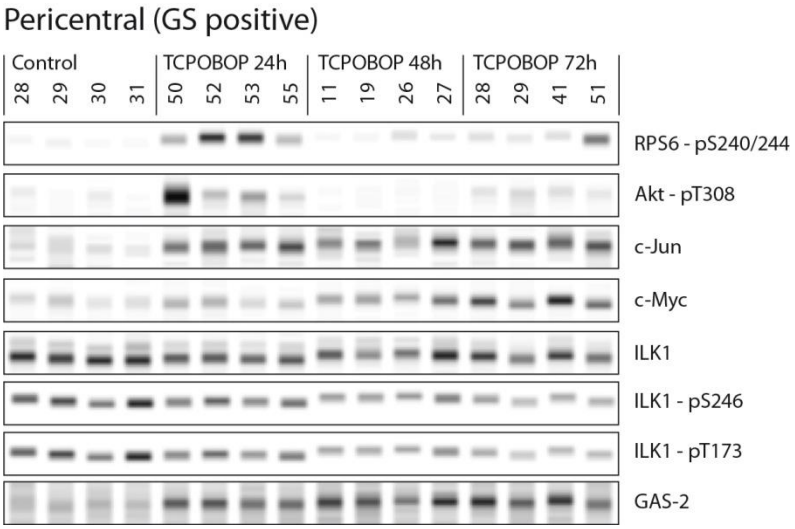

FIGURE 35 COLLECTION OF WESTERN-BLOT MIMICS

Shown is a selection of significantly changed analytes from the previous BETR analysis of the pericentral zone represented as Western-Blot mimics based on the background-subtracted raw data.

Taken together, there are many changes observed in protein expression and phosphorylation in the pericentral areas of the mouse livers during the TCPOBOP treatment time course. Some of them will be part of the discussion.

3.8.6 Zonation and drug response: periportal effects

The BETR analysis performed for the pericentral zones was also performed for the periportal zones. Data were normalized on the median of the periportal control group and log2 transformed. BETR analysis with a p-value <0.05 was performed. 36 analytes showed significant changes in this time course analysis.

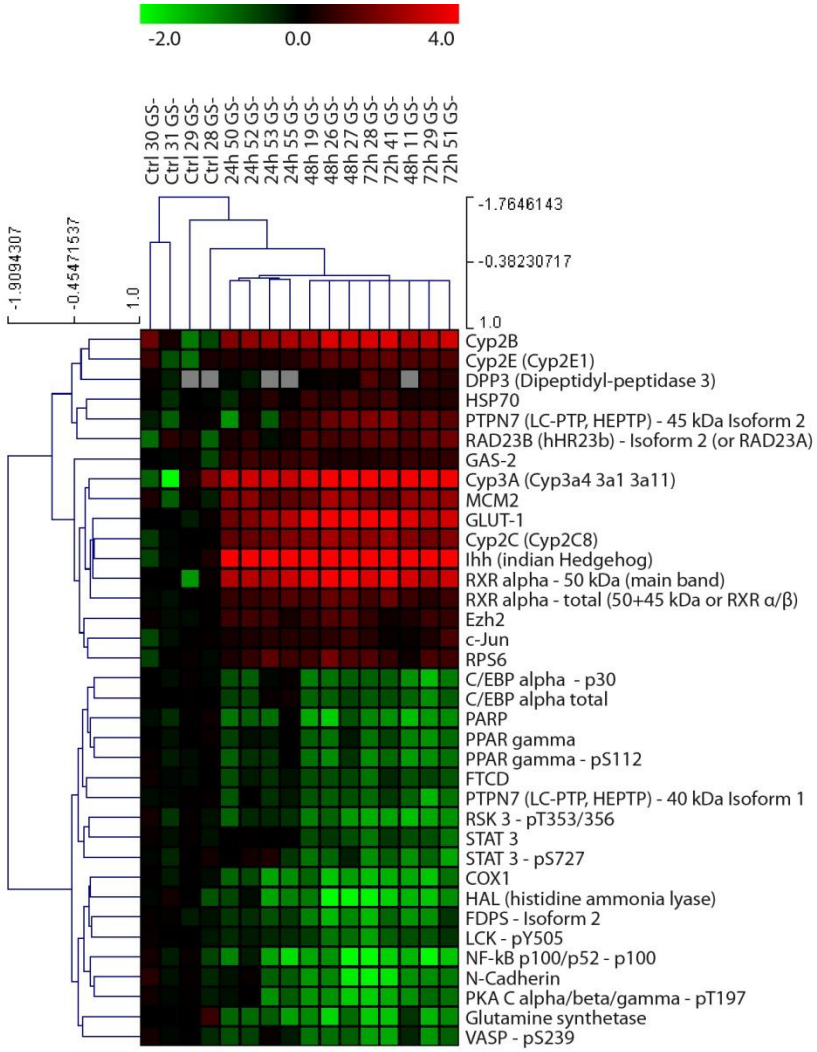

FIGURE 36 BETR TIME COURSE ANALYSIS OF THE PERIPORTAL AREAS

The heat map shows all 36 significant analytes ($p<0.05$) form the BETR analysis of the periportal zones again clustered by Pearson correlation to cluster analytes with similar behavior. The sample groups are almost completely clustered according to the time course; only the 48 hours and 72 hours TCPOBOP treatment groups are not properly clustered.

The observation that the 48 hours and 72 hours TCPOBOP treatment groups are not separated properly is based on the fact that most analytes do not show a continuous increase or decrease over time but they reach a plateau at 48 hours or in some cases go through a maximum effect followed by reduction.

Again, the Pearson correlation tree was used to identify analytes with similar behavior and diagrams showing the log2 fold change relative to the control group (medians with standard error) were generated and arranged according to the correlation tree of the heat map in figure 36.

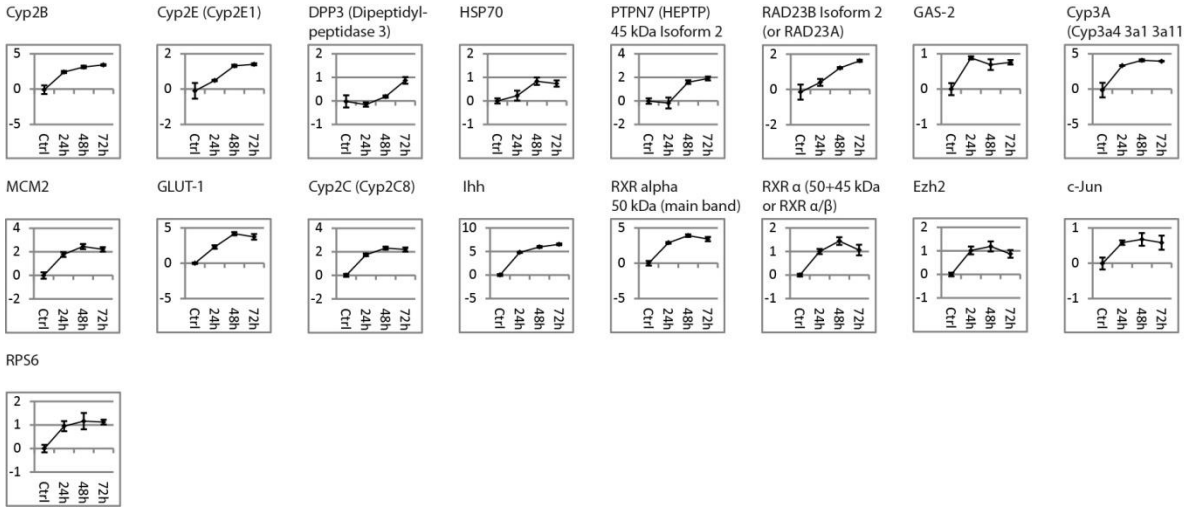

FIGURE 37 UP-REGULATED ANALYTES IN PERIPORTAL AREAS

Analytes which are up-regulated during TCPOBOP treatment time course in periportal areas based on BETR significant analytes. Data are shown in log2 fold change with standard error. Analytes are grouped by Pearson correlation corresponding to the analyte tree.

As mentioned, in the periportal zones there are not these clear increases or decreases over the time course than observed for the pericentral zones. Several of the up-regulated analytes observed in the periportal zones were also found up-regulated in the pericentral zones. An analyte which was not statistically significant in the pericentral zone is EZH2 which seems to be unaffected by TCPOBOP in the pericentral zones but is up-regulated in the periportal zones. EZH2 is a histone methyltransferase and part of the chromatin remodeling polycomb repressive complex 2 (PRC2). It is meant to be associated with hepatocyte proliferation and differentiation (Aoki et al., 2010).

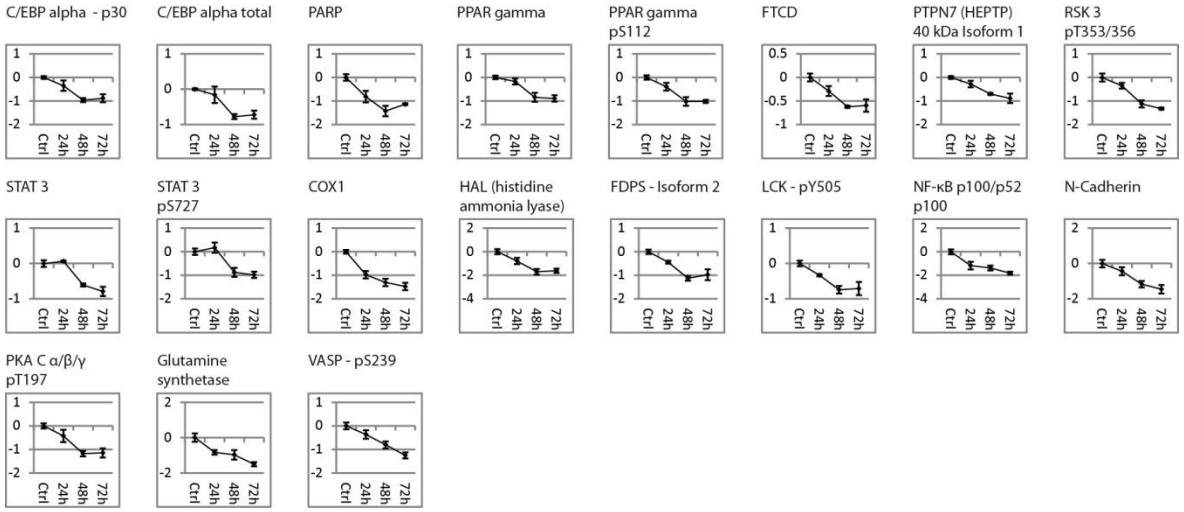

FIGURE 38 DOWN-REGULATED ANALYTES IN PERIPORTAL AREAS

Analytes which are down-regulated during TCPOBOP treatment time course on periportal side based on BETR significant analytes. Data are shown in log2 fold change with standard error. Analytes are grouped by Pearson correlation corresponding to the analyte tree.

As already seen for the pericentral zones there are several phosphorylations which are statistically significantly down-regulated. This observation is addressed in the discussion.

Interestingly, the analytes showing maxima at 24 or 48 hours TCPOBOP treatment which were significant in the analysis of the pericentral areas are not statistically significant in the periportal areas. The observed maxima were also found in the periportal areas but they were less distinctive.

The following figure shows some of the analytes which were found to be significantly changed during the TCPOBOP time course in the periportal areas, represented as Western-Blot mimics.

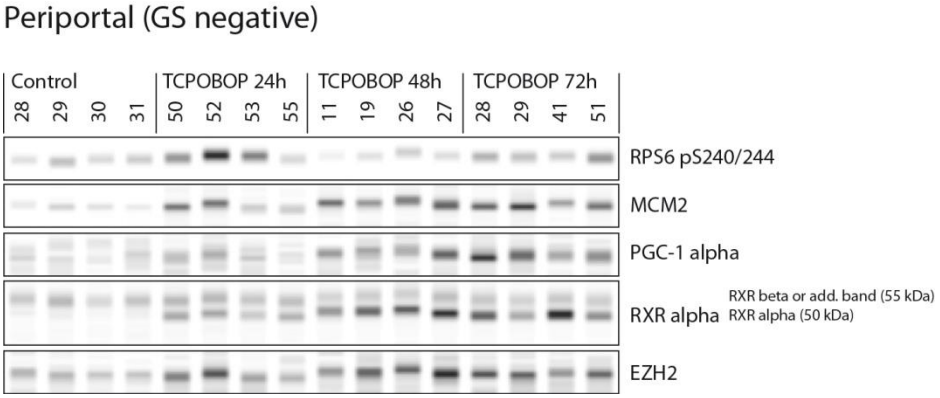

FIGURE 39 COLLECTION OF WESTERN-BLOT MIMICS

Shown are some of the analytes which show significant changes during the TCPOBOP time course in the periportal areas represented as Western-Blot mimics based on the background subtracted raw data. The phosphorylation of RPS6 also shows the peak at 24 hours after treatment but it was not found to be statistically significant by the BETR analysis. MCM2, PGC-1α and EZH2 show an induction in the time course. RXRα also shows an induction for the main band at 50 kDa while it also shows an additional band at 55 kDa which could represent RXRβ and does not show induction in the time course.

The number of analytes showing statistically significant changes in the TCPOBOP treatment time course in the periportal and pericentral areas shows that TCPOBOP has strong effects on cellular signaling. Some of the observed changes were found to a similar extend in periportal and pericentral zones while some effects were found to be restricted to one zone. The stronger effects in the time course were found in the pericentral zones. Some of the observations will be addressed in the following discussion.

3.8.7 Validation of the DigiWest results by immunohistochemistry

Some of the statistically significant analytes were stained on mouse liver sections for validation of the results. The IHC stains were performed by Elke Zabinsky in the group of Michael Schwarz. The observed periportal zonation of several phosphorylations was of special interest to confirm the DigiWest measurements. For each IHC stain, a GS stain was performed on a sequential section for identification of periportal and pericentral zones and a secondary antibody control was performed additionally to confirm signal specificity. All sections were formalin fixed and paraffin embedded except for the PTCH2 staining which showed the described cross reactivity with GS on formalin fixed sections. Therefore, a fresh frozen section was used.

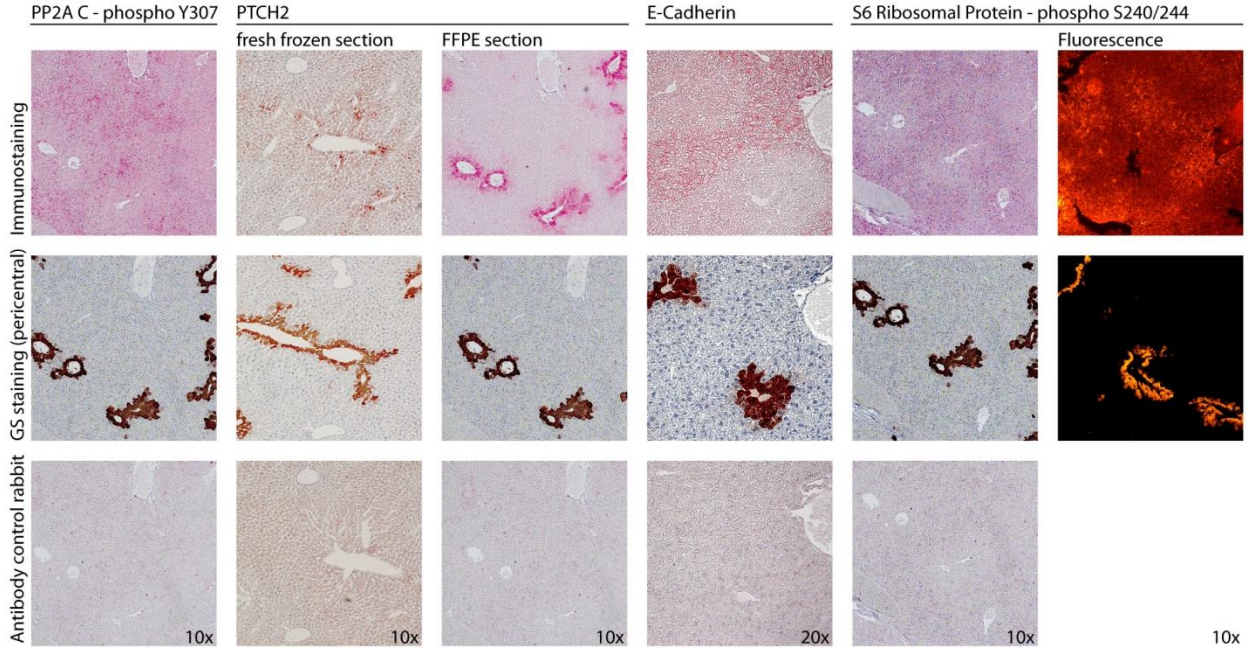

FIGURE 40 VALIDATION OF RESULTS BY IMMUNOHISTOCHEMISTRY

Immunohistochemical staining was performed for some analytes which showed statistically significant zonation in the DigiWest analysis. The periportal marker protein GS was stained on a sequential section for identification of the periportal and pericentral zones and a secondary antibody control was performed for validation of the signal specificity. The phosphorylation of the protein phosphatase PP2A C at Tyr307 shows the periportal zonation as observed in the DigiWest results. The same is true for the phosphorylation of S6 ribosomal protein (RPS6) which was additionally confirmed in a fluorescent stain. PTCH2 shows, as mentioned before, the observed pericentral zonation on fresh frozen and FFPE sections but on FFPE sections it shows cross-reactivity with GS. E-Cadherin is a known periportal marker.

The immunohistochemical stains confirmed the zonation of some proteins and phosphorylations observed in the DigiWest results. This is of special interest because several serine and threonine phosphorylations showed a periportal zonation which raised concern that this observation might have been an artefact. These images verify the results and prove the reliability of the DigiWest data. The following discussion also provides a reasonable explanation for the periportal zonation of the observed serine and threonine phosphorylations based on cellular signalling and zonation of phosphatases.

All antibodies used for IHC to validate the DigiWest data did either confirm the DigiWest results or did not show any staining as most of the antibodies used for DigiWest were not suited for IHC. None of the antibodies which were used for IHC showed conflictive results.

4 Discussion

Proteins play a pivotal role in cellular processes in health and disease. Changes in protein abundance and in the degree of posttranslational modifications indicate changes in the status of cells on the molecular level. Thereby, analysis of proteins improves our understanding of physiological and pathophysiological mechanisms. To gain insight into the complex interplay found in cellular signaling and to analyze the adaption of a cell or a living being to influences like drug treatment, it is necessary to look at as many factors as possible. Analysis using mass spectrometry has the advantage of being unbiased and allows de novo identification of changes in protein abundances or even in posttranslational modifications of proteins. Yet, the protein mixtures obtained from whole cells or tissues are often too complex for mass spectrometry analysis and laborious preprocessing steps are required to get this information. There are methods for specific depletion or enrichment like Kinobeads to reduce complexity to an analyzable level. Antibody based immunoassays are often better suited for the analysis of complex samples but the selection of antibodies brings in a bias. Nevertheless, immunoassays play a pivotal role in research and diagnostics. In research, Western-Blot is still a gold standard for semi-quantitative protein detection. Efforts in protein microarray technology resulted in an increased sample and analyte throughput but often combined with a loss of data quality. As in practice antibodies are often not perfect and show unspecific signal, the information of molecular weight generated by Western-Blot and identification of specific signal proved to be crucial.

Different methods have been developed that do provide an increased sample and analyte throughput and molecular weight information. The microwestern array, which spots the samples into a gel and runs them for approximately 9 mm before blotting onto a membrane, is a good example. Six samples are analyzed in parallel and up to 96 antibodies can be analyzed in one assay. Thereby, they address the sample and analyte throughput and introduce some limited information on molecular weight. The focus of this approach is on antibody throughput (Ciaccio, Wagner, Chuu, Lauffenburger, & Jones, 2010). Another method that needs to be mentioned is the Simple Western technology. This method uses capillary electrophoresis and by running up to 96 samples simultaneously, a high parallelization is achieved. Denaturing SDS-PAGE using gel containing capillaries separates proteins followed by immobilization by photo-activated capture chemistry. Antibody incubation is performed in the capillaries followed by chemiluminescent readout. The 96 capillaries can also be used to separate the same sample several times and incubation with different antibodies (Nguyen, Squaglia, Boge, & Fung, 2011; O'Neill et al., 2006).

The DigiWest method uses another approach with a focus on generation of high resolution molecular weight information, analyte throughput and on easy and reliable signal quantification. DigiWest represents a digitalized Western-Blot which allows generation of hundreds of identical replicas of a Western-Blot. It is a novel approach which combines advantages of Western-Blot and microarrays and thereby also provides new possibilities in protein research.

4.1 DigiWest

4.1.1 Development of the DigiWest method

A main part of this work was development of the DigiWest method, a system that utilizes standard Western-Blotting as integral part of its workflow. After gel electrophoresis and blotting, proteins are biotinylated on the blot and the lanes on the blots containing the separated proteins are cut into 96 strips, each 0.5 mm high, representing molecular weight fractions. All proteins contained in each fraction are eluted from the membrane strips and loaded onto Luminex beads. A collection of 384 distinct color-coded, magnetic Luminex bead-sets coated with NeutrAvidin is employed to load the eluted proteins. Each of the 96 molecular weight fractions is loaded onto a distinct bead-set and the 384 bead-sets allow loading of 4 initial Western-Blot lanes onto distinct bead-sets. After loading with proteins, the bead-sets are pooled into a DigiWest bead-mix. The information on the molecular weight fraction and its position on the initial Western-Blot are maintained in the color code of the beads. A bead-mix generated from one Western-Blot is sufficient for hundreds of antibody incubations in microtiter plate based assays. The signals obtained on each bead-set, for each antibody-incubation, are used to digitally reconstruct the initial Western-Blot. This is where the name is derived from.

This novel idea could be patent protected and the whole workflow realizing this approach had to be developed from scratch. Important aspects throughout the method development process were robustness and applicability in a routine workflow. A good quality and reproducibility of the initial blotting procedure including sample preparation and gel loading is mandatory. The use of a commercial system (NuPAGE) gave acceptable reproducibility and blotting homogeneity. The obtained reproducibility of the DigiWest method was comparable to regular Western-Blots with only a marginal increase of variation. Therefore the method is very robust. Cutting the lanes into 96 molecular weight fractions and the resulting distribution of the proteins on the fractions can lead to variation of the shape of the peaks in diagram representation, integration of the peak areas still results in robust signal intensities. This can be seen in the spike-in experiment where the peaks for the intrinsic ERK2 have very different shapes depending on the exact position of the cuts (Figure 17). An aspect which plays a role

here is that gels run slightly faster in the middle compared to the borders which leads to a slight shift when lanes are compared which are not directly adjacent. Biotinylation of the proteins on the membranes is very reproducible because the blots are biotinylated in a whole and all potentially interfering contaminants are washed off before biotinylation. Elution of the proteins from the molecular weight fractions in 96 well plates is a critical step and quantitative elution is required for reproducible results. An elaborate optimization was performed resulting in a simple protocol. The different NeutrAvidin coated bead sets represent the binding matrix for the biotinylated proteins. It is mandatory that all 384 bead-sets have the same biotin binding capacity to ensure reproducible loading of the biotinylated proteins. Irregularities in binding capacities could appear as a bias in the DigiWest results. A semi-automated coupling procedure employing the KingFisher magnetic particle processor resulted in high reproducibility of NeutrAvidin coupling and a CV below 3% for their biotin binding capacity was achieved for the used 384 bead-sets.

The assay buffer which is used for the antibody incubations has a strong impact and a new buffer was created based on a commercial ELISA buffer and supplemented with milk powder. This buffer showed a good performance for the vast majority of antibodies. A polymer based buffer was also developed which can be used to further increase signals.

Development of the DigiWest method resulted in a robust system with the main source of technical variance derived from the initial Western-Blots. The spike-in experiment shown in this thesis illustrates the high data quality and reproducibility that can be obtained with DigiWest. In this experiment, a constant amount of HepG2 cell lysate spiked with different amounts of GST-ERK2 was loaded onto the gel. The DigiWest bead-mixes were derived from 18 lanes which were distributed over 3 blots. The Western-Blot, which was performed to compare the results, was one blot with 15 lanes. The CV of the Western-Blot for intrinsic ERK2 was 6.44% and the CV for the DigiWest results using the same antibody was 9.57%. The increased CV is derived from the whole workflow including distribution over several blots. Similar DigiWest experiments containing fewer lanes which were processed using only one blot resulted in even lower CVs.

In this thesis only the commercial NuPAGE 4-12% Bis-Tris gels were used but as the DigiWest specific part of the method starts after proteins are blotted onto the membrane, all gel-separation systems which allow blotting of the proteins onto a membrane can be employed.

4.1.2 Data quality and performance

The data quality is also an important aspect. Molecular weight fractions of 0.5 mm result in 96 fractions covering the molecular weight range from more than 400 to about 10 kDa using the commercial mini gels. Reduction of the fraction size not only leads to a better resolution with shapelier peaks but also increases sensitivity and robustness. Smaller fractions lead to higher densities of the analytes on the individual Luminex bead-sets and distribution over more bead-sets also increases the overall binding capacity and reduces the background signal. The resolution of 96 fractions is good enough to differentiate for example ERK1 and ERK2 with 44 and 42 kDa. The two bands are often not completely separated as two peaks but appear as a double peak. The same is true for classical Western-Blots when the grayscale values are plotted into a diagram. So the limit for distinguishable peaks can be assumed to be about 5% difference in molecular weight and is comparable to standard Western-Blots.

A comparison of about 100 antibodies on Western-Blots and DigiWest showed a high similarity in the obtained band pattern (Appendix 1). Most antibodies showed the same additional bands for both methods. Differences between the two methods are mainly restricted to intensity and appearance of additional bands. Similar differences can be observed when Western-Blots are performed using BSA or milk powder as blocking reagents. Here, Western-Blots were performed using BSA as blocking reagent and for DigiWest a buffer was used which contains milk-powder.

The spike-in experiment showed that the linear range for DigiWest covers at least 3 orders of magnitude with good signal linearity. This experiment also proved that DigiWest allows absolute quantification of analytes if a known standard is used. The direct comparison of the DigiWest to the high-end infrared fluorescence based Licor Odyssey scanner proved that both systems have about the same sensitivity and signal linearity. The obvious advantage of the DigiWest method is the fact that the same amounts of sample and the same initial gel electrophoresis and blotting resulted in a bead-mix sufficient for 100 antibody incubations while the Western-Blot allowed only one antibody incubation.

4.1.3 Applicability of DigiWest

The innovation of the DigiWest method is that starting from one blot it provides hundreds of Western-Blot replicas. This allows detection of hundreds of analytes even on limited material like LCM samples. This was demonstrated in the experiment on mouse liver zonation where 200 antibody incubations were performed on LCM derived samples. The method is scalable in respect to the number of analytes and generation of a DigiWest bead-mix sufficient for 1000 antibodies or more is feasible, the main limitation for up-scaling is the amount of sample that can be loaded onto a lane on the initial gel. The bead-mixes

can be stored and used for follow-up assays. A scheduled stability test is still missing but bead-mixes were routinely used for additional assays after 6 months without observable disintegration.

The DigiWest method is also very economical in respect to buffer and antibody consumption compared to Western-Blots. DigiWest assays are run in microtiter plates and only 30 µl antibody dilution are needed per well. The DigiWest bead-mixes can be handled using pipettes or magnetic bead handling equipment allowing fast processing and providing the opportunity of automation solutions.

As mentioned in the introduction, a disadvantage of reverse phase protein microarrays is that they require advanced and complicated workflow and equipment. The DigiWest is based on the wide spread commercial Luminex platform. The workflow is obviously more complex than a classical Western-Blot but compared to the workflow of RPPMs, which includes pipetting robots and spotting robots, the Digi-West workflow is still pretty simple and besides Western-Blotting equipment and a Luminex instrument it needs only low-cost and low-tech equipment as long as no automation is required. Only for bead-coating and bead-plate preparation some robotic high-tech instruments were employed.

Taken together, DigiWest proved to be a robust method which creates hundreds of Western-Blot replicas with a good sensitivity, reproducibility and signal linearity. The experiments presented in this thesis show that it is possible to perform 200 Western-Blot-like analyses even from limited LCM samples and the Kinobead pulldowns show that it is also possible to analyze samples derived from affinity enrichment methods.

4.1.4 Properties of DigiWest

Transfer of the Western-Blot onto the bead-based Luminex platform results in completely changed properties. The bead-mixes can be seen as a kind of ‘liquid Western-Blot’ and allow assays in microtiter plates. The beads allow fast washing steps while for Western-Blots long washing steps are required, usually 5 times 5 or even 10 minutes. This is because Western-Blot membranes are a tree dimensional mesh with a thickness of 100 to 200 µm and an average pore size of typically 0.2 or 0.45 µm. Contrary to the typical saying ‘proteins are blotted onto a membrane’ they are actually blotted into a membrane, it is also possible to blot proteins through a membrane when blotting is performed for prolonged times. As proteins are blotted into a membrane and binding to the membrane is mainly based on hydrophobic interactions, accessibility and flexibility of the proteins are limited. On the DigiWest beads, proteins are immobilized on the surface of the beads with a flexible spacer. This results in increased flexibility and accessibility of the proteins and might explain the good sensitivity of the DigiWest method.

Another important property is that each aliquot of a bead-mix is – at least statistically – identical and each bead sets contains an unknown but defined mixture of proteins from a small molecular weight range. This allows global normalization strategies for example on the amount of loaded protein by on-bead protein determination using streptavidin-PE or by a marker analyte like β-Actin. An intrinsic molecular weight marker can be calculated based on the position of the peaks from a selection of analytes with different molecular weights to get a precise molecular weight marker. The digital Luminex data allow easy and fast quantification of the peaks without image processing as necessary for Western-Blot images. As DigiWest represents hundreds of Western-Blot replicas, it brings the Western-Blot towards a proteomic tool which allows system biology approaches from initial Western-Blots. The digital data can also be used to create images which look similar to real Western-Blots to represent data in a familiar way. Such Western-Blot mimics are shown several times in this thesis. An advantage of Western-Blot mimics compared to classical Western-Blots is that the digital data can be arranged as desired to represent the samples in the favored order and they allow combination of samples from several blots.

These features are not only distinctive differences to the classical Western-Blot but also to all other technologies for detection of molecular weight separated proteins. Besides the original idea of generating replicas of a Western-Blot, these properties can be exploited for new approaches for research as indicated in the outlook in chapter 4.4.

4.1.5 Issues and suggestions

An aspect which was not investigated in depth is the influence of biotinylation. The biotinylation reagent, which is reactive towards primary amino groups and therefore mainly modifies lysine residues, might have an influence on antibodies which bind a lysine-containing epitope. Some antibodies were selected known to have a lysine-residue in their epitope and they showed a specific peak at the correct molecular weight. As almost all antibodies which showed a specific band in a classical Western-Blot also showed a specific peak in the DigiWest data, biotinylation does not seem to be an issue and it is expected that only a fraction of the lysine residues is biotinylated. But biotinylation might have an effect on some antibodies.

As biotinylation is performed on primary amino groups, the number biotins on a protein should be dependent on the number of available amino groups which should lead to a bias in protein loading. Proteins which provide more primary amino groups might also provide more biotins and should therefore be more abundant on the DigiWest beads.

But, the main application of Western-Blots and therefore also of DigiWest is relative quantification and the relative abundance of a protein in a sample compared to another sample is determined. The influences of biotinylation should be the same for the same protein and antibody in each sample and therefore it should not represent an issue for relative quantification.
For absolute quantification, the biotinylation step could present an issue. In the experiment for absolute quantification presented in this thesis, the intrinsic protein ERK2 is quantified by usage of GST-ERK2 as standard, spiked into the samples. The GST-tag might have an influence on protein loading as it provides additional primary amino groups. A better setup for absolute quantification might be to use an untagged protein and process it on separate lanes of the gel. As mentioned, it is also expected that only a fraction of the lysine residues is biotinylated which might reduce the effect.

It is also expected that the proteins fold into secondary and tertiary structures after elution from the membrane which are not expected to represent the native conformations. Western-Blot antibodies are optimized for detection of denatured proteins and the expected folding of the proteins does not seem to be an issue as almost all antibodies which worked in Western-Blot also worked for DigiWest indicating that the epitopes are accessible. Without objective investigation, the direct comparisons of Western-Blots and DigiWest give the impression that DigiWest shows less unspecific signal.

The workflow might need some further improvements towards a higher grade of automation. Cutting of the membranes employing a cutting plotter represents an intermediately optimized step of the work-flow. It might be helpful to have a cutting tool which is optimized for this application.

Another aspect is the throughput in respect to the number of samples. At the moment 96 bead sets are used for each sample and 4 samples can be pooled into one DigiWest bead-mix. It is possible to increase the number of samples per bead-mix to 5. For more samples it is necessary to generate more bead-mixes. It is also necessary to keep empty lanes between the samples on the gel for cutting the membranes after blotting. This results in a limitation of 6 samples on a 15 well gel. The experiments in this thesis, especially the mouse liver LCM experiment using 32 samples, proved that it is possible to use several gels and several bead-mixes but the number of samples cannot unlimitedly be increased.
Therefore, DigiWest completely fulfills the initial idea of hundreds of replicas of a Western-Blot but it also in parts inherits the property of limited sample numbers from Western-Blot.

4.2 Lapatinib resistance in H292 cell line

The receptor tyrosine kinases EGFR (Her1) and Her2 are overexpressed in several types of tumors and therefore drugs targeting these receptors are frequently used in cancer treatment. A major issue with EGFR and Her2 inhibitors in cancer treatment is that tumors can acquire resistance to these drugs. This often leads to a relapse after an initially successful treatment. There seem to be several potential resistance mechanisms depending on the tumor type (C. R. Chong & Jänne, 2013).

In an experiment performed in cooperation with Benjamin Ruprecht (laboratory of Bernhard Küster, TUM) we investigated the changes occurring during resistance development of the lung cancer cell line H292 to the EGFR/Her2 inhibitor Lapatinib. As the targets of Lapatinib are receptor tyrosine kinases and several downstream signaling pathways are kinase cascades or involve kinases (Yarden & Sliwkowski, 2001) they represented a promising starting point for investigation. A Lapatinib resistant H292 cell line was generated in the laboratory of Bernhard Küster and Kinobeads were used to enrich kinases from the cell lysates of Lapatinib resistant and parental H292 cells. The kinase enriched fractions were analyzed by mass spectrometry. Statistical analysis resulted in a panel of 24 kinases which showed significant differences in protein abundance between the two cell lines and thereby were likely to be connected to the observed Lapatinib resistance.

Using the same kinase enriched material these 24 kinases were analyzed using the DigiWest approach. Mass spectrometry and DigiWest results showed good correlation (correlation coefficient 0.98) although they represent completely different methods for protein quantification. DigiWest was used to further investigate the Kinobead pulldowns and also the initial whole cell lysates were analyzed for kinase content and differences in phosphorylations.

The set of 24 significantly changed kinases contained 5 members of the Eph receptor tyrosine kinase family which are receptors for the Eph receptor-interacting (Ephrin) family of proteins (Pasquale, 2010). EphA2 (Myk2) and EphB4 (Myk1) were found down-regulated whereas EphA4, EphB3 and EphB6 were found up-regulated in the Lapatinib resistant cell line. Ephrins and Eph receptors provide complex signaling mechanisms which are not yet fully understood. They are involved in intercellular signaling and capable of signaling in both directions, from the cell with the Eph receptor and towards the cell with the receptor. Their role in cancer seems to be context dependent resulting in opposing outcomes in different tumors or cell lines. EphA2 and EphB4 have been observed being up or down regulated together but depending on the context, up-regulation resulted in increased or decreased cell motility and proliferation (Pasquale, 2010; Xi, Wu, Wei, & Chen, 2012). The Src family member Fyn which was found to be up-regulated in the identified set of kinases could also be involved in Ephrin signaling as Src tyrosine

kinase family members are involved in Eph signaling (Pasquale, 2010). Some kinases involved in cell cycle regulation were also found to be deregulated.

The DigiWest analysis of the whole cell lysates unveiled that the Lapatinib resistant cell line overexpresses EGFR more than 3-fold and Her2 more than 2-fold compared to the parental cell line which might be an adaption to the permanent presence of the inhibitor.

Another interesting observation is a kind of switch in dual-specific phosphatases (DUSPs). DUSP6 (MKP3) is massively down regulated in the resistant cell line while DUSP9 (MKP4) is up regulated. Both these phosphatases are involved in regulation of MAP kinase cascades which are downstream of the Lapatinib targets EGFR (Her1) and Her2 (Owens & Keyse, 2007; Yarden, 2001).

An Ingenuity pathway analysis performed by Benjamin indicated that p53 should be down-regulated in the Lapatinib resistant H292 cell line. As p53 is not a kinase, a DigiWest assay was performed on the whole cell lysates which confirmed the down-regulation of p53. This is in-line with published data which investigated resistance mechanisms for other EGFR/Her2 inhibitors in lung cancer cell lines including H292 based on clonal selection for resistant cells. They found that in this case the resistance mechanism is based on loss of p53 (S. Huang et al., 2011). We can show that p53 is also the key player for Lapatinib resistance in H292 cells and that p53 is down-regulated in reversibly resistant cells without clonal selection and without loss of p53. Therefore, loss of p53 might be a result of the selective pressure of permanent presence of Lapatinib and might give a survival advantage to these cells.

The combination of mass spectrometry and DigiWest combined with Ingenuity pathway analysis proved to be a powerful team. The mass spectrometry analysis and the pathway analysis were especially helpful in respect to a guided analyte selection for the DigiWest approach. And the analysis of the whole cell lysates combined with the Kinobead pulldowns gave the opportunity to analyze non-kinases. The experiment also shows that DigiWest can be used for analysis of co-immunoprecipitation-like affinity enriched samples.

The obtained data are only indicative for a mechanism that leads to Lapatinib resistance and follow-up experiments are missing. Nevertheless, the identification of p53 as key player in Lapatinib resistance in H292 lung cancer cells by an in-depth bioinformatics analysis of the generated data, combined with the experimental proof that p53 is down regulated in the resistant state, is an important observation. At this point we cannot completely exclude that the long term culture in Lapatinib containing medium could have resulted in partial clonal selection but the cells seemed to lose their induced resistance when cultured in Lapatinib free medium.

4.3 Mouse liver LCM

The liver is the major organ for blood homeostasis and has a wide range of metabolic functions including drug metabolism and therefore it is especially susceptible to toxic drug effects. Many studies on toxic drug effects and also on the effects of non-genotoxic carcinogens focus on the liver. As the liver is a complex organ with the lobules as building blocks which provide different metabolic competences within the different zones, it is helpful to look at the different functional zones individually to gain a better understanding of the function of the liver and of drug effects. It is known that several enzymes including drug-metabolizing enzymes underlie zonation (Kai O. Lindros, 1997; S. P. S. Monga & Cagle, 2010).

Here, the DigiWest approach was employed to investigate the different functional zones of liver lobules on protein level with a focus on cellular signaling. A comprehensive protein analysis was performed for a drug treatment time course with zonal resolution to obtain knowledge on signaling and drug response processes in periportal and pericentral hepatocytes.

In this experiment, which was performed in cooperation with Albert Braeuning from the Institute of Toxicology at University of Tübingen in the Laboratory of Michael Schwarz, the effects of the non-genotoxic carcinogen TCPOBOP were investigated. TCPOBOP is a phenobarbital-like tumor promoter and an agonist of the nuclear receptor CAR which induces hepatomegaly and liver hypertrophy followed by liver tumors in mice (Donthamsetty et al., 2011; S. P. S. Monga & Cagle, 2010).

Liver sections from TCPOBOP treated mice (controls and 24, 48 and 72 hours TCPOBOP treated groups) were generated and LCM was performed to isolate tissue from pericentral and periportal zones. A DigiWest analysis was performed with more than 200 antibodies.

A major question was feasibility of this approach as the resulting material was limited and less than usually used for a single Western-Blot. Another restraint was that proteins had to be formalin fixed to preserve posttranslational modifications during staining and LCM and reversion of formalin fixation impairs protein quality and yield. The experiment proved that it is possible to perform 200 DigiWest analyses from this limited material. It should be noted that in total about 660 antibodies were tested on appropriate material and not all potentially interesting analytes could be covered by the 204 antibodies which were employed in the main experiment.

To visualize the liver zones for laser capture microdissection, the sections were stained for the pericentral marker protein glutamine synthetase (GS) using a mouse derived GS specific antibody. Preparation of the sections was performed by Elke Zabinsky at the Institute of Toxicology. For LCM, areas positively stained for GS (1-2 cell layers) were collected as pericentral zones and areas of 1-2 cell layers surrounding GS negative vessels were collected as periportal zones. Therefore, the areas represent only

the proximal periportal and pericentral zones. The DigiWest analysis of the LCM derived samples resulted in a 470 fold enrichment of GS in the pericentral compared to the periportal areas. The periportal marker protein E-cadherin was not detectable in the pericentral areas. This indicates that the collected material presents pure preparations of periportal and pericentral areas from the mouse liver sections. Some other proteins known to be zonated were also investigated and showed the expected results. Different cytochrome P450 family members which were analyzed and are known to be induced by TCPOBOP also showed the expected inductions.

An aspect which is not discussed here but which should be kept in mind is that hepatocytes make only 60% of the cells and 80% of the volume of a liver. Therefore, some of the observed differences and changes might not be hepatocyte specific.

4.3.1 Reflection of potential issues

It is a common observation that some antibodies show additional bands and often it is not clear whether these represent protein isoforms or other proteins with similarity to the epitopes. There was an additional band observed for some antibodies which was at the molecular weight of GS (about 40 kDa) which exactly overlaid the bands for GS and showed the same zonation and decrease over the time course and another additional band at about 50 kDa showing pericentral zonation and induction in the time course. The DigiWest method allows identification of additional bands and only bands at the proper molecular weights were used for signal quantification. Interestingly, the use of some of the affected antibodies in IHC on tissue sections showed a staining pattern resembling the GS stain but only on formalin fixed sections. IHC on fresh-frozen sections did not show this staining. So probably the formalin treatment caused cross reactivity with GS and another protein for some antibodies.

During data analysis it turned out that most of the investigated serine and threonine phosphorylations which showed statistically significant zonation were periportally zonated. Since during LCM the periportal areas were collected first, followed by isolation of the pericentral areas, this observation caused some concerns. But in pre-experiments, in which the pericentral areas were collected first, these phosphorylations showed the same periportal zonation for these analytes which indicated that no artefacts were created. The immunohistochemical stains performed by Elke for some analytes and also some of the periportally zonated phosphorylations confirmed the DigiWest results. The following discussion provides a possible explanation for the periportal tendency of phosphorylations based on a cellular signaling mechanism.

A decrease for several analytes was observed over the TCPOBOP treatment time course. A possible explanation could be hypertrophy during TCPOBOP treatment and therefore a reduction of the number of cells in the samples. In a liver with enlarged hepatocytes, more structural and metabolic proteins relative to signaling proteins might be present. Drug metabolizing proteins that are induced may contribute to the observed relative decrease. The obtained data were normalized on the total protein amount. For LCM, an area of about 3.7 mm^2 (a volume of about 0.037 mm^3) was collected for each sample and the total protein amount in this volume did not change during TCPOBOP treatment. Therefore, the samples represent a defined amount of protein and also a defined volume of liver tissue. The number of cells was not determined but the TCPOBOP induced hypertrophy should result in a decrease in cell number during the time course when a defined volume is examined. The normalization on the protein amount did not show any tendency which might have resulted in a bias. The effects on cellular signaling resulting from this potential effect cannot be assessed.

4.3.2 Liver zonation and regulation of metabolism

A major function of the liver is to maintain blood homeostasis. This includes regulation of content of glucose, lipids and other metabolites and nutrients and adaption to different situations. Many of the enzymes required for these functions underlie zonation. The composition of the blood entering the liver through the portal vein underlies strong variations. The content and composition of nutrients depends on the feeding state and also the circadian rhythm and many of the detoxifying enzymes are induced by presence of xenobiotics. To adapt to these variations, the enzymatic equipment of the liver varies not only within the zones but also depending on feeding, circadian rhythm and presence of hormones, xenobiotics and other metabolites. For successful blood maintenance the liver is equipped with sensory systems. Many of the sensors are nuclear receptors which, upon activation by ligands or signaling events, induce expression of metabolic enzymes (Arias, 2009; Dufour & Clavien, 2009; Schibler, Ripperger, & Brown, 2003).

Cellular signaling underlying liver zonation and metabolic adaption is complex and integrates many signals from different sensory systems. Some details and key players are uncovered. It is known that inversion of the blood flow in the liver leads to inversed zonation of several but not all zonated enzymes. That means that blood flow itself and the resulting gradients in oxygen, nutrients, hormones and others play a role (Thurman & Kauffman, 1985).

Studies from the Eighties shed some light on metabolic characteristics of the liver zones. A comprehensive review on metabolic zonation of the liver summarizing the knowledge from that time is available

from Rolf Gebhardt (R Gebhardt, 1992). Oxygen uptake was found to be about 2-fold higher in periportal regions when compared to pericentral regions (Matsumura & Thurman, 1984). Plasma concentration of Insulin was found to be about 2-fold higher in the portal vein compared to the central vein (BALKS & JUNGERMANN, 1984) and a periportally zonated binding of the epidermal growth factor (EGF) using I^{125}-labelled EGF was observed (Chabot, Walker, & Pelletier, 1986; St Hilaire, Hradek, & Jones, 1983).

4.3.2.1 Known signaling pathways involved in liver zonation

A gradient in β-catenin signaling plays an important role in liver zonation (S. P. S. Monga & Cagle, 2010). Periportal hepatocytes express APC which is a negative regulator of β-catenin. Pericentral hepatocytes do not express APC causing accumulation of active β-catenin (Benhamouche et al., 2006). E-Cadherin which is only expressed in the periportal zone traps β-catenin to the membrane and prevents nuclear translocation (Orsulic, Huber, Aberle, Arnold, & Kemler, 1999). In the nucleus, β-catenin acts as a co-activator and can interact with transcription factors of the TCF/LEF family. These transcription factors bind Wnt-response-elements and lead to β-catenin-mediated gene transcription (Benhamouche et al., 2006; S. P. S. Monga & Cagle, 2010).

The antibodies used for the DigiWest data set contained antibodies for β-catenin, active (non-phosphorylated) β-catenin and phosphorylated β-catenin but no significant zonation was observed. This is in line with the fact that the zonation of β-catenin cannot be measured or detected in IHC (personal communication from Albert Braeuning) and is because β-catenin predominantly localizes at the membrane and in the cytoplasm (S. P. Monga, Pediaditakis, Mule, Stolz, & Michalopoulos, 2001). DigiWest is not capable of distinguishing nuclear and cytoplasmic or membrane-bound β-catenin which might explain that β-catenin did not show zonation in the analysis. The hypothesis of the role of β-catenin in liver zonation is based on knock-out models resulting in livers which do not show zonation for important zonation markers and resemble either a pericentral gene expression pattern for these markers when APC is knocked out or a periportal pattern when β-catenin is knocked out (Benhamouche et al., 2006; S. P. S. Monga & Cagle, 2010).

MAP kinase signaling is also meant to play an important role in liver zonation. This hypothesis is based on the observation that β-catenin mutated tumors resemble more pericentral gene and marker protein expression while tumors harboring an activating mutation in Ha-Ras or B-Raf resemble more periportal gene and marker protein expression. Experiments on transgenic mice further support this hypothesis (Braeuning, Ittrich, Köhle, Buchmann, & Schwarz, 2007; Braeuning, Menzel, et al., 2007; Hailfinger, Jaworski, Braeuning, Buchmann, & Schwarz, 2006). For the phosphorylation of ERK1/2 there was no

zonation observed with a very slight and not significant periportal tendency. The DigiWest results showed 2-fold pericentral zonation of phosphorylated MEK1/2 which is not in line with this hypothesis and is a contentious point. This phosphorylation would be expected to be periportally zonated as it is downstream of EGF receptor and upstream of ERK and as MAPK signaling is postulated to be periportally zonated (Braeuning, Ittrich, et al., 2007; Kolch, 2005). A similar discrepancy has been described for female rats where phosphorylated ERK was found to be pericentrally zonated (Hvid et al., 2011). Again the intracellular distribution which cannot be accessed by DigiWest might play a role.

4.3.2.2 New insights into liver zonation: Hedgehog signaling

The first part of the data analysis considered the zonation found in the untreated livers of the control group. Known zonation markers (GS and E-cadherin) and several enzymes known to underlie zonation showed the expected results. In respect to cellular signaling some new findings were made that point to a role of hedgehog-signaling in liver zonation. The group of Rolf Gebhardt described Hedgehog signaling being pericentrally zonated in the liver based on the observation of Ihh (indian Hedgehog) zonation (Rolf Gebhardt & Matz-Soja, 2014; Matz-Soja et al., 2014; Matz-Soja, Hovhannisyan, & Gebhardt, 2013) although in the publication from 2013 they mention a periportal zonation.

Here I show that PTCH2, which is a hedgehog signaling receptor, is completely pericentrally zonated. The IHC staining of PTCH2 on fresh-frozen mouse liver sections performed by Elke Zabinsky validated the zonation. Ihh, one of the known ligands of the Ptch receptors, was also part of the DigiWest analysis. It was barely detectable in the control group and the obtained signals did not show a significant zonation. A strong induction of Ihh to a similar extend in both zones was observed after TCPOBP treatment in the time course. The IHC staining performed by Elke showed that after TCPOBOP treatment Ihh is zonated in the mid-lobular zone and less expressed in the pericentral and periportal zones. In the untreated liver Ihh was located in ‘spots’ in between the hepatocytes which might represent other kinds of cells and did not show zonation. The mid-lobular zonation of Ihh explains that in the DigiWest results Ihh did not show zonation as only the proximal periportal and the pericentral zones were investigated. Hedgehog signaling will be discussed in some more detail in the section for the TCPOBOP treatment. Staining of Ihh is shown in figure 43.

4.3.2.3 New insights into liver zonation: HNF4α

The nuclear receptor HNF4α is seen as an important player in the liver as it occupies 12% of hepatic promoters yet it does not show zonation (Gougelet et al., 2014; K O Lindros, Oinonen, Issakainen, Nagy,

& Thorgeirsson, 1997; S. P. S. Monga & Cagle, 2010). However, HNF4α plays a role in expression of pericentral and periportal genes, the interaction of HNF4α with Lef1 is required for expression of the pericentral marker GS while HNF4α alone seems to repress GS expression. It was found that HNF4α alone might be sufficient for expression of several periportally expressed genes (Colletti et al., 2009; S. P. S. Monga & Cagle, 2010). Important crosstalk has also been found for Tcf-4 and HNF4α. Tcf-4 interacting with β-catenin binds to Wnt-responsive elements of β-catenin induced genes while Tcf-4 binds to HNF4 responsive elements of genes repressed by β-catenin (Gougelet et al., 2014). HNF4α is phosphorylated at Ser313 (uniprot and phosphosite plus databases) yet this phosphorylation site is referred to as Ser304 in their references (Hong, Varanasi, Yang, & Leff, 2003; Zhongyan Wang, Salih, & Burke, 2011). The phosphorylation site is located in the interaction domain of HNF4α and prevents formation of homo-dimers; the kinase responsible for this phosphorylation is AMPKα (Hong et al., 2003).

The DigiWest analysis found HNF4α not being zonated but phosphorylation of HNF4α at Ser313 showed a more than 2-fold enrichment on the periportal side. The activating phosphorylation of AMPKα at Thr172 was also found to be periportally zonated (1.7 fold). If the HNF4α phosphorylation in the interaction domain would also prevent interaction of HNF4α with Lef1, Tcf-4 and other transcription factors, this could explain the observation that HNF4α plays a role in expression of both pericentrally and periportally expressed genes either as HNF4α alone on the periportal side or interacting with other transcription factors on the pericentral side, or at least with differing interaction partners dependent on the phosphorylation. This observation needs further investigation.

4.3.2.4 New insights into liver zonation: phosphatases

Some phosphatases showed a zonated distribution. The dual-specific phosphatase DUSP4 was found to be 4.7-fold periportally zonated in the DigiWest results. DUSP4 expression is known to be induced by activated AMPK and seems to be required for inhibition of gluconeogenesis (Berasi et al., 2006).

An about 5-fold periportal zonation of PP1γ, the catalytic subunit of PP1, was found. PP1 is, as is PP2A, a holoenzyme comprised of catalytic and regulatory subunits. PP1 and the PP1γ subunit do not only underlie the circadian rhythm (Schmutz et al., 2011) but it is also involved in regulation of glycogen metabolism by dephosphorylating and activating glycogen synthase. To regulate glycogen metabolism it is anchored to the glycogen particles via a glycogen-targeting regulatory subunit. These subunits were not investigated. It is known that in the liver the glycogen-targeting subunit PPP1R3G is upregulated upon fasting and downregulated upon feeding while other glycogen-targeting regulatory subunits of PP1

are downregulated upon fasting (Luo et al., 2011). Zonation of PP1γ alone is not sufficient to draw a full picture.

The data on zonation of proteins and protein phosphorylations in the control group show that the inhibitory phosphorylation of PP2A C, the catalytic subunit of PP2A, is more than 8-fold enriched in the periportal zone and as a consequence of this inhibition, several targets of PP2A and targets thereof show a periportal zonation for serine and threonine phosphorylation. PP2A is one of the major serine/threonine phosphatases in mammalian cells (Virshup & Shenolikar, 2009). Besides Src and Lck, Insulin and EGF receptors have been identified as kinases which can phosphorylate PP2A (J. Chen et al., 1992). Src phosphorylation at Tyr527 and Tyr416 did not show zonation and Lck phosphorylation at Tyr505 showed a pericentral zonation. Therefore, the inhibitory phosphorylation might be derived from EGF and Insulin receptor.

4.3.2.5 New insights into liver zonation: phosphorylation of proteins

Besides the analytes mentioned already, several serine and threonine phosphorylations showed a periportal zonation. This can be explained by the inhibitory phosphorylation of PP2A at Tyr307. IHC stainings were performed to confirm the zonation. PP2A can dephosphorylate AMPK (S. P. Davies, Helps, Cohen, & Hardie, 1995) and also Akt and S6 kinase (T. Wang et al., 2010), the kinase phosphorylating RPS6, which are both phosphorylated by PDK1 (Bononi et al., 2011; Shiojima & Walsh, 2006). Phosphorylation of RPS6 in the liver increases massively after feeding in an insulin dependent manner (Lu et al., 2012).

Active PP2A dephosphorylates and thereby inhibits AMPK which was shown to promote HSP70 expression (T. Wang et al., 2010). This might provide the explanation for the observed pericentral zonation of HSP70. As PP2A is inhibited in the periportal zone, the activating phosphorylation of AMPKα and RPS6 are higher and the activating phosphorylation of Akt at Ser473 is also expected to be higher in the periportal zone. Akt phosphorylation at Thr308 was measured and did not show significant zonation, phosphorylation of Ser473 could not be investigated.

AMPK is meant to be an energy sensor of the cell and can be phosphorylated at Thr172 in response to calcium flux, different kinds of cellular stress and several hormones (Kahn, Alquier, Carling, & Hardie, 2005; Mihaylova & Shaw, 2011; Towler & Hardie, 2007). HNF4α is not only a target of AMPK but integrates many signals resulting in several phosphorylations and acetylations and HNF4α is involved in different protein complexes (Daigo et al., 2011; Um et al., 2011; Xue & Kahn, 2006). It is also involved in regulation of circadian transcription (Reddy et al., 2007).

A study on AMPK activity in periportal and pericentral hepatocytes isolated from rat livers by Witters et al. showed 2-fold pericentral zonation of AMPK activity in fasted rats which almost vanished after refeeding (Witters, Gao, Kemp, & Quistorff, 1994). This is not in line with the DigiWest results which show periportal zonation in ad libitum fed mice, but data comparison is difficult as the time consuming process of cell perfusion and isolation may have led to changes in phosphorylation in this study.

PAK1/2 phosphorylation at Ser144/Ser141 showed an 8-fold periportal zonation. The role of PAK1/2 (p21 activated protein kinase) in the liver is not yet completely clear but it seems to play a role in glucose homeostasis. PAK1 is involved in insulin secretion in β-cells and also seems to be involved in insulin signaling in the liver (Y.-T. A. Chiang et al., 2014; Zhanxiang Wang, Oh, Clapp, Chernoff, & Thurmond, 2011). PAK2 was identified as an AMPK substrate (Banko et al., 2011). Several serine residues in PAK2 are phosphorylated by AMPK although the direct substrate of AMPK is possibly Ser20 which induces autophosphorylation at several sites including Ser144/Ser141. This phosphorylation is meant to significantly contribute to activation (C. Chong, Tan, Lim, & Manser, 2001; Molli, Li, Murray, Rayala, & Kumar, 2009). The phosphorylation of Integrin linked kinase ILK1 at Ser246 and Thr173 is directly connected to this observation. Both of these phosphorylation sites on ILK have been shown to be substrates of PAK. Phosphorylation on Ser246 and Thr173 seems to inhibit nuclear localization of ILK (Acconcia, Barnes, Singh, Talukder, & Kumar, 2007; Hannigan, McDonald, Walsh, & Dedhar, 2011).

All these observations and connections mentioned above are represented in figure 41 for illustration. This might draw a clearer picture.

4.3.2.6 New insights into liver zonation: Nuclear receptors and coregulators

PPARγ is a nuclear receptor involved in regulation of lipid and glucose metabolism. Phosphorylation of PPARγ at Ser112 can be caused by MAP-kinases and CDKs, the function of this phosphorylation is not clear yet (Ahmadian et al., 2013). PPARγ was found to be periportally zonated in the DigiWest results. Phosphorylation of PPARγ at Ser112 showed the same zonation as did the PPARγ coactivator PGC-1α phosphorylation at Ser571. The coregulator PGC-1α is again a protein that integrates signals from many sources and plays a critical role in glucose, lipid and energy homeostasis. It is meant to be a master regulator of mitochondrial biogenesis and can interact with a variety of nuclear hormone receptors including HNF4α (Jäger, Handschin, St-Pierre, & Spiegelman, 2007; Lin, Handschin, & Spiegelman, 2005; Oberkofler et al., 2002). Insulin signaling involving the kinase Akt has been shown to induce the inhibitory PGC-1α phosphorylation at Ser571 (Ser570 in mouse) (X. Li, Monks, Ge, & Birnbaum, 2007; W. Wang & Wong, 2010). PGC-1α is phosphorylated by S6 kinase at Ser568 and Ser572 (Lustig et al., 2011),

the phosphorylation which was measured at Ser570 (in mouse) is derived from Akt (X. Li et al., 2007), which attenuates binding to HNF4α and inhibits gluconeogenesis while these phosphorylations seem to have no impact on mitochondrial biogenesis or β-oxidation of fatty acids (Lustig et al., 2011). The observed phosphorylation of RPS6 indicates higher S6 kinase activity in the periportal zone and therefore the phosphorylations at Ser568 and Ser572 might also show periportal zonation.

4.3.2.7 Insulin signaling and liver zonation

Insulin signaling regulates glucose and lipid homeostasis and is associated with several signaling pathways including regulation of cellular growth. As most investigations are performed utilizing cultured cells and insulin is part of the endocrine system, it seems to be clear that not all of the observed pathways and signaling events are relevant for the physiological functions of insulin (Saltiel, 1996). Although the insulin receptor is a tyrosine kinase, its activation results in up- and down-regulation of several serine and threonine phoshorylations indicating important roles for kinases and also phosphatases (Saltiel, 1996). PDK1 was identified as potential missing link (Cohen, Alessi, & Cross, 1997) and the link from insulin receptor to Akt was filled by PI3K (Vanhaesebroeck & Alessi, 2000). The phosphatases which might be involved were forgotten as the question of how the tyrosine kinase activity of insulin receptor is translated into serine and threonine phosphorylations seemed to be solved. Although there has been intense effort in deciphering insulin signaling and many players were identified, insulin signaling is still not fully understood (Cohen, 2006).

The study on liver zonation was not designed for investigation of insulin signaling. Nevertheless the data on cellular signaling with a focus on phosphorylation in liver zonation provide insights into physiological insulin signaling in the liver. Besides a periportal zonation of PDK1 (1.7-fold) several serine and threonine phosphorylations and also several phosphatases were found to underlie zonation. These include the serine/threonine phosphatases PP1 and PP2A.

The high degree of inhibitory phosphorylation of PP2A observed in the DigiWest results should result in much higher PP2A activity in the pericentral zone and might explain the observed tendency of periportal zonation for several serine and threonine phosphorylations as PP2A is one of the major serine and threonine phosphatases in mammalian cells and has a broad range of substrates (Virshup & Shenolikar, 2009; Westermarck & Hahn, 2008).

The following figure represents a possible connectivity for most of the analytes which were discussed above. The core component is the periportal zonation of the inhibitory phosphorylation of PP2A which might be derived from activated insulin and EGF receptors.

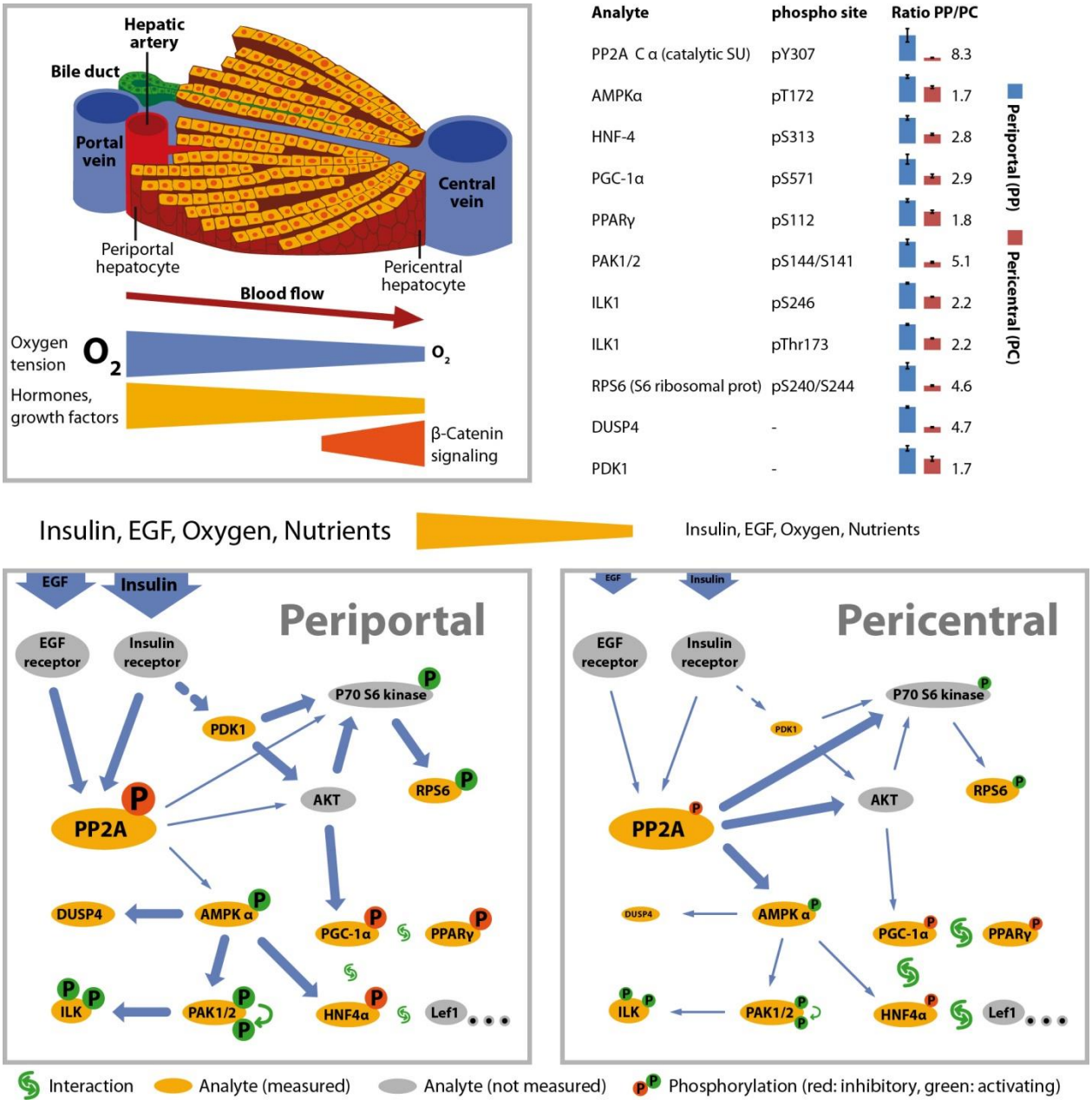

FIGURE 41 OVERVIEW OF THE OBSERVATIONS FOR ZONATED SIGNALING IN THE LIVER

Shown is a detail of a liver lobule with some of the known characteristics highlighted. The illustration is adopted from Angélique Gougelet and Sabine Colnot (Gougelet & Colnot, 2012) *and in smaller parts from Albert Braeuning* (Braeuning et al., 2006)*. The data represent most of the data mentioned in the discussion above. There are small bar diagrams with standard error for all given analytes with the periportal data shown in blue and the pericentral data in red. Data are normalized to the higher value. The ratios of periportal to pericentral (not in log2) are given.*

The lower part shows a possible connection of the observations in respect to cellular signaling. As the mice were not starved, insulin is expected about 2-fold higher in the periportal zones as is EGF signaling. Insulin itself and the receptors were not analyzed. Activated insulin and EGF receptors on the periportal side can phosphorylate protein phosphatase 2 (PP2A) at the inhibitory Tyr307. Inhibited PP2A cannot dephosphorylate AMPKα, S6 kinase or Akt resulting in increased activity of these kinases. On the periportal side, insulin also leads to activation of PDK1 which phosphorylates Akt at Ser473 (which could not be measured) and S6 kinase, which can also be phosphorylated by Akt, which then phosphorylates the transcriptional coactivator PGC-1α at Ser571 (Ser570 in mouse). Neighboring phosphorylation sites at Ser568 and Ser572 of PGC-1α which are phosphorylated by S6 kinase might also be periportally zonated but were not measured and are not included in the illustration. Besides PAK 1/2, AMPK phosphorylates HNF4α at the inhibitory Ser residue in the interaction domain. Activated PAK1/2 can phosphorylate ILK1 at the 2 phosphorylation sites.

On the pericentral side, where insulin and EGF are reduced and PDK1 is also less expressed, PP2A shows less inhibition resulting in less active AMPK, S6 kinase and Akt which results in less phosphorylation of the targets. As the phosphorylations which inhibit or change interaction of HNF4α and PGC-1α with other proteins are reduced, this might result in protein interaction and formation of transcription regulating complexes.

On the periportal side the phosphorylations of HNF4α, PGC-1α and PPARγ might inhibit their interactions with each other or other proteins like Lef1 or might lead to a switch in interaction partners.

The core component of this proposed connectivity is the periportally zonated inhibitory phosphorylation of PP2A resulting in active AMPKα and RPS6 and probably also active Akt. The periportal zonation of PDK1 might support this. The central role of the inhibition of PP2A is of special interest as this could mean that the specificity of the cellular signal and regulation of the downstream phosphorylations is more derived from the phosphatase.

4.3.2.8 Consequences for metabolic zonation

Active AMPK induces DUSP4 expression and leads to suppression of gluconeogenesis via down regulation of PEPCK and glucose-6-phosphatase, the rate limiting and hormonally controlled enzymes in gluconeogenesis (Berasi et al., 2006). The protein interactions of PGC-1α with PPARγ and with HNF4α also play an important role in glucose metabolism. As mentioned, the phosphorylations of these proteins are meant to inhibit their interactions although for PPARγ it is not fully clear. If not inhibited, PGC-1α is meant to

activate a fasting response including gluconeogenesis, fatty-acid β-oxidation, ketogenesis and bile-acid homeostasis by coactivating key hepatic transcription factors (Lin et al., 2005). Interaction of PGC-1α with HNF4α is also required for gluconeogenesis and expression of the rate limiting enzymes PEPCK and glucose-6-phosphatase (Rhee et al., 2003). AMPKα and its target PAK1/2 are meant to play an important role in membrane translocation of the insulin responsive glucose transporter GLUT4 resulting in increased glucose uptake (Y. A. Chiang & Jin, 2014; Viana et al., 2006).

As the mice in this study were fed ad libitum and no starved mice were investigated, it is not clear how the observed phosphorylations might depend on the feeding state and whether the adaptions to changes in feeding and related hormones would affect the periportal or the pericentral hepatocytes. But as the initial triggers of the proposed connectivity are meant to be insulin and EGF, the signaling might adjust in the way that the phosphorylations are reduced in the periportal zones. Depending on the contribution of EGF this could also be a minor change.

4.3.2.9 Conclusions

The blood entering the liver through the portal vein underlies high variations in content and composition of nutrients and also metabolism regulating hormones whereas the blood leaving the liver through the central vein needs to be in the physiological range. Therefore, it might make sense that the regulatory phosphorylations of critical regulators for energy metabolism are periportally zonated. Phosphorylation of AMPKα, HNF4α, PPARγ, PCG-1α and also PAK1/2 and RPS6 could provide links for regulation of metabolism to these variations and to the circadian rhythm. It is not clear whether the inhibitory PPARγ phosphorylation is linked to activated AMPKα or not, but it is known that activated AMPK can inhibit PPARγ transcriptional activity (Sozio, Lu, Zeng, Liangpunsakul, & Crabb, 2011).

The proposed connectivity puts PP2A into a central role. As mentioned, this phosphatase is a major serine and threonine phosphatase with a broad range of substrates. The inhibitory phosphorylation of PP2A shows a strong peak at 24 hours after TCPOBOP treatment which is also observed for the phosphorylation of RPS6 and phosphorylation of Akt at Thr308 but not for phosphorylation of AMPK and several other proteins. This implies an important role for the regulatory subunits of PP2A which were not part of this analysis. PP2A is a holo-enzyme that contains regulatory subunits which influence substrate specificity and lead to precisely regulated phosphatase activity (Virshup & Shenolikar, 2009). The measured inhibitory phosphorylation is on the catalytic subunit.

Besides the discussed observations, other interesting differences between periportal and pericentral areas of the analyzed liver sections were found. Table 2 in the results section summarizes all analytes showing statistically significant zonation (more than 2-fold, $p < 0.05$).

This study was designed to investigate changes in cellular signaling in the TCPOBOP treatment time course. For investigation of differences in cellular signaling in respect to feeding state and insulin it would have been helpful to add different feeding states like starved mice or mice fed with different diets like high fat, high carbohydrate and high protein diets. For investigation of circadian rhythm dependencies the day/night cycle might be incorporated. Therefore, further investigations are necessary.

4.3.3 TCPOBOP time course – effects with zonal resolution

TCPOBOP is a prototypical non-genotoxic carcinogen and the most potent phenobarbital-like inducer. It binds the nuclear receptor CAR and induces expression of genes associated with xenobiotic detoxification and proliferation. Hepatomegaly and liver hypertrophy are observed within the first two days after administration resulting in an increase of liver mass by 2 to 3 fold. This is meant to be a physiological process as a larger liver provides higher drug metabolizing capacity. This mitogenic process needs to be tightly controlled and terminated in time (Donthamsetty et al., 2011). CAR agonists like phenobarbital and TCPOBOP specifically promote β-catenin mutated hepatocellular carcinoma (Braeuning et al., 2011)(personal communication Albert Braeuning). It is still not clear why phenobarbital-like non-genotoxic carcinogens specifically promote tumors harboring an activating β-catenin mutation.

In this experiment, protein expression was investigated in separated proximal periportal and pericentral areas from mouse liver sections for a time course of 3 days after TCPOBOP injection. The DigiWest method allowed measuring protein expression and phosphorylation using about 200 antibodies resulting in a wide-ranging, yet biased, selection of analytes. Aim of this experiment was to gain deeper insights into changes in cellular signaling induced by TCPOBOP.

As shown in the results section, there are many changes occurring after TCPOBOP administration. Some analytes show the same or similar behavior in pericentral and periportal zones but some TCPOBOP induced effects are focused or even restricted to just one zone.

As this is the first time that cellular signaling was investigated in mouse livers with zonal resolution and in a study with a drug-treatment time course, the data set is difficult to interpret. The large data-set would need further analysis using systems biology approaches and pathway mapping. Therefore, the following section just highlights some observations.

4.3.3.1 Stress response and oxidative stress upon TCPOBOP treatment

The inhibitory phosphorylation of PP2A shows a massive peak 24 hours after treatment (about 40-fold increase in the pericentral zone and about 6-fold in the periportal zone reaching a similar level in both zones) indicating a substantial disturbance of cellular signaling. The high standard error at the 24 hour time point might indicate that the effect peaks sharply and the maximum is not met perfectly in the one day resolution of the time course. A peak showing an appropriate hyper-phosphorylation at the 24 hours TCPOBOP treatment time point was also observed for Akt pThr308 and RPS6 pSer240/244 but it was not observed for other substrates of PP2A like AMPKα which indicates an important role for the regulatory

subunits of PP2A and their regulation of substrate specificity. Akt pThr308 is involved in liver regeneration (Haga et al., 2009) and RPS6 pSer240/244 is associated with increased proliferation and protein synthesis (Stewart & Thomas, 1994). Phosphorylation of ERK1/2 at Thr202/Tyr204 also showed a slight peak at 24 hours but less than factor 2. The representation of the whole data-set in figure 27 in the results part indicates that several analytes show a slight peak at the 24 hours treatment time-point.

Increased PP2A phosphorylation in response to oxidative stress has been described (Jin Jung et al., 2013). The inhibitory PP2A phosphorylation has been described to mediate a stress survival response in retinal cells showing a massive peak in response to reactive oxygen species which was not observable when reactive oxygen species were scavenged (Finnegan, Mackey, & Cotter, 2010). Therefore the observed peak in PP2A phosphorylation could be based on oxidative stress.

The induction of c-Myc, HSP70 and DPP3 in the TCPOBOP treatment time course were found to be restricted to the pericentral zone. Induction of c-Myc by TCPOBOP has been described and was meant to be a key mediator of direct liver hyperplasia (Blanco-Bose et al., 2008). c-Myc expression is induced during liver regeneration and upon treatment with several chemicals (Donthamsetty et al., 2011; Hickling et al., 2010; Makino, Hayashi, & Sugimura, 1984) but it has been shown that deletion of c-Myc does not impair liver regeneration (F. Li et al., 2006). c-Myc has manifold functions including induction of apoptosis and regulation of metabolism (Dang, 1999). Myc dependent apoptosis has been shown to result from oxidative stress and to be prevented by glutamine (Xu, Nguyen, Lo, & Czaja, 1997; Yuneva, Zamboni, Oefner, Sachidanandam, & Lazebnik, 2007). The pericentrally zonated GS might therefore support survival of the stressed pericentral cells.

HSP70 is induced by several kinds of stress including oxidative stress and it is also induced during liver regeneration. It protects cells against stress-induced apoptosis (Konishi et al., 1995; Mosser, Caron, Bourget, Denis-Larose, & Massie, 1997; Wolf et al., 2014).

DPP3 (Dipeptidyl-peptidase 3) was shown to bind Keap1 and replace Nrf2 which prevents Nrf2 ubiquitination and activates Nrf2-dependent transcription (Hast et al., 2013). Nrf2 plays an important role in defense against reactive oxygen species and induces an antioxidant response (W. Chen et al., 2009). Nrf2 is meant to redirect metabolism of glucose and glutamine into anabolic pathways (Mitsuishi et al., 2012).

The restriction of the induction of c-Myc, HSP70 and also DPP3 to the pericentral zone might indicate that the pericentral zone is more affected by oxidative stress upon TCPOBOP treatment.

The antibody directed against RAD23B, which is a protein involved in DNA damage repair (Friedberg, 2001), showed periportal zonation and no significant changes in the time-course. But the antibody detected an additional band which could represent isoform 2 of RAD23B or it could represent RAD23A.

This additional band showed pericentral zonation and induction in the treatment time-course with a stronger pericentral effect. This might indicate increased DNA damage in the pericentral zone which might result from the oxidative stress. But as it could also be an additional band this needs further investigation.

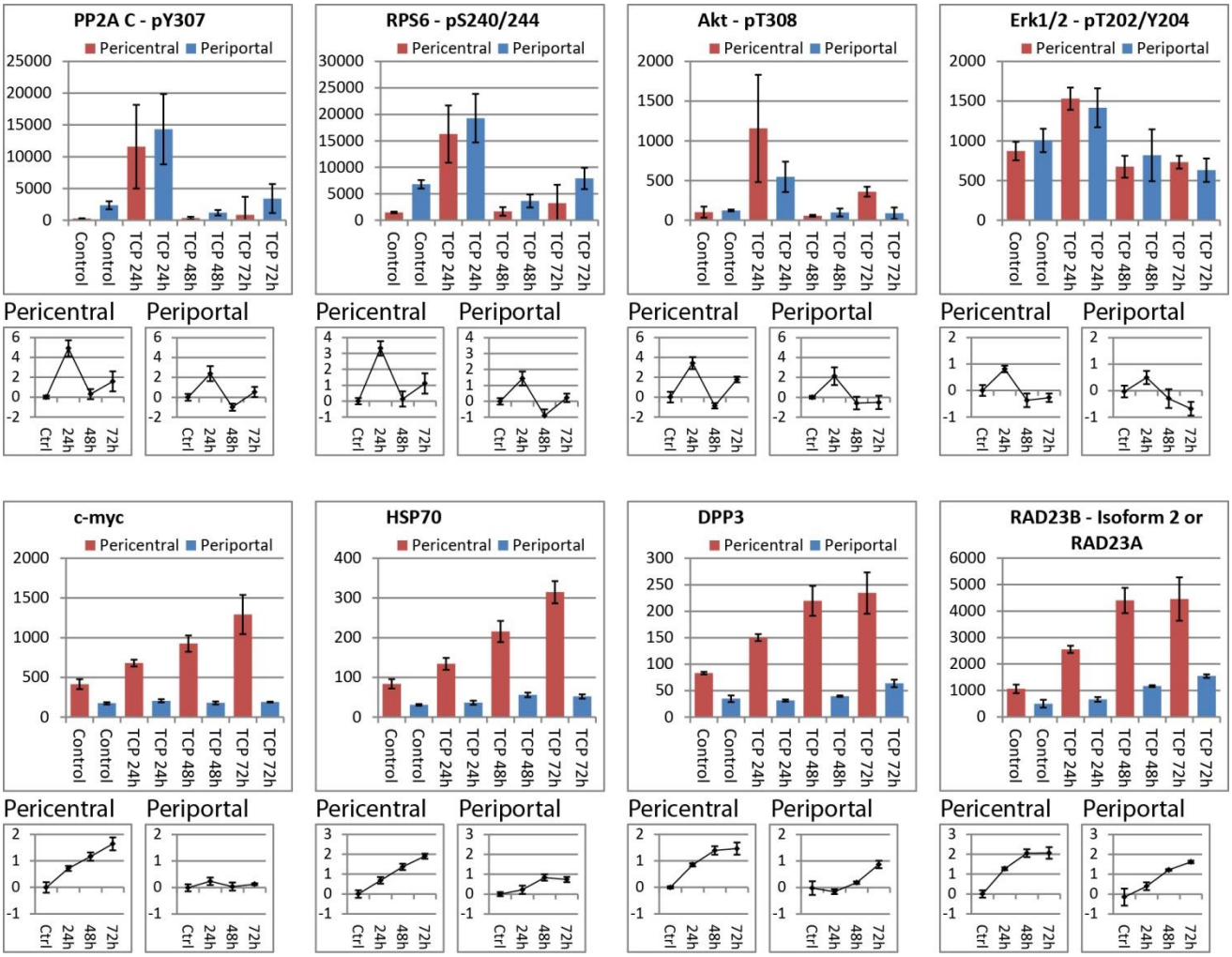

FIGURE 42 SOME OF THE TCPOBOP INDUCED EFFECTS MENTIONED IN THE DISCUSSION

Shown are some of the analytes showing significant changes in the TCPOBOP time course mentioned in the discussion so far. The data are shown in diagrams representing the AFI values (relative fluorescence units) with standard error for the pericentral zone in red and for the periportal zone in blue. The smaller diagrams represent the same data but as log2-fold changes relative to the control (normalized on median of control) with standard error. The phosphorylations of PP2A at Tyr307, RPS6 at Ser240/244 and Akt at Thr308 show a strong peak at 24 hours TCPOBOP treatment with a high standard error at this time point. The phosphorylation of ERK1/2 at Thr202/Tyr204 shows a slight and not statistically significant peak. c-

Myc, HSP70, DPP3 and the additional band obtained with the antibody directed against RAD23B which could represent isoform 2 or RAD23A all show a pericentral zonation with an induction during the time-course while they show no or less induction in the periportal zone.

4.3.3.2 Proliferative and other effects

MCM2 (Minichromosome maintenance protein 2) has been observed on mRNA level to be induced by TCPOBOP (Leoni et al., 2011). The DigiWest data show that it is induced in both zones upon TCPOBOP treatment. MCM2 plays an important role in cell proliferation and is often used as proliferation marker (Blow & Hodgson, 2002).

Activation of Hedgehog signaling was shown to play an important role in liver regeneration after partial hepatectomy and under conditions which might induce apoptosis (Ochoa et al., 2010; Omenetti et al., 2011). The DigiWest data show a massive increase of the Hedgehog ligand Ihh (about 100-fold) in the TCPOBOP treatment time course in both zones. As the hedgehog receptor PTCH2 was found to be pericentrally zonated, there could be a pericentrally zonated activation of hedgehog signaling induced by TCPOBOP. PTCH1 could not be measured and therefore it is not clear how it is expressed in the liver. The differences between PTCH2 and PTCH1 are not known yet, the two hedgehog receptors seem to provide, at least in parts, redundant functionality (Alfaro, Roberts, Kwong, Bijlsma, & Roelink, 2014).

Immature ductal cells and stellate cells have been reported to produce hedgehog ligands in response to injury-associated factors. This enriches the injured liver with hedgehog ligands and stimulates hedgehog responsive cells. Mature hepatocytes are not meant to be hedgehog responsive (Choi, Omenetti, Syn, & Diehl, 2011). It has also been reported that apoptotic stimuli trigger mature hepatocytes to produce Ihh (Choi et al., 2011; Jung et al., 2010) which might connect to the proposed oxidative stress and apoptosis related functions of c-Myc and HSP70 and might be part of a stress survival response.

The IHC staining for Indian hedgehog showed thin areas in between the hepatocytes positive for Ihh which could be stellate cells. After TCPOBOP treatment, the whole liver showed a strong staining for Ihh including the hepatocytes with a stronger staining in the mid-lobular zone (see figure 43 b)). The finding that PTCH2 is expressed in the pericentral zone might indicate that pericentral hepatocytes could be hedgehog responsive. As hedgehog signaling is often associated with differentiation and precursor cells, the hepatocytes might, at least slightly, dedifferentiate to reactivate their mitotic abilities. The zonation of the hedgehog receptor PTCH2 and the consequences of the induction of the ligand Ihh on hedgehog signaling need further investigation including the downstream proteins Smo, Gli1-3 and target proteins to investigate the hedgehog responsiveness.

The glucose transporter GLUT1 was found to be pericentrally zonated in the liver which is in line with literature (Bilir et al., 1993). In the TCPOBOP treatment time-course, GLUT1 is induced in both zones with a stronger induction in the periportal zone resulting in the same level in both zones. This could indicate a higher energy demand upon treatment.

RXRα is induced upon TCPOBOP treatment. It shows a slower but stronger induction in the periportal zone. RXRα is a nuclear receptor predominantly expressed in the liver where it plays important roles in regulation of metabolism and gene expression. It has the ability to hetero-dimerize with numerous other nuclear receptors and thereby controls specific gene transcription (Evans & Mangelsdorf, 2014; Zhan et al., 2012). It also hetero-dimerizes with CAR and PXR.

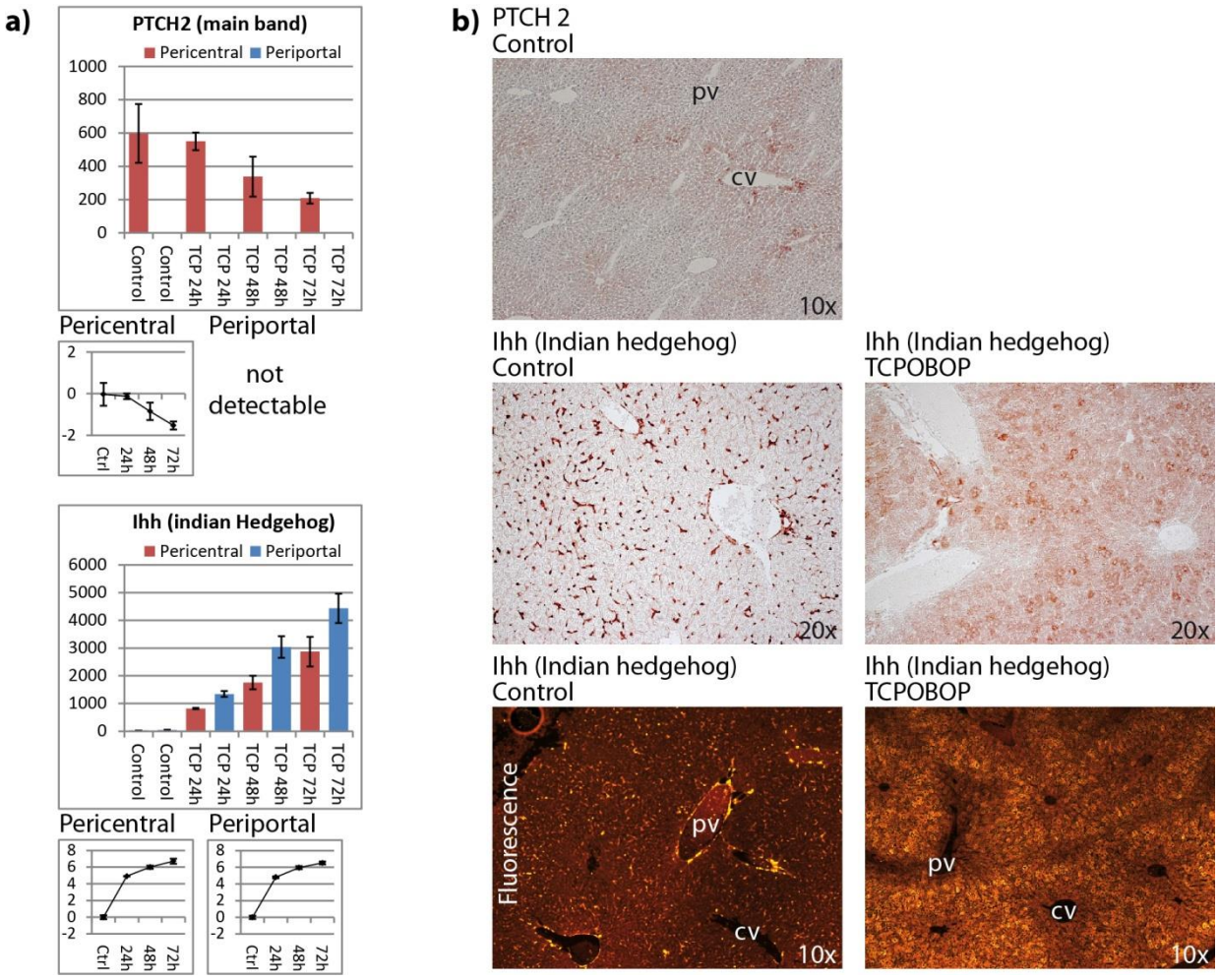

FIGURE 43 HEDGEHOG LIGAND IHH AND RECEPTOR PTCH2 IN THE TCPOBOP TREATMENT TIME-COURSE

a) *The data obtained for PTCH2 and Ihh represented as diagrams in AFI (relative fluorescence units) with standard error. PTCH2 was only detectable in the pericentral zone and shows a decrease in the time-course. Ihh is about 100-fold induced in the time-course in both zones (red is periportal and blue is*

pericentral). The smaller diagrams show the log2-fold changes relative to the control group with standard error. Data were normalized on the median of the corresponding control group.

***b)** IHC staining of PTCH2 and Ihh. The stainings were performed by Elke Zabinsky. PTCH2 staining is shown on a fresh-frozen liver section of a control mouse and shows a pericentral zonation. Ihh was stained on formalin fixed, paraffin embedded sections from a control mouse and a mouse treated with TCPOBOP for 72 hours. In the control mouse, Ihh staining shows a pattern which seems to be cells in between the hepatocytes which could be stellate cells. The zones cannot be assigned for the sections. The staining does not show a clear zonation. In the TCPOBOP treated liver all the hepatocytes show Ihh staining with a midlobular zonation. The intensities of the pictures cannot be compared as the microscope automatically searched for the ideal contrast. The staining was also performed using fluorescence and the zones are indicated by pv (portal vein) and cv (central vein). In the 10x magnification, the pattern in the control mouse is not so clear but Ihh is also located in between the hepatocytes. In the TCPOBOP treated mouse again all hepatocytes show Ihh staining and the stronger staining in the midlobular zone is clearly visible.*

4.3.3.3 PP2A is involved in TCPOBOP induced CAR activation

The nuclear receptor CAR which is activated by phenobarbital and TCPOBOP is retained in the cytoplasm and upon drug induced activation, it translocates into the nucleus (Kawamoto et al., 1999). Dephosphorylation of CAR at Ser202 seems to be necessary for nuclear translocation which is performed by PP2A (Hosseinpour, Moore, Negishi, & Sueyoshi, 2006). It was shown that the CAR-HSP90 complex, which is located in the cytoplasm, recruits PP2A upon Phenobarbital treatment which might induce CAR translocation to the nucleus (Yoshinari, Kobayashi, Moore, Kawamoto, & Negishi, 2003). The observed zonation of PP2A phosphorylation in the DigiWest results should result in low periportal and high pericentral PP2A activity.

PP2A itself has been described as tumor suppressor and inhibitors of PP2A have been described as tumor promoters (Fujiki, Sueoka, & Suganuma, 2013; Haystead et al., 1989; Westermarck & Hahn, 2008). As mentioned, for retinal cells the inhibitory PP2A phosphorylation has been described to mediate a stress survival response. They observed a massive peak in PP2A phosphorylation within 15 minutes as response on reactive oxygen species (Finnegan et al., 2010).

Therefore, the observation on the inhibitory phosphorylation of PP2A is interesting, showing a strong peak after 24 hours of TCPOBOP treatment. This effect shows a strong variation in between the animals resulting in high standard deviations which might result from a very sharp peak which cannot be resolved in the 4 time points. Yet after 24 hours, in the pericentral zone a minimum increase of 10.6-fold

(maximum of control group compared to minimum of 24 hours treatment group) and a maximum increase of 155-fold (minimum of control group compared to maximum of 24 h treatment group) were seen. The median increase for the peak at 24 hours is 40-fold for the pericentral zone and 6-fold for the periportal zone. The amount of phosphorylated PP2A reaches a similar level in both zones at 24 hours. This should result in a massive inhibition of PP2A after 24 hours and as PP2A is a major serine and threonine kinase it represents a massive disturbance in cellular signaling which might have wide ranging effects. As inhibitors of PP2A have been described as tumor promoters, the proliferation peak induced at 24 to 48 hours after TCPOBOP treatment and the resulting increase in liver mass which has been seen as a physiological process meant to increase the detoxifying capacity of the liver (Donthamsetty et al., 2011), might possibly be a pathophysiologic effect based on an overdrive of a stress survival response and the massive inhibition of PP2A.

4.3.3.4 Wnt-signaling might be down-regulated

Expression of the zonation marker glutamine synthetase has been shown to be regulated by β-catenin and might be a target of the Wnt/β-catenin pathway (Cadoret et al., 2002) and overexpression of glutamine synthetase is associated with β-Catenin mutations in mouse liver tumors (Loeppen et al., 2002). Besides the massive zonation of glutamine synthetase, the DigiWest results show a decrease of GS over the TCBPOBOP treatment time course of about 2-fold (72 hours compared to control) for periportal and pericentral zones. β-catenin itself and Wnt3a, the only Wnt protein measured in this experiment, also show a decrease during the time. This might indicate that β-catenin signaling could be reduced during TCPOBOP treatment. But as mentioned, several analytes and phosphorylations show a decrease over the time course. As the samples represent a defined volume of liver tissue this might be associated with the increase in cell size and the analytes might hence still be present in the same number in the cells but due to the volume increase their concentration might decrease. The effect on cellular signaling resulting from this phenomenon cannot be accessed.

4.3.4 Conclusions from the mouse liver LCM experiment

The main part of this work was development of the DigiWest method. Therefore, an important aspect is the technical side. The DigiWest approach successfully allowed analysis of laser-capture microdissected material. The additional bands which appeared for some antibodies in a formalin-dependent manner underline the value of the molecular weight resolution which the DigiWest approach provides. The estimated about 2.5 µg of protein per sample which are barely enough for a single Western-Blot were

used for 204 antibody incubations and allowed a comprehensive analysis of the proximal periportal and pericentral zones from mouse livers. An additional advantage of the LCM based approach was the possibility to analyze phosphorylation of proteins which is impaired by perfusion-based approaches.

The analysis of the proximal liver zones in the untreated control group gave new insights into cellular signaling in the liver zones and highlighted the role of serine and threonine phosphorylations, kinases and phosphatases.

The analysis of the TCPOBOP treatment showed that there are manifold changes upon TCPOBOP treatment. The proper interpretation of all these changes demands for advanced bioinformatics and systems biology approaches. Even without these analyses the results show that there are substantial differences between the periportal and the pericentral zones indicating that oxidative stress might be restricted to the pericentral zone and the inhibitory phosphorylation of PP2A and the massive peak thereof at 24 hours might indicate a massive disturbance in cellular signaling upon TCPOBOP treatment. The data also unveiled the pericentral zonation of the hedgehog receptor PTCH2 which, combined with the strong induction of Ihh, might result in activation of hedgehog signaling.

Several of the results need further investigations as they represent new observations which have not yet been described. The experiment proved that the DigiWest method can be used for comprehensive analyses of limited LCM samples.

Although several pre-experiments were performed, all the data on mouse liver shown in this thesis were derived from one single DigiWest experiment which additionally underlines the value of the method.

4.4 Conclusions and outlook

The DigiWest method generates hundreds of replicas of a Western-Blot. It results in a bead-mix which contains the size-separated proteins from the initial Western-Blot and retains the molecular weight information in the color code of the beads. A bead-mix is sufficient for hundreds of antibody incubations while the results are highly comparable to classical Western-Blots. Thereby, it bridges the gap between Western-Blot and microarrays and brings the Western-Blot towards a systems-biology tool. As the DigiWest method mainly uses Western-Blotting equipment and the now wide-spread Luminex technology, it represents an interesting method which could be implemented in other laboratories without major investments.

Tissues represent the 'natural environment' of cells and therefore the most relevant material for research but they are not very popular as they are heterogeneous and contain for example different types of cells, stroma and blood vessels obstructing proper analyses. This can be solved by isolation of cells by LCM but most methods for protein analysis are not capable of or struggle with analysis of LCM samples. As demonstrated with the mouse liver LCM experiment, the DigiWest method can be used for comprehensive analyses of LCM isolated samples. In experiments which are not shown in this thesis, where hematoxylin and eosin (H&E) stained sections were used without formalin fixation and cells were isolated using the Arcturus system, the analysis worked even better. Therefore, DigiWest could promote analysis of tissue and LCM samples as it allows hundreds on analyses from limited material.

The DigiWest method completely changes the properties of the 'blot'. The bead-mixes can be handled like a liquid and pipetted or magnetic bead handling equipment can be employed providing the possibility for automation. Washing steps are fast as the proteins on the beads are better accessible for washing buffers but also for antibodies and other reagents. Assays are performed in microtiter plates and each aliquot of a bead-mix is statistically identical and contains the same proteins on the same bead-sets. These features are not only distinctive differences to the classical Western-Blot but also to all other technologies for detection of molecular weight separated proteins. Besides the original idea of generating replicas of a Western-Blot, these properties can be exploited for new approaches for research.

The nature of identical replicates can be used for pattern analysis for example using human serum samples instead of antibodies. Incubation of serum samples on DigiWest bead-mixes loaded with pathogen lysates can be used for analysis of reactivity of the serum antibodies towards the pathogen proteins. The resulting patterns on the size-resolved proteins can be used for classification of e.g. patients that are/were infected and non-infected. Using the pattern instead of an absolute signal could result in better classification compared to ELISA or similar approaches. The feasibility of this approach

has already been shown in a successful experiment performed by Anette Döttinger in our group using human sera and bacteria lysates. A similar approach might be possible for cancer diagnostics. Human tumor samples could be used to analyze reactivity of serum contained antibodies in a pattern analysis which might even allow differentiation of tumor types based on the patterns.

The Kinobead pulldowns shown in this thesis are similar to co-immunoprecipitations (co-IPs) which can therefore also be analyzed by DigiWest in a more comprehensive way which might allow analysis of large protein complexes and their dynamics under different conditions.

Another application which has not yet been tested could be experiments similar to Far-Western-Blot for protein interaction analysis or similar approaches. The better accessibility and flexibility of the proteins might bring a further advantage compared to Western-Blot besides the higher output.

It is also possible to perform enzymatic reactions on the DigiWest bead-mixes. The immobilized proteins could for example be dephosphorylated by phosphatases to test the phosphorylation specificity of antibodies. Therefore, an aliquot of a DigiWest bead-mix can be enzymatically dephosphorylated and used to compare the antibody specific signal to the signal obtained on an aliquot of the original bead-mix. DigiWest bead-mixes are generally ideal for antibody characterization as they allow fast and automatable assays with high reproducibility and high throughput. DigiWest might also be useful for RPPM as it could be used for prescreening of antibodies on the samples of interest and might thereby increase the reliability of the RPPM results.

DigiWest provides a new possibility to bring Western-Blot applications and variations to a higher output and the unique features of DigiWest provide the possibility to develop new ideas.

5 Methods

5.1 Sample preparation

5.1.1 Samples for method development

The samples used during method development were already lysed in CLB1 and protein content was determined in a Bradford assay. Samples were prepared in commercial NuPAGE LDS sample buffer according to the manufacturer's instructions. Preparations were composed of 1/4th volume 4x LDS sample buffer, 1/10th volume 10x NuPAGE Reducing Agent, the desired amount of sample and the remaining volume ddH_2O. Sample preparations were incubated on a Thermomixer comfort or a Mastercycler gradient for 10 minutes at 70°C prior to application to the gels.

5.1.2 GST-ERK2 spike-in experiment

HepG2 lysate was spiked with GST-ERK2 in a 1:4 dilution series. The preparations contained 10 µg HepG2 lysate and 20 ng, 5 ng, 1.25 ng, 0.31 ng, 78 pg or 19.5 pg of the GST-ERK protein per 12 µl.

HepG2 lysate (in CLB1 lysis buffer, 6.08 mg/ml protein) was prepared in LDS sample buffer according to the manufacturer's instructions. 1320 µl were prepared containing 1100 µg protein. 12 µl (10 µg protein) were applied to the gel for each lane.

Therefore: 677 µl H2O, 330 µl of 4x LDS sample buffer, 132 µl of 10x reducing agent and 181 µl sample were mixed.

GST-ERK2 was obtained from Millipore (#14-536) with a concentration of 1.463 mg/ml. 3 µl were mixed with 6 µl H2O resulting in a concentration 487.7 µg/ml.

294 µl of the HepG2 preparation was mixed with 1.005 µl diluted GST-ERK2 (490 ng) resulting in 20 ng GST-ERK2 per 12 µl. The remaining HepG2 preparation (1026 µl) was adjusted with 3.5 µl H2O. The GST-ERK2 spiked and the un-spiked HepG2 preparations were used to prepare a 1:4 dilution series. 200 µl of the HepG2 preparation were mixed with 66.67 µl of the GST-ERK2 spiked HepG2 preparation resulting in 5 ng GST-ERK2 per 12µl. This preparation was used for the next dilution step. 6 dilutions (from 20 ng to about 20 pg per 12 µl, overall dilution factor of 1024) were prepared. Samples were denatured at 70°C for 10 minutes. 12 µl were applied per lane.

For DigiWest, 3 replicates of each dilution were used resulting in 18 lanes. They were distributed over 3 blots (empty lanes between the protein-loaded lanes were needed for cutting the membrane). For Western-Blots, the 3 higher concentrations were applied in duplicates, the 3 lower concentrations in

triplicates resulting in 15 lanes per blot. 4 Western-Blots were prepared, 2 were blotted onto PVDF membranes, 2 on nitrocellulose membranes.

5.1.3 LCM of mouse liver sections

The TCPOBOP treatment study was performed by Albert Braeuning as described (Braeuning et al., 2011) and the sections were prepared by Elke Zabinsky at the Institute of Toxicology. Frozen mouse liver tissue was cut into 10 µm sections, placed on slides (MembraneSlide 1.0 PEN, Zeiss). Sections were formalin fixed and stained with a mouse-derived anti-glutamine synthetase (GS) antibody. These sections were stored at -80°C till used. The mouse liver tissue sections were derived from 16 animals, 4 replicates of each treatment condition. They were either treated with corn oil or with TCPOBOP for 24, 48 and 72 hours. Some more sections from mouse livers with corn oil and 48 hours TCPOBOP treatment were prepared for pretests.

For laser capture microdissection, the stained sections were stored on dry ice. One section per day was equilibrated to room temperature and placed on the PALM MicroBeam. Areas around the central veins (GS stained areas) and areas around non-stained blood vessels which should represent portal triads were collected. About the same width as seen for GS staining was chosen (1-2 cell layers). An area of about 3.7 mm² was collected on AdhesiveCap 200 opaque (Zeiss) for central vein and portal vein regions. Each sample was collected on 6 caps with an area of about 0.6 mm² per cap. The caps containing the collected areas were stored at room temperature till the LCM of the section was completed (8 hour in average). The collected samples were then placed on dry ice and later stored at -80°C. So the 16 sections for the main experiment resulted in 32 samples each composed of 6 caps.

For lysis, the areas from each sample were pooled into 0.5 ml vials by adding 10 µl of 100% ethanol to each cap and transfer into the vials. The vials containing about 60 µl ethanol and the LCM material were stored at -80°C. The next day they were dried in a speed-vac. The lysis buffer had the following composition. 500 µl lysis buffer: 275 µl TPER, 125 µl 4x LDS, 100 µl Reducing Agent. 15 µl of this buffer was added to each sample and incubated for 1 hour at 95°C, 1200 rpm on a Thermomixer comfort. Samples were stored at -80°C and used as is for gel electrophoresis.

5.1.4 H292 cell lysates and Kinobead pulldowns

These samples were provided by Benjamin Ruprecht, TUM, laboratory of Bernhard Küster. Samples were provided in 2x LDS sample buffer containing 2x Reducing Agent. Cell lysates were diluted in the same buffer to a concentration of 25 µg protein per 15 µl volume. Preparation of the Kinobead pulldowns was

performed as follows: 13 µl pulldown (in 2x LDS) + 5 µl of LDS buffer containing Reducing Agent (80 µl 4x LDS + 20 µl Reducing Agent). Samples were incubated at 50°C for 30 minutes following Benjamin's instructions.

5.2 Electrophoresis and blotting

5.2.1 Electrophoresis (SDS PAGE)

The commercial NuPAGE gel electrophoresis system was used for all gel electrophoresis experiments mentioned. Gels were NuPAGE 4-12% Bis-Tris Protein Gels. They contain a gradient from 4 to 12% poly-acrylamide. All gels used were 1 mm thick, the number of lanes varied depending on the experiment. Gels were unpacked, rinsed with ddH_2O and placed in the corresponding chambers. NuPAGE MES SDS running buffer was prepared using 40 ml 20x buffer and adding ddH_2O to a volume of 800 ml per chamber. The inner chamber was supplemented with 500 µl NuPAGE Antioxidant. 5 µl SeeBlue Plus 2 pre-stained protein standard was used as molecular weight marker. For DigiWest experiments the marker was applied twice, usually in the outer left and the outer right lanes.

Samples were loaded and gels were run at 150 V for 90 minutes on ice. For DigiWest experiments every second lane was left empty. This was necessary for cutting the membranes after blotting. For the H292 cell lysates and Kinobead pulldowns NuPAGE MOPS buffer was used and gels were run at 100 V for 3.5 hours on ice following Benjamin's instructions.

Gels for protein determination were usually just run for 20 to 45 minutes.

5.2.2 Western-Blotting

Blotting onto membranes was based on the wet blotting method. Again the commercial NuPAGE system was used. Blotting modules were the XCell SureLock Mini-Cells. NuPAGE Transfer buffer was used. Transfer buffer was (per blotting module) 25 ml 20x NuPAGE Transfer buffer, 50 ml methanol, filled to 500 ml with ddH_2O. Transfer setup was as follows: 3 transfer sponges soaked with transfer buffer, 2 Whatman papers soaked with transfer buffer, gel, membrane soaked with transfer buffer, 2 soaked Whatman papers, 2 soaked sponges. Transfer conditions were: 30 V, 200 mA, 60-75 minutes. In earlier experiments transfer was performed on ice, later at room temperature.

Membranes were, depending on the experiment, nitrocellulose or PVDF membranes. Membranes and Whatman papers had a size of 7.5x8.5 cm. For DigiWest experiments PVDF membranes were used which were pre-wetted in 100% methanol for 20-30 seconds.

5.2.3 Ponceau S staining

After blotting, a Ponceau S stain was performed for quality control and in case of DigiWest experiments for labelling of the lane positions. Nitrocellulose membranes were stained directly. PVDF membranes were washed/blocked in PBST for about 15 minutes prior to staining. Membranes were stained in Ponceau S solution for 5 minutes and washed in ddH_2O till the proteins were visible. In case of DigiWest experiments a pencil was used to label the protein lane positions. Images of each blot were taken using the Fuji LAS-4000. Blots were destained in TBST till no Ponceau S was visible anymore. For DigiWest experiments blots were destained and washed in PBST for 30 minutes with several rounds of buffer exchange.

5.2.4 Immuno-detection

For Western Blot incubations, blots were blocked in either 3% BSA or 3% milk powder in TBST for about 1 hour. Antibody dilutions were prepared in either 1% BSA or 1% milk powder in TBST. Blots were placed in 15 ml or 50 ml tubes and incubated with the primary antibody overnight on a wobble roller at 4°C. For small blots in 15 ml tubes, 2.5 ml antibody dilution were used, for whole blots in 50 ml tubes 4 ml. Blots were washed 5 times for 5 minutes in TBST. For 15 ml tubes 5 ml TBST were used for washing, for 50 ml tubes 10 ml were used. Secondary antibodies were prepared in the same buffer than the primary antibodies and incubated for 1 hour at room temperature, in case of fluorescently labelled antibodies in the dark. After washing 5 times for 5 minutes blots were prepared for readout.

For fluorescent LICOR Odyssey readout blots were dried between Whatman paper and readout was performed using the dry blots. Blots were pre-scanned with different laser power settings to find the optimal setting (highest intensity without saturated pixels) for high resolution readout.

For chemiluminescent readout using the Fuji LAS-4000 the SuperSignal West Pico chemiluminescent substrate was used. Working solution was prepared freshly following the manufacturer's instructions. Blots were incubated for 5 minutes in the chemiluminescent substrate then placed on the LAS-4000 tray, soaked with the chemiluminescent substrate, covered with a glass plate and exposed on the LAS-4000 in an incremental series. The image with the longest exposure time without any saturation was chosen for further processing.

5.2.5 Western-Blot quantification

Western Blot quantification was performed using the Fuji MultiGauge software.

5.3 Luminex bead preparation (final workflow conditions)

5.3.1 Coating of MagPlex beads with NeutrAvidin

Coupling conditions were optimized over time. The following conditions represent the latest coupling conditions which were used for the main 384-plex DigiWest bead-mixes.

Coupling of NeutrAvidin to Luminex MagPlex bead-sets was performed employing a KingFisher 96 automated magnetic particle processor. 400 bead sets were coated with NeutrAvidin. These bead sets were used to compose a 384-plex consisting of 4 times 96 bead sets. The KingFisher 96 was equipped with a 96 head for deep well plates. The coupling procedures took place in KingFisher 96 KF plates using tip combs for deep well plates.

MagPlex magnetic Luminex beads were delivered in vials containing 1 ml bead suspension with a concentration of 12.5 million beads/ml. Beads were vortexed vigorously for 30 seconds and placed in an ultrasonic bath for 10 seconds. Beads were vortexed again directly before pipetting them into the bead plates. To reduce stickiness of the KingFisher consumables, all buffers were supplemented with Triton X-100 (see buffer compositions).

500 µl of each bead set were used. The first round of bead-coating was performed for 16 bead sets followed by four rounds of 96 bead sets each. 2 bead plates were used to provide the beads to the KingFisher. 5 µl of a 2.5% Triton X-100 solution in ddH_2O were pipetted to each well followed by 250 µl bead suspension. 2 more plates were filled with 200 µl/well activation buffer (100 mM phosphate buffer, pH 6.2, 0.01% Triton-X100).

In the first program, the KingFisher pooled the 2 bead plates and used the 2 activation buffer plates for washing followed by release of the pooled beads in the second activation buffer plate.

The coupling procedure worked as follows:

The KingFisher was equipped with 8 plates providing all buffers and solutions necessary. Beads were transferred to the activation plate which was prepared directly before the program was started. The activation plate contained 150 µl/well activation mix (5 mg/ml EDC and 5 mg/ml sulfo-NHS in activation buffer). The activation of the carboxylated Luminex beads to sulfo-NHS esters was performed for 20 minutes (4 rounds of 1 minute mixing and 4 minutes incubation). The next 2 plates contained 200 µl/well coupling buffer (50 mM MES, pH 5.0, 0.01% Triton X-100) for washing followed by the coupling plate which contained 150 µl/well of 500 µg/ml NeutrAvidin in coupling buffer. Coupling was performed for 2 hours (12 rounds of 1 minute mixing and 9 minutes incubation). After coupling, the beads were washed in 2 plates containing 200 µl/well CBS (‘carboxy block store’, 1% BSA in PBS, 0.05% sodium azide, 0.05%

Tween-20 (in later coupling procedure the Tween-20 was omitted)). The beads were finally released in a plate containing 200 µl CBS.

Beads were pipetted into 1.5 ml vials, wells were washed once with 200 µl CBS. The vials were placed in a magnet stand, buffer was removed and 1 ml CBS was added to each bead-set.

5.3.2 Quality control

500 µl CBS were pipetted into a 1.5 ml vial which was placed on a magnet stand. Bead sets were vortexed vigorously before use. 5 µl of each bead set were pipetted into the 1.5 ml vial. When the vial was full, some buffer was removed. After 5 µl of all 400 bead sets were pipetted into the vial, the buffer was removed and 1 ml CBS was added.

5.3.2.1 Bead count

500 µl of this 400-plex bead-mix was transferred to a new vial for loading control. The remaining 500 µl bead-mix were placed on a magnet stand, buffer was discarded and 1250 µl CBS were added. 8 replicates of 100 µl of this bead-mix were added to an assay plate. Readout was performed on a Luminex FlexMap 3D with the settings: count to 10000 and 50 µl volume. The count to 10000 cannot be reached so the instrument measures all beads in the solution till the volume limit is reached. The number of beads which were measured of each set can be used to back-calculate the bead concentration of each set. The calculated concentrations were used to adjust the 400 bead sets to a concentration of 4000 beads/µl.

5.3.2.2 Biotin binding capacity

The 500 µl bead-mix from above was placed in a magnet stand and buffer was removed. Beads were resuspended in 180 µl CBS. A biotinylated c-Myc peptide was used for testing the biotin binding capacity. The peptide had the sequence biotin-Doa-Doa-EQKLISEEDL. 40 µl of a 1 mg/ml solution were added to the bead-mix. Loading of the peptide onto the beads was performed for 2 hours on a Thermomixer at 900 rpm, 25°C. Beads were washed 5 times with 500 µl CBS and resuspended in 300 µl CBS.

Anti-c-Myc antibody (clone 9E10) was used for the loading control assay. A dilution series of anti-c-Myc-antibody was prepared (1 µg/ml, 0.2 µg/ml and 0.04 µg/ml) in CBS and a blank (CBS).

50 µl/well CBS were pipetted into an assay plate. 10 µl/well of the peptide-loaded bead-mix were added to 16 wells, preincubated for some minutes, placed on a magnet plate and buffer was discarded. 50 µl of the antibody dilution were added to the beads with 4 replicates each. Antibody was incubated for 2 hour on a Thermomixer at 750 rpm, 23°C. After 3 times washing with 100 µl PBST on a magnet plate, anti-

mouse-PE secondary antibody was added (50 µl/well, 2.5 µg/ml in CBS) and incubated for 1 hour at 750 rpm, 23°C. After washing 3 times with PBST on a magnet plate, 100 µl/well PBST were added for readout on a Luminex FlexMap 3D.

5.3.2.3 DigiWest bead plate composition

The bead sets used were the Luminex MagPlex bead sets 001 to 400. Some of the bead sets had to be excluded due to a technical problem leading to a shift of some bead sets out of their classification region in one corner of the 3-dimensional classification space. So these bead sets were excluded from the 384-plex DigiWest bead-mix. Some more bead sets were excluded due to their performance in the biotin binding capacity test. The selected 384 bead sets had a biotin binding capacity with a CV below 3% and were adjusted to a concentration of 4000 beads/µl. They were arranged in 4 blocks with 96 bead sets according to their bead set ID.

5.3.2.4 Bead plate preparation

200 µl/well of the 4 x 96 bead sets were pipetted into 4 96 well V-shape plates. These plates were used as master-plates to generate DigiWest bead plates containing a defined number of beads per well. This was done employing a BioMek FX pipetting robot which was equipped with a 96 pipetting head. 96 well V-shape plates were filled with 50 µl/well CBS and placed in the BioMek FX together with the master plate. Usually 40000 beads/well (10 µl) or 20000 beads/well (5 µl) were pipetted by the robot into each plate. Plates were labelled and vacuum sealed. These plates were stored at 4°C in the dark till used.

5.4 DigiWest (final workflow conditions)

5.4.1 Membrane processing

After Ponceau S staining and washing in PBST for 30 minutes with several rounds of buffer exchange, membranes were biotinylated. For each blot an aliquot NHS-PEG12-Biotin (50 mM, 20 µl in DMSO) was diluted in 20 ml PBST resulting in a concentration of 50 µM and added to the membrane. The reaction was performed at room temperature on a shaker for 1 hour at speed 30/minute and an angle of 6° in the dark. Blots were washed with PBST 3 times for 1 minute and dried between 2 Whatman papers.

Dried membranes were placed on a template printed on 120 g/m² paper and fixed with tape. The used templates were self-made Adobe Illustrator files. Membranes were covered with a piece of 120 g/m² paper. The template with the protected membrane was placed on a Silhouette cutting mat and placed in a Silhouette SD cutting plotter. Each lane containing separated proteins (every second) was cut into 96 horizontal strips which were usually 6 mm wide and 0.5 mm high.

5.4.2 Protein Elution

Elution buffer was 8 M urea, 1% Triton X-100 in 100 mM Tris-HCl buffer pH 9.5 (final concentration due to the volume of the urea was about 60-65 mM).

Each lane was folded or cut in the middle as the wells of 96 well plates have a diameter below 6 mm. The 96 strips were picked using a forceps and sorted into 96 well plates resulting in 1 plate per lane. 10 µl/well of the elution buffer was added. Plates were sealed with plate sealing tape and incubated on either Thermomixer comfort or a TiMix 5 control equipped with 2 decks for 16 plates at 1200 rpm for 90 minutes at room temperature.

5.4.3 Protein loading onto Luminex beads

Before bead loading, 90 µl of 5% BSA in PBST with 0.05% sodium azide was added to each well of the plates containing membrane snippets and eluted proteins to dilute the denaturing elution buffer. In earlier experiments a 3% BSA solution was used. Plates were placed on a shaker for some seconds. Bead plates were prepared ready to use and stored at 4°C till used as described. A KingFisher 96 PCR magnet head was used manually. A KingFisher 96 tip comb for PCR magnets was pre-blocked in the 3% or 5% BSA solution from above for some minutes. Then a KingFisher 96 PCR head and the comb were used to transfer the beads from the DigiWest bead plates to the plates containing the diluted and eluted proteins. Plates were sealed with a plate sealing tape and incubated on either Thermomixer comfort or TiMix 5 control over night at room temperature at either 750 rpm or 650 rpm.

5.4.3.1 Blocking of remaining biotin binding sites

An aliquot of the NHS-PEG12-Biotin was mixed with 500 µl TBST and incubated overnight at room temperature (left on the workbench). The inactivated biotinylation reagent was used to block the remaining biotin binding sites on the Luminex beads. The biotinylation reagent was diluted with TBST to a volume sufficient for 4 to 6 plates. 5 µl of the diluted biotin was added to each well and incubated for 1 hour at room temperature.

5.4.3.2 Pooling the beads to a DigiWest bead-mix

A PickPen 8-magnet tool and corresponding silicone tips were used to pool the beads into one bead-mix. All 4 plates containing the 384-plex representing 4 Western-Blot lanes were pooled. In several experiments the beads from the 4 plates were pooled into one plate using a KingFisher 96-well magnet prior to the PickPen pooling procedure. The beads were then transferred into 1.5 ml vials, washed 3

times with 500 µl CBS employing a magnet stand and then resuspended in CBS to a concentration of 40 beads/set/µl.

5.4.4 DigiWest assays

The assay layouts were individually designed for each experiment mainly depending on the number of samples and the resulting number of DigiWest bead-mixes.

DigiWest assays were performed in 96 well half-area plates (Corning). The assay buffer for the final workflow was blocking reagent for ELISA (Roche) supplemented with 0.2% milk powder, 0.05% Tween-20 and 0.02% sodium azide. Antibodies were diluted in assay buffer. Antibodies were usually used in a concentration about 5 times higher than recommended for Western-Blots and not more than 1 µg/ml. For example antibodies from Cell Signaling which are recommended to be diluted 1:1000 were used in a 1:200 dilution.

Plates were filled with 50 µl assay buffer per well. The DigiWest bead-mix or bead-mixes were added, usually 5 µl of the bead-mixes containing 40 beads/ID/µl resulting in 200 beads/ID/well. Beads were pre-incubated in assay buffer for some minutes. Plates were placed on magnet plates and buffer was discarded. 30 µl/well of the antibody dilutions were added, plates were sealed with plate sealing tape and incubated overnight on a Thermomixer comfort at 750 rpm and 15°C. The next day the plates were washed twice with PBST (100 µl/well) on a magnet plate. PE-labelled secondary antibodies were diluted 1:200 in assay buffer (2.5 µg/ml). 30 µl were added per well and incubated for 1 hour at 750 rpm, 23°C. Plates were washed twice and 100 µl/well PBST was added for readout.

Readout settings on the Luminex FlexMap 3D were count to 50 beads per set, 90 µl volume and due to the bigger size of the MagPlex beads compared to the MicroPlex beads an increased gate. Depending on the bead recovery in the first assay of each DigiWest bead-mix or bead-mixes the count was lowered to 40 or 35 beads which represent the absolute minimum for stable assays.

5.4.5 Data analysis

As DigiWest is a completely new method there was no data analysis software. Therefore I created an Excel based analysis tool. This tool is described in detail in the method development section.

5.4.6 Western-Blot mimics

For generation of the Western-Blot mimics the background subtracted Luminex data were used. Background subtraction was performed either using the species specific blank or the bead-set specific background. The background subtracted data were normalized to values between 0 and 1 and loaded into the TM4 Microarray Software Suite (MEV) which created gray-scale maps using a black and white color scheme with 0 represented in white and 1 in black. The images were saved and a Gaussian diffusor was applied in Photoshop with a radius of half the element height.

5.5 Protein determination

5.5.1 Coomassie (Bradford)

A Bradford (Coomassie) Protein Assay Kit was used according to the manufacturer's instructions. A BSA standard was prepared in the same buffer as the corresponding samples. In cases when the samples were diluted for the assay, the standard was prepared in the same dilution. The standard concentrations usually covered the range from 1000 µg/ml to 25 µg/ml and a blank. 5 µl of the standards, blank and samples were pipetted to a 96 well F-bottom plate (Greiner) in duplicates or triplicates. 200 µl of the Coomassie reagent was added. The plates were placed on a shaker for 30 seconds and then incubated for 10 minutes at room temperature. Readout was performed on a FLUOstar OPTIMA.

5.5.2 BCA (bicinchoninic acid)

A BCA Protein Assay Kit was used according to the manufacturer's instruction. The BSA standard was prepared as described for Coomassie protein determination.

5.5.3 In gel

For very limited samples which were directly prepared in LDS sample buffer or in Laemmli buffer it was necessary to perform the protein determination in gel as no protein assay was compatible with these buffers and sensitive enough.

Krypton stain was used for in gel protein stain. A sample which was related to the samples of interest was used as standard. For example for mouse liver LCM samples a mouse liver lysate was used. The standard sample was used in 4 different concentrations based on best guess for the samples of interest in a 1:2 dilution series. The standards and aliquots of the samples were run on a gel as described in the electrophoresis section.

Either Krypton Flourescent Protein Stain or Krypton Infrared Protein Stain was used according to the manufacturer's instruction. Usually the standard procedure or an intermediate between standard and rapid procedure was used. Readout was performed on the Odyssey scanner (Licor) for the infrared variant or on the Typhoon Trio (GE Healthcare) for the 'fluorescent' variant.

For quantification the MultiGauge software was used. In contrast to Western-Blot quantification not a single band was chosen for quantification but a wide range representing the whole or the majority of the lanes.

5.6 Gel staining

5.6.1 Krypton

See in-gel protein determination.

5.7 Statistical analysis

For statistical analysis the TM4 Microarray Software Suite (MEV) was used which has the R statistical language packets implemented (Saeed et al., 2006). The experiment-specific tests are described in the results part. In general, data were normalized on the median or mean of the corresponding control group and log2 transformed prior to statistical analysis. The settings for the individual tests are also described in the results part.

6 Materials

6.1 Reagents and consumables

6.1.1 Buffers and solutions

Basic buffers

Buffer Name	Composition	Supplier
PBS (Dulbecco's)	PBS 10x, BP399	Thermo Fisher Scientific, Walthab, MA, USA
PBS (Dulbecco's)		PAA Laboratories, Pasching, Austria
TBS	10 mM Tris, 150 mM NaCl in ddH2O pH 7,4	
Tris/HCl	100 mM Tris, adjusted with HCl in ddH2O, pH 9.5	

Composed buffers

Buffer Name	Composition	Supplier
Activation Buffer	100 mM phosphate, pH 6.2, 0.01% Triton X-100, ddH2O	
Antioxidant	NuPAGE Antioxidant	Life Technologies, Carlsbad, CA, USA
Assay buffer	0.05% Tween 20, 0.2% milk powder, 0.05% sodium azide, in BRE	
Blocking Reagent for Elisa (BRE)	Blocking Reagent for Elisa, 11112589001	Roche, Rotkreuz, Risch, Switzerland
Bradford Reagent	Pierce Coomassie Assay Reagent	Thermo Fisher Scientific, Waltham, MA, USA
CLB1 lysis buffer	Zeptosens Reverse Array Lysis Buffer CLB1	Bayer Technology Services, Leverkusen
Coupling Buffer	50 mM MES, pH5.0, 0.01% Triton X-100, ddH2O	
Elution buffer	8 M urea, 1% Triton X100 in 100 mM Tris/HCl pH 9.5	
Gel-Staining	Krypton protein stain	Thermo Fisher Scientific, Walthab, MA, USA
	Krypton infrared protein stain	Thermo Fisher Scientific, Walthab, MA, USA
LDS sample buffer	NuPAGE LDS Sample Buffer	Life Technologies, Carlsbad, CA, USA
Lowry reagent	DC Protein Assay Kit	Bio-Rad Laboratories, Hercules, CA, USA
PBST	0,1 % (v/v) Tween 20 in PBS	
Ponceau S solution	0.1% (w/v) Ponceau S, 1% acetic acid, ddH2O	
Protein ladders	Odyssey Protein Molecular Weight Marker;	LI-COR Biosciences, Lincoln, NE, USA;
	SeeBlue Plus2 Pre-Stained Standard	Life Technologies, Carlsbad, CA, USA
Reducing agent	NuPAGE Sample Reducing Agent	Life Technologies, Carlsbad, CA, USA
Running buffers	NuPAGE MES SDS Running Buffer	Life Technologies, Carlsbad, CA, USA
	NuPAGE MOPS SDS Running Buffer	Life Technologies, Carlsbad, CA, USA
Storage buffer (CBS)	1% BSA, 0.05% sodium azide, (0.05% Tween 20), in PBS	
Streptavidin-PE	Streptavidin-R-Phycoerythrin	Dianova, Hamburg
TBST	0,1 % (v/v) Tween 20 in TBS	
T-PER	T-PER Tissue Protein Extraction Reagent	Thermo Fisher Scientific, Walthab, MA, USA
Transfer buffer	NuPAGE Transfer Buffer	Life Technologies, Carlsbad, CA, USA
Western blotting substrate	SuperSignal West Pico Chemiluminescent Substrate	Thermo Fisher Scientific, Waltham, MA, USA

6.1.2 Chemicals and reagents

Product	Supplier
Acetic acid	Carl Roth, Karlsruhe
Biotin-c-myc peptide (custom)	NMI Peptides, Reutlingen
BSA (Fraktion V, protease free)	Carl Roth, Karlsruhe
DMSO	Sigma-Aldrich, St. Louis, MO, USA
EDC	Thermo Fisher Scientific, Walthab, MA, USA
Glycerol	Sigma-Aldrich, St. Louis, MO, USA

Product	Supplier
GST-ERK2 fusion protein	Millipore / Merck, Darmstadt
HCl	Sigma-Aldrich, St. Louis, MO, USA
KCl	Sigma-Aldrich, St. Louis, MO, USA
Krypton Protein Stain	Thermo Fisher Scientific, Walthab, MA, USA
Krypton Infrared Protein Stain	Thermo Fisher Scientific, Walthab, MA, USA
MES	Sigma-Aldrich, St. Louis, MO, USA
Methanol	Carl Roth, Karlsruhe
MgCl2	Merck, Darmstadt
Milk powder	Carl Roth, Karlsruhe
Na2HPO4	Carl Roth, Karlsruhe
NaCl	Sigma-Aldrich, St. Louis, MO, USA
NaH2PO4	Carl Roth, Karlsruhe
NaHCO3	Merck, Darmstadt
NaN3 (Sodium azide)	Sigma-Aldrich, St. Louis, MO, USA
NaOH	Carl Roth, Karlsruhe
NHS-LC-LC-Biotin	Thermo Fisher Scientific, Walthab, MA, USA
NHS-PEG12-Biotin	Thermo Fisher Scientific, Walthab, MA, USA
Ponceau S	Carl Roth, Karlsruhe
PVA (different chain lengths))	Sigma-Aldrich, St. Louis, MO, USA
PVP (PVP-360)	Sigma-Aldrich, St. Louis, MO, USA
PVP (different chain lengths)	ICN Biomedicals, Aurora, Ohio, USA
	Sigma-Aldrich, St. Louis, MO, USA
SDS	Sigma-Aldrich, St. Louis, MO, USA
sNHS	Thermo Fisher Scientific, Walthab, MA, USA
Tris	Carl Roth, Karlsruhe
Triton X-100	Sigma-Aldrich, St. Louis, MO, USA
Triton X-100	VWR, Radnor, PA, USA
Tween 20	Merck, Darmstadt
Urea	Sigma-Aldrich, St. Louis, MO, USA

6.1.3 Secondary antibodies

Antigen	Species	Label	Supplier	Product #
anti-Goat IgG (H+L)	Donkey	HRP	Jackson Dianova	705-035-147
anti-Goat IgG (H+L)	Donkey	IRDye 800CW	LI-COR Biosciences	926-32214
anti-Goat IgG (H+L)	Donkey	RPE (PE)	Jackson Dianova	705-116-147
anti-Mouse IgG (H+L)	Goat	HRP	Jackson Dianova	115-035-062
anti-Mouse IgG (H+L)	Donkey	RPE (PE)	Jackson Dianova	715-116-151
anti-Mouse IgG (H+L)	Goat	RPE (PE)	Jackson Dianova	115-116-146
anti-Mouse IgG (H+L)	Donkey	IRDye 800CW	LI-COR Biosciences	926-32212
anti-Rabbit IgG (H+L)	Donkey	HRP	Jackson Dianova	711-035-152
anti-Rabbit IgG (H+L)	Donkey	RPE (PE)	Jackson Dianova	711-116-152
anti-Rabbit IgG (H+L)	Donkey	IRDye 800CW	LI-COR Biosciences	926-32213
anti-Rat IgG (H+L)	Donkey	HRP	Jackson Dianova	712-035-153
anti-Rat IgG (H+L)	Donkey	RPE (PE)	Jackson Dianova	712-116-153
anti-Rat IgG (H+L)	Goat	IRDye 800CW	LI-COR Biosciences	926-32219
anti-Sheep IgG (H+L)	Donkey	RPE (PE)	Jackson Dianova	713-116-147
Streptavidin		RPE (PE)	Jackson Dianova	016-110-084

6.1.4 Primary antibodies

Antigen	P-Sites	Species	Distributor	Product #	Lot #
14-3-3 sigma		gt	R&D	AF4424	ZLC01-07051
4E-BP1		rb	Epitomics	1557-1	YC111401
4E-BP1 – phospho	Ser65	rb	Cell Signaling	9451	14
ABL2		rb	Epitomics	5431-1	
ABL2 (phosphorylated) antibody		rb	Biorbyt	orb34396	
Acetyl-CoA Carboxylase – phospho	Ser79	rb	Cell Signaling	3661	10
ADAM12		rb	abcam	ab137468	GR128068-2
AHR		sheep	R&D	AF6697	CFAL0111021
Ahr		rb	Biomol	SA-210	
Akt		rb	Cell Signaling	4685	
Akt		rb	Cell Signaling	4691	11
Akt		rb	Cell Signaling	9272	11
Akt – phospho	Ser473	rb	Cell Signaling	4060	5
Akt – phospho	Thr308	rb	Cell Signaling	9275	
Alcohol dehydrogenase beta subunit (Aldh1A1)		rb	Epitomics	2052-1	YE0226012
AMPK alpha		rb	Cell Signaling	2532	3
AMPK alpha – phospho	Thr172	rb	Cell Signaling	2535	13
Anti-Folate Binding Protein (Folate Receptor, FOLR1)		rb	Epitomics	ab125030	
Anti-SIK3		rb	Epitomics	ab88495	
A-Raf		rb	Cell Signaling	4432	2
ASK1		rb	CST	8662	
ASK1 Phospho	Ser83	rb	CST	3761	
ASK1 Phospho	Thr845	rb	CST	3765	
ASL (argininosuccinate lyase)		rb	Atlas/Sigma	HPA016646	R06318
ATF3		rb	Sigma	HPA001562	A70381
ATM		rb	Cell Signaling	2873	3
ATM – phospho	Ser 1981	ms	Millipore	MAB3806	2015985
Aurora A – phospho	Thr288	rb	Cell Signaling	3079	3
Aurora A (AIK)		rb	Cell Signaling	4718	
Aurora A/B/C – phospho	T288/T232/T198	rb	Cell Signaling	2914	3
Aurora A/B/C – phospho	T288/T232/T198	rb	Cell Signaling	2914	3
Aurora B (AIM1)		rb	Cell Signaling	3094	2
Axin1		rb	Cell Signaling	3323	1
Bad		rb	Cell Signaling	9292	6
Bad – phospho	Ser112	ms	Cell Signaling	9296	2
Bax		rb	Cell Signaling	2772	6
Bcl2		rb	Cell Signaling	2870	2
Bcl-xL		rb	Cell Signaling	2764	4
beta-Actin		ms	Sigma	A1978	012M4821
beta-Catenin		rb	Biosource	AHO0462	25439-06S
beta-Catenin – phospho	Ser675	rb	Cell Signaling	9567	1
beta-Catenin – phospho	Thr41/Ser45	rb	Cell Signaling	9565	2
beta-Catenin – phospho	Ser552	rb	Cell Signaling	9566	2
beta-Catenin (non-pospho Ser33/37/Thr41; active)		rb	Cell Signaling	8814	3
Bmf		rb	Cell Signaling	4692	1
b-Raf		rb	Upstate	07-583	
b-Raf – phospho	Ser445	rb	Cell Signaling	2696	
BRCA1		rb	Cell Signaling	9010	2
BRCA1 – phospho	Ser1524	rb	Cell Signaling	9009	2
C/EBP alpha		rb	Cell Signaling	8178	0001

Antigen	P-Sites	Species	Distributor	Product #	Lot #
Caseinkinase 1 alpha		rb	Cell Signaling	2655	1
Caseinkinase 1 delta		ms	Abcam	ab85320	GR3957
Caseinkinase 1 epsilon		rb	Invitrogen	487600	070629237D1
Caseinkinase 1 epsilon		ms	Nanotools	0172-100	
Caseinkinase 2 alpha		rb	Cell Signaling	2656	1
Caspase 3		rb	Cell Signaling	9662	
Caspase 7		rb	Cell Signaling	9492	
Caspase 8		ms	Cell Signaling	9746	
Caspase 9		ms	Cell Signaling	9508	
Caveolin-1		rb	Cell Signaling	3238	3
CD36		rb	Epitomics	5777-1	YI081203CS
cdc2 – phospho	Tyr15	rb	Cell Signaling	4539	
cdc2 (CDK1)		ms	Cell Signaling	9116	
CDK6		ms	CST	3136P	
CDK6 (126hosphor-Tyr13) antibody		rb	Biorbyt	orb15013	
CDK6 (126hosphor-Tyr24) antibody		rb	Biorbyt	orb15014	
CDKN2B (p15 INK4B, CDN2B, MTS2)		rb	Cell Signaling	4822	
c-Jun		rb	Cell Signaling	9165	2
c-Jun – phospho	Ser63	rb	Cell Signaling	2361	1
c-Jun – phospho	Ser73	rb	Cell Signaling	9164	3
c-Kit		rb	Epitomics	1522-1	GR90061-1
c-myc		rb	Cell Signaling	9402	3
c-myc clone 9E10, Helmholtz Zentrum München		ms	E. Kremmer	custom	
c-myc - phospho	Thr58/Ser62	rb	Epitomics	1203-1	C04017
c-myc - phospho	Thr58/Ser62	rb	Epitomics	1203-1	GR104962-1
Cofilin		rb	Cell Signaling	5175	0001
Cofilin - phospho	Ser3	rb	Cell Signaling	3313	4
Cox1		rb	Cell Signaling	9896	1
Cox2		rb	Cell Signaling	4842	2
c-Raf		rb	Cell Signaling	9422	2
c-Raf - phospho	Ser259	rb	Cell Signaling	9421	4
CREB		rb	Cell Signaling	9197	1
CREB - phospho	Ser133	rb	Cell Signaling	9198	10
CREB - phospho	Ser133	rb	Cell Signaling	9191	8
Crk (p38)		rb	Epitomics	1779-1	YD032001
Crk (p38) - phospho	Tyr221	rb	Epitomics	2132-1	YE060603
CXCR4		rb	Calbiochem	PC389	D00086510
Cyclin A		rb	abcam	ab53054	332779
Cyclin A2		rb	Epitomics	1547-1	C10191
Cyclin B1		ms	Cell Signaling	4135	4
Cyclin B1 - phospho	Ser133	rb	Cell Signaling	4133	1
Cyclin D1		ms	Cell Signaling	2926	7
Cyp2B		rb	Dr Wolf, gift		
Cyp2C8		rb	Puracyp	Hu-A004	RaPh/B#6
Cyp2E1		rb	StressGen		
Cyp3A4, 3A1, 3A11		ms	Millipore	MAB10041	PSO1482596
Cytokeratin 18		ms	Cell Signaling	4548	1
Cytokeratin 7		rb	Epitomics	2181-1	YE040203
Cytokeratin 8		ms	Santa Cruz	sc-8020	
Cytokeratin 8 - phospho	Ser23	rb	Epitomics	2147-1	YE062501
Dicer1		ms	Millipore	MABN461	Q2095733
DKK1		rb	Biorbyt	orb27676	

Antigen	P-Sites	Species	Distributor	Product #	Lot #
DPP3 (Dipeptidyl-peptidase 3)		rb	Epitomics	S1902	39757
DUSP1 - phospho - (MKP-1)	Ser296/318	rb	Abcam	ab78898	
DUSP1 (MKP1)		rb	Millipore	07-535	
DUSP10 (MKP-5)		rb	Cell Signaling	3483	
DUSP4		rb	abcam	ab72593	713785
DUSP5 (VH3)		rb	Sigma	D8819	
DUSP6 (MKP3, MKP-3, PYST1)		rb	Epitomics	2138-1	YE061201C
DUSP9 (MKP4, MKP-4)		rb	ProteinTech	14484-1-AP	05-May-09
Dvl2		rb	Cell Signaling	3224	1
Dvl3		rb	Cell Signaling	3218	1
E2F-3		ms	Millipore	05-551	NG1911119
E2F4		rb	biorbyt	orb10571	A1502
E-Cadherin		rb	Cell Signaling	3195	
E-Cadherin - phospho	Ser838/Ser840	rb	Epitomics	2239-1	
eEF2		rb	Cell Signaling	2332	5
eEF2 - phospho	Thr56	rb	Cell Signaling	2331	7
EGFR		rb	Cell Signaling	4405	1
EGFR - phospho	Tyr845	rb	Cell Signaling	2231	7
EGFR - phospho	Tyr1068	rb	Cell Signaling	2234	13
EGFR - phospho	Tyr992	rb	Cell Signaling	2235	7
EGR1		rb	Cell Signaling	4153	3
eIF2 alpha		rb	Cell Signaling	9722	7
eIF2 alpha - phospho	Ser51	rb	Cell Signaling	3597	4
eIF4E		rb	Cell Signaling	2067	1
eIF4E - phospho	Ser209	rb	Cell Signaling	9741	4
Elk-1		rb	Cell Signaling	9182	3
Elk-1 - phospho	Ser383	rb	Cell Signaling	9181	4
EphA2		rb	CST	6997P	
EphA2 Phospho	Tyr594	rb	CST	3970	
EphA2 Phospho	Ser897	rb	CST	6347	
EphA2 Phospho	Tyr588	rb	CST	7423	
EphA2 Phospho	Tyr772	rb	CST	8244	
EPHA4 (phospho-Tyr596) antibody		rb	Biorbyt	orb126908	
EphA4 antibody		rb	Biorbyt	orb38212	
EphB3 antibody		rb	Biorbyt	orb38239	
EphB4 antibody		rb	Biorbyt	orb38241	
EphB6		rb	abcam	ab70181	855934
EphB6 antibody		rb	Biorbyt	orb38245	
Ephrin B Phospho	Tyr324/329	rb	CST	3481	
Erk1/2 (MAPK p44/42)		rb	Cell Signaling	4695	14
Erk1/2 (MAPK p44/42) - phospho	Thr202/Tyr204	rb	Cell Signaling	4370	7
Ets-1		ms	Bonn		
Ezh2		rb	Cell Signaling	5246	5
Ezrin / Radixin / Moesin		rb	Cell Signaling	3142	3
Ezrin / Radixin / Moesin - phospho	Thr567/564/558	rb	Cell Signaling	3149	11
FAK		rb	Cell Signaling	3285	9
FAK - phospho	Tyr397	rb	Cell Signaling	8556	1
FAK 1		rb	Epitomics	2146-1	YE052404C
FAK 1 - phospho	Tyr861	rb	Epitomics	2153-1	YE070902
FAK 1 - phospho	Tyr576/Tyr577	rb	Epitomics	2183-1	YE080103C
FDPS (farnesyl diphosphate synthase)		rb	Atlas/Sigma	HPA028200	R27252
Frizzled-1		rb	abcam	ab71342	GR121802-1

Antigen	P-Sites	Species	Distributor	Product #	Lot #
FTCD		rb	biorbyt	orb36816	E5977
Fyn		rb	Cell Signaling	4023	2
Fyn		rb	CST	4023P	
Gab1		rb	Cell Signaling	3232	3
GADD45B		rb	Epitomics	5833-1	GR80581-12
GAPDH		rb	Abcam	ab9485	
GAS2		rb	Epitomics	3347-1	YH053106C
GCN5L2		rb	Cell Signaling	3305	4
GLDC		rb	biorbyt	orb40195	E9357
GLS2 (Glutaminase 2)		rb	Atlas	HPA038608	H89921
GLUT-1		rb	Millipore	07-1401	2373314
Glutaminsynthetase		rb	Sigma	G2781	061K4811
GSK3 alpha/beta - phospho	Ser21/9	rb	Cell Signaling	9331	15
GSK3 beta		rb	Cell Signaling	9315	11
GSK3 beta		rb	Cell Signaling	9332	4
GSK3 beta - phospho	Ser9	rb	Cell Signaling	9336	3
HAL (histidine ammonia lyase)		rb	Atlas/Sigma	HPA038547	R35558
Ha-ras		rb	Upstate	05-775	26823
Her2		rb	Dako	A0485	00018437
Her2 - phospho	Tyr877	rb	Cell Signaling	2241	
Her2 - phospho	Tyr1221/Tyr1222	rb	Cell Signaling	2243	8
Her2 - phospho	Tyr1248	rb	Biosource	44904	0104
hHR23b		rb	abcam	ab86781	957974
HIF1 alpha		rb	Cell Signaling	3716	2
HIF1 beta (ARNT)		rb	Cell Signaling	3718	1
Histon Deacetylase 1 (HDAC1)		rb	Cell Signaling	2062	1
Histon Deacetylase 2		rb	Epitomics	1603-1	YC-12-16-06
Histon Deacetylase 3 (HDAC3)		rb	Epitomics	1580-1	YC120108
Histon H3		rb	Cell Signaling	9715	0
Histon H3 - acetyl	Lys9	rb	Cell Signaling	9649	9
Histon H3 - acetyl	Lys9	rb	Cell Signaling	9671	2
Histon H3 - dimethyl	Lys4	rb	Epitomics	1347-1	C07063
Histon H3 - phospho	Ser10	rb	Cell Signaling	9701	13
Histon H4 - acetyl	Lys8	rb	Epitomics	1796-1	YD062903
HNF-4 alpha (HNF-4A)		gt	Santa Cruz	sc-6556	
HNF-4 alpha (HNF-4A) - phospho	Ser313	rb	biorbyt	orb5454	A3963
HSP 70		rb	Cell Signaling	4876	2
IDH1 (Isocitrate dehydrogenase [NADP] cytoplasmic)		rb	Cell Signaling	8137	1
IDH2		ms	abcam	ab55271	GR98694-1
Ihh		rb	abcam	Ab52919	GR61013-15
IkappaB alpha		ms	Cell Signaling	4814	4
IkappaB alpha		rb	Cell Signaling	9242	5
IkappaB alpha - phospho	Ser32	rb	Cell Signaling	9241	7
IKKε		rb	CST	2905	
IKKε Phospho	Ser172	rb	CST	8766	
ILK1		rb	Cell Signaling	3862	2
ILK1 - phospho	Thr173	rb	biorbyt	orb6213	A4945
ILK1 - phospho	Ser246	rb	biorbyt	orb6214	A4946
INSL4		rb	abcam	ab75061	633606
Integrin beta1		ms	Transduction Lab.	I41720	4
IPP-2 (PPP1R2, IPP2, PP1 Inhibitor 2) - phospho	Thr72	rb	abcam	ab27850	686457
IRAK4		rb	Cell Signaling	4363	2

Antigen	P-Sites	Species	Distributor	Product #	Lot #
IRAK4 - phospho	Thr345/Ser346	rb	Cell Signaling	11927	1
IRE1 alpha		rb	Cell Signaling	3294	4
JNK/SAPK		rb	Cell Signaling	9252	
JNK/SAPK		rb	Cell Signaling	9258	7
JNK/SAPK - phospho	Thr183/Tyr185	rb	Cell Signaling	4668	7
JNK/SAPK - phospho	Thr183/Tyr185	rb	Cell Signaling	9251	8
KSR1		rb	abcam	ab52196	791002
KSR1 - phospho	Ser392	rb	Cell Signaling	4951	2
LATS2		rb	CST	5888	
Lck - phospho	Tyr505	rb	Cell Signaling	2751	5
LIMK1		rb	CST	3842	
LIMK1 Phospho	Thr508 / Thr505	rb	CST	3841	
LRP6		rb	Cell Signaling	3395	1
LRP6 - phospho	Ser1490	rb	Cell Signaling	2568	3
LRRK2		rb	CST	5559	
LRRK2 Phospho	Ser910	rb	Epitomics	5098-1	
LRRK2 Phospho	Ser935	rb	Epitomics	5099-1	
Mcl-1		rb	Cell Signaling	5453	1
Mcl-1 - phospho	Ser159/Thr163	rb	Cell Signaling	4579	1
MCM2		rb	Cell Signaling	3619	3
MEK1		rb	Cell Signaling	9124	
MEK1 - phospho	Thr292	rb	Epitomics	2233-1	YE100906
MEK1/2 - phospho	Ser217/221	rb	Cell Signaling	9121	7
MEK1/2 - phospho	Ser217/221	rb	Cell Signaling	9154	
MEK2		rb	Cell Signaling	9125	1
MERTK		rb	abcam	ab95925	GR121529-1
MKK3/6 - phospho	Ser189/207	rb	Cell Signaling	9236	
MKK3/MKK6 Phospho	S218/T222,S207/T211	rb	RnD	AF4930	
MKK4		rb	Epitomics	1658-1	YD021301
MKK4 (SEK1) - phospho	Ser257/Thr261	rb	Cell Signaling	9156	2
MKK6		rb	Epitomics	1821-1	
MKK7		rb	Cell Signaling	4172	3
MKK7 - phospho	Ser271/Thr275	rb	Cell Signaling	4171	2
MLK3 - phospho	Thr277/Ser281	rb	Sigma	M6318	094K0766
MLK3 (MAP3K11)		rb	Epitomics	2000-1	YE010205
MLK3 -phospho (MAP3K11)	Thr277/Ser281	rb	Cell Signaling	2811	2
Mnk1		rb	Cell Signaling	2195	1
Mnk1 - phospho	Thr197/202	rb	Cell Signaling	2111	3
MSK1		rb	Cell Signaling	3489	1
MSK1 - phospho	Ser360	rb	Epitomics	2154-1	YE071202
MSK1 - phospho	Ser212	rb	R&D	AF1036	FKC03
mTOR		rb	Cell Signaling	2983	1
mTOR - phospho	Ser2448	rb	Cell Signaling	2971	9
MUC1 (CD227)		ms	Chemicon	CBL264	2641911LC
N-Cadherin		rb	Cell Signaling	4061	3
NF-κB p100/p52		rb	Cell Signaling	4882	4
NF-κB p105/p50		rb	Epitomics	1559-1	YG012101C
NF-κB p105/p50		rb	Cell Signaling	3035	3
NF-κB p65		rb	Cell Signaling	3034	
NF-κB p65		rb	Cell Signaling	4764	3
NF-κB p65 - phospho	Ser536	rb	Cell Signaling	3033	6
NIK		rb	Cell Signaling	4994	2

Antigen	P-Sites	Species	Distributor	Product #	Lot #
Numb		rb	Cell Signaling	2756	2
p21/Waf1/Cip1		rb	Cell Signaling	2947	5
p27(Kip1) - phospho - (CDKN1B)	Ser10	rb	Epitomics	2187-1	YE081401
p27(Kip1) (CDKN1B)		ms	Cell Signaling	3698	1
p38/MAPK		rb	Cell Signaling	9212	
p38/MAPK - phospho	Thr180/Tyr182	rb	Cell Signaling	9211	
p53		rb	Cell Signaling	2527	4
p53		rb	Cell Signaling	9282	4
p53 - acetyl	Lys305	rb	Epitomics	3308-1	GR44067-4
p53 - phospho	Ser392	rb	Cell Signaling	9281	4
p53 - phospho	Ser20	rb	Cell Signaling	9287	5
p70 S6 kinase		rb	Cell Signaling	2708	1
PAI-1		rb	Cell Signaling	11907	1
PAK 1/2 - phospho	Ser144/Ser141	rb	Cell Signaling	2606	2
PAK 2		rb	Cell Signaling	2608	3
PAK 4		rb	Cell Signaling	3242	2
PAK 4/5/6 - phospho	S474/S602/S560	rb	Cell Signaling	3241	5
PAK1/2/3 - phospho	Ser141	rb	Biosource	44-940G	0301
PARP		rb	Cell Signaling	9542	5
PDGF Receptor beta		rb	Cell Signaling	4564	1
PDGF Receptor beta - phospho	Tyr751	rb	Cell Signaling	3161	5
PDK1		rb	Cell Signaling	3062	10
PERK		rb	Cell Signaling	3192	1
PERK - phospho	Thr980	rb	Cell Signaling	3179S	10
PGC-1 alpha		ms	Calbiochem	KP9803	D00151286
PGC-1 alpha - phospho	Ser571	rb	R&D	AF6650	CEBA0111101
Phospho-Fyn(Tyr530) antibody		rb	Biorbyt	orb99261	
PI3-kinase p110 subunit alpha		rb	Cell Signaling	4255	
PI3-kinase p85		rb	Cell Signaling	4292	4
PI3-kinase p85 alpha		rb	Epitomics	1675-1	YF-05-06-11C
PKA C alpha		rb	Cell Signaling	4782	1
PKA C alpha/beta - phospho	Thr197	rb	Biosource	44-988	0104
PKA C alpha/beta/gamma - phospho	Thr197	rb	Cell Signaling	4781	2
PKA Substrate - phospho	Ser/Thr	rb	Cell Signaling	9621	4
PKC (pan) - phospho	Ser660	rb	Cell Signaling	9371	3
PKC alpha/beta II - phospho	Thr638/641	rb	Cell Signaling	9375	3
PKCθ		rb	CST	12206	
PKCθ Phospho	Thr538	rb	CST	9377P	
PKG-1		rb	Cell Signaling	3248	2
PLC gamma I		rb	Cell Signaling	2822	3
PLC gamma I - phospho	Tyr783	rb	Cell Signaling	2821	3
PP1 alpha		rb	Millipore	06-221	1350289
PP1 alpha - phospho	Thr320	rb	Epitomics	2167-1	YE072306
PP1 gamma		rb	Calbiochem	539543	D00114312
PP2A C		rb	Cell Signaling	2259	
PP2A C - phospho	Tyr307	rb	R&D	AF3989	
PPAR alpha		rb	abcam	ab8934	
PPAR alpha - phospho	Ser12	rb	abcam	ab3484	
PPAR gamma		rb	biorbyt	orb11291	B2538
PPAR gamma - phospho	Ser112	rb	biorbyt	orb5574	A3704
PRL-1 (PTP4A1)		gt	ProSci	46-225	

Antigen	P-Sites	Species	Distributor	Product #	Lot #
PTCH2		rb	Cell Signaling	2470	1
PTEN		rb	Cell Signaling	9552	3
PTEN - phospho	Ser380	rb	Cell Signaling	9551	6
PTPN7 (LC-PTP, HEPTP)		rb	ProteinTech	15286-1-AP	01-May-09
PTPN7 (LC-PTP, HEPTP)		rb	Atlas	HPA019118	R08192
PTP-PEST (PTPN12, PTN12)		rb	Bethyl	A301-302A	A301-302A
PXR (NR1I2)		rb	Biorbyt	orb131805	
Pyk2 - phospho	Tyr402	rb	Cell Signaling	3291	
Pyk2 / FAK 2		rb	Epitomics	1480-1	
RACK1		ms	BD Biosciences	610177	
Rad51		rb	Epitomics	3161-1	YH031704C
Raptor		rb	Cell Signaling	2280	10
Raptor - phospho	Ser792	rb	Cell Signaling	2083	4
Ras		rb	Cell Signaling	8955	1
RBPSUH		rb	Cell Signaling	5313	1
RKIP (PBP, PEBP, PEBP1)		rb	Cell Signaling	4742	1
RSK 1		rb	Upstate	06-668	
RSK 1 - phospho	Thr573	rb	Epitomics	2185-1	GR72730-3
RSK 1 (p90RSK) - phospho	Ser380	rb	Cell Signaling	9341	
RSK 1/2/3		rb	Cell Signaling	9347	0005
RSK 3 - phospho	Thr353/356	rb	Epitomics	2012-1	C04223
RSK 4		rb	Epitomics	2102-1	YE041203
RSK 4 - phospho	Ser235	rb	Epitomics	2151-1	YE051803
RXR alpha		ms	R&D	PP-K8508-00	
RXR alpha		rb	Santa Cruz	sc-553	
S6 Ribosomal Protein		rb	Cell Signaling	2217	1
S6 Ribosomal Protein - phospho	Ser240/244	rb	Cell Signaling	2215	9
SDS (serine dehydratase)		rb	Atlas/Sigma	HPA039230	R36967
Shh		rb	Cell Signaling	2207	2
SHP-2		rb	Epitomics	1609-1	YC121206
SIK3 (KIAA0999) antibody		rb	Biorbyt	orb29515	
Slug		rb	Cell Signaling	9585	3
Smad1		rb	Cell Signaling	6944	1
Smad2 - phospho	Ser245/250/255	rb	Cell Signaling	3104	2
Smad2 - phospho	Ser245/250/255	rb	Cell Signaling	3104	2
Smad2 - phospho	Ser465/467	rb	Cell Signaling	3108	7
Smad2/3		rb	Cell Signaling	3102	8
Smad3		rb	Cell Signaling	9523	5
Smad3 - phospho	Ser423/425	rb	Cell Signaling	9520	10
SPRED2		rb	abcam	ab50535	545611
SPRY2 (Protein sprouty homolog 2)		rb	Millipore	07-524	31940
SPRY3 (Spry-3, Sprouty 3)		rb	Sigma (ASB)	AV50519	QC22737
Src		rb	Cell Signaling	2109	4
Src - phospho	Tyr527	rb	Cell Signaling	2105	9
Src Family - phospho	Tyr416	rb	Cell Signaling	6943	1
STAT 1		rb	Cell Signaling	9172	10
STAT 3		rb	Cell Signaling	4904	2
STAT 3 - phospho	Ser727	rb	Cell Signaling	9134	5
STAT 3 - phospho	Tyr705	ms	Cell Signaling	9138	2
STAT 5		rb	Cell Signaling	9310	4
STEP (PTPN5, PTN5)		rb	Cell Signaling	4817	1
Superoxiddismutase (Cu/Zn)		rb	StressGen	SOD-100	102411

Antigen	P-Sites	Species	Distributor	Product #	Lot #
TAK1		rb	Cell Signaling	4505	3
TAK1 - phospho	Ser412	rb	Cell Signaling	9339	1
TBK1 (NAK) - phospho	Ser172	rb	Cell Signaling	5483	1
TCF4		rb	Cell Signaling	2565	3
Thrombospondin 2		ms	BD		
Thymidin Phosphorylase (ECGF1)		rb	Abnova	H00001890	09091 WULZ
Topoisomerase 1		rb	Abcam	ab85038	940503
VASP - phospho	Ser157	rb	Cell Signaling	3111	5
VASP - phospho	Ser239	rb	Cell Signaling	3114	5
VEGFR 2 (FLK-1)		rb	Cell Signaling	9698	1
Vimentin		rb	Cell Signaling	5741	1
Wnt3A		rb	Millipore	09-162	DAM1764519
YAP		rb	Cell Signaling	4912	0
YAP - phospho	Ser127	rb	Cell Signaling	4911	
γ-Catenin		rb	Cell Signaling	2309	1

6.1.5 Primary antibodies for IHC

Antigen	P-Sites	Species	Distributor	Product #
E-Cadherin			From the Institute of Toxiciology	
Glutaminsynthetase			From the Institute of Toxiciology	
PP2A C - phospho	Tyr307	rb	R&D	AF3989
PTCH2		rb	Cell Signaling	2470
S6 Ribosomal Protein - phospho (RPS6)	Ser240/244	rb	Cell Signaling	5364
Ihh (indian hedgehog)		rb	Abcam (Epitomics)	Ab52919

6.1.6 Consumables

Type	Format	Distributor
Vials	0.5 ml, 0.65 ml, 1.5 ml, 2 ml, 15 ml, 50 ml	Biozym Scientific,Hessisch Oldendorf
		Greiner Bio-One, Frickenhausen
		Mettler-Toledo, Columbus, OH, USA
		neoLab, Heidelberg
		Starlab, Hamburg
		Thermo Fisher Scientific, Waltham, MA, USA
		Eppendorf, Hamburg
Beads	MicroPlex, MagPlex	Luminex
Blotting paper		GE Healthcare, Chalfont St Giles, UK
Gels	NuPAGE Novex 4 – 12 % Bis-Tris Gels 1,0 mm, different formats	Life Technologies, Carlsbad, CA, USA
King fisher consumables	Plates, combs	Thermo Fisher Scientific, Waltham, MA, USA
LCM slides	MembraneSlide 1.0 PEN	Carl Zeiss AG, Jena
LCM caps	AdhesiveCAp 200 opaque	Carl Zeiss AG, Jena
Membranes	PVDF, nitrocellulose	Millipore / Merck, Darmstadt
		GE Healthcare, Chalfont St Giles, UK
		BioRad, Hercules, California, USA
		Merck, Darmstadt
Pipette tips		VWR, Radnor, PA, USA
		Mettler-Toledo, Columbus, OH, USA
		Starlab, Hamburg

Type	Format	Distributor
		Beckman Coulter, Brea, CA, USA
Plates	96-well plates	Thermo Fisher Scientific, Waltham, MA, USA
		Greiner Bio-One, Frickenhausen
		Corning , New York, NY, USA
Plate sealing tape		Thermo Fisher Scientific, Waltham, MA, USA
Vacuum bags		Landig + Lava GmbH , Bad Saulgau

6.2 Equipment

6.2.1 Instruments / lab equipment

Application	Product	Supplier
Balance	Explorer E12140	OHAUS, Pine Brook, NJ, USA
Bead readout instruments	FLEXMAP 3D, Luminex 100	Luminex, Austin, TX, USA
Centrifuges	5415D, 5417R	Eppendorf, Hamburg, Germany
	Universal 30F	Hettich, Tuttlingen, Germany
Cutting plotter	Silhouette SD	Silhouette America, West Orem, UT, USA
Gel electrophoresis	XCell SureLock Mini-Cell	Life Technologies, Carlsbad, CA, USA
Gel blotting	XCell II Blot Module	Life Technologies, Carlsbad, CA, USA
Heating block	Mastercycler gradient, Thermomixer comfort	Eppendorf, Hamburg, Germany
Horizontal tube rotator	RM5	Assistent, Sondheim, Germany
LCM microscope	Palm Microbeam	Carl Zeiss AG, Jena, Germany
Magnetic bead handling	PickPen 8-channel	Bio-Nobile, Pargas, Finland
	Plate magnets for 96 well plates	Luminex, TX, USA
	DynaMag™- Spin Magnet	Life Technologies, Carlsbad, CA, USA
	KingFisher96, KingFisher Flex	Thermo Fisher Scientific, Waltham, MA, USA
Mixer	Vortex Genie 2	Scientific Industries, Bohemia, NY, USA
Pipettes	PIPETMAN Neo	Gilson, Middleton, WI, USA
Pipettes electronic	Xplorer, Research pro	Eppendorf, Hamburg, Germany
Pipetting robot	Biomek FX	Beckman Coulter, Brea, CA, USA
pH meter	pH-Meter 766	Knick, Berlin, Germany
Power source	Power Ease 500	Life Technologies, Carlsbad, CA, USA
Shakers	Polymax 2040 (gels + membranes)	Heidolph, Schwabach, Germany
	DRS-12 (membranes)	NeoLab, Heidelberg, Germany
	KL-2 (gels + membranes)	Edmund Bühler GmbH, Hechingen
	Thermomixer comfort (Vials + MTP)	Eppendorf, Hamburg, Germany
	TiMix 5 control (MTP)	Edmund Bühler GmbH, Hechingen
Spectrometer	Fluostar OPTIMA	BMG Labtech, Offenburg, Germany
Speedvac	BaVaCo-M Mini-30	Bachofer, Reutlingen, Germany
Stirrer	RCT basic	IKA Werke, Staufen, Germany
Ultrasonic bath	SONOREX	Bandelin, Berlin, Germany
Vacuum sealer		Landig + Lava GmbH , Bad Saulgau, Germany
Western-Blot readout / gel documentation	ODYSSEY Infrared Imaging System	LI-COR Biosciences, Lincoln, NE, USA
	ImageQuant LAS 4000 mini	GE Healthcare, Chalfont St Giles, UK
	Typhoon Trio	GE Healthcare, Chalfont St Giles, UK
Water purification system	arium 61316	Sartorius Stedim Biotech, Göttingen, Germany

6.3 Software

Software	Distributor
Creative Suite CS5 (Illustrator, Photoshop, Acrobat)	Adobe Systems, San Jose, CA, USA
DigiWest Analysis tool, based on Excel	self-made
ImageJ 1.42q	Wayne Rasband (NIH), NIH Bethesda, Maryland, USA
Mendeley	Mendeley Ltd., New York, NY, USA
Multi Gauge V 3.0	FUJIFILM, Minato, Tokio, Japan
Odyssey V 3.0	LI-COR Biosciences, Lincoln, NE, USA
Office 2010 (Word, Power Point, Excel)	Microsoft, Redmond, WA, USA
TM4 Microarray Software Suite, MeV Version 4.8.1	Dana-Farber Cancer Institute, Boston, MA, USA
XLfit 5.3.1.3	IDBS, Guildford, Surrey, GB
Xponent, different versions	Luminex, Austin, TX, USA
Diverse control software for the instruments	See instruments

7 Abbreviations

Abbreviation	Explanation
°C	degree Celsius
µ	micro
µl	microliter
µM	micromolar
µm	micrometer
2D	two dimensional
3D	three dimensional
Å	Angstrom
AFI	assembled fluorescence units
ATP	Adenosine triphosphate
BCA	Bicinchoninic acid assay
BETR	Bayesian Estimation of Temporal Regulation
BSA	bovine serum albumine
Ca	Calcium
CAR	Constitutive androstane receptor
CBS	carboxy block store (storage buffer)
CCD	Charge-coupled device
CLB1	Cell lysis buffer 1
cm	centimeter
co-IP	co-immunoprecipitation
CV	Coefficient of variation
ddH_2O	purified water (18.2 MΩ)
DEN	diethylnitrosamine
DNA	deoxyribonucleic acid
DUSP	dual specific phosphatases
e.g.	Latin “exempli gratia”
ECL	Enhanced chemiluminescence
EDC	1-Ethyl-3-(3-dimethylaminopropyl)carbodiimide
EGF	Epidermal growth factor
ELISA	Enzyme-linked immunosorbent assay
f	fempto
FFPE	formalin-fixed, paraffin-embedded
fM	femptomolar
GPI	Glycosylphosphatidylinositol
GS	Glutamine synthetase
GST	Glutathione S-transferase
h	hour
HRP	Horseradish peroxidase
IC50	half maximal inhibitory concentration
i.e.	id est
I125	Iodine 125
IHC	Immunohistochemistry
k	kilo
Kd	Dissociation constant
kDa	kilo dalton
L	Liter
LCM	laser capture microdissection
LIMMA	Linear Model for Microarray Analysis
M	molar
m	milli
M	mega
mA	milli ampere

Abbreviation	Explanation
MAP-kinase	mitogen-activated protein kinase
MES	2-(N-morpholino)ethanesulfonic acid
MFI	median fluorescence intensity
mg	milligramm
MKP	MAP kinase phosphatase
ml	milliliter
mm	millimeter
mM	millimolar
MOPS	3-(N-morpholino)propanesulfonic acid
MS	mass spectrometry
MΩ	mega Ω
ng	nanogramm
NGC	non-genotoxic carcinogen
NHS	N-Hydroxysuccinimide
nl	nano liter
nm	nanometer
nM	nanomolar
PAGE	Polyacrylamide gel electrophoresis
PBS	Phosphate buffered saline
PE	Phycoerythrin
PEG	Polyethylene glycol
pg	picogramm
pH	Unit for acidity
pI	isoelectric point
PMT	photomultiplier tube
PVA	Polyvinyl alcohol
PVDF	Polyvinylidene fluoride
PVP	Polyvinylpyrrolidone
RPPM	Reevrse phase protein microarray
S	serine
SDS	Sodium dodecyl sulfate
SEM	Standard error of mean
Ser	serine
sNHS	sulfo-NHS
SU	sub unit
T	threonine
TBS	Tris-buffered saline
TCPOBOP	substance described in the text
Thr	threonine
TPER	Tissue protein extraction reagent
Tris	tris(hydroxymethyl)aminomethane
TUM	Technical University Munich
Tyr	tyrosine
USA	United States of America
UV	Ultra violett
V	Volt
VBA	Visual Basic for Applications
w/v	weight/volume
WB	Western-Blot
Y	tyrosine
Ω	Ohm

8 Curriculum vitae

Personal information removed for online publication

9 Presentations, publications, awards

Poster presentation at Keystone Symposia: Proteomics, Interactomes

Stockholm, Sweden 2012

Poster presentation at Cold Spring Harbor Laboratories: Mechanisms & Models of Cancer

Cold Spring Harbor, NY, USA 2014

Talk at the 'Arbeitstagung Mikromethoden in der Proteinchemie'

Bochum, Germany 2012

Young Talent Award at the 'Arbeitstagung Mikromethoden in der Proteinchemie'

Winner of the Serva Electrophoresis Award

Bochum, Germany 2012

Science2Start award of 'BioRegio STERN'

Winner of the 1st price together with Markus Templin

Esslingen, Germany 2014

Patent on the DigiWest Method

DE102011109063 B3 Verfahren zum Nachweis von Biomolekülen

CA 2842995 A1 / PCT/EP2012/062403 Method for detecting biomolecules

Publications

The DigiWest method is planned for publication

The Mouse liver LCM data are planned for publication

Wuchter, J., Beuter, S., Treindl, F., Herrmann, T., Zeck, G., Templin, M. F., & Volkmer, H. (2012). **A comprehensive small interfering RNA screen identifies signaling pathways required for gephyrin clustering**. The Journal of Neuroscience : The Official Journal of the Society for Neuroscience, 32(42), 14821–34. doi:10.1523/JNEUROSCI.1261-12.2012

Lempiäinen, H., Couttet, P., Bolognani, F., Müller, A., Dubost, V., Luisier, R., … Moggs, J. G. (2013). **Identification of Dlk1-Dio3 imprinted gene cluster noncoding RNAs as novel candidate biomarkers for liver tumor promotion**. Toxicological Sciences : An Official Journal of the Society of Toxicology, 131(2), 375–86. doi:10.1093/toxsci/kfs303

10 Acknowledgement

First and foremost, I want to thank my Supervisor Markus Templin for giving me the opportunity to develop the DigiWest method which is based on his idea and for his support.

A special thanks to Albert Bräuning, Michael Schwarz and Elke Zabinsky for their cooperation and support on the mouse liver LCM experiment. Albert performed the mouse study and Elke prepared the liver sections and performed the IHC staining. Michael and Albert supported me with their profound knowledge on mouse liver and non-genotoxic carcinogens.

Also big thanks to Benjamin Ruprecht and Bernhard Küster for their cooperation and support on the Lapatinib resistance experiment. Benjamin prepared the H292 cell lysates, performed the Kinobead pulldown, mass spectrometry analysis and also the Ingenuity analysis.

And of course I also want to thank all my colleagues in the group of Markus Templin and at the NMI.

11 Literature

Acconcia, F., Barnes, C. J., Singh, R. R., Talukder, A. H., & Kumar, R. (2007). Phosphorylation-dependent regulation of nuclear localization and functions of integrin-linked kinase. *Proceedings of the National Academy of Sciences of the United States of America*, *104*(16), 6782–7. http://doi.org/10.1073/pnas.0701999104

Ahmadian, M., Suh, J. M., Hah, N., Liddle, C., Atkins, A. R., Downes, M., & Evans, R. M. (2013). PPARγ signaling and metabolism: the good, the bad and the future. *Nature Medicine*, *19*(5), 557–66. http://doi.org/10.1038/nm.3159

Alfaro, A. C., Roberts, B., Kwong, L., Bijlsma, M. F., & Roelink, H. (2014). Ptch2 mediates the Shh response in Ptch1-/- cells. *Development (Cambridge, England)*, *141*(17), 3331–9. http://doi.org/10.1242/dev.110056

Anderson, N. L. (2002). The Human Plasma Proteome: History, Character, and Diagnostic Prospects. *Molecular & Cellular Proteomics*, *1*(11), 845–867. http://doi.org/10.1074/mcp.R200007-MCP200

Anderson, P. J. (1985). The recovery of nitrocellulose-bound protein. *Analytical Biochemistry*, *148*(1), 105–110. http://doi.org/10.1016/0003-2697(85)90634-7

Aoki, R., Chiba, T., Miyagi, S., Negishi, M., Konuma, T., Taniguchi, H., … Iwama, A. (2010). The polycomb group gene product Ezh2 regulates proliferation and differentiation of murine hepatic stem/progenitor cells. *Journal of Hepatology*, *52*(6), 854–63. http://doi.org/10.1016/j.jhep.2010.01.027

Arias, I. (2009). *Wiley: The Liver: Biology and Pathobiology, 5th Edition - Irwin Arias, Allan Wolkoff, James Boyer, et al*.

Aryee, M. J., Gutiérrez-Pabello, J. A., Kramnik, I., Maiti, T., & Quackenbush, J. (2009). An improved empirical bayes approach to estimating differential gene expression in microarray time-course data: BETR (Bayesian Estimation of Temporal Regulation). *BMC Bioinformatics*, *10*(1), 409. http://doi.org/10.1186/1471-2105-10-409

Aydinlik, H., Nguyen, T. D., Moennikes, O., Buchmann, A., & Schwarz, M. (2001). Selective pressure during tumor promotion by phenobarbital leads to clonal outgrowth of beta-catenin-mutated mouse liver tumors. *Oncogene*, *20*(53), 7812–6. http://doi.org/10.1038/sj.onc.1204982

Baker, M. (2015). Reproducibility crisis: Blame it on the antibodies. *Nature*, *521*(7552), 274–276. http://doi.org/10.1038/521274a

BALKS, H.-J., & JUNGERMANN, K. (1984). Regulation of peripheral insulin/glucagon levels by rat liver. *European Journal of Biochemistry*, *141*(3), 645–650. http://doi.org/10.1111/j.1432-1033.1984.tb08240.x

Banko, M. R., Allen, J. J., Schaffer, B. E., Wilker, E. W., Tsou, P., White, J. L., … Brunet, A. (2011). Chemical genetic screen for AMPKα2 substrates uncovers a network of proteins involved in mitosis. *Molecular Cell*, *44*(6), 878–92. http://doi.org/10.1016/j.molcel.2011.11.005

Bantscheff, M., Eberhard, D., Abraham, Y., Bastuck, S., Boesche, M., Hobson, S., … Drewes, G. (2007). Quantitative chemical proteomics reveals mechanisms of action of clinical ABL kinase inhibitors. *Nature Biotechnology*, *25*(9), 1035–44. http://doi.org/10.1038/nbt1328

Benetti, R., Del Sal, G., Monte, M., Paroni, G., Brancolini, C., & Schneider, C. (2001). The death substrate Gas2 binds m-calpain and increases susceptibility to p53-dependent apoptosis. *The EMBO Journal*, *20*(11), 2702–14. http://doi.org/10.1093/emboj/20.11.2702

Benhamouche, S., Decaens, T., Godard, C., Chambrey, R., Rickman, D. S., Moinard, C., … Colnot, S. (2006). Apc tumor suppressor gene is the "zonation-keeper" of mouse liver. *Developmental Cell*, *10*(6), 759–70. http://doi.org/10.1016/j.devcel.2006.03.015

Berasi, S. P., Huard, C., Li, D., Shih, H. H., Sun, Y., Zhong, W., … Martinez, R. V. (2006). Inhibition of gluconeogenesis through transcriptional activation of EGR1 and DUSP4 by AMP-activated kinase. *The Journal of Biological Chemistry*, *281*(37), 27167–77. http://doi.org/10.1074/jbc.M602416200

Bianconi, E., Piovesan, A., Facchin, F., Beraudi, A., Casadei, R., Frabetti, F., … Canaider, S. (2013). An estimation of the number of cells in the human body.

Bilir, B., Gong, T., Kwasiborski, V., Shen, C., Fillmore, C., Berkowitz, C., & Gumucio, J. (1993). Novel control of the position-dependent expression of genes in hepatocytes. The GLUT-1 transporter. *J. Biol. Chem.*, *268*(26), 19776–19784.

Blanco-Bose, W. E., Murphy, M. J., Ehninger, A., Offner, S., Dubey, C., Huang, W., … Trumpp, A. (2008). C-Myc and its target FoxM1 are critical downstream effectors of constitutive androstane receptor (CAR) mediated direct liver hyperplasia. *Hepatology (Baltimore, Md.)*, *48*(4), 1302–11. http://doi.org/10.1002/hep.22475

Blow, J. J., & Hodgson, B. (2002). Replication licensing — Origin licensing: defining the proliferative state? *Trends in Cell Biology*, *12*(2), 72–78. http://doi.org/10.1016/S0962-8924(01)02203-6

Bolt, H. M., Foth, H., Hengstler, J. G., & Degen, G. H. (2004). Carcinogenicity categorization of chemicals-new aspects to be considered in a European perspective. *Toxicology Letters*, *151*(1), 29–41. http://doi.org/10.1016/j.toxlet.2004.04.004

Bononi, A., Agnoletto, C., De Marchi, E., Marchi, S., Patergnani, S., Bonora, M., … Pinton, P. (2011). Protein kinases and phosphatases in the control of cell fate. *Enzyme Research*, *2011*, 329098. http://doi.org/10.4061/2011/329098

Boorman, G. A., Maronpot, R. R., & Eustis, S. L. (1994). Rodent Carcinogenicity Bioassay: Past, Present, and Future. *Toxicologic Pathology*, *22*(2), 105–111. http://doi.org/10.1177/019262339402200204

Braeuning, A., Heubach, Y., Knorpp, T., Kowalik, M. A., Templin, M., Columbano, A., & Schwarz, M. (2011). Gender-specific interplay of signaling through β-catenin and CAR in the regulation of

xenobiotic-induced hepatocyte proliferation. *Toxicological Sciences : An Official Journal of the Society of Toxicology*, *123*(1), 113–22. http://doi.org/10.1093/toxsci/kfr166

Braeuning, A., Ittrich, C., Köhle, C., Buchmann, A., & Schwarz, M. (2007). Zonal gene expression in mouse liver resembles expression patterns of Ha-ras and beta-catenin mutated hepatomas. *Drug Metabolism and Disposition: The Biological Fate of Chemicals*, *35*(4), 503–7. http://doi.org/10.1124/dmd.106.013656

Braeuning, A., Ittrich, C., Köhle, C., Hailfinger, S., Bonin, M., Buchmann, A., & Schwarz, M. (2006). Differential gene expression in periportal and perivenous mouse hepatocytes. *The FEBS Journal*, *273*(22), 5051–61. http://doi.org/10.1111/j.1742-4658.2006.05503.x

Braeuning, A., Menzel, M., Kleinschnitz, E.-M., Harada, N., Tamai, Y., Köhle, C., … Schwarz, M. (2007). Serum components and activated Ha-ras antagonize expression of perivenous marker genes stimulated by beta-catenin signaling in mouse hepatocytes. *The FEBS Journal*, *274*(18), 4766–77. http://doi.org/10.1111/j.1742-4658.2007.06002.x

Cadoret, A., Ovejero, C., Terris, B., Souil, E., Lévy, L., Lamers, W. H., … Perret, C. (2002). New targets of beta-catenin signaling in the liver are involved in the glutamine metabolism. *Oncogene*, *21*(54), 8293–301. http://doi.org/10.1038/sj.onc.1206118

Chabot, J. G., Walker, P., & Pelletier, G. (1986). Distribution of epidermal growth factor binding sites in the adult rat liver. *The American Journal of Physiology*, *250*(6 Pt 1), G760–4.

Chang, L., & Karin, M. (2001). Mammalian MAP kinase signalling cascades. *Nature*, *410*(6824), 37–40. http://doi.org/10.1038/35065000

Chen, J., Martin, B. L., & Brautigan, D. L. (1992). Regulation of protein serine-threonine phosphatase type-2A by tyrosine phosphorylation. *Science (New York, N.Y.)*, *257*(5074), 1261–4.

Chen, W., Sun, Z., Wang, X.-J., Jiang, T., Huang, Z., Fang, D., & Zhang, D. D. (2009). Direct interaction between Nrf2 and p21(Cip1/WAF1) upregulates the Nrf2-mediated antioxidant response. *Molecular Cell*, *34*(6), 663–73. http://doi.org/10.1016/j.molcel.2009.04.029

Chiang, Y. A., & Jin, T. (2014). p21-Activated protein kinases and their emerging roles in glucose homeostasis. *American Journal of Physiology. Endocrinology and Metabolism*, *306*(7), E707–22. http://doi.org/10.1152/ajpendo.00506.2013

Chiang, Y.-T. A., Ip, W., Shao, W., Song, Z. E., Chernoff, J., & Jin, T. (2014). Activation of cAMP signaling attenuates impaired hepatic glucose disposal in aged male p21-activated protein kinase-1 knockout mice. *Endocrinology*, *155*(6), 2122–32. http://doi.org/10.1210/en.2013-1743

Choi, S. S., Omenetti, A., Syn, W.-K., & Diehl, A. M. (2011). The role of Hedgehog signaling in fibrogenic liver repair. *The International Journal of Biochemistry & Cell Biology*, *43*(2), 238–44. http://doi.org/10.1016/j.biocel.2010.10.015

Chong, C. R., & Jänne, P. A. (2013). The quest to overcome resistance to EGFR-targeted therapies in cancer. *Nature Medicine*, *19*(11), 1389–400. http://doi.org/10.1038/nm.3388

Chong, C., Tan, L., Lim, L., & Manser, E. (2001). The mechanism of PAK activation. Autophosphorylation events in both regulatory and kinase domains control activity. *The Journal of Biological Chemistry*, *276*(20), 17347–53. http://doi.org/10.1074/jbc.M009316200

Ciaccio, M. F., Wagner, J. P., Chuu, C.-P., Lauffenburger, D. A., & Jones, R. B. (2010). Systems analysis of EGF receptor signaling dynamics with microwestern arrays. *Nature Methods*, *7*(2), 148–55. http://doi.org/10.1038/nmeth.1418

Cohen, P. (2006). The twentieth century struggle to decipher insulin signalling. *Nature Reviews. Molecular Cell Biology*, *7*(11), 867–73. http://doi.org/10.1038/nrm2043

Cohen, P., Alessi, D. R., & Cross, D. A. . (1997). PDK1, one of the missing links in insulin signal transduction? *FEBS Letters*, *410*(1), 3–10. http://doi.org/10.1016/S0014-5793(97)00490-0

Colletti, M., Cicchini, C., Conigliaro, A., Santangelo, L., Alonzi, T., Pasquini, E., … Amicone, L. (2009). Convergence of Wnt signaling on the HNF4alpha-driven transcription in controlling liver zonation. *Gastroenterology*, *137*(2), 660–72. http://doi.org/10.1053/j.gastro.2009.05.038

Daigo, K., Kawamura, T., Ohta, Y., Ohashi, R., Katayose, S., Tanaka, T., … Hamakubo, T. (2011). Proteomic analysis of native hepatocyte nuclear factor-4α (HNF4α) isoforms, phosphorylation status, and interactive cofactors. *The Journal of Biological Chemistry*, *286*(1), 674–86. http://doi.org/10.1074/jbc.M110.154732

Dang, C. V. (1999). c-Myc Target Genes Involved in Cell Growth, Apoptosis, and Metabolism. *Mol. Cell. Biol.*, *19*(1), 1–11.

Davies, H., Bignell, G. R., Cox, C., Stephens, P., Edkins, S., Clegg, S., … Futreal, P. A. (2002). Mutations of the BRAF gene in human cancer. *Nature*, *417*(6892), 949–54. http://doi.org/10.1038/nature00766

Davies, S. P., Helps, N. R., Cohen, P. T., & Hardie, D. G. (1995). 5'-AMP inhibits dephosphorylation, as well as promoting phosphorylation, of the AMP-activated protein kinase. Studies using bacterially expressed human protein phosphatase-2C alpha and native bovine protein phosphatase-2AC. *FEBS Letters*, *377*(3), 421–5. http://doi.org/10.1016/0014-5793(95)01368-7

Donthamsetty, S., Bhave, V. S., Kliment, C. S., Bowen, W. C., Mars, W. M., Bell, A. W., … Michalopoulos, G. K. (2011). Excessive hepatomegaly of mice with hepatocyte-targeted elimination of integrin linked kinase following treatment with 1,4-bis [2-(3,5-dichaloropyridyloxy)] benzene. *Hepatology (Baltimore, Md.)*, *53*(2), 587–95. http://doi.org/10.1002/hep.24040

Dufour, J.-F., & Clavien, P.-A. (2009). *Signaling Pathways in Liver Diseases*. Springer Science & Business Media.

Dundas, C. M., Demonte, D., & Park, S. (2013). Streptavidin-biotin technology: improvements and innovations in chemical and biological applications. *Applied Microbiology and Biotechnology*, *97*(21), 9343–53. http://doi.org/10.1007/s00253-013-5232-z

Durrant, I. (1994). Enhanced chemiluminescent detection of horseradish peroxidase labeled probes. *Methods in Molecular Biology (Clifton, N.J.)*, *31*, 147–61. http://doi.org/10.1385/0-89603-258-2:147

Evans, R. M., & Mangelsdorf, D. J. (2014). Nuclear Receptors, RXR, and the Big Bang. *Cell*, *157*(1), 255–66. http://doi.org/10.1016/j.cell.2014.03.012

Finnegan, S., Mackey, A. M., & Cotter, T. G. (2010). A stress survival response in retinal cells mediated through inhibition of the serine/threonine phosphatase PP2A. *The European Journal of Neuroscience*, *32*(3), 322–34. http://doi.org/10.1111/j.1460-9568.2010.07301.x

Friedberg, E. C. (2001). How nucleotide excision repair protects against cancer. *Nature Reviews. Cancer*, *1*(1), 22–33. http://doi.org/10.1038/35094000

Fujiki, H., Sueoka, E., & Suganuma, M. (2013). Tumor promoters: from chemicals to inflammatory proteins. *Journal of Cancer Research and Clinical Oncology*, *139*(10), 1603–14. http://doi.org/10.1007/s00432-013-1455-8

Fukushima, S., Kinoshita, A., Puatanachokchai, R., Kushida, M., Wanibuchi, H., & Morimura, K. (2005). Hormesis and dose-response-mediated mechanisms in carcinogenesis: evidence for a threshold in carcinogenicity of non-genotoxic carcinogens. *Carcinogenesis*, *26*(11), 1835–45. http://doi.org/10.1093/carcin/bgi160

Gabriel, J. (2007). *The Biology of Cancer*. John Wiley & Sons.

Gebhardt, R. (1992). Metabolic zonation of the liver: regulation and implications for liver function. *Pharmacology & Therapeutics*, *53*(3), 275–354.

Gebhardt, R., & Matz-Soja, M. (2014). Liver zonation: Novel aspects of its regulation and its impact on homeostasis. *World Journal of Gastroenterology : WJG*, *20*(26), 8491–8504. http://doi.org/10.3748/wjg.v20.i26.8491

Gomperts, B. D., Kramer, I. M., & Tatham, P. E. R. (2009). *Signal Transduction*. Academic Press.

Gougelet, A., & Colnot, S. (2012). A Complex Interplay between Wnt/β-Catenin Signalling and the Cell Cycle in the Adult Liver. *International Journal of Hepatology*, *2012*, 816125. http://doi.org/10.1155/2012/816125

Gougelet, A., Torre, C., Veber, P., Sartor, C., Bachelot, L., Denechaud, P.-D., … Colnot, S. (2014). T-cell factor 4 and β-catenin chromatin occupancies pattern zonal liver metabolism in mice. *Hepatology (Baltimore, Md.)*, *59*(6), 2344–57. http://doi.org/10.1002/hep.26924

Häfeli, U., Schütt, W., Teller, J., & Zborowski, M. (Eds.). (1997). *Scientific and Clinical Applications of Magnetic Carriers*. Boston, MA: Springer US. http://doi.org/10.1007/978-1-4757-6482-6

Haga, S., Ozaki, M., Inoue, H., Okamoto, Y., Ogawa, W., Takeda, K., … Todo, S. (2009). The survival pathways phosphatidylinositol-3 kinase (PI3-K)/phosphoinositide-dependent protein kinase 1 (PDK1)/Akt modulate liver regeneration through hepatocyte size rather than proliferation. *Hepatology (Baltimore, Md.)*, *49*(1), 204–14. http://doi.org/10.1002/hep.22583

Hagen, J. von. (2011). *Proteomics Sample Preparation*. John Wiley & Sons.

Hailfinger, S., Jaworski, M., Braeuning, A., Buchmann, A., & Schwarz, M. (2006). Zonal gene expression in murine liver: lessons from tumors. *Hepatology (Baltimore, Md.)*, *43*(3), 407–14. http://doi.org/10.1002/hep.21082

Hanahan, D., & Weinberg, R. A. (2000). The Hallmarks of Cancer. *Cell*, *100*(1), 57–70. http://doi.org/10.1016/S0092-8674(00)81683-9

Hanahan, D., & Weinberg, R. A. (2011). Hallmarks of cancer: the next generation. *Cell*, *144*(5), 646–674.

Hannigan, G. E., McDonald, P. C., Walsh, M. P., & Dedhar, S. (2011). Integrin-linked kinase: not so "pseudo" after all. *Oncogene*, *30*(43), 4375–85. http://doi.org/10.1038/onc.2011.177

Hast, B. E., Goldfarb, D., Mulvaney, K. M., Hast, M. A., Siesser, P. F., Yan, F., … Major, M. B. (2013). Proteomic analysis of ubiquitin ligase KEAP1 reveals associated proteins that inhibit NRF2 ubiquitination. *Cancer Research*, *73*(7), 2199–210. http://doi.org/10.1158/0008-5472.CAN-12-4400

Haystead, T. A., Sim, A. T., Carling, D., Honnor, R. C., Tsukitani, Y., Cohen, P., & Hardie, D. G. (1989). Effects of the tumour promoter okadaic acid on intracellular protein phosphorylation and metabolism. *Nature*, *337*(6202), 78–81. http://doi.org/10.1038/337078a0

Hermanson, G. T. (2008). *Bioconjugate Techniques*.

Hernández, L. G., van Steeg, H., Luijten, M., & van Benthem, J. (2009). Mechanisms of non-genotoxic carcinogens and importance of a weight of evidence approach. *Mutation Research*, *682*(2-3), 94–109. http://doi.org/10.1016/j.mrrev.2009.07.002

Hickling, K. C., Hitchcock, J. M., Oreffo, V., Mally, A., Hammond, T. G., Evans, J. G., & Chipman, J. K. (2010). Evidence of oxidative stress and associated DNA damage, increased proliferative drive, and altered gene expression in rat liver produced by the cholangiocarcinogenic agent furan. *Toxicologic Pathology*, *38*(2), 230–43. http://doi.org/10.1177/0192623309357946

Hoeijmakers, J. H. J. (2009). DNA damage, aging, and cancer. *The New England Journal of Medicine*, *361*(15), 1475–85. http://doi.org/10.1056/NEJMra0804615

Hong, Y. H., Varanasi, U. S., Yang, W., & Leff, T. (2003). AMP-activated protein kinase regulates HNF4alpha transcriptional activity by inhibiting dimer formation and decreasing protein stability. *The Journal of Biological Chemistry*, *278*(30), 27495–501. http://doi.org/10.1074/jbc.M304112200

Hosseinpour, F., Moore, R., Negishi, M., & Sueyoshi, T. (2006). Serine 202 regulates the nuclear translocation of constitutive active/androstane receptor. *Molecular Pharmacology*, *69*(4), 1095–102. http://doi.org/10.1124/mol.105.019505

Huang, S., Benavente, S., Armstrong, E. A., Li, C., Wheeler, D. L., & Harari, P. M. (2011). p53 modulates acquired resistance to EGFR inhibitors and radiation. *Cancer Research*, *71*(22), 7071–9. http://doi.org/10.1158/0008-5472.CAN-11-0128

Huang, W., Zhang, J., Washington, M., Liu, J., Parant, J. M., Lozano, G., & Moore, D. D. (2005). Xenobiotic stress induces hepatomegaly and liver tumors via the nuclear receptor constitutive androstane

receptor. *Molecular Endocrinology (Baltimore, Md.)*, *19*(6), 1646–53. http://doi.org/10.1210/me.2004-0520

Hvid, H., Fels, J. J., Kirk, R. K., Thorup, I., Jensen, H. E., Hansen, B. F., & Oleksiewicz, M. B. (2011). In situ phosphorylation of Akt and ERK1/2 in rat mammary gland, colon, and liver following treatment with human insulin and IGF-1. *Toxicologic Pathology*, *39*(4), 623–40. http://doi.org/10.1177/0192623311406936

Jäger, S., Handschin, C., St-Pierre, J., & Spiegelman, B. M. (2007). AMP-activated protein kinase (AMPK) action in skeletal muscle via direct phosphorylation of PGC-1alpha. *Proceedings of the National Academy of Sciences of the United States of America*, *104*(29), 12017–22. http://doi.org/10.1073/pnas.0705070104

Jaworski, M., Buchmann, A., Bauer, P., Riess, O., & Schwarz, M. (2005). B-raf and Ha-ras mutations in chemically induced mouse liver tumors. *Oncogene*, *24*(7), 1290–5. http://doi.org/10.1038/sj.onc.1208265

Jin Jung, K., Hyun Kim, D., Kyeong Lee, E., Woo Song, C., Pal Yu, B., & Young Chung, H. (2013). Oxidative stress induces inactivation of protein phosphatase 2A, promoting proinflammatory NF-κB in aged rat kidney. *Free Radical Biology & Medicine*, *61*, 206–17. http://doi.org/10.1016/j.freeradbiomed.2013.04.005

Jørgensen, C. S., Jagd, M., Sørensen, B. K., McGuire, J., Barkholt, V., Højrup, P., & Houen, G. (2004). Efficacy and compatibility with mass spectrometry of methods for elution of proteins from sodium dodecyl sulfate-polyacrylamide gels and polyvinyldifluoride membranes. *Analytical Biochemistry*, *330*(1), 87–97. http://doi.org/10.1016/j.ab.2004.03.012

Jung, Y., Witek, R. P., Syn, W.-K., Choi, S. S., Omenetti, A., Premont, R., … Diehl, A. M. (2010). Signals from dying hepatocytes trigger growth of liver progenitors. *Gut*, *59*(5), 655–65. http://doi.org/10.1136/gut.2009.204354

Kahn, B. B., Alquier, T., Carling, D., & Hardie, D. G. (2005). AMP-activated protein kinase: ancient energy gauge provides clues to modern understanding of metabolism. *Cell Metabolism*, *1*(1), 15–25. http://doi.org/10.1016/j.cmet.2004.12.003

Kambhampati, D. (2006). *Protein Microarray Technology*. John Wiley & Sons.

Karp, G. (2009). *Cell and Molecular Biology: Concepts and Experiments*. John Wiley & Sons.

Kawamoto, T., Sueyoshi, T., Zelko, I., Moore, R., Washburn, K., & Negishi, M. (1999). Phenobarbital-responsive nuclear translocation of the receptor CAR in induction of the CYP2B gene. *Molecular and Cellular Biology*, *19*(9), 6318–22.

Kholodenko, B. N. (2006). Cell-signalling dynamics in time and space. *Nature Reviews. Molecular Cell Biology*, *7*(3), 165–76. http://doi.org/10.1038/nrm1838

Klein, C. B., & Costa, M. (1997). DNA methylation, heterochromatin and epigenetic carcinogens. *Mutation Research/Reviews in Mutation Research*, *386*(2), 163–180. http://doi.org/10.1016/S1383-5742(96)00052-X

Kodama, S., & Negishi, M. (2008). Phenobarbital Confers its Diverse Effects by Activating the Orphan Nuclear Receptor Car.

Kolch, W. (2005). Coordinating ERK/MAPK signalling through scaffolds and inhibitors. *Nature Reviews. Molecular Cell Biology*, *6*(11), 827–37. http://doi.org/10.1038/nrm1743

Konishi, T., Karasaki, Y., Nomoto, M., Ohmori, H., Shibata, K., Abe, T., … Higashi, K. (1995). Induction of Heat Shock Protein 70 and Nucleolin and Their Intracellular Distribution during Early Stage of Liver Regeneration. *J. Biochem.*, *117*(6), 1170–1177.

Korf, U. (2011). *Protein Microarrays: Methods and Protocols*. Humana Press.

Krauss, G. (2006). *Biochemistry of Signal Transduction and Regulation* (Vol. 2). John Wiley & Sons.

Leoni, V. P., Ledda-Columbano, G. M., Pibiri, M., Saliba, C., Perra, A., Kowalik, M. A., … Columbano, A. (2011). Expression of c-jun is not mandatory for mouse hepatocyte proliferation induced by two nuclear receptor ligands: TCPOBOP and T3. *Journal of Hepatology*, *55*(5), 1069–78. http://doi.org/10.1016/j.jhep.2011.02.016

Li, F., Xiang, Y., Potter, J., Dinavahi, R., Dang, C. V, & Lee, L. A. (2006). Conditional deletion of c-myc does not impair liver regeneration. *Cancer Research*, *66*(11), 5608–12. http://doi.org/10.1158/0008-5472.CAN-05-4242

Li, X., Monks, B., Ge, Q., & Birnbaum, M. J. (2007). Akt/PKB regulates hepatic metabolism by directly inhibiting PGC-1alpha transcription coactivator. *Nature*, *447*(7147), 1012–6. http://doi.org/10.1038/nature05861

Lin, J., Handschin, C., & Spiegelman, B. M. (2005). Metabolic control through the PGC-1 family of transcription coactivators. *Cell Metabolism*, *1*(6), 361–70. http://doi.org/10.1016/j.cmet.2005.05.004

Lindros, K. O. (1997). Zonation of cytochrome P450 expression, drug metabolism and toxicity in liver. *General Pharmacology: The Vascular System*, *28*(2), 191–196. http://doi.org/10.1016/S0306-3623(96)00183-8

Lindros, K. O., Oinonen, T., Issakainen, J., Nagy, P., & Thorgeirsson, S. S. (1997). Zonal distribution of transcripts of four hepatic transcription factors in the mature rat liver. *Cell Biology and Toxicology*, *13*(4-5), 257–62.

Loeppen, S., Schneider, D., Gaunitz, F., Gebhardt, R., Kurek, R., Buchmann, A., & Schwarz, M. (2002). Overexpression of Glutamine Synthetase Is Associated with {beta}-Catenin-Mutations in Mouse Liver Tumors during Promotion of Hepatocarcinogenesis by Phenobarbital. *Cancer Res.*, *62*(20), 5685–5688.

Lombard, D. B., Chua, K. F., Mostoslavsky, R., Franco, S., Gostissa, M., & Alt, F. W. (2005). DNA repair, genome stability, and aging. *Cell*, *120*(4), 497–512. http://doi.org/10.1016/j.cell.2005.01.028

Lu, M., Wan, M., Leavens, K. F., Chu, Q., Monks, B. R., Fernandez, S., … Birnbaum, M. J. (2012). Insulin regulates liver metabolism in vivo in the absence of hepatic Akt and Foxo1. *Nature Medicine*, *18*(3), 388–95. http://doi.org/10.1038/nm.2686

Luo, X., Zhang, Y., Ruan, X., Jiang, X., Zhu, L., Wang, X., … Chen, Y. (2011). Fasting-induced protein phosphatase 1 regulatory subunit contributes to postprandial blood glucose homeostasis via regulation of hepatic glycogenesis. *Diabetes*, *60*(5), 1435–45. http://doi.org/10.2337/db10-1663

Lustig, Y., Ruas, J. L., Estall, J. L., Lo, J. C., Devarakonda, S., Laznik, D., … Spiegelman, B. M. (2011). Separation of the gluconeogenic and mitochondrial functions of PGC-1 through S6 kinase. *Genes & Development*, *25*(12), 1232–1244. http://doi.org/10.1101/gad.2054711

Makino, R., Hayashi, K., & Sugimura, T. (1984). C-myc transcript is induced in rat liver at a very early stage of regeneration or by cycloheximide treatment. *Nature*, *310*(5979), 697–698. http://doi.org/10.1038/310697a0

Malarkey, D. E., Johnson, K., Ryan, L., Boorman, G., & Maronpot, R. R. (2005). New insights into functional aspects of liver morphology. *Toxicologic Pathology*, *33*(1), 27–34. http://doi.org/10.1080/01926230590881826

Mathews, S. T., Plaisance, E. P., & Kim, T. (2009). Imaging systems for westerns: chemiluminescence vs. infrared detection. *Methods in Molecular Biology (Clifton, N.J.)*, *536*, 499–513. http://doi.org/10.1007/978-1-59745-542-8_51

Matsumura, T., & Thurman, R. G. (1984). Predominance of glycolysis in pericentral regions of the liver lobule. *European Journal of Biochemistry*, *140*(2), 229–234. http://doi.org/10.1111/j.1432-1033.1984.tb08091.x

Matz-Soja, M., Aleithe, S., Marbach, E., Böttger, J., Arnold, K., Schmidt-Heck, W., … Gebhardt, R. (2014). Hepatic Hedgehog signaling contributes to the regulation of IGF1 and IGFBP1 serum levels. *Cell Communication and Signaling : CCS*, *12*, 11. http://doi.org/10.1186/1478-811X-12-11

Matz-Soja, M., Hovhannisyan, A., & Gebhardt, R. (2013). Hedgehog signalling pathway in adult liver: a major new player in hepatocyte metabolism and zonation? *Medical Hypotheses*, *80*(5), 589–94. http://doi.org/10.1016/j.mehy.2013.01.032

Melnick, R. L., Kohn, M. C., & Portier, C. J. (1996). Implications for risk assessment of suggested nongenotoxic mechanisms of chemical carcinogenesis. *Environmental Health Perspectives*, *104 Suppl* , 123–34.

Michaud, G. A., Salcius, M., Zhou, F., Bangham, R., Bonin, J., Guo, H., … Schweitzer, B. I. (2003). Analyzing antibody specificity with whole proteome microarrays. *Nature Biotechnology*, *21*(12), 1509–12. http://doi.org/10.1038/nbt910

Mihaylova, M. M., & Shaw, R. J. (2011). The AMPK signalling pathway coordinates cell growth, autophagy and metabolism. *Nature Cell Biology*, *13*(9), 1016–23. http://doi.org/10.1038/ncb2329

Milone, M. C. (2012). *Therapeutic Drug Monitoring*. *Therapeutic Drug Monitoring*. Elsevier. http://doi.org/10.1016/B978-0-12-385467-4.00003-8

Mitsuishi, Y., Taguchi, K., Kawatani, Y., Shibata, T., Nukiwa, T., Aburatani, H., … Motohashi, H. (2012). Nrf2 redirects glucose and glutamine into anabolic pathways in metabolic reprogramming. *Cancer Cell*, *22*(1), 66–79. http://doi.org/10.1016/j.ccr.2012.05.016

Molli, P. R., Li, D. Q., Murray, B. W., Rayala, S. K., & Kumar, R. (2009). PAK signaling in oncogenesis. *Oncogene*, *28*(28), 2545–55. http://doi.org/10.1038/onc.2009.119

Monga, S. P., Pediaditakis, P., Mule, K., Stolz, D. B., & Michalopoulos, G. K. (2001). Changes in WNT/beta-catenin pathway during regulated growth in rat liver regeneration. *Hepatology (Baltimore, Md.)*, *33*(5), 1098–109. http://doi.org/10.1053/jhep.2001.23786

Monga, S. P. S., & Cagle, P. T. (2010). *Molecular Pathology of Liver Diseases*. Springer Science & Business Media.

Mosser, D., Caron, A., Bourget, L., Denis-Larose, C., & Massie, B. (1997). Role of the human heat shock protein hsp70 in protection against stress- induced apoptosis. *Mol. Cell. Biol.*, *17*(9), 5317–5327.

Nguyen, U., Squaglia, N., Boge, A., & Fung, P. A. (2011). The Simple Western[trade]: a gel-free, blot-free, hands-free Western blotting reinvention, *8*(11). http://doi.org/10.1038/nmeth.f.353

Nika, K., Charvet, C., Williams, S., Tautz, L., Bruckner, S., Rahmouni, S., … Mustelin, T. (2006). Lipid raft targeting of hematopoietic protein tyrosine phosphatase by protein kinase C theta-mediated phosphorylation. *Molecular and Cellular Biology*, *26*(5), 1806–16. http://doi.org/10.1128/MCB.26.5.1806-1816.2006

O'Neill, R. A., Bhamidipati, A., Bi, X., Deb-Basu, D., Cahill, L., Ferrante, J., … Vander Horn, P. B. (2006). Isoelectric focusing technology quantifies protein signaling in 25 cells. *Proceedings of the National Academy of Sciences of the United States of America*, *103*(44), 16153–8. http://doi.org/10.1073/pnas.0607973103

Oberkofler, H., Esterbauer, H., Linnemayr, V., Strosberg, A. D., Krempler, F., & Patsch, W. (2002). Peroxisome proliferator-activated receptor (PPAR) gamma coactivator-1 recruitment regulates PPAR subtype specificity. *The Journal of Biological Chemistry*, *277*(19), 16750–7. http://doi.org/10.1074/jbc.M200475200

Ochoa, B., Syn, W.-K., Delgado, I., Karaca, G. F., Jung, Y., Wang, J., … Diehl, A. M. (2010). Hedgehog signaling is critical for normal liver regeneration after partial hepatectomy in mice. *Hepatology (Baltimore, Md.)*, *51*(5), 1712–23. http://doi.org/10.1002/hep.23525

Ogawa, H., & Kawamata, S. (1995). Periportal expression of the serine dehydratase gene in rat liver. *The Histochemical Journal*, *27*(5), 380–387. http://doi.org/10.1007/BF02389024

Omenetti, A., Choi, S., Michelotti, G., & Diehl, A. M. (2011). Hedgehog signaling in the liver. *Journal of Hepatology*, *54*(2), 366–73. http://doi.org/10.1016/j.jhep.2010.10.003

Orsulic, S., Huber, O., Aberle, H., Arnold, S., & Kemler, R. (1999). E-cadherin binding prevents beta-catenin nuclear localization and beta-catenin/LEF-1-mediated transactivation. *J. Cell Sci.*, *112*(8), 1237–1245.

Owens, D. M., & Keyse, S. M. (2007). Differential regulation of MAP kinase signalling by dual-specificity protein phosphatases. *Oncogene*, *26*(22), 3203–13. http://doi.org/10.1038/sj.onc.1210412

Pasquale, E. B. (2010). Eph receptors and ephrins in cancer: bidirectional signalling and beyond. *Nature Reviews. Cancer*, *10*(3), 165–80. http://doi.org/10.1038/nrc2806

Reddy, A. B., Maywood, E. S., Karp, N. A., King, V. M., Inoue, Y., Gonzalez, F. J., … Hastings, M. H. (2007). Glucocorticoid signaling synchronizes the liver circadian transcriptome. *Hepatology (Baltimore, Md.)*, *45*(6), 1478–88. http://doi.org/10.1002/hep.21571

Rhee, J., Inoue, Y., Yoon, J. C., Puigserver, P., Fan, M., Gonzalez, F. J., & Spiegelman, B. M. (2003). Regulation of hepatic fasting response by PPARgamma coactivator-1alpha (PGC-1): requirement for hepatocyte nuclear factor 4alpha in gluconeogenesis. *Proceedings of the National Academy of Sciences of the United States of America*, *100*(7), 4012–7. http://doi.org/10.1073/pnas.0730870100

Ruijter, J. M., Gieling, R. G., Markman, M. M., Hagoort, J., & Lamers, W. H. (2004). Stereological measurement of porto-central gradients in gene expression in mouse liver. *Hepatology (Baltimore, Md.)*, *39*(2), 343–52. http://doi.org/10.1002/hep.20068

Saeed, A. I., Bhagabati, N. K., Braisted, J. C., Liang, W., Sharov, V., Howe, E. A., … Quackenbush, J. (2006). TM4 microarray software suite. *Methods in Enzymology*, *411*, 134–93. http://doi.org/10.1016/S0076-6879(06)11009-5

Saltiel, A. R. (1996). Diverse signaling pathways in the cellular actions of insulin. *Am J Physiol Endocrinol Metab*, *270*(3), E375–385.

Scanlon, V. C. (2007). *Essentials of Anatomy and Physiology*.

Schibler, U., Ripperger, J., & Brown, S. A. (2003). Peripheral Circadian Oscillators in Mammals: Time and Food. *Journal of Biological Rhythms*, *18*(3), 250–260. http://doi.org/10.1177/0748730403018003007

Schmutz, I., Wendt, S., Schnell, A., Kramer, A., Mansuy, I. M., & Albrecht, U. (2011). Protein phosphatase 1 (PP1) is a post-translational regulator of the mammalian circadian clock. *PloS One*, *6*(6), e21325. http://doi.org/10.1371/journal.pone.0021325

Schulte-Hermann, R. (1985). Tumor promotion in the liver. *Archives of Toxicology*, *57*(3), 147–158. http://doi.org/10.1007/BF00290879

Shiojima, I., & Walsh, K. (2006). Regulation of cardiac growth and coronary angiogenesis by the Akt/PKB signaling pathway. *Genes & Development*, *20*(24), 3347–65. http://doi.org/10.1101/gad.1492806

Sozio, M. S., Lu, C., Zeng, Y., Liangpunsakul, S., & Crabb, D. W. (2011). Activated AMPK inhibits PPAR-{alpha} and PPAR-{gamma} transcriptional activity in hepatoma cells. *American Journal of Physiology. Gastrointestinal and Liver Physiology*, *301*(4), G739–47. http://doi.org/10.1152/ajpgi.00432.2010

St Hilaire, R. J., Hradek, G. T., & Jones, A. L. (1983). Hepatic sequestration and biliary secretion of epidermal growth factor: evidence for a high-capacity uptake system. *Proceedings of the National Academy of Sciences of the United States of America*, *80*(12), 3797–801.

Stewart, M. J., & Thomas, G. (1994). Mitogenesis and protein synthesis: a role for ribosomal protein S6 phosphorylation? *BioEssays : News and Reviews in Molecular, Cellular and Developmental Biology*, *16*(11), 809–15. http://doi.org/10.1002/bies.950161107

Taussig, M. J., Stoevesandt, O., Borrebaeck, C. A. K., Bradbury, A. R., Cahill, D., Cambillau, C., … Uhlén, M. (2007). ProteomeBinders: planning a European resource of affinity reagents for analysis of the human proteome. *Nature Methods*, *4*(1), 13–7. http://doi.org/10.1038/nmeth0107-13

Templin, M. F., Stoll, D., Schrenk, M., Traub, P. C., Vöhringer, C. F., & Joos, T. O. (2002). Protein microarray technology. *Trends in Biotechnology*, *20*(4), 160–166. http://doi.org/10.1016/S0167-7799(01)01910-2

Thorpe, G. H., Kricka, L. J., Moseley, S. B., & Whitehead, T. P. (1985). Phenols as enhancers of the chemiluminescent horseradish peroxidase-luminol-hydrogen peroxide reaction: application in luminescence-monitored enzyme immunoassays. *Clinical Chemistry*, *31*(8), 1335–41.

Thurman, R. G., & Kauffman, F. C. (1985). SUblobularcompartmentationofpharmacologicevents (scope): Metabolic fluxes in periportal and pericentral regions of the liver lobule. *Hepatology*, *5*(1), 144–151. http://doi.org/10.1002/hep.1840050128

Towbin, H., Staehelin, T., & Gordon, J. (1979). Electrophoretic transfer of proteins from polyacrylamide gels to nitrocellulose sheets: procedure and some applications. *Proceedings of the National Academy of Sciences of the United States of America*, *76*(9), 4350–4.

Towler, M. C., & Hardie, D. G. (2007). AMP-activated protein kinase in metabolic control and insulin signaling. *Circulation Research*, *100*(3), 328–41. http://doi.org/10.1161/01.RES.0000256090.42690.05

Uhlen, M., Fagerberg, L., Hallstrom, B. M., Lindskog, C., Oksvold, P., Mardinoglu, A., … Ponten, F. (2015). Tissue-based map of the human proteome. *Science*, *347*(6220), 1260419–1260419. http://doi.org/10.1126/science.1260419

Uhlen, M., Oksvold, P., Fagerberg, L., Lundberg, E., Jonasson, K., Forsberg, M., … Ponten, F. (2010). Towards a knowledge-based Human Protein Atlas. *Nature Biotechnology*, *28*(12), 1248–50. http://doi.org/10.1038/nbt1210-1248

Um, J.-H., Pendergast, J. S., Springer, D. A., Foretz, M., Viollet, B., Brown, A., … Chung, J. H. (2011). AMPK regulates circadian rhythms in a tissue- and isoform-specific manner. *PloS One*, *6*(3), e18450. http://doi.org/10.1371/journal.pone.0018450

Vanhaesebroeck, B., & Alessi, D. R. (2000). The PI3K-PDK1 connection: more than just a road to PKB. *The Biochemical Journal*, *346 Pt 3*, 561–76.

Viana, A. Y. I., Sakoda, H., Anai, M., Fujishiro, M., Ono, H., Kushiyama, A., … Asano, T. (2006). Role of hepatic AMPK activation in glucose metabolism and dexamethasone-induced regulation of AMPK expression. *Diabetes Research and Clinical Practice*, *73*(2), 135–42. http://doi.org/10.1016/j.diabres.2005.12.011

Virshup, D. M., & Shenolikar, S. (2009). From promiscuity to precision: protein phosphatases get a makeover. *Molecular Cell*, *33*(5), 537–45. http://doi.org/10.1016/j.molcel.2009.02.015

Volmat, V., & Pouysségur, J. (2001). Spatiotemporal regulation of the p42/p44 MAPK pathway. *Biology of the Cell*, *93*(1-2), 71–79. http://doi.org/10.1016/S0248-4900(01)01129-7

Voshol, H., Ehrat, M., Traenkle, J., Bertrand, E., & van Oostrum, J. (2009). Antibody-based proteomics: analysis of signaling networks using reverse protein arrays. *The FEBS Journal*, *276*(23), 6871–9. http://doi.org/10.1111/j.1742-4658.2009.07395.x

Wang, T., Yu, Q., Chen, J., Deng, B., Qian, L., & Le, Y. (2010). PP2A mediated AMPK inhibition promotes HSP70 expression in heat shock response. *PloS One*, *5*(10), e13096. http://doi.org/10.1371/journal.pone.0013096

Wang, W., & Wong, C.-W. (2010). Statins enhance peroxisome proliferator-activated receptor gamma coactivator-1alpha activity to regulate energy metabolism. *Journal of Molecular Medicine (Berlin, Germany)*, *88*(3), 309–17. http://doi.org/10.1007/s00109-009-0561-1

Wang, Z., Oh, E., Clapp, D. W., Chernoff, J., & Thurmond, D. C. (2011). Inhibition or ablation of p21-activated kinase (PAK1) disrupts glucose homeostatic mechanisms in vivo. *The Journal of Biological Chemistry*, *286*(48), 41359–67. http://doi.org/10.1074/jbc.M111.291500

Wang, Z., Salih, E., & Burke, P. A. (2011). Quantitative analysis of cytokine-induced hepatocyte nuclear factor-4α phosphorylation by mass spectrometry. *Biochemistry*, *50*(23), 5292–300. http://doi.org/10.1021/bi200540w

Weber, G. F. (2007). *Molecular Mechanisms of Cancer*.

Westermarck, J., & Hahn, W. C. (2008). Multiple pathways regulated by the tumor suppressor PP2A in transformation. *Trends in Molecular Medicine*, *14*(4), 152–60. http://doi.org/10.1016/j.molmed.2008.02.001

Wild, D. (2013). *The Immunoassay Handbook: Theory and applications of ligand binding, ELISA and related techniques*.

Witters, L. A., Gao, G., Kemp, B. E., & Quistorff, B. (1994). Hepatic 5'-AMP-activated protein kinase: zonal distribution and relationship to acetyl-CoA carboxylase activity in varying nutritional states. *Archives of Biochemistry and Biophysics*, *308*(2), 413–9. http://doi.org/10.1006/abbi.1994.1058

Wolf, J. H., Bhatti, T. R., Fouraschen, S., Chakravorty, S., Wang, L., Kurian, S., … Levine, M. H. (2014). Heat shock protein 70 is required for optimal liver regeneration after partial hepatectomy in mice. *Liver Transplantation : Official Publication of the American Association for the Study of Liver Diseases and the International Liver Transplantation Society*, *20*(3), 376–85. http://doi.org/10.1002/lt.23813

Xi, H.-Q., Wu, X.-S., Wei, B., & Chen, L. (2012). Eph receptors and ephrins as targets for cancer therapy. *Journal of Cellular and Molecular Medicine*, *16*(12), 2894–909. http://doi.org/10.1111/j.1582-4934.2012.01612.x

Xu, Y., Nguyen, Q., Lo, D. C., & Czaja, M. J. (1997). c-myc-Dependent hepatoma cell apoptosis results from oxidative stress and not a deficiency of growth factors. *Journal of Cellular Physiology*, *170*(2), 192–9. http://doi.org/10.1002/(SICI)1097-4652(199702)170:2<192::AID-JCP11>3.0.CO;2-K

Xue, B., & Kahn, B. B. (2006). AMPK integrates nutrient and hormonal signals to regulate food intake and energy balance through effects in the hypothalamus and peripheral tissues. *The Journal of Physiology*, *574*(Pt 1), 73–83. http://doi.org/10.1113/jphysiol.2006.113217

Yarden, Y. (2001). The EGFR family and its ligands in human cancer. *European Journal of Cancer*, *37*, 3–8. http://doi.org/10.1016/S0959-8049(01)00230-1

Yarden, Y., & Sliwkowski, M. X. (2001). Untangling the ErbB signalling network. *Nature Reviews. Molecular Cell Biology*, *2*(2), 127–37. http://doi.org/10.1038/35052073

Yoshinari, K., Kobayashi, K., Moore, R., Kawamoto, T., & Negishi, M. (2003). Identification of the nuclear receptor CAR:HSP90 complex in mouse liver and recruitment of protein phosphatase 2A in response to phenobarbital. *FEBS Letters*, *548*(1-3), 17–20. http://doi.org/10.1016/S0014-5793(03)00720-8

Yuneva, M., Zamboni, N., Oefner, P., Sachidanandam, R., & Lazebnik, Y. (2007). Deficiency in glutamine but not glucose induces MYC-dependent apoptosis in human cells. *The Journal of Cell Biology*, *178*(1), 93–105. http://doi.org/10.1083/jcb.200703099

Zhan, Q., Fang, Y., He, Y., Liu, H.-X., Fang, J., & Wan, Y.-J. Y. (2012). Function annotation of hepatic retinoid x receptor α based on genome-wide DNA binding and transcriptome profiling. *PloS One*, *7*(11), e50013. http://doi.org/10.1371/journal.pone.0050013

11.1 List of figures

11.2 List of tables

12 Appendices

12.1 Appendix 1: Comparison of Western-Blots to DigiWest

Shown are comparisons of classical Western-Blots and DigiWest data as described in section 3.5.1. The sample which was used for the Western-Blots and for generation of the DigiWest bead-mix was a HepG2 lysate. For each of the 104 antibodies a classical Western-Blot is shown on the left, the DigiWest data in a reduced diagram in the middle with the specific signal highlighted in black and a grayscale-map representing the DigiWest data as Western-Blot mimic on the right.


14-3-3 sigma
4E-BP1 - phospho Ser65
4E-BP1
Akt
Alcohol dehydrogenase beta subunit
AMPK alpha - phospho Thr172
AMPK alpha
Aurora A/B/C - phospho T288/T232/T198
Aurora B (AIM1)
Axin 1
Western Blot
DigiWest
Greyscale Map

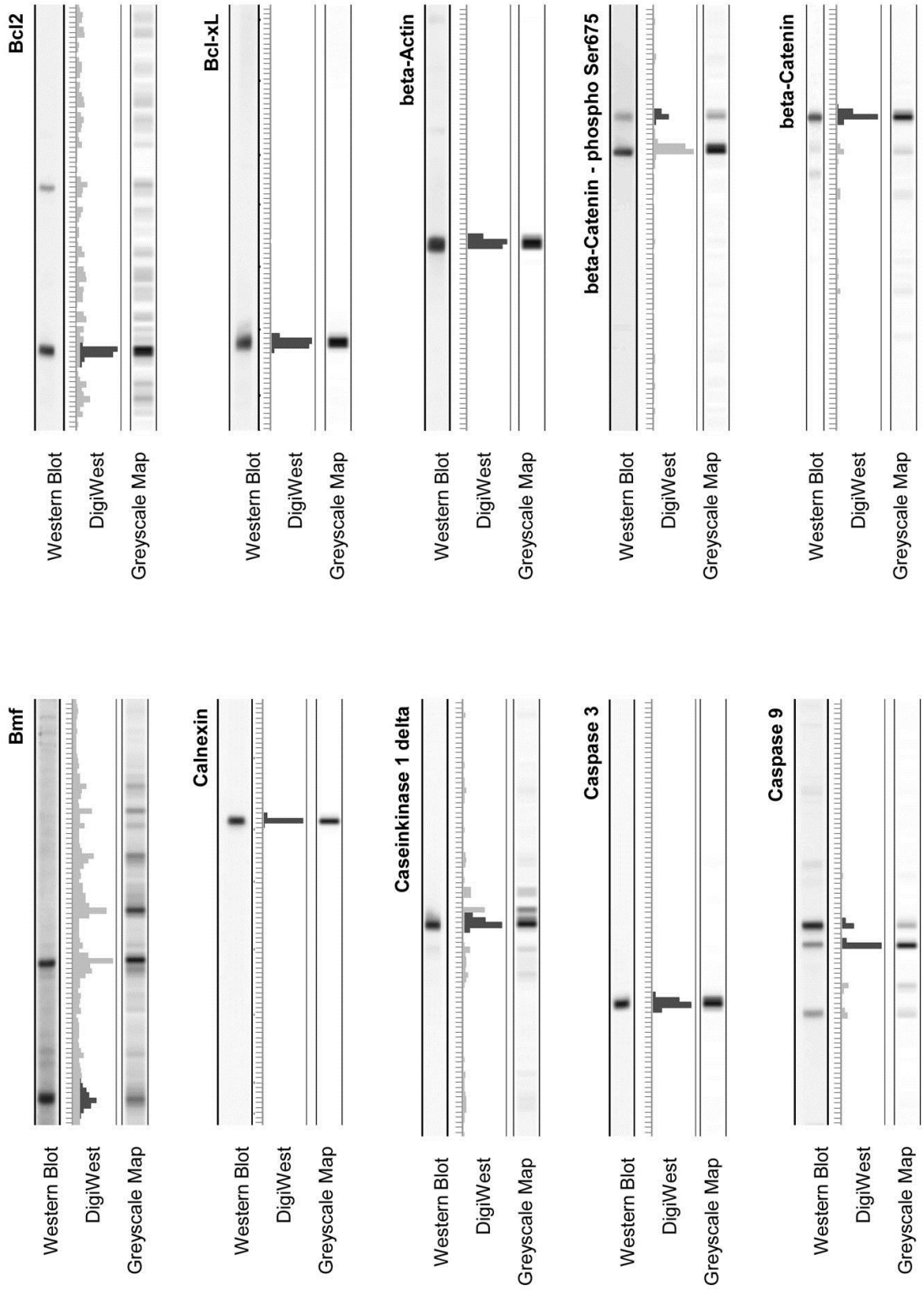
Bcl2
Western Blot
DigiWest
Greyscale Map
Bcl-xL
Western Blot
DigiWest
Greyscale Map
beta-Actin
Western Blot
DigiWest
Greyscale Map
beta-Catenin - phospho Ser675
Western Blot
DigiWest
Greyscale Map
beta-Catenin
Western Blot
DigiWest
Greyscale Map
Bmf
Western Blot
DigiWest
Greyscale Map
Calnexin
Western Blot
DigiWest
Greyscale Map
Caseinkinase 1 delta
Western Blot
DigiWest
Greyscale Map
Caspase 3
Western Blot
DigiWest
Greyscale Map
Caspase 9
Western Blot
DigiWest
Greyscale Map


cdc2 - phospho Tyr15
cdc2 (CDK1)
CDKN2B (p15 INK4B)
c-myc - phospho Thr58/Ser62
c-myc
Cofilin - phospho Ser3
Cofilin
c-Raf - phospho Ser259
c-Raf
CREB - phospho Ser133
Western Blot
DigiWest
Greyscale Map

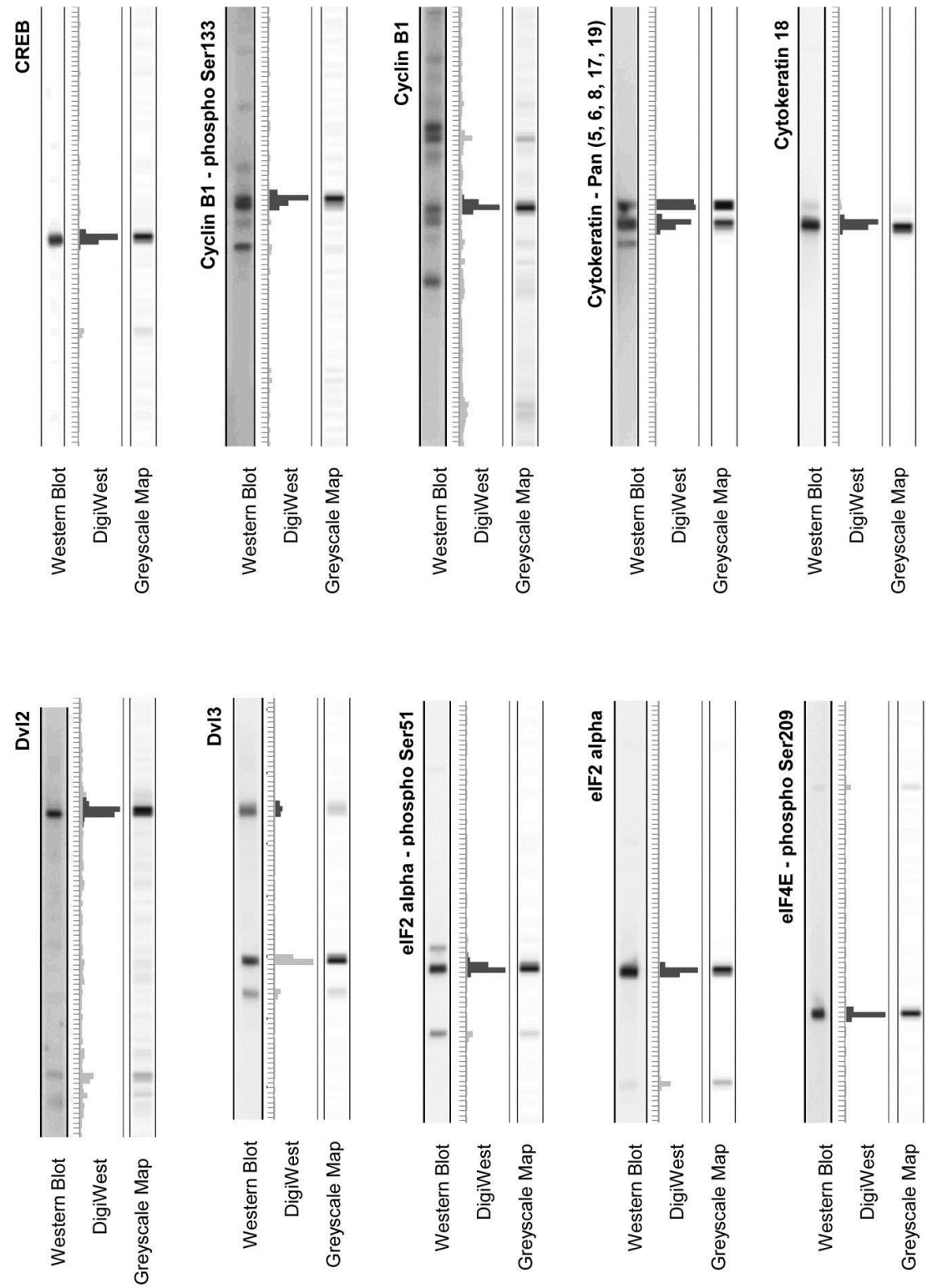
CREB
Western Blot
DigiWest
Greyscale Map
Cyclin B1 - phospho Ser133
Western Blot
DigiWest
Greyscale Map
Cyclin B1
Western Blot
DigiWest
Greyscale Map
Cytokeratin - Pan (5, 6, 8, 17, 19)
Western Blot
DigiWest
Greyscale Map
Cytokeratin 18
Western Blot
DigiWest
Greyscale Map
Dvl2
Western Blot
DigiWest
Greyscale Map
Dvl3
Western Blot
DigiWest
Greyscale Map
eIF2 alpha - phospho Ser51
Western Blot
DigiWest
Greyscale Map
eIF2 alpha
Western Blot
DigiWest
Greyscale Map
eIF4E - phospho Ser209
Western Blot
DigiWest
Greyscale Map

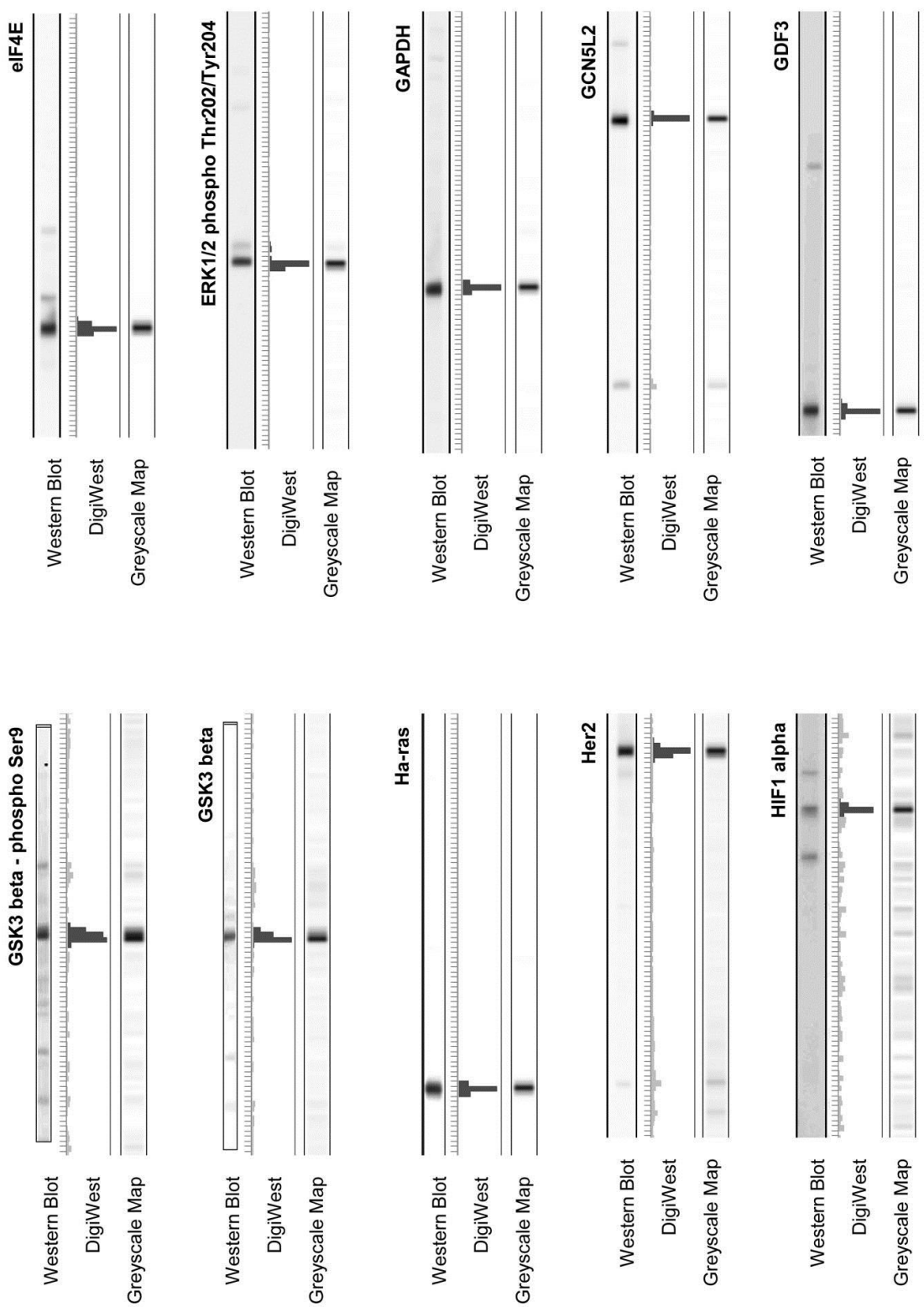
eIF4E
Western Blot
DigiWest
Greyscale Map
ERK1/2 phospho Thr202/Tyr204
Western Blot
DigiWest
Greyscale Map
GAPDH
Western Blot
DigiWest
Greyscale Map
GCN5L2
Western Blot
DigiWest
Greyscale Map
GDF3
Western Blot
DigiWest
Greyscale Map
GSK3 beta - phospho Ser9
Western Blot
DigiWest
Greyscale Map
GSK3 beta
Western Blot
DigiWest
Greyscale Map
Ha-ras
Western Blot
DigiWest
Greyscale Map
Her2
Western Blot
DigiWest
Greyscale Map
HIF1 alpha
Western Blot
DigiWest
Greyscale Map

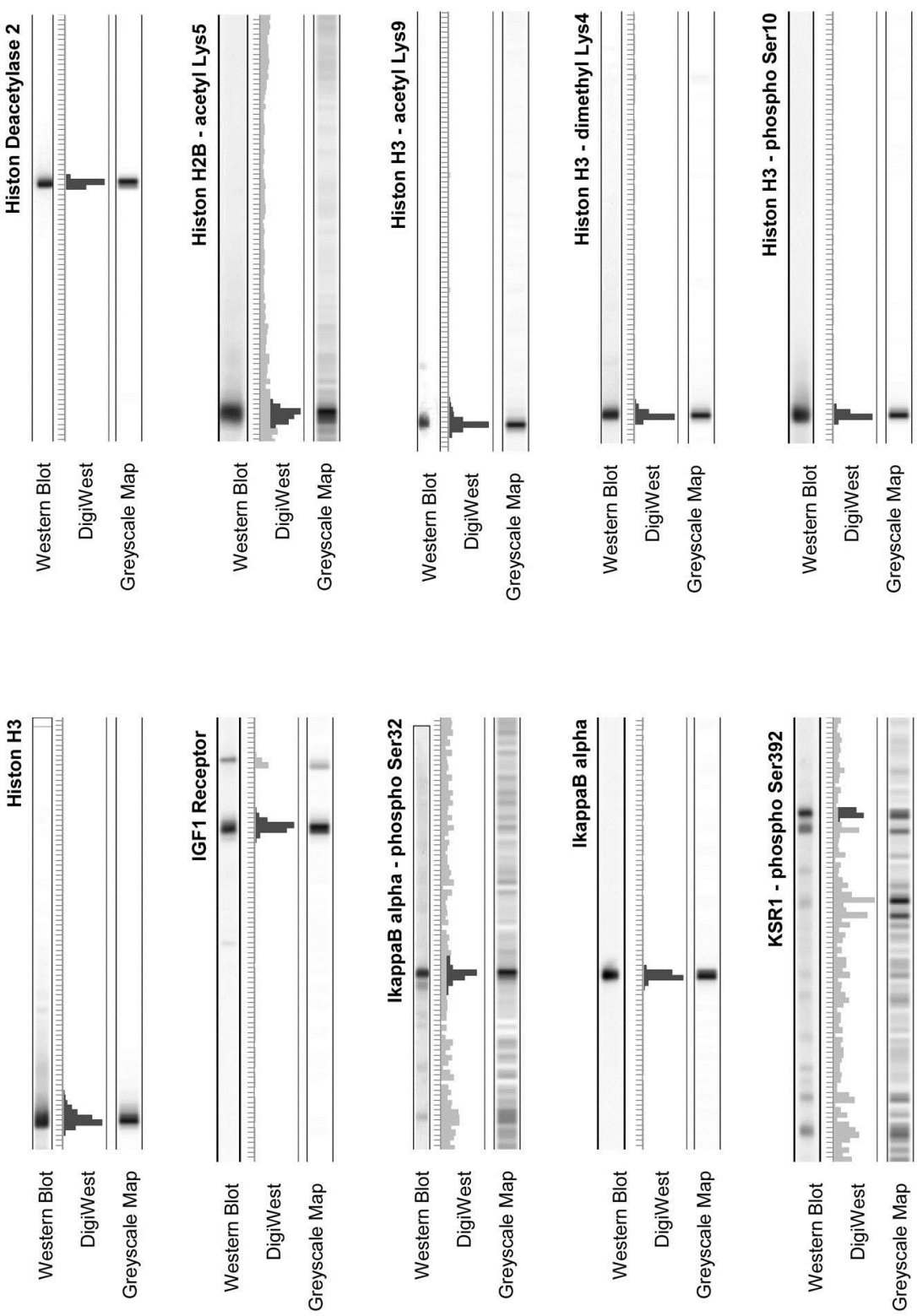
Histon Deacetylase 2
Western Blot
DigiWest
Greyscale Map
Histon H2B - acetyl Lys5
Western Blot
DigiWest
Greyscale Map
Histon H3 - acetyl Lys9
Western Blot
DigiWest
Greyscale Map
Histon H3 - dimethyl Lys4
Western Blot
DigiWest
Greyscale Map
Histon H3 - phospho Ser10
Western Blot
DigiWest
Greyscale Map
Histon H3
Western Blot
DigiWest
Greyscale Map
IGF1 Receptor
Western Blot
DigiWest
Greyscale Map
IkappaB alpha - phospho Ser32
Western Blot
DigiWest
Greyscale Map
IkappaB alpha
Western Blot
DigiWest
Greyscale Map
KSR1 - phospho Ser392
Western Blot
DigiWest
Greyscale Map

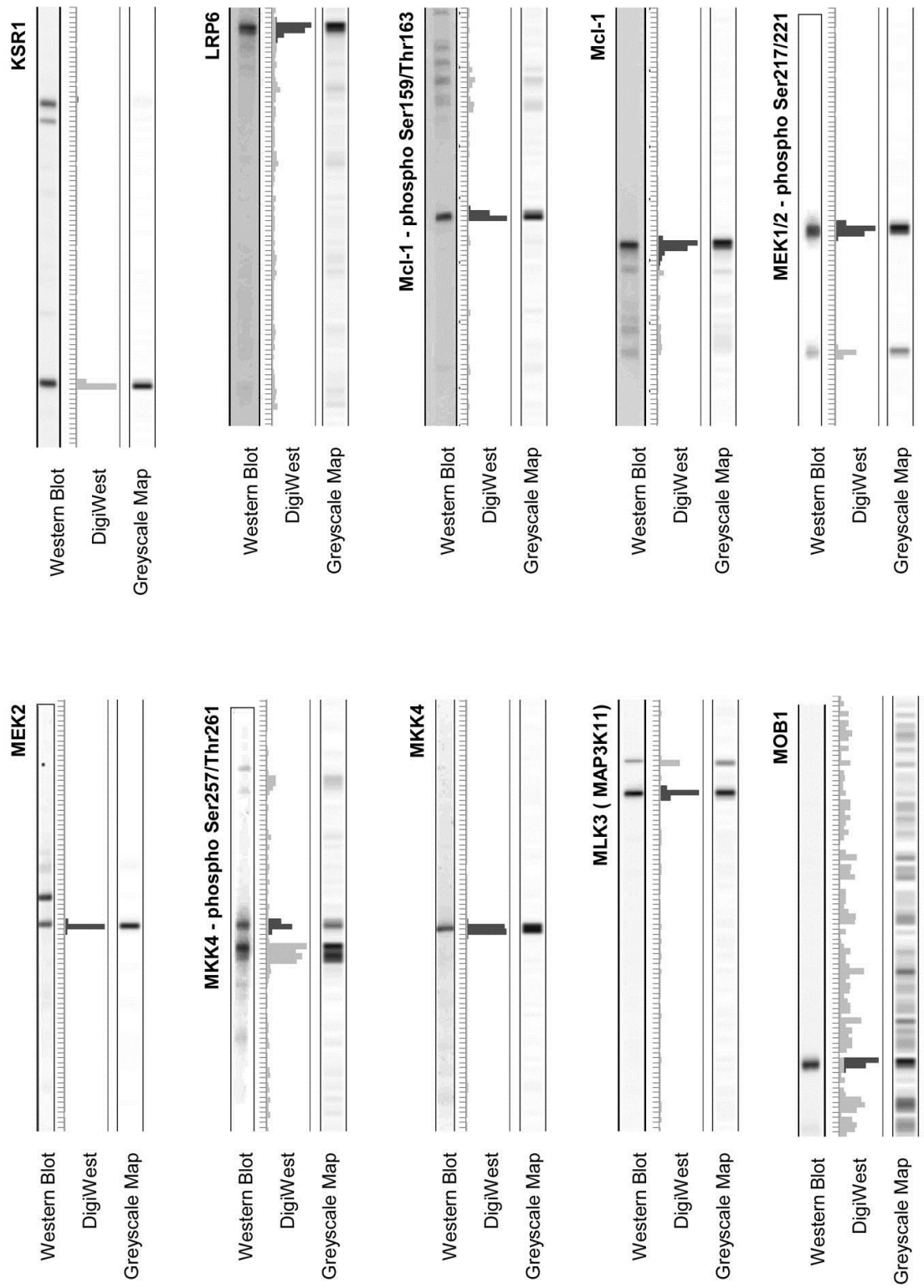
KSR1
Western Blot
DigiWest
Greyscale Map
LRP6
Western Blot
DigiWest
Greyscale Map
Mcl-1 - phospho Ser159/Thr163
Western Blot
DigiWest
Greyscale Map
Mcl-1
Western Blot
DigiWest
Greyscale Map
MEK1/2 - phospho Ser217/221
Western Blot
DigiWest
Greyscale Map
MEK2
Western Blot
DigiWest
Greyscale Map
MKK4 - phospho Ser257/Thr261
Western Blot
DigiWest
Greyscale Map
MKK4
Western Blot
DigiWest
Greyscale Map
MLK3 (MAP3K11)
Western Blot
DigiWest
Greyscale Map
MOB1
Western Blot
DigiWest
Greyscale Map

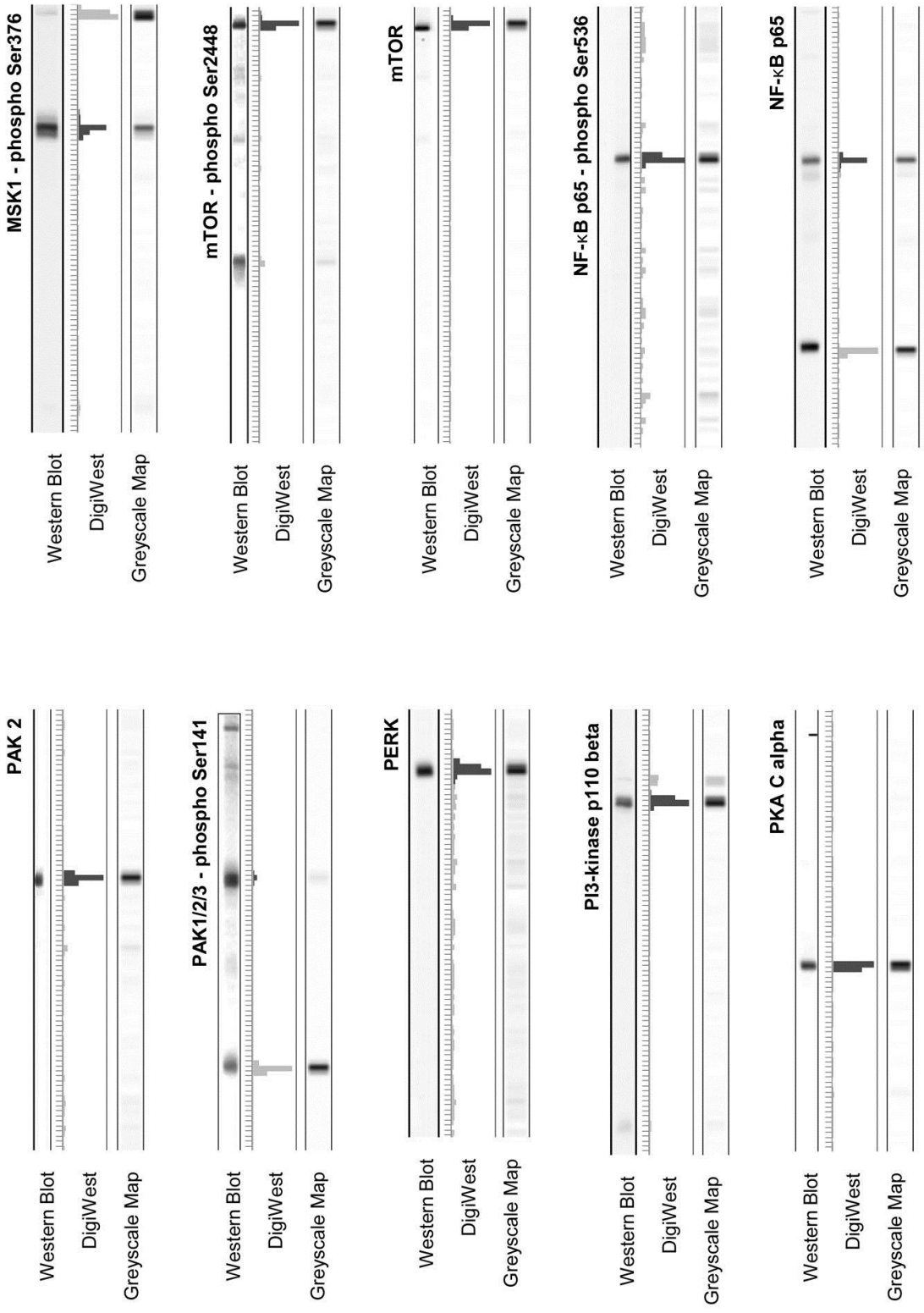
MSK1 - phospho Ser376
mTOR - phospho Ser2448
mTOR
NF-κB p65 - phospho Ser536
NF-κB p65
PAK 2
PAK1/2/3 - phospho Ser141
PERK
PI3-kinase p110 beta
PKA C alpha
Western Blot
DigiWest
Greyscale Map

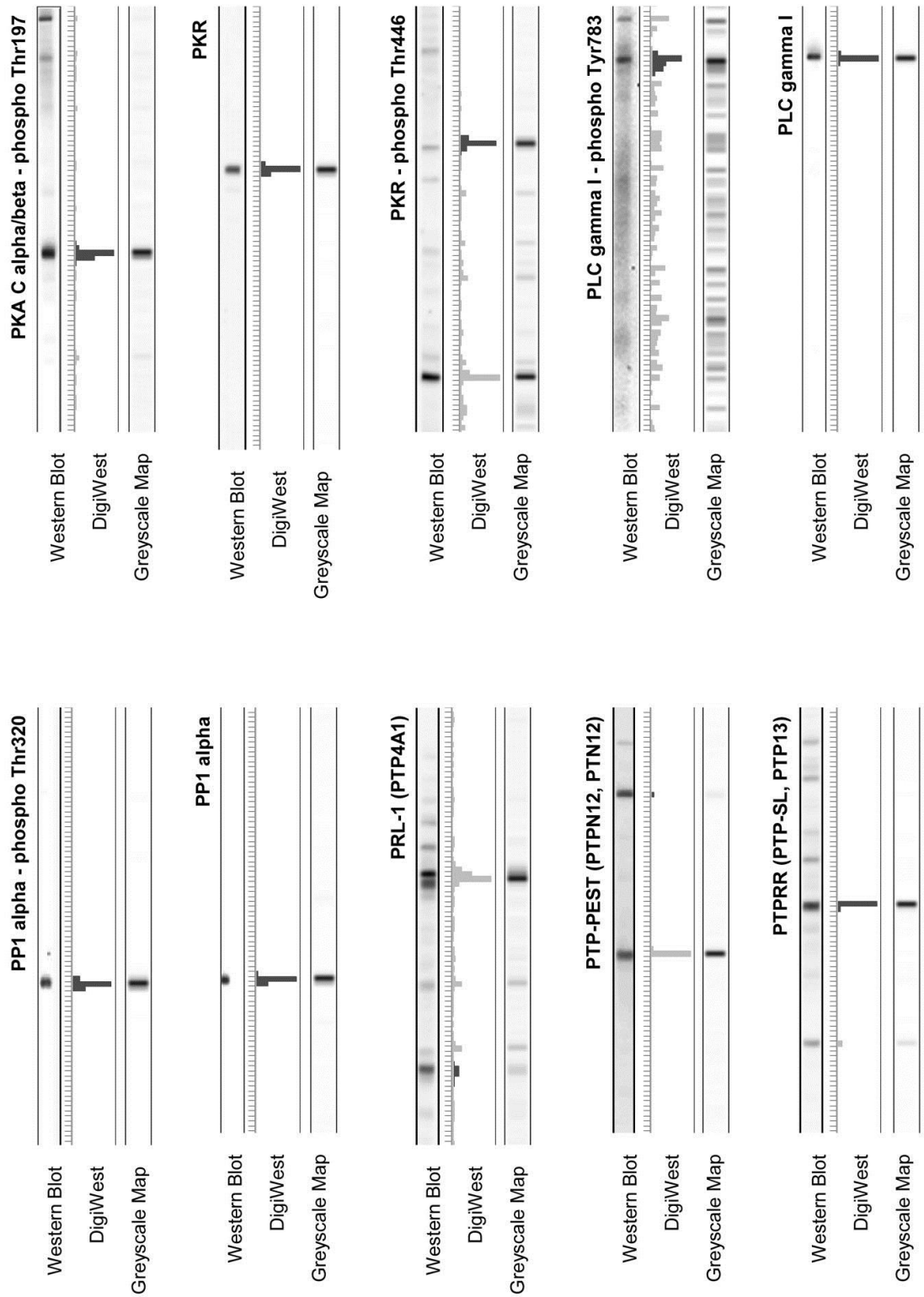
PKA C alpha/beta - phospho Thr197
Western Blot
DigiWest
Greyscale Map
PKR
Western Blot
DigiWest
Greyscale Map
PKR - phospho Thr446
Western Blot
DigiWest
Greyscale Map
PLC gamma I - phospho Tyr783
Western Blot
DigiWest
Greyscale Map
PLC gamma I
Western Blot
DigiWest
Greyscale Map
PP1 alpha - phospho Thr320
Western Blot
DigiWest
Greyscale Map
PP1 alpha
Western Blot
DigiWest
Greyscale Map
PRL-1 (PTP4A1)
Western Blot
DigiWest
Greyscale Map
PTP-PEST (PTPN12, PTN12)
Western Blot
DigiWest
Greyscale Map
PTPRR (PTP-SL, PTP13)
Western Blot
DigiWest
Greyscale Map

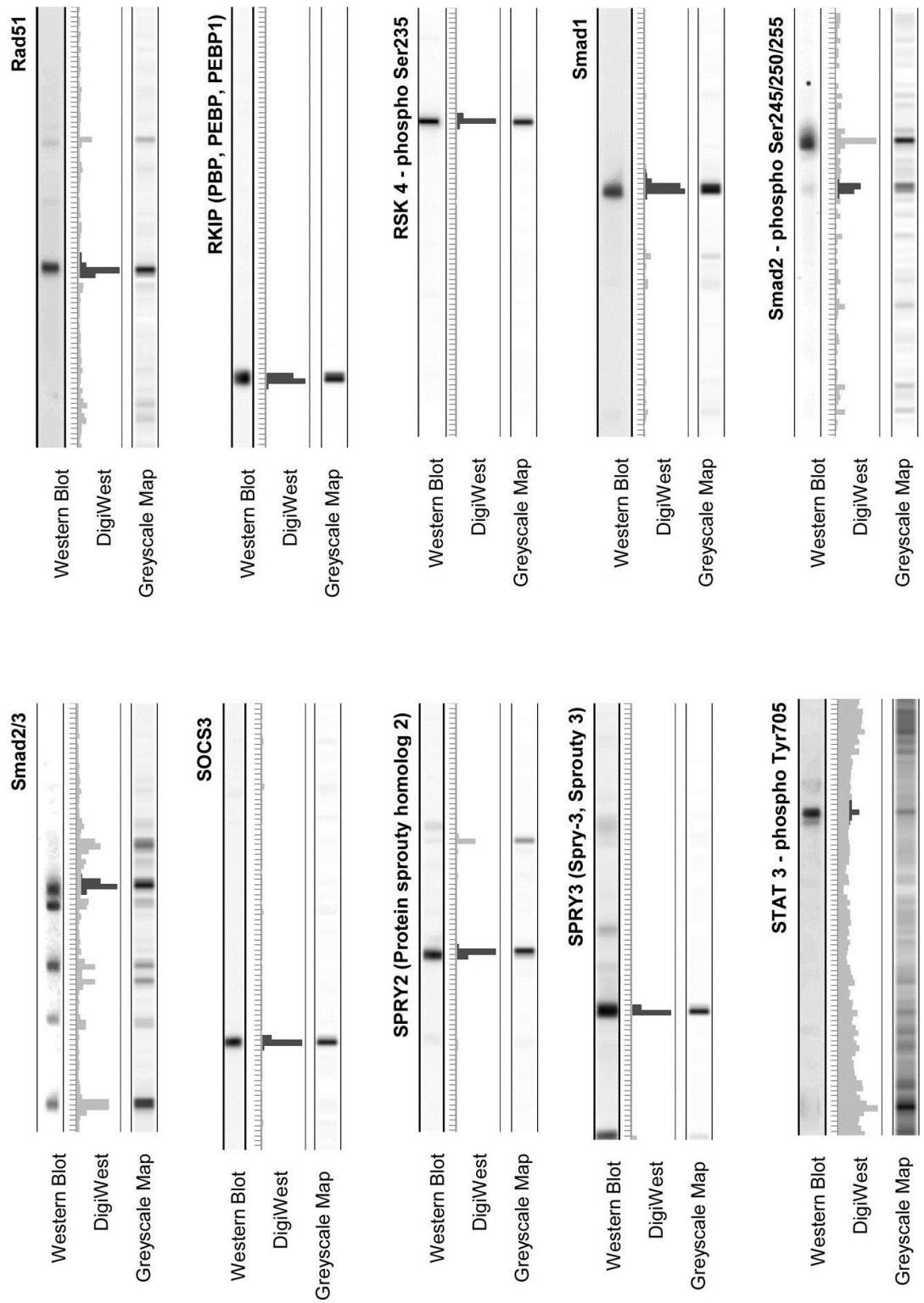
Rad51
Western Blot
DigiWest
Greyscale Map
RKIP (PBP, PEBP, PEBP1)
Western Blot
DigiWest
Greyscale Map
RSK 4 - phospho Ser235
Western Blot
DigiWest
Greyscale Map
Smad1
Western Blot
DigiWest
Greyscale Map
Smad2 - phospho Ser245/250/255
Western Blot
DigiWest
Greyscale Map
Smad2/3
Western Blot
DigiWest
Greyscale Map
SOCS3
Western Blot
DigiWest
Greyscale Map
SPRY2 (Protein sprouty homolog 2)
Western Blot
DigiWest
Greyscale Map
SPRY3 (Spry-3, Sprouty 3)
Western Blot
DigiWest
Greyscale Map
STAT 3 - phospho Tyr705
Western Blot
DigiWest
Greyscale Map

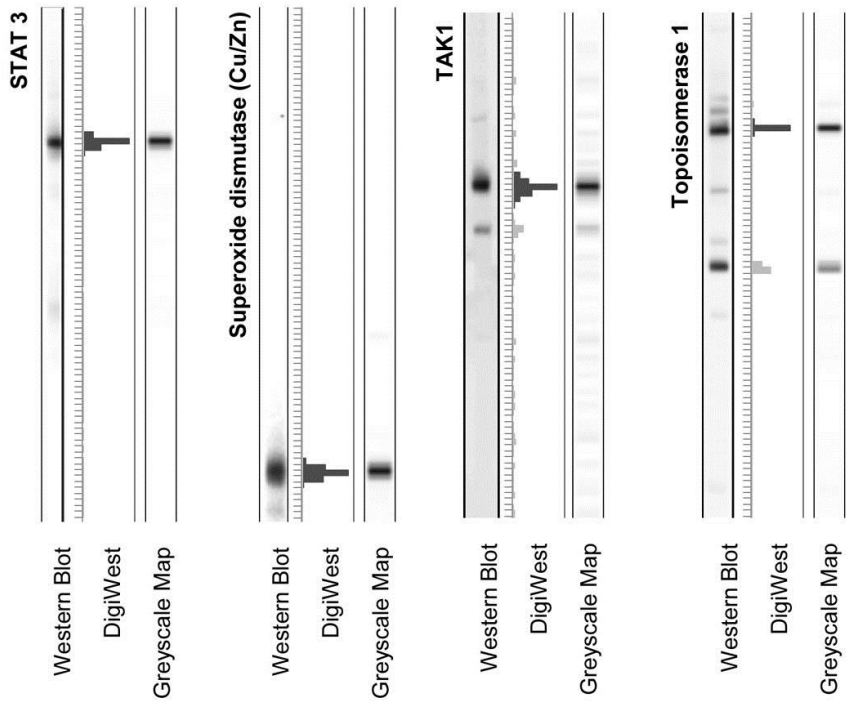

12.2 Appendix 2: GST-ERK2 spike-in complete experiment

This appendix is part of the experiment shown section 3.5.3. The figure in the appendix shows all replicates from the spike-in experiment including the technical replicates and the repeated measurements. The table shows the quantified signal from the DigiWest measurements (in [AFI], relative fluorescence units) and from quantification of the Western-Blot also in relative fluorescence units.

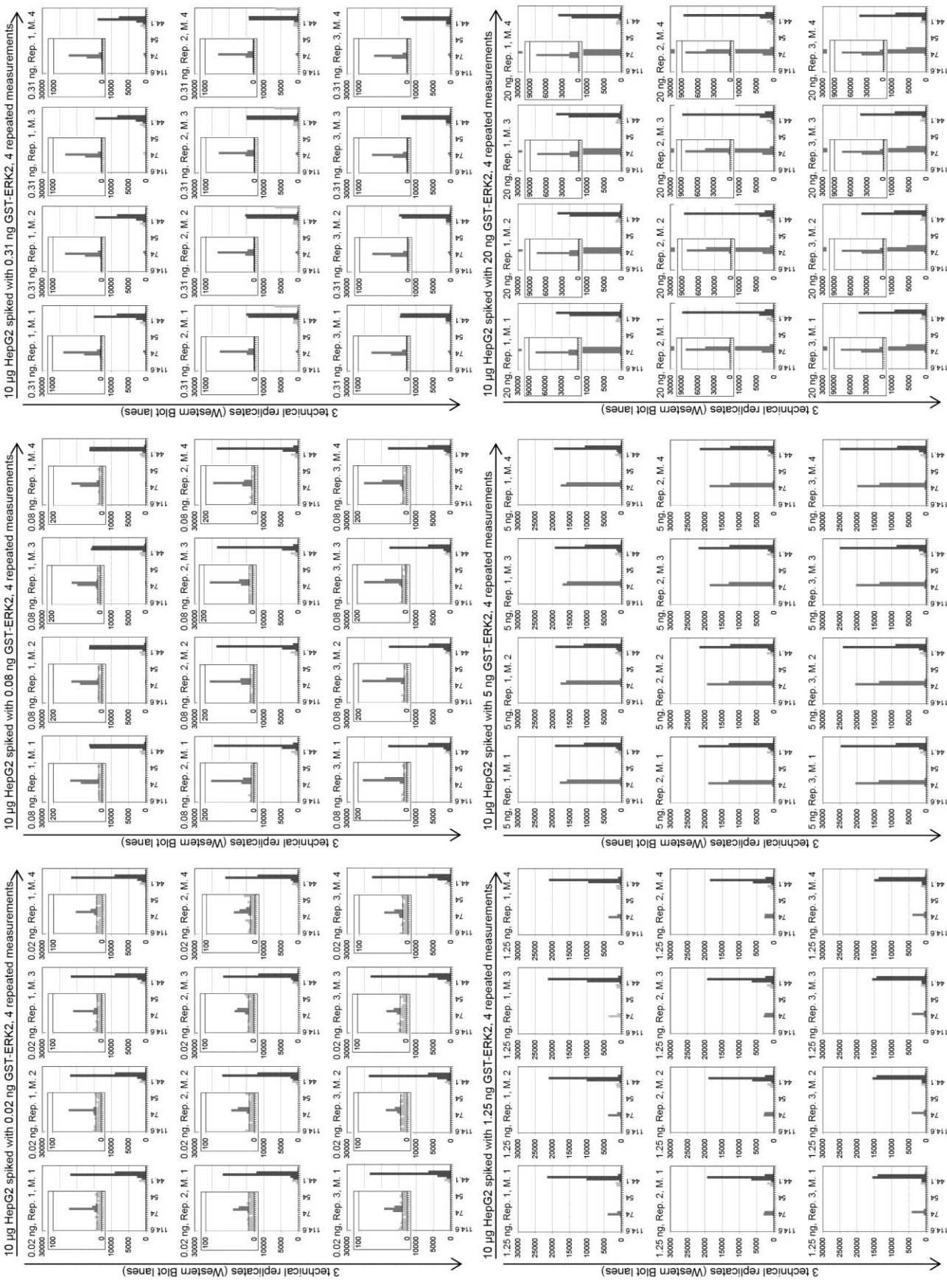
10 µg HepG2 spiked with 0.31 ng GST-ERK2, 4 repeated measurements
10 µg HepG2 spiked with 20 ng GST-ERK2, 4 repeated measurements
10 µg HepG2 spiked with 0.08 ng GST-ERK2, 4 repeated measurements
10 µg HepG2 spiked with 5 ng GST-ERK2, 4 repeated measurements
10 µg HepG2 spiked with 0.02 ng GST-ERK2, 4 repeated measurements
10 µg HepG2 spiked with 1.25 ng GST-ERK2, 4 repeated measurements
3 technical replicates (Western Blot lanes)

DigiWest

GST-ERK2 quantification
(Spike-in per 10 µg HepG2 Lysate, relative signal)

		Replicate 1	Replicate 2	Replicate 3	Mean	CV (%)
20 ng	Meas. 1	111610	132187	123061		
	Meas. 2	110545	131069	121013	121546	7.58
	Meas. 3	109539	133063	121319		
	Meas. 4	110796	132258	122093		
5 ng	Meas. 1	34446	32902	35241		
	Meas. 2	34452	33242	35176	33923	3.15
	Meas. 3	33635	32368	34849		
	Meas. 4	34339	32063	34365		
1.25 ng	Meas. 1	5458	5860	5568		
	Meas. 2	5339	5771	5471	5469	4.37
	Meas. 3	5212	5727	5450		
	Meas. 4	5095	5503	5178		
0.31 ng	Meas. 1	1208	993	1118		
	Meas. 2	1159	1051	1159	1097	6.02
	Meas. 3	1149	1046	1117		
	Meas. 4	1074	1006	1086		
0.08 ng	Meas. 1	217	241	270		
	Meas. 2	215	275	260	249	10.91
	Meas. 3	228	252	264		
	Meas. 4	215	251	302		
0.02 ng	Meas. 1	85	60	73		
	Meas. 2	78	75	77	73	9.38
	Meas. 3	67	64	74		
	Meas. 4	73	71	79		

Intrinsic ERK2
(in 10 µg HepG2 lysate, relative signal)

		Replicate 1	Replicate 2	Replicate 3	Mean	CV (%)
20 ng	Meas. 1	34953	33795	29330		
	Meas. 2	34518	33194	28654	32399	9.57
	Meas. 3	35208	33441	28729		
	Meas. 4	33745	33003	30158		
5 ng	Meas. 1	32769	37621	35915		
	Meas. 2	32763	36971	35567		
	Meas. 3	32522	37395	36033		
	Meas. 4	32608	36794	35699		
1.25 ng	Meas. 1	33006	29025	32337		
	Meas. 2	32512	28286	32558		
	Meas. 3	32573	28731	32674		
	Meas. 4	31866	27581	31418		
0.31 ng	Meas. 1	27349	31321	32156		
	Meas. 2	26813	32022	31902		
	Meas. 3	26737	31581	31398		
	Meas. 4	25480	30164	30841		
0.08 ng	Meas. 1	33943	31263	27490		
	Meas. 2	34069	30510	27039		
	Meas. 3	32726	30317	27053		
	Meas. 4	33933	30173	27490		
0.02 ng	Meas. 1	34688	37989	34494		
	Meas. 2	34682	37824	34829		
	Meas. 3	34465	37132	34060		
	Meas. 4	34419	36704	33692		

Western-Blot on Licor Odyssey

GST-ERK2 quantification
(Spike-in per 10 µg HepG2 Lysate, relative signal)

	Replicate 1	Replicate 2	Replicate 3	Mean	CV%
20 ng	318473100	329781002		324127051	NA
5 ng	135073639	134463994		134768817	NA
1.25 ng	36316470	36196382		36256426	NA
0.31 ng	8911814	9002800	9625102	9179905	4.23
0.08 ng	2586263	2532097	2636531	2584964	2.02
0.02 ng	1108895	1177614	924245	1070252	12.24

Intrinsic ERK2 (in 10 µg HepG2 lysate)
(in 10 µg HepG2 lysate, relative signal)

	Replicate 1	Replicate 2	Replicate 3	Mean	CV%
20 ng	106277100	107386932			
5 ng	108356255	109254315		116739348	6.58
1.25 ng	108724000	109124584			
0.31 ng	115500031	121316792	124221951		
0.08 ng	125092496	122582478	119270453		
0.02 ng	123804788	126355252	123822790		

12.3 Appendix 3: Data from the mouse liver LCM experiment

This table contains all DigiWest data from the Mouse liver LCM experiment. All analytes which gave analyzable signal at the correct molecular weight are contained. Data are given in [AFI], normalized on total protein amount (streptavidin-PE). ‘GS+’ is the proximal pericentral zone and ‘GS-‘ is the proximal periportal zone. The numbers behind the time-points represent the animal identifiers.

	Control GS+				Control GS-				24 h TCP GS+				24 h TCP GS-			
Analyte	**Ctrl 28 GS+**	**Ctrl 29 GS+**	**Ctrl 30 GS+**	**Ctrl 31 GS+**	**Ctrl 28 GS-**	**Ctrl 29 GS-**	**Ctrl 30 GS-**	**Ctrl 31 GS-**	**24h 50 GS+**	**24h 52 GS+**	**24h 53 GS+**	**24h 55 GS+**	**24h 50 GS-**	**24h 52 GS-**	**24h 53 GS-**	**24h 55 GS-**
ADAM12	160	200	187	204	149	312	193	180	127	155	88	99	204	323	127	185
AHR (Aryl Hydrocarbon Receptor)	849	1773	2029	1859	1721	2485	1298	1679	2092	2171		1583	2037	2667	1423	2216
Akt	914	1260	986	1016	792	1048	879	873	972	1112	968	993	849	875	791	1021
Akt - pT308		102	314	103	122	125	155	96	3510	803	1511	521	971	59	649	446
AMPK alpha	150	73	53	72	222	161	152	169	49	72	147	135	184	222	261	367
AMPK alpha - pT172	2010	2272	2949	2540	3791	4432	4859	3770	1710	1920	1402	1678	3734	4324	3307	3697
A-Raf	278	322	187	152	264	172	203	189	156	198	328	333	204	231	222	262
ASL (argininosuccinate lyase)	3344	7190	7813	7676	9454	25820	22335	25167	6867	7988	2128	2335	18989	23574	7059	7736
Bax	48	56		41	45	51	41	59	71	63	79	100	49	42		
beta-Actin	67618	86022	40613	80899	85426	104922	41985	94533	76090	95594	63030	104972	91844	102378	93273	107177
beta-Catenin	7454	7160	9197	5682	9525	8290	11864	6480	4805	4705	7808	7523	6660	7475	10733	10938
beta-Catenin - p S552	1955	1949	2505	1363	2681	2409	3286	1913	1035	994	1123	1223	1656	1803	1831	2164
beta-Catenin - p S675	1309	1409	1773	1100	1639	1515	2282	1174	845	894	1154	1157	1118	1308	1397	1533
beta-Catenin (non-pS33/37/T41 - active)	90	94	74	84	203	150	111	63	78	67	111	119	88	131	175	214
C/EBP alpha - p30	1631	1803	2109	1584	2120	2423	2304	2033	1252	1041	1440	1296	1417	1317	2115	2471
C/EBP alpha - p42	1741	1848	1789	1827	2056	2017	1921	2080	1239	916	1645	1568	1534	1497	2682	2804
C/EBP alpha total	3372	3651	3898	3411	4176	4440	4224	4112	2491	1957	3085	2864	2951	2813	4798	5274
Caseinkinase 1 alpha	133	157	87	153	203	150	111	211	160	146	240	195	130	180	222	206
Caseinkinase 2 alpha	399	403	289	438	425	424	360	334	405	415	563	608	415	416	521	532
Catenin gamma	60	51	64	33	114	105	87	56	137	48	45	55	52	67	127	144
CDKN2B (p15 INK4B, CDN2B, MTS2)	687	1594	1283	2139	589	1567	1013	1699	1589	1974	418	421	1729	1487	473	570
c-Jun		40	30		110	108	67	91	99	115	150	169	128	145	156	152
c-myc	449	607	379	317	200	155	194	136	706	771	566	655	216	244	196	152
COX1	1541	1676	2485	1940	1262	1464	1462	1174	1221	1461	1100	1310	766	899	547	624
CREB	147	168	170	233	216	193	121	161	165	175	247	231	208	202	258	234
CREB - pS133	329	325	386	317	398	471	392	499	378	312	312	495	364	470	596	611
Cyclin A					1263	1081	1157	1073					1094	1211	1935	1680
Cyp2B	5469	3363	33843	15550	7024	5248	35145	14024	37549	39485	53778	47573	44569	53022	60171	72358
Cyp2C (Cyp2C8)	82667	62324	55550	41347	34816	34273	23910	31632	97947	100953	148538	130381	97284	103105	117129	136219
Cyp2E (Cyp2E1)	106574	74028	81468	59633	2787	1090	4007	1311	83711	82150	138079	128454	2926	2834	2658	3061
Cyp3A (Cyp3a4 3a1 3a11)	62903	45965	21853	12647	46661	15985	6598	1611	241864	234245	336431	270103	111524	115119	117181	103546
DKK1	649	536	589	496	870	502	506	472	533	414	560	949	560	482	607	1037
DPP3 (Dipeptidyl-peptidase 3)	81	91	86	81			41	29	149	151	146	174	33	29		
DUSP4	3170	2111	2518	2548	12651	11653	10576	12129	2852	1649	2346	2910	11029	11578	16102	18752
E2F4	78516	65830	60894	38792	120194	96330	105460	72512	27885	33423	38513	54721	57463	73011	86322	133271
E-Cadherin					7290	7381	7740	5953					7760	8880	7552	8280
E-Cadherin - pS838/S840					14387	12464	15311	10313					13529	16817	14559	15146
EEF2	1768	2835	3175	2305	2917	2333	2569	1590	2410	2726	1426	2281	2139	2902	1517	1940
eEF2 pT56	21795	24216	31355	19693	25822	19026	27305	15163	21639	23723	22226	26555	19059	22830	21458	22946
EGR1	81	98	147	87	55	64	97	66	100	132	142	103	67	61	72	59
eIF2 alpha	9597	11969	8382	10914	9482	11589	8792	10911	12360	12762	12332	12683	11407	11753	11662	11568
eIF2 alpha - pS51	85	201	307	297	89	156	203	214	443	286	245	375	209	160	167	209
eIF4E	1325	1558	1057	1264	1114	1619	1204	1290	1816	2173	2865	1924	1631	1641	2027	1698
Erk1/2 - ERK1	418	530	484	547	701	697	705	522	447	495	530	618	606	711	697	842
Erk1/2 - ERK2	979	1081	872	935	1051	1219	840	913	912	993	1085	935	833	965	967	1032
Erk1/2 - pT202/Y204 - ERK1	395	159	257	219	419	366	351	278	458	424	437	594	311	437	776	481
Erk1/2 - pT202/Y204 - ERK2	755	425	650	616	793	903	334	520	1080	819	1086	1328	580	923	1309	992
Erk1/2 - pT202/Y204 - total	1150	584	907	836	1213	1270	685	798	1538	1243	1524	1922	891	1360	2084	1473
Erk1/2 - total	1398	1612	1356	1482	1752	1916	1544	1436	1359	1488	1615	1553	1439	1676	1662	1874
Ets-1	322	309	403	333	299	307	254	226	271	373	552	431	227	334	192	332
Ezh2	70	91	77	99	69	60	74	60	78	125	74	128	127	137	134	84
Ezrin / Radixin / Moesin	78	120	61	70	122	103	108	82	73	82	91	90	83	97	117	93
Ezrin / Radixin / Moesin - pT567/564/558	1034	432	1466	381	538	284	969	279	412	446	808	806	287	325	472	518
FAK	140	116	200	57	191	160	358	107	66	87	54	142	129	163	212	203
FAK - pY397	131	116	333	84	145	147	421	119		126		89	152	143		165
FDPS - Isoform 1	591	1305	983	1363	857	1952	1183	2220	977	1641	744	798	1527	2532	779	978
FDPS - Isoform 2	346	358	664	495	688	656	841	848	284	431	250	343	565	593	491	555
FDPS - total	938	1663	1649	1857	1545	2608	2026	3068	1262	2072	992	1142	2092	3125	1271	1534
FTCD	113	88	149	138	1332	1197	1547	1228	117	139	103	130	835	1113	984	1153
Fyn	509	535	552	581	588	684	686	525	386	553	451	373	431	507	521	510
Gab1	613	612	855	734	647	649	1022	495	498	484	447	538	775	888	667	554
Gadd45 beta	105	342	181	488	36	221	103	179	260	312	176	184	101	214	38	43
GAPDH	33	33			63	68	73	71	50	41			68	79	42	70
GAS-2	102	100	123	74	1320	2283	2045	1874	282	293	332	263	3599	4036	3524	3636
GLS2 (Glutaminase 2)		37	56	31	121	176	199	269					119	178	211	205
GLUT-1	579	560	389	298	72	52	62	60	295	289	773	545	211	253	361	463
Glutaminsynthetase	916859	890495	1045050	953850	5316	2746	2830	2715	758972	813109	828246	971226	1575	1557	1687	1142
GSK3 alpha/beta - pS21/9 - alpha	105	89	119	92	172	217	135	151	139	210	164	108	194	247	133	151
GSK3 alpha/beta - pS21/9 - beta	199	138	187	102	204	167	188	156	208	278	193	167	150	190	149	180
GSK3 alpha/beta - pS21/9 - total	304	225	306	195	376	384	323	306	346	488	357	274	343	439	280	330
GSK3 beta	2747	2683	2651	2330	2244	2275	1846	2038	2126	1897	2094	2523	1787	1841	1812	2098
GSK3 beta - pS9	322	212	247	145	294	331	225	170	314	399	252	248	223	323	255	229
HAL (histidine ammonia lyase)	124	212	87	147	710	1173	1083	1444	148	145	95	175	767	1051	455	547
Histon Deacetylase 1 (HDAC1)	53	52		56	36	61	49	78	45	57	79	80	52	70		62
Histon Deacetylase 3 (HDAC3)	41	43		26		36		49	37		57	50	39		68	51
Histon H3 - acetyl K9	7212	6091	6527	6489	9078	7952	9226	8617	4763	6787	5441	5633	7263	7178	6923	8341
HNF-4 - pS313	406	286	372	482	1415	1051	1008	1135	252	275	330	355	946	1193	1511	1221
HNF-4 alpha	710	575	404	418	569	720	465	525	553	561	164	663	403	722	967	552
HSP70	62	79	117	88	30	32	33	24	97	131	170	138	24	39	49	34
IDH1 ([NADP] cytoplasmic)	2664	4384	3975	4439	1657	2706	2288	2393	4994	5234	2775	2778	2323	2769	1566	1959
IDH2	3090	2516	1430	2090	2777	2772	3098	2893	2439	2707	5346	4719	2932	3921	4128	4242
Ihh (indian Hedgehog)	47	22	24	31	67	51	33	45	778	813	831	883	1211	1482	1113	1544
IkappaB alpha	41	70		40	72	66	39	65	75	36	47	125	59	38	74	103

	Control GS+				Control GS-				24 h TCP GS+				24 h TCP GS-			
ILK1	575	476	662	422	594	602	966	615	395	425	510	494	432	528	648	526
ILK1 - pS246	109238	97912	101469	113290	248451	230855	218883	222680	75649	91168	96072	104791	215329	240440	292952	279271
ILK1 - pThr173	75237	68261	69468	79468	179774	161140	158305	157565	49871	59595	60103	68849	157832	165983	215907	206005
INSL4	1321	1220	1360	1716	466	509	1013	595	1181	1435	1869	1712	978	888		1581
IRAK4 - Isoform 1	456	371	489	430	551	565	539	526	366	383	488	510	372	467	723	694
IRAK4 - p T345/S346 - Isoform 2	85	120	59	86	90	107	59	90	108	124	150	135	80	90	84	92
JNK/SAPK (p46)	135	124	89	146	77	177	150	94	128	143		178	126	113	152	154
JNK/SAPK (p54)	156	273	180	144	209	340	203	214	262	146	315	150	210	158	271	317
JNK/SAPK - total	290	396	269	290	287	516	354	307	390	288		330	336	272	423	471
KRAS GTPase	157	105	121	132	91	131	105	100	92	124	132	134	76	93	85	92
KSR1 - pS392	501	312	826	444	787	596	1200	784	529	439	878	802	564	584	1076	1198
LCK - pY505	1748	2009	2226	1787	1149	1332	1505	1266	1543	1765	1396	1424	1021	1122	1039	1019
MCM2	81	114	114	49	92	126	155	65	280	393	152	193	444	521	286	312
MEK1/2 - p Ser217/221	98	70	49	143	33	36	39	52	95	105	112	80	68	56	69	40
N-Cadherin	3467	3560	5323	3880	1327	1819	2618	1483	3687	4259	1609	2504	1474	1864	977	1007
NF-κB p100/p52 - p100		166	71	53	200	332	372	247					139	246	117	85
NF-κB p105/p50 - p50	1624	1599	1157	1406	1404	1382	1455	1359	1279	1370	1253	1432	1333	1535	1857	1839
NF-κB p65	125	158	159	131	144	133	169	155	146	198	152	115	177	171	127	135
Numb	1061	1279	1326	1086	1005	1487	1859	1053	792	943	1121	1006	950	1269	1457	1387
p38/MAPK	129	223	191	211	146	194	143	132	197	144	139	127	130	133	102	107
p38/MAPK - pT180/Y182	225	276	429	368	146	314	240	296	214	186	186	123	150	203	154	206
p53	269	212	111	112	506	422	547	256	85	145	200	233	272	425	556	783
p70 S6 kinase	269	415	366	365	239	328	285	313	337	450	337	378	309	314	258	308
PAK 1/2 - p S144/S141	90	100	76	147	466	553	319	496	60	99	139	93	480	761	713	675
PAK 4	178	154	239	119	206	193	243	114	100	135	118	160	113	192	176	258
PAK 4/5/6 - pS474/602/560	96	96	154	88	136	121	132	56	67	92	78	120	80	76	104	102
PARP	6586	5860	4920	3418	10263	9144	7872	6628	2139	2528	2205	3870	4388	5047	4620	9156
PDGF Receptor beta	56	69	90	57	251	186	223	107	61	47		35	168	203	231	315
PDK1	123	181	87	128	176	248	173	250	408	222	207	165	277	273	202	205
PGC1 alpha - pS571	665	440	627	180	1987	1473	1625	614	377	1017	340	519	1537	2436	1436	1302
PI3-kinase p85	164	181	239	155	150	146	200	91	132	173	156	224	105	131	120	126
PI3-kinase p85 alpha	33	43	51	26	26	29	50	29	27	36	41	50		32		55
PKA C alpha/beta - pT197	2915	2889	2611	2390	2215	2668	2818	2482	2805	2962	2335	2243	2135	2451	2366	2258
PKA C alpha/beta/gamma - pT197	418	518	549	313	269	331	386	301	329	373	214	247	287	313	143	192
PKA Substrate - pSer/Thr - band at 100 kDa	245	276	394	188	359	246	322	141	190	211	159	321	231	333	208	304
PKA Substrate - pSer/Thr - band at 35 kDa	83	70	54	63	75	76		48	87	67	116	99	70	50		80
PKC (pan) - pS660	355	452	397	332	645	796	782	492	272	368	292	307	539	590	628	647
PKC alpha/beta II - pT638/641	1116	1228	1155	812	2507	2288	2689	1920	660	805	863	822	1829	1824	2326	2091
PKG-1	50	116	76	63	67	157	187	106	53	71		78	82	99	149	212
PP1 alpha		1094	646	937	746	1750	1256	1650	636	788	1525		1620	2047		
PP1 alpha - pT320	250	306	313	274	320	391	270	229	346	318	417	385	339	337	315	440
PP1 gamma	2353	1594		1453	11586	9409	7015	7169	1463	1752	1297	1519	12549	14062	11308	12801
PP2A C - pY307	290	280	320	197	1392	2423	4352	2305	3396	19335	30585	3805	6964	21692	25473	2782
PPAR gamma	28486	22669	25205	18114	53638	45699	47554	41718	7577	11264	9805	15680	32692	42480	40225	49830
PPAR gamma - pS112	1201	882	1030	744	1843	1566	1919	1461	262	428	359	614	1006	1309	1284	1752
PTCH2 (main band)	176	479	716	1007					588	679	432	513				
PTEN	855	774	639	671	852	722	724	616	725	711	753	639	601	738	691	764
PTEN - pS380	330	358	333	272	386	341	439	308	312	312	380	294	338	365	341	302
PTPN7 (LC-PTP, HEPTP) - 40 kDa Isoform 1	738	730	540	553	1446	1378	1218	1255	501	762	371	540	821	1284	1010	1164
PTPN7 (LC-PTP, HEPTP) - 45 kDa Isoform 2	511	324	409	458	265	269	194	136	1058	1267	1847	1434	101	295	139	403
PTPN7 (LC-PTP, HEPTP) - 52 kDa Isoform 3	858	914	1185	634	1824	1917	1884	1961	814	924	1024	1168	1577	2138	1307	1534
RACK1	20337	28321	15091	24752	19389	27268	15380	23394	25186	27333	23586	22868	25980	26146	23383	23762
RAD23B - Isoform 1	238			261	702	756	478	838	211	269		292	731	890	732	938
RAD23B - Isoform 1+2 (or RAD23A/B)	1109			1880	989	1474	753	1674	2718	2702		2895	1410	1780	1188	1583
RAD23B (hHR23b) - Isoform 2 (or RAD23A)	872	1077	1046	1619	285	718	275	835	2506	2433	3054	2603	680	890	456	644
RBPSUH	384	418	380	359	367	471	430	385	332	392	400	340	377	437	449	449
RSK 1/2/3	56	50	54	33	86	72	87	30				54	43	51	53	
RSK 3 - pT353/356	98	158	174	139	234	290	336	197	92	120	121	209	149	211	212	201
RXR alpha - 45 kDa (add. band, or RXR beta)	1036	1012	983	1129	1218	1362	1108	1043	1027	1189	1596	1375	1289	1233	1704	1802
RXR alpha - 50 kDa (main band)	362	246	286	114	193	73	164	172	1100	896	1099	1173	1231	1271	1166	1658
RXR alpha - 50+45 kDa or RXR alpha/beta	1398	1259	1267	1243	1412	1435	1272	1215	2127	2085	2695	2546	2520	2503	2869	3459
RPS6	325	234	90	312	354	442	264	399	466	566	1153	836	522	690	1075	765
RPS6 - pS240/244	1666	1577	1412	911	4039	7308	7503	6300	8507	22732	31127	9820	13297	25907	25270	7328
SDS (serine dehydratase)	345	421	537	784	4736	7171	8751	9344	524	544	285	332	6552	7016	5072	5582
SerpinE1 / PAI1	1451	1307	2388	1775	1533	1926	1251	1283	1722	1764	739	1189	1511	2509	945	1246
SHP-2	221	406	383	392	200	330	320	278	344	374	167	243	277	317	143	147
Smad1	109	95		88	103	108	126	63	141	98	242	187	112	90	182	231
Smad3	37	62	87	62	77	71	123	72	56	96	48	39	68	78	55	93
SPRED2	33	54	47	51		30	65	43	48	50	62	63	29	33	51	
SPRY2 (Protein sprouty homolog 2)	1011	1629	722	1463	230	693		947	1750	1413	988	1099	786	838	430	712
SPRY3 (Sprouty 3)	68224	61318	53529	60061	86220	87764	65971	85132	59008	60332	80289	70731	86876	81509	114302	113846
Src	3867	2538	3828	2785	4179	3664	4713	3147	1854	2496	4348	4371	2639	3214	4625	6009
Src - pY527	2233	3549	3627	3225	2293	4257	3549	3292	2762	3273	1823	2014	2573	3416	1697	1804
Src Family - pY416	69	204	337	229	100	232	415	228	183	152	147	147	173	211	128	179
STAT 1	1281	2000	2082	1555	1443	1753	2220	1715	1731	1908	1540	1796	1616	2035	1597	1881
STAT 3	1836	2429	2446	2003	2091	2555	2686	2111	2232	2298	2104	2296	2406	2461	2338	2470
STAT 3 - pS727	108	142	151	128	209	171	158	133	168	172	111	152	162	211	241	121
Strep	224904	224904	224904	224904	224904	224904	224904	224904	224904	224904	224904	224904	224904	224904	224904	224904
Superoxiddismutase (Cu/Zn)	1119	1387	1872	1658	632	880	922	851	1688	1744	1334	1326	985	775	714	853
TBK1/NAK - pS172	36	55	56	39	68	83	108	56	32	40	74	74	50	56	95	85
TCF4	59	116	70	127		56		56	104	96	41	54	47	49		
Topoisomerase 1	2146	1966	3922	2279	3550	1908	3523	1930	2092	2399	2036	3011	2192	3036	2335	2647
VASP - pS239	84	74	129	89	125	166	202	149	44	29	60	50	101	109	176	136
Wnt3A	5883	12445	6379	14718	13582	35229	7732	20800	11059	10434	2526	4212	18050	21725	4912	6786

	48 h TCP GS+				48 h TCP GS-				72 h TCP GS+				72 h TCP GS-			
Analyte	48h 11 GS+	48h 19 GS+	48h 26 GS+	48h 27 GS+	48h 11 GS-	48h 19 GS-	48h 26 GS-	48h 27 GS-	72h 28 GS+	72h 29 GS+	72h 41 GS+	72h 51 GS+	72h 28 GS-	72h 29 GS-	72h 41 GS-	72h 51 GS-
ADAM12	55	69	62	77	90	144	72	148	45	47	41	49	143	94	123	120
AHR (Aryl Hydrocarbon Receptor)	760	1042	1474	1280	1216	1610	868	1579	996	1519	1653	1203	1081	899	1960	2427
Akt	801	809	711	707	743	675	695	654	521	646	693	842	522	631	644	763
Akt - pT308	41	86	74	43	152	44	44	255	196	458	435	286	116	40	64	353
AMPK alpha	136	92	108	86	351	284	330	309	93	132	123	83	283	149	212	152
AMPK alpha - pT172	1612	1303	1156	1266	4102	3318	3240	3342	977	958	1307	1228	2639	2002	3107	2656
A-Raf	323	179	343	337	317	250	209	321	303	276	253	231	280	79	289	268
ASL (argininosuccinate lyase)	3453	3255	1472	1209	11421	13262	5000	3927	1104	3293	1498	3239	3693	12760	5168	13082
Bax	65	87	75	55	43	37	97	68	36	52	52	86	33	90	65	61
beta-Actin	55791	72392	50476	77788	76354	86223	64960	91420	50044	63356	49686	68256	83795	78288	83226	82513
beta-Catenin	3658	4545	5475	5439	5859	5654	9926	8128	4613	3364	4944	3475	6856	5379	7731	5071
beta-Catenin - p S552	783	1100	1011	1197	1592	1431	1914	2233	1025	921	1416	921	2027	1390	2248	1500
beta-Catenin - p S675	637	950	962	832	933	1069	1436	1193	734	607	884	694	1105	860	1131	891
beta-Catenin (non-pS33/37/T41 - active)	72	122	176	144	158	143	325	303	95	62	106	62	194	157	182	107
C/EBP alpha - p30	646	828	676	829	991	1098	1172	1305	696	368	632	673	1298	786	1305	1106
C/EBP alpha - p42	801	988	842	836	1382	1291	1346	1627	744	478	719	683	1275	1130	1442	1413
C/EBP alpha total	1446	1817	1518	1665	2373	2389	2518	2933	1440	846	1351	1356	2573	1915	2746	2520
Caseinkinase 1 alpha	143	119	190	235	175	174	264	227	139	102	157	78	139	176	205	75
Caseinkinase 2 alpha	378	451	511	452	441	401	475	490	382	309	350	409	392	438	380	419
Catenin gamma			52	26	64	42	65	71	33		46		71	54	70	44
CDKN2B (p15 INK4B, CDN2B, MTS2)	524	423	303	291	678	682	331	253	294	739	393	750	367	843	429	898
c-Jun	89	83	78	136	114	153	165	207	86	102	150	137	155	143	114	224
c-myc	716	941	913	1212	195	165	142	230	1258	917	2087	1324	190	191	177	199
COX1	1107	990	905	1033	536	774	460	565	721	920	952	1012	468	455	512	727
CREB	106	57	80	90	149	107	112	134	43	130	110	107	97	95	130	186
CREB - pS133	163	149	183	176	298	271	385	347	143	171	119	200	349	241	218	361
Cyclin A					768	745	1189	1249					1068	561	1113	576
Cyp2B	69072	64213	87816	84103	77795	73393	121628	109187	88943	53534	114592	86193	117988	93518	130169	108642
Cyp2C (Cyp2C8)	127307	98770	163813	153290	145618	148590	207161	179981	141342	89053	192258	129508	156727	116969	208648	144552
Cyp2E (Cyp2E1)	95339	76701	128428	124938	4950	4521	5625	5282	86846	50947	117996	69450	5661	5212	6227	5206
Cyp3A (Cyp3a4 3a1 3a11)	271271	322760	411778	352500	174831	146611	208872	228655	344375	259451	461932	332693	192524	177842	166575	171910
DKK1		318		332		312	462	562	344		360		473			367
DPP3 (Dipeptidyl-peptidase 3)	240	197	199	318		37	42	40	335	185	284	174	90	66	61	58
DUSP4	1051	1065	1136	1772	8025	9503	10123	12907	921	463	1273	750	9072	4170	12374	9565
E2F4	14129	15794	17060	40032	47863	48902	56912	86776	18678	22903	16303	17820	64357	56503	55499	46455
E-Cadherin					6897	7532	8405	7055					5926	6761	5856	7128
E-Cadherin - pS838/S840					14269	12846	16323	13956					11757	9534	11245	14514
EEF2	1527	1632	1359	1205	1676	1771	2026	1844	1037	1535	1391	1463	1242	1589	1649	1762
eEF2 pT56	17749	18559	18645	15053	19734	16817	23042	17733	12761	17770	18167	18057	14954	16547	17535	18052
EGR1	129	115	122	192	53	94	83	148	151	113	253	212	108	71	145	106
eIF2 alpha	10446	8674	8549	8698	9228	9945	8363	7617	7639	8451	9107	9552	7247	9506	9256	10030
eIF2 alpha - pS51	553	482	161	138	187	191	83	98	255	344	360	753	89	175	170	314
eIF4E	1154	1230	1454	1578	1082	1030	1448	1132	1361	1340	1796	1995	1193	1303	1484	1477
Erk1/2 - ERK1	509	517	469	611	725	645	798	815	347	363	563	389	484	678	572	645
Erk1/2 - ERK2	957	817	775	831	905	904	1107	942	664	734	925	917	733	996	836	705
Erk1/2 - pT202/Y204 - ERK1	197	205	391	225	245	251	588	254	239	235	198	320	418	208	169	290
Erk1/2 - pT202/Y204 - ERK2	465	482	738	246	633	510	1500	481	650	342	413	533	751	341	375	425
Erk1/2 - pT202/Y204 - total	662	686	1129	472	878	761	2088	736	889	578	611	852	1170	548	544	717
Erk1/2 - total	1466	1335	1244	1443	1630	1549	1906	1757	1011	1098	1489	1306	1217	1676	1408	1350
Ets-1	323	334	193	201	247	208	208	208	241	213	297	218	154	240	273	236
Ezh2	77	96	117	84	91	129	167	174	81	102	124	61	115	126	78	121
Ezrin / Radixin / Moesin	73	69	80	114	67	68	82	91	95	54	94	52	89	52	131	82
Ezrin / Radixin / Moesin - pT567/564/558	199	236	923	418	115	138	354	194	457	160	495	160	222	80	236	131
FAK	104	78	120	80	211	132	160	176	67	67	88	68	150	107	174	108
FAK - pY397	102			76	112		122	119		69	104		79		117	119
FDPS - Isoform 1	804	770	747	829	1109	1794	963	1474	986	892	1039	1305	1329	1050	2708	2199
FDPS - Isoform 2	161	249	147	259	334	373	277	364		209	196	280	273	345	434	576
FDPS - total	965	1020	894	1089	1443	2166	1242	1838		1101	1234	1585	1603	1395	3142	2774
FTCD	234	166	105	227	826	833	830	882	184	205	371	240	671	894	1028	802
Fyn	236	872		503	353	519	753	321	288	267	427	452		641	464	497
Gab1	397	251	241	371	581	628	421	719	297	195	323	292	701	218	1014	778
Gadd45 beta	207	253	86	93	72	141	37	56	76	189	103	256	30	136		72
GAPDH	44	42			89	76		39	39	37	32	61	57	62	71	55
GAS-2	280	324	205	312	3583	4261	2732	2800	263	240	363	287	2869	3348	3283	3521
GLS2 (Glutaminase 2)				35	149	173	239	221					128	87	163	129
GLUT-1	929	504	979	1133	757	877	1404	1419	1114	391	1532	674	1066	496	1676	628
Glutaminsynthetase	649542	648096	631175	606444	2100	1310	861	1536	470973	494718	554123	628302	906	1024	948	1304
GSK3 alpha/beta - pS21/9 - alpha	100	120	101	133	148	148	175	128	43	56	76	168	96	185	115	234
GSK3 alpha/beta - pS21/9 - beta	168	129	138	136	180	154	138	177	84	118	108	161	125	156	126	157
GSK3 alpha/beta - pS21/9 - total	268	249	239	269	328	302	313	306	126	174	184	329	222	342	241	392
GSK3 beta	2335	2106	2020	1777	2080	1793	1771	1478	1484	1489	1963	1734	1387	1717	1478	1501
GSK3 beta - pS9	240	161	176	186	225	199	253	233	123	148	173	286	171	202	159	170
HAL (histidine ammonia lyase)	109	113	69	69	413	568	280	289	98	97	56	78	291	380	353	519
Histon Deacetylase 1 (HDAC1)	41	54	69	39		73		60	31	37		32	29	36	29	
Histon Deacetylase 3 (HDAC3)	39	40	34	51	44	37	48	55	34	21			38	49	60	27
Histon H3 - acetyl K9	5308	3706	5671	3955	5729	7682	6829	6923	2710	3464	4910	4062	5380	5082	5136	6211
HNF-4 - pS313	122	327	170	250	613	735	965	1021	127	93	161	235	635	436	1066	732
HNF-4 alpha	176	971	294	419	144	336	460	212	177	151	261	438	138	683	500	480
HSP70	208	306	223	182	43	62	50	71	285	392	344	270	56	48	70	48
IDH1 ([NADP] cytoplasmic)	3147	3175	2335	2320	2035	2341	1515	1478	2190	3135	3168	3993	1362	2478	1895	2777
IDH2	3714	3106	4516	4875	3476	3070	4919	4867	3162	2279	3604	2651	3298	3337	3757	3100
Ihh (indian Hedgehog)	1564	1274	1951	2398	2345	2422	3657	3784	3117	1559	4134	2630	5062	3196	5439	3797
IkappaB alpha	63	40	68	37	79	53	89	101		35	30	59	34	60	40	

	48 h TCP GS+				48 h TCP GS-				72 h TCP GS+				72 h TCP GS-			
ILK1	388	301	403	462	432	426	561	590	337	296	472	367	479	402	587	422
ILK1 - pS246	49009	54734	62571	71206	148731	162566	212604	224854	43409	35246	50233	47981	172986	121837	211500	164734
ILK1 - pThr173	31323	34755	37710	43261	107916	119929	140982	153564	26521	20253	29521	28999	116751	80624	140888	108797
INSL4			967	928	670	368	946	921	409	1663	1186	780	396	714	856	653
IRAK4 - Isoform 1		349	239	369	305	260	407	606	228		443	262	349	230	446	361
IRAK4 - p T345/S346 - Isoform 2	107	105	109	110	96	111	95	61	80	111	61	136	65	117	74	118
JNK/SAPK (p46)	99	243	149	170	192	121	119	130	88	161	147		126	107	126	154
JNK/SAPK (p54)	188	163	316	200	312	185	247	176	145	163	213	137	153	188	210	268
JNK/SAPK - total	288	406	465	370	503	307	367	306	233	324	360		279	296	336	422
KRAS GTPase	101	98	61	122	71	58	107	97	78	71	83	65	89	69	77	70
KSR1 - pS392	327	329	485	517	568	403	690	955	362	285	416	372	488	493	618	500
LCK - pY505	1067	1207	849	969	843	929	676	713	590	743	804	1033	530	816	772	981
MCM2	382	243	423	379	568	365	746	627	253	424	349	417	445	613	341	569
MEK1/2 - p Ser217/221	79	107	87	33	46	43	42	26	49	65	72	71	32	47	30	29
N-Cadherin	1692	1487	1675	1275	751	710	790	453	994	1369	931	1243	432	765	472	834
NF-κB p100/p52 - p100		33		24	106	116	128	67			36		68	73	91	98
NF-κB p105/p50 - p50	1303	1110	1027	1114	1441	1244	1227	1289	775	819	919	1095	1018	1157	1069	1118
NF-κB p65	133	90	75	131	123	120	76	126	73	93	111	116	105	60	115	130
Numb	852	741	888	927	768	1153	714	1017	554	490	783	658	884	528	1262	889
p38/MAPK	144	141	82	74	149	115	68	56	70	93	89	122	61	116	73	90
p38/MAPK - pT180/Y182	439	981	1277	310	141	420	665	171	84	128	49	289	323	208	106	234
p53	89	470	374	235	188	283	875	517	99	141	196	191	227	526	369	333
p70 S6 kinase	386	371	270	324	269	354	287	234	282	314	320	349	225	201	225	247
PAK 1/2 - p S144/S141	52	69	50	57	198	302	381	541	26		49	40	306	157	451	188
PAK 4	140	240	405	575	107	160	171	449	149	342	76	41	241	336	110	250
PAK 4/5/6 - pS474/602/560	76	76	74	74	53	58	55	85	51	42	80	64	50		93	65
PARP	977	1135	879	2916	3006	3341	2718	5443	1322	1744	1378	1715	4058	3628	3802	3932
PDGF Receptor beta	38	64		74	144	163	370	422	55		63	27	263	145	155	92
PDK1	161	211			113	210	267		143	264	72	66	217	231	248	117
PGC1 alpha - pS571	397	260	372	367	1310	1470	1434	1113	211	324	204	302	789	1197	1176	1281
PI3-kinase p85	130	212	121	135	81	94	125	108	141	131	137	147	112	148	104	73
PI3-kinase p85 alpha		107	105	122		24		27	24		42	43		100		43
PKA C alpha/beta - pT197	2496	2843	2123	1685	2162	1953	1960	1579	1640	2188	2100	2038	1369	1886	1531	1713
PKA C alpha/beta/gamma - pT197	204	207	193	139	142	137	143	102	144	190	159	197	101	175	120	170
PKA Substrate - pSer/Thr - band at 100 kDa	194	203	230	142	255	230	283	216	133	185	186	183	197	204	171	205
PKA Substrate - pSer/Thr - band at 35 kDa	63	64	93	85		64	78	51	70	76	89	66	51	87	46	38
PKC (pan) - pS660	223	275	208	266	479	532	475	489	208	176	175	301	510	408	404	412
PKC alpha/beta II - pT638/641	652	736	650	796	1977	1628	1834	1699	473	421	610	712	1462	1261	1679	1539
PKG-1	50	113		114	65	109	95	81	29	31	40	34	60	112	60	116
PP1 alpha	471	488			996	832			446	432				978	306	688
PP1 alpha - pT320	333	190	257	250	230	304	331	241	172	212	282	198	243	241	203	238
PP1 gamma	906			830	8129	8835	10460	8328	802		947		9891	6670	13054	9186
PP2A C - pY307	208	282	1036	439	912	1040	2776	1352	768	624	938	12196	3288	3554	2479	12176
PPAR gamma	6330	6088	5616	11851	22733	27406	24647	41370	5076	5557	6499	6890	24570	20508	32539	25717
PPAR gamma - pS112	226	257	227	527	719	900	783	1285	227	270	305	271	788	784	939	898
PTCH2 (main band)	273	404	733	186					187	178	231	320				
PTEN	792	620	693	509	791	694	764	579	458	529	558	660	516	702	662	684
PTEN - pS380	386	331	332	276	381	346	354	253	238	208	278	344	205	328	294	313
PTPN7 (LC-PTP, HEPTP) - 40 kDa Isoform 1	141	189	211	229	755	826	794	854	187	146	177	252	732	482	952	690
PTPN7 (LC-PTP, HEPTP) - 45 kDa Isoform 2	2644	1469	3198	2899	637	534	755	897	2845	1390	3817	2355	956	772	1075	632
PTPN7 (LC-PTP, HEPTP) - 52 kDa Isoform 3	1010	1239	1720	2085	831	976	1023	1635	2093	908	3006	1410	1116	761	1449	1300
RACK1	16135	12320	14513	10746	15054	18161	16562	12681	10511	12784	12085	12718	11403	15681	13085	15407
RAD23B - Isoform 1	208			289	543	509	495	677	159		213		571	292	677	541
RAD23B - Isoform 1+2 (or RAD23A/B)	4778			4518	1734	1780	1598	1819	4953		6639		2016	1878	2180	2295
RAD23B (hHR23b) - Isoform 2 (or RAD23A)	4569	2656	4760	4228	1192	1271	1102	1142	4794	2467	6425	4107	1446	1586	1503	1754
RBPSUH	202	274	293	265	218	265	335	296	191	178	193	265	252	204	237	284
RSK 1/2/3	66			53	59	57	96	77	37		69	31	85	89	103	48
RSK 3 - pT353/356	43	84	48	74	92	129	150	112	49	65	112	112	101	103	106	117
RXR alpha - 45 kDa (add. band, or RXR beta)	640	624	938	1013	861	958	1207	1302	591	530	617	604	947	830	983	1023
RXR alpha - 50 kDa (main band)	934	669	1056	1176	1826	2202	3058	2918	1223	617	1303	701	1930	1229	3411	1707
RXR alpha - 50+45 kDa or RXR alpha/beta	1574	1293	1994	2188	2687	3160	4265	4221	1814	1148	1920	1305	2877	2057	4394	2729
RPS6	644	601	1002	1015	452	784	1443	907	515	328	645	720	970	853	691	788
RPS6 - pS240/244	1010	1294	4544	2073	2124	3331	7744	3974	2805	2446	3699	16776	7804	7980	6319	15256
SDS (serine dehydratase)	517	306	236	151	5292	6393	4302	2914	198	389	279	446	3324	4839	4819	6945
SerpinE1 / PAI1	740	775	561	523	824	1022	800	1233	666	446	755	734	949	968	1316	1174
SHP-2	304	223	101	83	249	233	136	181	98	177	125	210	109	157	192	239
Smad1	160	176	182	249	132	157	191	214	150	101	171	126	161	130	189	106
Smad3	52	47	65	59	55	50	110	65	42	50	69	57	57	46	63	43
SPRED2	60	89	67	84	28	36	36	43	71	39	121	104	50	28	57	30
SPRY2 (Protein sprouty homolog 2)	931	818	595	706	558	641	365	394	637	740	631	790	303	631	376	524
SPRY3 (Sprouty 3)	40053	35624	41098	50394	48812	57768	77377	66847	33227	24177	36121	31532	59667	41185	58739	50537
Src	1998	2050	2885	3042	2564	2987	3851	4381	2188	1341	2747	2155	3301	2082	3709	2574
Src - pY527	2238	2292	1385	1383	2394	2526	1416	1445	881	1778	1225	2148	1029	2132	1267	2221
Src Family - pY416	108	134	74	92	99	104	85	92	99	77	141	163	109	109	116	189
STAT 1	1148	2063	984	1518	1115	1580	1473	1150	1122	1502	1579	1510	1334	1967	1582	1605
STAT 3	1404	1587	1375	1345	1526	1531	1711	1515	946	1018	1341	1222	1199	1514	1728	1199
STAT 3 - pS727	63	90	91	81	74	86	92	138	47	83	45	82	74	92	96	65
Strep	224904	224904	224904	224904	224904	224904	224904	224904	224904	224904	224904	224904	224904	224904	224904	224904
Superoxiddismutase (Cu/Zn)	867	685	900	717	617	575	548	457	834	880	1032	987	514	674	519	658
TBK1/NAK - pS172	53	39	41	72	59	38	49	60	40	35	40	53	54	47	60	60
TCF4	57	40		35	49	37	60			24		49	25	49	42	44
Topoisomerase 1	1276	1232	2587	1436	1569	1825	3808	2180	1035	1156	920	1099	1748	1377	1142	1788
VASP - pS239	31	47	44	70	128	81	85	95	35	31	37	53	64	68	62	92
Wnt3A	2956	2860	2083	1536	8144	11148	3892	3155	1328	2133	1161	2218	3745	7133	5065	8205

12.4 Appendix 4: Data from the Lapatinib resistance experiment

This table contains all DigiWest data from the Lapatinib resistance experiment. All analytes which gave analyzable signal at the correct molecular weight are contained. Data are given in [AFI], data are not normalized. 'KB PD' is short for Kinobead pull-down.

	H292 Control Lysate			H292 Resistant Lysate			H292 Control KB PD			H292 Resistant KB PD		
	Lysate 1	Lysate 2	Lysate 3	Lysate 1	Lysate 2	Lysate 3	KB PD 1	KB PD 2	KB PD 3	KB PD 1	KB PD 2	KB PD 3
Analyte	[AFI]	[AFI]	[AFI]	[AFI]	[AFI]	[AFI]	[AFI]	[AFI]	[AFI]	[AFI]	[AFI]	[AFI]
Abl2	504	556	469	468	404	452	2558	3184	2967	1941	2012	2198
ABL2 (phosphorylated)	257	288	325	161	117	119	3028	3287	3155	1866	2177	2154
AHR	1271	1191	1171	1256	862	1375						
Akt	70890	72361	73044	75848	81811	75933	214019	218137	185963	205763	188962	180614
Akt - phospho Ser473	69	75	81	34	33	23	318	254	202	102	106	95
Akt - phospho Thr308	13	23	29	21	31	17	409	550	512	431	205	235
AMPK alpha	2457	2422	2181	1731	1833	1625	11069	11860	9692	6871	7669	6614
AMPK alpha - phospho Thr172	4832	4869	4392	2303	2202	2243	34161	35075	32039	19568	20926	18752
ASK1	85	94	86	79	53	68	724	759	658	243	222	219
ASK1 Phospho Thr845	51	46	49	30	16	17	1007	1051	977	316	296	284
ATF3	3083	3210	3183	2832	2757	2940						
ATM	644	540	816	471	418	505	118	156	154	55	35	40
Aurora A - phospho Thr288	33	28	26	143	160	151						
Aurora A (AIK)	321	330	334	102	91	79	5899	5808	3900	1315	1137	885
Aurora A/B/C - phospho Thr288/Thr232/Thr198	59	26	39	29	39	25	166	208	143	79	72	79
Aurora B (AIM1)	92	111	89	41	29	26	432	404	329	95	119	104
beta-Actin	271450	271186	254977	294429	277161	259552	5092	4017	2469	5281	3253	3293
beta-Catenin	46410	44486	37109	72109	68666	68062	2760	2785	1431	2208	2294	2506
beta-Catenin - phospho Ser675	10613	9696	8113	19291	17706	16892	550	489	259	462	493	538
beta-Catenin - phospho Thr41/Ser45	65	61	42	103	102	94						
b-Raf	105	125	99	108	123	101	812	802	474	596	656	589
b-Raf - phospho Ser445	1531	1513	1294	1256	1171	1139	6913	7135	4707	5433	5659	5180
Caseinkinase 1 epsilon	1368	1655	1345	1298	1313	1135	979	640	589	364	293	220
Caspase 3	11367	11257	10470	12523	12419	13293	67	48	64	67	85	76
Caspase 7	5986	5809	5479	12356	11651	12039	95	98	77	193	234	254
Caspase 8	1998	1963	1725	840	808	871						
Caspase 9	1032	902	816	3172	3210	3027						
Caveolin-1	8381	9549	9836	2352	2494	2588	332	339	265	115	86	94
cdc2 - phospho Tyr15	961	899	828	619	640	642	1806	1748	1447	1321	1224	1287

	H292 Control Lysate			H292 Resistant Lysate			H292 Control KB PD			H292 Resistant KB PD		
cdc2 (CDK1)	8672	9746	7796	3646	3682	4052	1943	1444	1603	275	347	360
CDK6	95	79	80	375	398	425	23	8	15	69	90	77
CDK6 (phospho-Tyr13)	3277	2149	1846	3922	2568	2947	456	482	507	731	557	456
CDK6 (phospho-Tyr24)	468	278	207	404	205	221	764	627	628	346	289	243
CDKN2B (p15 INK4B, CDN2B, MTS2)	187330	180745	160777	207908	190461	205396						
c-Jun	37	34	25	30	48	34						
c-Jun - phospho Ser63	195	166	183	116	120	124						
c-Jun - phospho Ser73	92	85	74	110	74	94						
c-Kit												
c-myc	1073	945	950	739	801	754						
c-myc - phospho Thr58/Ser62	2665	2865	2935	2684	2262	2179						
Crk (p38)	1096	1032	926	976	937	910						
Crk (p38) - phospho Tyr221												
Cyclin A2	125	167	139	143	147	122						
Cyclin B1	801	692	691	182	137	156	3063	3005	2503	182	174	170
Cyclin B1 - phospho Ser133	196	224	203	167	197	162						
Cyclin D1	420	341	319	288	219	285						
Cytokeratin 7	71440	67790	74837	51024	44915	48292	20219	11158	9315	7943	7052	8601
Cytokeratin 8	4008	3940	4594	1145	897	1086	795	612	522	213	167	209
Cytokeratin 8 - phospho Ser23	432	437	543	264	246	262	551	539	293	200	267	256
DUSP1 - phospho - (MKP-1) Ser296/318	183	99	87	181	125	78						
DUSP1 (MKP1)	4369	3250	2889	5261	3936	3784						
DUSP10 (MKP-5)	302	244	205	158	142	154						
DUSP5 (VH3)	197	196	169	191	186	187						
DUSP6 (MKP3)	541	540	448	32	34	27						
DUSP9 (MKP4, MKP-4)	986	571	533	5262	4857	5002	140	137	136	266	177	126
E-Cadherin	44784	50096	43821	72565	73979	72414	1778	2183	1247	1415	907	1053
E-Cadherin - phospho Ser838/Ser840	84059	93627	84345	105570	114051	105951	5336	6576	3718	3028	1963	2044
EGFR	12169	16160	12012	36640	53335	41327	63777	71488	57802	73	76	71
EGFR - phospho Tyr1068	2038	2384	2059	467	521	417	2815	2832	2585			
EGFR - phospho Tyr845	472	532	497	182	170	188	677	861	705			
EGFR - phospho Tyr992	1253	1502	1206	1864	2394	1810	4772	5204	4602			
EphA2	2528	2901	2480	835	828	854	53089	55271	53066	16049	17402	15870
EphA2 Phospho Ser897	158	137	128				2762	2707	2690	170	196	176
EphA2 Phospho Tyr588	250	331	328	296	377	347	5419	5681	5386	5476	5978	5679
EphA2 Phospho Tyr594	119	124	123	139	114	101	2583	2693	2447	2454	2878	2519
EphA2 Phospho Tyr772	2422	2669	2621	2113	2035	1919	43197	45251	43454	27382	28379	27402
EphA4							31	23	22	113	152	128
EPHA4 (phospho-Tyr596)							269	293	231	314	281	267
EphB3							67	74	58	248	310	310
EphB4							844	874	820	234	235	210
EphB6												
EphB6												
Ephrin B Phospho Tyr324/329	89	90	93	118	113	127	6465	7520	5706	4592	2777	2832
Erk1/2	37139	35016	28686	36486	36381	34368	334116	327959	293328	349849	382168	378960
Erk1/2 (MAPK p44/42) - phospho Thr202/Tyr204	1515	1664	1495	569	581	577	15951	14333	12591	6020	5680	6068
FAK 1	573	620	505	634	543	579	24898	29941	31527	18860	24714	25256
FAK 1 - phospho Tyr576/Tyr577	154	170	137	221	222	225	2907	3323	3337	3463	3826	3779
FAK 1 - phospho Tyr861				153	197	158	122	118	108	115	139	150
Folate Binding Protein (Folate Receptor, FOLR1)												
Fyn	461	491	434	1182	1112	1164	2964	2933	2534	11651	11869	11705
Fyn - phospho Tyr530	9169	8114	8526	6882	6531	6593	171340	165707	140987	150366	141554	125728
GSK3 beta	6833	6786	6779	4802	4738	4562	55376	49899	43613	36331	31169	28604
GSK3 beta - phospho Ser9	448	478	458	225	205	216	7492	6746	5359	3479	2900	2449
Her2	3933	4472	3934	9547	9754	9677	211	259	155	173	132	137
Her2 - phospho Tyr1248	2958	4247	3199	1110	1552	1379	1848	1632	2004			
Her2 - phospho Tyr877												
HIF1 alpha												
HIF-1beta (ARNT)	3694	3279	3053	1808	1631	1528						
IKKε	592	482	493	99	91	83	6222	6862	5195	827	837	703
IKKε Phospho Ser172												
IRAK4	1614	1438	1534	2949	2041	2180	1023	1093	787	2748	2167	2251
IRAK4 Phospho Thr345/Ser346	35	40	29	191	207	206	165	169	114	787	783	753
JNK/SAPK	3253	3325	3114	2475	3348	3163	33010	31671	24305	31852	32565	29554
JNK/SAPK - phospho Thr183/Tyr185	214	193	170	228	237	231	448	420	368	67	62	56
LATS2	26	30	32	162	105	127	275	305	310	880	969	926
LIMK1	2376	2493	2321	1430	1322	1370	6128	6357	4787	2758	2812	2494
LIMK1 Phospho Thr508 / Thr505	77	71	65	59	48	59	1472	1199	940	1089	1145	940
LRRK2	79	67	100	77	79	103	290	311	421	97	112	82
LRRK2 Phospho Ser910							80	93	108	26	46	43
LRRK2 Phospho Ser935							108	121	131	20	19	27
MEK1	8026	8740	7873	3914	4076	4046	1139	1064	805	510	458	440
MEK1 - phospho Thr292	480	423	403	263	204	207	82	79	82	42	39	41
MEK1/2 - phospho Ser217/221	676	690	669	408	386	362	170	159	151	96	87	81
MKK3/6 - phospho Ser189/207	83	71	58	70	77	40	218	202	174	605	678	530
MKK3/MKK6 Phospho S218/T222 S207/T211	808	582	584	768	742	743	1714	1492	1467	3962	3809	3700
MKK6	1962	2001	1601	4217	4064	4137	19777	17232	15066	57832	55929	55694
MKK7	805	801	831	1060	1026	979						
MKK7 - phospho Ser271/Thr275	234	254	158	305	172	235						
MLK3 (MAP3K11)	303	307	316	270	300	300	2879	2963	1933	1576	2215	1818
MLK3 -phospho (MAP3K11) Thr277/Ser281												
Mnk1	773	895	815	1491	1523	1488	206	187	155	218	218	213
Mnk1 - phospho Thr197/202	1139	1053	1047	831	719	744	600	555	537	228	262	265
NF-κB p100/p52	2423	3029	2776	1695	1618	1682	116	121	114	55	78	72
NF-κB p105/p50	21740	23331	21924	20659	21229	20087	1273	1078	758	675	696	635

	H292 Control Lysate			H292 Resistant Lysate			H292 Control KB PD			H292 Resistant KB PD		
NF-κB p65	4219	3820	3741	5734	5064	5115	306	348	170	266	232	243
NF-κB p65 - phospho Ser536	576	606	539	511	591	554						
NIK	62	66	56	87	89	99	517	648	502	280	329	278
p21/Waf1/Cip1	2723	2746	2406	1107	1064	1204						
p27(Kip1) - phospho - (CDKN1B) Ser10	2865	2735	2445	13684	12913	13358						
p27(Kip1) (CDKN1B)	941	872	762	2947	2670	2772						
p38/MAPK	3051	3511	2950	2717	3035	2629	107223	101467	91429	112247	122314	118966
p38/MAPK - phospho Thr180/Tyr182	100	85	74	97	45	55	2456	2242	2135	2100	2121	2038
p53	1801	1870	1755	580	494	539	130				55	73
p53												
p53 - phospho Ser20			44									
p53 - phospho Ser392	244	293	274	146	108	124						
PI3-kinase p110 subunit alpha	205	258	213	207	237	208						
PI3-kinase p85	204	210	215	379	384	348	38	57	48	53	58	46
PKCθ	126	125	116	29	27	20	1057	1385	806	100	109	107
PKCθ Phospho Thr538	129	114	114	25	32	26	1172	1472	919	117	109	110
PP1 alpha	6210	5671	4638	5550	6561	5482						
PP1 alpha - phospho Thr320	3515	3263	2773	3175	3124	2764						
PP2A C	11368	11346	10783	9232	8943	8959						
PP2A C - phospho Tyr307	2227	2490	2213	1942	1884	1829						
PTEN	6263	5907	5369	10726	10010	10279						
PTEN - phospho Ser380	2223	1911	1855	3667	3405	3440						
PTPN7 (LC-PTP, HEPTP)	4992	4135	4144	4252	3246	3401						
PTP-PEST (PTPN12, PTN12)	946	1040	915	814	920	995						
Pyk2 - phospho Tyr402	951	821	776	947	936	911	9897	10676	11167	12980	14934	14857
Pyk2 / FAK 2	813	1049	968	2474	2512	2744	19880	20336	22105	43334	45116	40518
RSK 1	3120	3332	3290	7920	8469	8466	25031	29735	20088	79645	74120	72776
RSK 1 - phospho Thr573							1811	1937	1480	1394	1614	1333
RSK 1 (p90RSK) - phospho Ser380							702	808	642	248	302	256
RSK 1/2/3	12221	12097	10718	32732	31238	32964	86063	96201	76349	200290	207071	201109
RSK 4							291	225	201	338	393	303
RSK 4 - phospho Ser235	666	795	689	1110	1169	1153	23880	28003	18783	66254	60846	56956
RXR	1144	1145	1066	1139	1222	1214						
RXR alpha												
SIK3	241	245	182	258	183	223	811	924	1051	486	426	520
SIK3 (KIAA0999)	2697	2266	2443	3258	3204	2847	296	327	200	269	223	263
Smad2 - phospho Ser245/250/255	76	62	92	34	38	31						
Smad2 - phospho Ser465/467												
Smad2/3	4245	3683	3793	4955	4495	4352	197	190	168	201	110	161
Smad3 - phospho Ser423/425												
Src	7739	6908	6829	5484	4897	4704	76401	74750	63646	64814	61679	59917
Src - phospho Tyr416	3732	4102	3871	1530	1426	1326	30619	31795	27220	16500	14591	13897
Src - phospho Tyr527	30676	30661	31306	29540	27479	27323	198634	191105	169539	227147	215388	205945
STEP (PTPN5, PTN5)	48048	47641	54025	96846	85334	102418						
TAK1	4594	4426	3936	5163	4698	4856						
TAK1 - phospho Ser412	1264	1337	1174	1266	1137	1224						
Thrombospondin 2												
YAP	1507	1342	1216	2652	2743	2535						
YAP - phospho Ser127	1723	1659	1414	4134	4257	4123						